

# Active Brownian Motion

An Agent Based Study of  
Active Brownian Particles With Energy Depots

Fraser Miles Baigent

Thesis submitted to the University of Strathclyde for  
the degree of Doctor of Philosophy

Department of Chemical and Process Engineering

2025

---

This thesis is the result of the author's original research. It has been composed by the author and has not been previously submitted for examination which has led to the award of a degree. The copyright of this thesis belongs to the author under the terms of the United Kingdom Copyright Acts as qualified by University of Strathclyde Regulation 3.50. Due acknowledgement must always be made of the use of any material contained in, or derived from, this thesis.

Signed: 

Date: 29th April 2025

“If you want to overcome the whole world, overcome yourself.”

— Fyodor Mikhailovich Dostoevsky (The Possessed)

# Acknowledgements

Thank you to the EPSRC for funding this Ph.D program and thesis, and to the Department of Chemical and Process Engineering at University of Strathclyde for hosting me from my first day of undergraduate study until the end of this journey.

I am forever grateful to my two academic supervisors and mentors, Mark Haw and Leo Lue. Mark's patience and guidance was critical in the completion of this thesis, and his support at the most challenging points set me up for any and all success I have had since. Thanks to Leo for teaching me how to turn unbounded curiosity into actions and results, for introducing me to Emacs, and for helping me to realise that coding could be more than just a tool and could also be a career. Without these two I wouldn't be where I am today.

To my amazing wife Oksana I'm thankful for all of the patience and support over the years. After all of the challenges we've been through, she has stood by my side through it all — this thesis is dedicated to you and our beautiful son, Dmitriy, who puts everything into perspective.

Thanks to Abdul Wadood, whom I met on my first day of undergraduate study and whose support helped me to completion. All

---

of our sojourns to the Lab, games of squash, and chats about deep literature, philosophy, sport and hobbies are cherished memories. Thanks to Chris Campbell for being a stand-up man and friend and a great example of how to be an efficient Ph.D student, as well as squash opponent. To Chris Boyle for being the definition of a creative coder and sharing my enthusiasm for computer-science nerdiness and inspiring me to become a better developer as well as for being on the other end of the IRC terminal. To Andy McGuire for sage advice and wisdom as I worked on completing this thesis, as sharp a mind I know but also a great and kind man.

Thanks to Dr. Paul Mulheran and Prof. Ashleigh Fletcher for nurturing my love of teaching through opportunities to tutor in their classes, and for all of the interesting discussions that arose.

To all of the other Ph.D. students, thanks for the lunchtime debates and discussion — Martin, Andrew, Rab, Scott, David, David M, Carla, Craig, Daria, Francesco, Ivan, Alessia, Kelly, Precious, Maclean, Callum, and all the others who shared in the experience and made coming into the office fun and interesting.

I'd also like to thank my parents, without whose support this study could not have been completed and who always supported and encouraged my interests in science and mathematics from an early age.

A final thanks to all of the open source and free software, languages, tools and libraries used in the execution and writing of this thesis — Linux, Emacs, C++, L<sup>A</sup>T<sub>E</sub>X, python (matplotlib, numpy

---

and Fenics in particular); thanks to all of the contributors!

# Abstract

Active Brownian particles (ABPs) are Brownian particles (on the scale of nano- to micro-metres) which are also subject to an additional active component of motion. This may be as a result of a physical propulsion from the particle itself, or as the result of an external force acting upon the particle.

One way of modelling these ABPs is through the energy depot (ED) model. ED particles contain an internal depot capable of storing and consuming energy in order to accelerate. We aim to better understand particle behaviour when the depot energy and velocity are independently calculated and improve the clarity in the literature of when the commonly made adiabatic assumption holds.

We run agent based simulations of individual particles with energy depots in 1-D and capture the results. By varying the uptake of energy from the surroundings and the rate of consumption, we observe different particle dynamics in the velocity-energy phase-space.

We find that when constrained to a single dimension, the depot behaviour becomes more adiabatic as energy uptake and conversion rates increase. We compare our results to the literature and add resolution to behaviours in non-adiabatic parameter regimes where the update rate of depot energy and particle velocity are on the

---

same timescale. Particles are categorised into 4 sub-types dependent on the emergent behaviour from the given input parameters. We note that for non-adiabatic particles there are two emergent behaviours — one near to the stationary points in velocity-energy phase-space where the particle approaches the adiabatic limit; and one at low velocities, where particles exhibit behaviour more similar to a simple Ornstein–Uhlenbeck (OU) particle, or a particle starting from rest. We stochastically model particles switching between these behaviours and model the time distributions as a power law.

# Contents

|          |   |           |
|----------|---|-----------|
| <b>1</b> | <b>Introduction</b>                                 | <b>1</b>  |
| 1.1      | Thesis Overview                                     | 1         |
| <b>2</b> | <b>Literature review</b>                            | <b>5</b>  |
| 2.1      | Introduction  | 5         |
| 2.1.1    | Brownian Motion                                     | 5         |
| 2.1.2    | Active Brownian Motion                              | 6         |
| 2.1.3    | Conclusions   | 13        |
| 2.2      | Active Brownian Particle Simulations                | 14        |
| 2.2.1    | Introduction  | 14        |
| 2.3      | Modelling Brownian Motion                           | 14        |
| 2.3.1    | Agent Based Approaches                              | 15        |
| 2.3.2    | Group Motion of Active Brownian Particles           | 18        |
| 2.4      | Energy Depot Model                                  | 20        |
| 2.4.1    | Parameters  | 20        |
| 2.4.2    | Theoretical Summary                                 | 21        |
| 2.4.3    | Adiabatic Assumption Of Motion                      | 23        |
| 2.4.4    | Other Models  | 26        |
| 2.4.5    | External Fields                                     | 28        |
| 2.4.6    | Multiple Particle Systems                           | 29        |
| 2.4.7    | Conclusion  | 30        |
| 2.5      | Conclusion  | 34        |
| <b>3</b> | <b>Theory and Methodologies</b>                     | <b>36</b> |
| 3.1      | Brownian Motion                                     | 36        |
| 3.1.1    | Langevin Equations & the Ornstein-Uhlenbeck Process | 37        |
| 3.1.2    | Underdamped & Overdamped Motion                     | 39        |
| 3.1.3    | Fokker-Planck Equation                              | 40        |
| 3.1.4    | Deterministic Limits of Particles in 1D             | 41        |
| 3.1.5    | Survival Probability and First Passage Time in 1-D  | 42        |
| 3.2      | Statistical Theory of Random Motion                 | 46        |
| 3.2.1    | Markov Processes                                    | 46        |
| 3.2.2    | Statistical Mean Values                             | 47        |
| 3.3      | Active Brownian Motion                              | 49        |
| 3.3.1    | The Active Force                                    | 49        |
| 3.3.2    | Multiple Particle Interactions                      | 50        |
| 3.3.3    | The Energy Depot Model                              | 50        |
| 3.4      | Energy Depot Model                                  | 51        |
| 3.4.1    | Model Description                                   | 51        |
| 3.4.2    | Langevin Equations                                  | 52        |
| 3.4.3    | Adiabatic Assumption                                | 52        |
| 3.4.4    | Active Friction                                     | 53        |
| 3.4.5    | Stationary Velocity & Bifurcation Point             | 56        |
| 3.4.6    | Fokker-Planck Equation                              | 57        |
| 3.5      | Stochastic Calculus                                 | 61        |
| 3.5.1    | Heun Method   | 61        |
| 3.5.2    | Autocorrelation                                     | 63        |
| 3.5.3    | Switching Time Distribution                         | 64        |

---

|          |  |            |
|----------|--|------------|
| 3.5.4    | Power Law Fit For Switching Time . . . . .                                       | 65         |
| 3.5.5    | Chi-Squared Testing . . . . .  | 65         |
| <b>4</b> | <b>Ensemble Average Behaviour of Particles with Energy Depots in 1-D</b>         | <b>67</b>  |
| 4.1      | Introduction . . . . .   | 68         |
| 4.1.1    | Simulation Motivation and Experimental Outline . . . . .                         | 68         |
| 4.1.2    | Model Parameters . . . . .   | 71         |
| 4.1.3    | Simulation Parameters and Assumptions . . . . .                                  | 72         |
| 4.1.4    | Simulation Methodology . . . . .   | 77         |
| 4.2      | Time Evolution of 1-D ED Particles Starting From Rest . . . . .                  | 80         |
| 4.2.1    | Introduction . . . . .   | 80         |
| 4.2.2    | Methodology . . . . .  | 81         |
| 4.2.3    | Results . . . . .  | 82         |
| 4.2.4    | Discussion of Results . . . . .  | 85         |
| 4.2.5    | Conclusions . . . . .  | 91         |
| 4.3      | Steady-State Particle Velocity Distributions . . . . .                           | 95         |
| 4.3.1    | Introduction . . . . .   | 95         |
| 4.3.2    | Simulation Parameters . . . . .  | 95         |
| 4.3.3    | Results . . . . .  | 97         |
| 4.3.4    | Low Activity Particles . . . . .   | 116        |
| 4.3.5    | Conclusions . . . . .  | 118        |
| 4.4      | Particle Motion in Velocity-Energy Phase-Space . . . . .                         | 122        |
| 4.4.1    | Introduction . . . . .   | 122        |
| 4.4.2    | Simulation Parameters . . . . .  | 123        |
| 4.4.3    | Methodology . . . . .  | 123        |
| 4.4.4    | Particle Motion through $v - e$ Phase-Space . . . . .                            | 125        |
| 4.4.5    | Scatter Plot of Trajectories ( $d_0 = 0.1$ ) . . . . .                           | 127        |
| 4.4.6    | Results . . . . .  | 131        |
| 4.4.7    | Conclusions . . . . .  | 144        |
| 4.5      | Chapter Conclusions . . . . .  | 148        |
| <b>5</b> | <b>Directional Switching of 1-D Active Brownian Particles With Energy Depots</b> | <b>149</b> |
| 5.1      | Introduction . . . . .   | 150        |
| 5.2      | Particle Switching Time Distributions . . . . .                                  | 151        |
| 5.2.1    | Introduction . . . . .   | 151        |
| 5.2.2    | Simulation Parameters . . . . .  | 152        |
| 5.2.3    | Methodology . . . . .  | 153        |
| 5.2.4    | Results . . . . .  | 154        |
| 5.2.5    | Conclusion . . . . .   | 159        |
| 5.3      | Velocity and Energy Before and After Switches . . . . .                          | 162        |
| 5.3.1    | Introduction . . . . .   | 162        |
| 5.3.2    | Methodology . . . . .  | 162        |
| 5.3.3    | Results . . . . .  | 163        |
| 5.4      | Fitting Parameters to Switching Time Distributions . . . . .                     | 170        |
| 5.4.1    | Introduction . . . . .   | 170        |
| 5.4.2    | Methodology . . . . .  | 170        |
| 5.4.3    | Results . . . . .  | 173        |
| 5.5      | Velocity & Energy Autocorrelation Functions . . . . .                            | 182        |
| 5.5.1    | Introduction . . . . .   | 182        |
| 5.5.2    | Simulation Parameters . . . . .  | 184        |
| 5.5.3    | Methodology . . . . .  | 184        |
| 5.5.4    | Results . . . . .  | 185        |
| 5.5.5    | Conclusions . . . . .  | 193        |
| <b>6</b> | <b>Conclusions</b>   | <b>197</b> |
| 6.1      | Conclusions of This Work . . . . .   | 197        |
| 6.1.1    | This Work in Context . . . . .   | 197        |
| 6.1.2    | 1-D ED Particles in the Physical World . . . . .                                 | 199        |
| 6.2      | Future work . . . . .  | 201        |
| 6.2.1    | Extension to Present Work . . . . .  | 201        |
| 6.2.2    | Beyond the Present . . . . .   | 204        |

---

|          |   |            |
|----------|---|------------|
| 6.3      | Concluding Thoughts . . . . .                                     | 207        |
| <b>7</b> | <b>Appendices</b>   | <b>216</b> |
| 7.1      | Differential Chapman-Kolmogorov Equation . . . . .                | 216        |
| 7.2      | Fokker-Planck Equation . . . . .                                  | 218        |
| 7.3      | Derivation of Ornstein-Uhlenbeck Fokker-Planck Equation . . . . . | 219        |
| 7.4      | Derivation of Solution to OU FPE . . . . .                        | 220        |
| 7.5      | Velocity-Energy Scatter Plots . . . . .                           | 223        |
| 7.6      | First Passage Time Probability . . . . .                          | 228        |
| 7.7      | Stationary Solution of Adiabatic Energy Depot FPE . . . . .       | 230        |

# List of Tables

|     |   |      |
|-----|---|------|
| 1   | Reference table for mathematical symbols used throughout the thesis presented with dimensions $\mathcal{L}$ (length), $\tau$ (time), $\mathcal{M}$ (mass), $\mathcal{T}$ (temperature). . . . .   | viii |
| 2   | Reference table for abbreviations used throughout the thesis. . . . .   | ix   |
| 2.1 | Summary table of parameters for ED model and corresponding simulations. . . . .   | 33   |
| 4.1 | Summary table of parameters for ED model . . . . .  | 71   |
| 4.2 | Summary of simulation parameters kept constant throughout experiments. . . . .  | 72   |
| 4.3 | Dimensionless groups used without simulations and calculations. . . . .   | 74   |
| 4.4 | Reference table for dimensionless simulation parameter sets used. . . . .   | 76   |
| 4.5 | Summary of simulation results for ensemble average dimensionless energy and ensemble average dimensionless velocity at steady-state (taken as $t = 100.0$ for all simulations). Deterministic adiabatic energy fixed point $e_0(\beta)$ and velocity bifurcation point $\beta = (v_0^2)$ are also listed for reference. . . . . | 87   |
| 4.6 | Summary of statistical means and standard deviations for simulations over all 20 parameter pairings. The mean and standard deviation of the absolute values of the velocity are also shown, as they are more useful in analysing bimodal distributions. . . . .   | 99   |
| 4.7 | Ratios of standard deviations and mean to the absolute stationary velocity $ v_0 ^D$ for all cases. . . . .   | 112  |
| 4.8 | Summary of observed behaviour types based upon definitions for all parameter variation cases. . . . .   | 116  |
| 5.1 | Dimensionless standard deviation of velocity ( $\sigma_{vD}$ ) and mean value of the dimensionless absolute velocity ( $\mu_{vD}(t)$ ) and mean dimensionless energy ( $\mu_{eD}$ ) measured immediately before and after a directional switch for all parameter sets. . . . .  | 167  |
| 5.2 | Summary of fitted effective diffusion $D_{\text{eff}}$ and fitting error $\chi_{\text{OU}}^2$ for all cases for switching time fits at short timescales (lower $\tau_s$ — where particles exhibit OU-like behaviour) calculated using the OU first hitting time distribution model eq. (5.4.1). . . . .                         | 174  |
| 5.3 | Summary of fitted reference time ( $\tau_0$ ), decay rate ( $\lambda$ ) and scaling factor ( $h_0$ ) along with corresponding statistical errors for switching time fits at long-timescales using the power-law decay model eq. (5.4.2). . . . .  | 174  |

# List of Figures

|     |  |    |
|-----|--|----|
| 2.1 | Examples of different theoretical synthetic spherical active Brownian particles outlined by Golestanian et al. [26] — (a) Janus swimmer (b) Saturn swimmer with an <i>equatorial belt</i> (c) <i>Three-Slice Design</i> (as Saturn but with a wider equator). These three designs for different spherical swimmers exhibit swimming behaviour. $\mu$ is the mobility of the swimmer; $\alpha$ is the chemical activity; $\theta$ is the latitude angle (used with permission). . . .   | 10 |
| 2.2 | (A) Illustration of QD (red sphere) and AP (green molecules) conjugate producing self-assembled fibres (purple structures) from fuel micelles (black/yellow/purple) in the fluid. (B) Dephosphorylation reaction resulting in formation of fibres and resultant accelerated motion. [1]. . . . .   | 12 |
| 3.1 | Solution to particle survival distribution from eq. (3.1.16) for an absorbing boundary at $v_c = 0$ for different positive starting velocities $v_{t_0}$ . Particles starting at higher velocities are less likely to reverse direction quickly than those starting slower. $\gamma_0 = 1.0$ , $D = 0.1$ .   | 44 |
| 3.2 | Solution to particle survival distribution from eq. (3.1.17) for an absorbing boundary at $v_c = 0$ for different positive starting velocities $v_{t_0}$ . Slower initial velocities lead to a higher probability of changing directions at lower values of survival time $\tau$ . $\gamma_0 = 1.0$ , $D = 0.1$ . . . . .  | 45 |
| 3.3 | Graphical representation of the active friction eq.(3.4.8) for adiabatic particles. For values of $\gamma(v) < 0$ (the pumping region) the particle is “pumped” and the velocity increases, depleting the internal depot. For values of $\gamma(v) > 0$ (the reduced drag, or dissipation region) the particle is dragged as with static friction, however the active motion reduces this drag force. At the stationary velocity $v_0$ (eq. (3.4.9)), the active and static friction components are balanced and the particle maintains a steady velocity. Adapted from[67]. Sample values $\gamma_0 = 1.0$ , $d_0 = 0.7$ , $q_0 = 10.0$ , $c = 1.0$ . . . . . | 54 |
| 3.4 | Velocity and energy streamlines for a deterministic particle with ED. The lines show the particle motion in $(v, e)$ -space always tending towards the stationary points at $(v_0, e_p)$ — darker red lines correspond to a higher gradient of motion through the phase space, with lighter orange corresponding to a lesser gradient. Example values: $q_0 = 2.0$ , $c = 0.001$ , $d_0 = 6.0$ , $\gamma_0 = 1.0$ . . . . .  | 55 |
| 3.5 | Plot showing $e_0$ curves vs. $v$ for varying values of constant energy uptake rate $q_0$ . The black dashed line shows $e_p$ , the threshold for pumping behaviour defined in eq. (3.4.7). The points where $e_0 = e_p$ is the stationary velocity $v_0$ . For $\beta < 0$ the $e_0$ line never meets $e_p$ . If $\beta = 0$ then the lines intersect at $v = 0$ only. $d_0 = 4.0$ , $c = 0.01$ , $\gamma_0 = 1.0$ . . . . .  | 57 |
| 3.6 | Normalised steady-state velocity distribution for particles with energy depots for different values of $q_0$ . There is an emergence of bimodal distribution for particles with $\beta > 0$ . As $q_0$ is increasing, the stationary velocity value also increases and the distributions move apart. There is no large effect on the variance of the velocities. The bimodal distribution gives an interesting case where $\langle v \rangle = 0$ but $\langle v^2 \rangle = \beta$ . $D$ has no effect on the value of $\beta$ . $D = 0.1$ , $d_0 = 4.0$ , $c = 0.01$ , $\gamma_0 = 1.0$ . . . . .  | 59 |
| 4.1 | Ratio of $D/\gamma_0$ for spherical Brownian particles in water. The line shows the expected value of this ratio for a constant temperature system of real particles over a range of possible radii. $T = 298.15 K$ , $\eta = 0.001 Pa s$ . . . . .  | 73 |
| 4.2 | Top: Distribution of ratio of simulated energy $e_{sim}$ to calculated adiabatic energy $e_0(v_i)$ . Bottom: $e_i$ for both simulated and calculated energies over a 20 time-unit trajectory. Parameters: $D = 0.1$ , $\gamma_0 = 1.0$ , $c = 0.001$ , $d_0 = 10.0$ , $q_0 = 10.0$ , $\Delta t = 0.01$ . . . . .   | 79 |

---

|      |   |     |
|------|---|-----|
| 4.3  | Average values $\langle  v  \rangle_{SS}$ for particles starting from rest with empty energy depots ( $v(0) = 0$ , $e(0) = 0$ ) for all cases A1-E4. Simulations of varying $d_0$ values are grouped with the same $q_0$ values in each subplot. Other parameters $\gamma_0 = 1.0$ , $D = 0.1$ , $c = 0.001$ , $\Delta t = 0.001$ .   | 83  |
| 4.4  | Average values of $ v(t) $ for particles starting from rest with empty energy depots ( $v(0) = 0$ , $e(0) = 0$ ) for all cases A1-E4 presented with log – log axes. Simulations of varying $d_0$ values are grouped with similar $q_0$ values in each subplot. Other parameters $\gamma_0 = 1.0$ , $D = 0.1$ , $c = 0.001$ , $\Delta t = 0.001$ .   | 84  |
| 4.5  | Average value of $e(t)$ for particles starting from rest with empty energy depots ( $v(0) = 0$ , $e(0) = 0$ ) for all cases A1-E4. Other parameters $\gamma_0 = 1.0$ , $D = 0.1$ , $c = 0.001$ , $\Delta t = 0.001$ .   | 85  |
| 4.6  | Average value of $e(t)$ for particles starting from rest with empty energy depots ( $v(0) = 0$ , $e(0) = 0$ ) for all cases A1-E4. Other parameters $\gamma_0 = 1.0$ , $D = 0.1$ , $c = 0.001$ , $\Delta t = 0.001$ .   | 86  |
| 4.7  | Velocity distributions of underdamped Brownian particles showing analytical solution to OU FPE (green line), Gillespie methodology[79] for an exact numerical solution to the OU process (blue circles) and normalised histogram of stochastic simulation for an inactive ED particle (orange crosses).   | 97  |
| 4.8  | Stochastic and analytical dimensionless velocity distributions for $d_0 = 0.1$ with varying $q_0$ (top-left: A1, top-right: A2, bottom-left: A3, bottom-right: A4). Other parameters $\gamma_0 = 1.0$ , $D = 0.1$ , $c = 0.001$ .   | 100 |
| 4.9  | Stochastic and analytical dimensionless velocity distributions for $d_0 = 1.0$ with varying $q_0$ (top-left: B1, top-right: B2, bottom-left: B3, bottom-right: B4). Other parameters $\gamma_0 = 1.0$ , $D = 0.1$ , $c = 0.001$ .   | 104 |
| 4.10 | Stochastic and analytical dimensionless velocity distributions for $d_0 = 2.0$ with varying $q_0$ (top-left: C1, top-right: C2, bottom-left: C3, bottom-right: C4). Other parameters $\gamma_0 = 1.0$ , $D = 0.1$ , $c = 0.001$ .   | 107 |
| 4.11 | Stochastic and analytical dimensionless velocity distributions for $d_0 = 6.0$ with varying $q_0$ (top-left: D1, top-right: D2, bottom-left: D3, bottom-right: D4). Other parameters $\gamma_0 = 1.0$ , $D = 0.1$ , $c = 0.001$ .   | 109 |
| 4.12 | Stochastic and analytical dimensionless velocity distributions for $d_0 = 1.0$ with varying $q_0$ (top-left: E1, top-right: E2, bottom-left: E3, bottom-right: E4). Other parameters $\gamma_0 = 1.0$ , $D = 0.1$ , $c = 0.001$ .   | 111 |
| 4.13 | Dimensionless velocity distributions for particles with $q_0 = 0.1$ shown alongside an inactive OU distribution and an inactive OU distribution with $\sigma_v = 1.41$ .  | 117 |
| 4.14 | Velocity and energy streamlines for a deterministic particle with ED. The lines show the particle motion in $(v, e)$ -space always tending towards the stationary points at $(v_0, e_p)$ . Example values: $q_0 = 2.0$ , $c = 0.001$ , $d_0 = 6.0$ , $\gamma_0 = 1.0$ .   | 126 |
| 4.15 | Scatter plot of particle velocity and energy at intervals of $\Delta t = 0.1$ (top-left: A1, top-right: A2, bottom-left: A3, bottom-left: A4). Each green point shows the depot energy to an instance where a particle was found at velocity $v$ throughout the trajectory. The lines show the adiabatic energy $e_0(v)$ (red) and the pumping energy $e_p$ (blue). The stationary points are found at the intersections of these two lines. Trajectory length $t_{\text{end}} = 30000.0$ . Other parameters $d_0 = 0.1$ , $\gamma_0 = 1.0$ , $D = 0.1$ , $c = 0.001$ . | 128 |
| 4.16 | Energy-velocity scatter from trajectories of varying values of $q_0$ , $d_0 = 0.1$ (top-left: A1, top-right: A2, bottom-left: A3, bottom-left: A4). Other parameters $t_{\text{end}} = 30000.0$ , $n_p = 1$ , $\gamma_0 = 1.0$ , $D = 0.1$ , $c = 0.001$ .  | 132 |
| 4.17 | Energy-velocity scatter from trajectories of varying values of $q_0$ , $d_0 = 1.0$ (top-left: B1, top-right: B2, bottom-left: B3, bottom-left: B4). Other parameters $t_{\text{end}} = 30000.0$ , $n_p = 1$ , $\gamma_0 = 1.0$ , $D = 0.1$ , $c = 0.001$ .  | 135 |
| 4.18 | Energy-velocity scatter from trajectories of varying values of $q_0$ , $d_0 = 2.0$ (top-left: C1, top-right: C2, bottom-left: C3, bottom-left: C4). Other parameters $t_{\text{end}} = 30000.0$ , $n_p = 1$ , $\gamma_0 = 1.0$ , $D = 0.1$ , $c = 0.001$ .  | 137 |
| 4.19 | Energy-velocity scatter from trajectories of varying values of $q_0$ , $d_0 = 6.0$ (top-left: D1, top-right: D2, bottom-left: D3, bottom-left: D4). Other parameters $t_{\text{end}} = 30000.0$ , $n_p = 1$ , $\gamma_0 = 1.0$ , $D = 0.1$ , $c = 0.001$ .  | 139 |
| 4.20 | Energy-velocity scatter from trajectories of varying values of $q_0$ , $d_0 = 10.0$ (top-left: E1, top-right: E2, bottom-left: E3, bottom-left: E4). Other parameters $t_{\text{end}} = 30000.0$ , $n_p = 1$ , $\gamma_0 = 1.0$ , $D = 0.1$ , $c = 0.001$ .   | 141 |
| 5.1  | Switching time distributions for particles with varying $q_0$ at $d_0 = 0.1$ (cases A1-A3). Other parameters $\Delta t = 0.1$ , $\gamma_0 = 1.0$ , $D = 0.1$ , $c = 0.001$ .  | 155 |
| 5.2  | Switching time distributions for particles with varying $q_0$ at $d_0 = 1.0$ (Cases B1-B3). Other parameters $\Delta t = 0.1$ , $\gamma_0 = 1.0$ , $D = 0.1$ , $c = 0.001$ .  | 156 |

---

|      |   |     |
|------|---|-----|
| 5.3  | Switching time distributions for particles with varying $q_0$ at $d_0 = 2.0$ (Cases C1-C3). Other parameters $\Delta t = 0.1, \gamma_0 = 1.0, D = 0.1, c = 0.001$ . . . . .   | 157 |
| 5.4  | Switching time distributions for particles with varying $q_0$ at $d_0 = 6.0$ (Cases D1-D3). Other parameters $\Delta t = 0.1, \gamma_0 = 1.0, D = 0.1, c = 0.001$ . . . . .   | 158 |
| 5.5  | Switching time distributions for particles with varying $q_0$ at $d_0 = 10.0$ (Cases E1-E3). Other parameters $\Delta t = 0.1, \gamma_0 = 1.0, D = 0.1, c = 0.001$ . . . . .  | 159 |
| 5.6  | Distributions of $v$ (upper plot) and $e$ (lower plot) for particles immediately before & after switching with varying values of $q_0$ at $d_0 = 0.1$ (Cases A1-A3). Other parameters $\Delta t = 0.1, \gamma_0 = 1.0, D = 0.1, c = 0.001$ . . . . .  | 163 |
| 5.7  | Distributions of $v$ (upper plot) and $e$ (lower plot) for particles immediately before & after switching with varying values of $q_0$ at $d_0 = 1.0$ (Cases B1-B3). Other parameters $\Delta t = 0.1, \gamma_0 = 1.0, D = 0.1, c = 0.001$ . . . . .  | 163 |
| 5.8  | Distributions of $v$ (upper plot) and $e$ (lower plot) for particles immediately before & after switching with varying values of $q_0$ at $d_0 = 2.0$ (Cases C1-C3). Other parameters $\Delta t = 0.1, \gamma_0 = 1.0, D = 0.1, c = 0.001$ . . . . .  | 164 |
| 5.9  | Distributions of $v$ (upper plot) and $e$ (lower plot) for particles immediately before & after switching with varying values of $q_0$ at $d_0 = 6.0$ (Cases D1-D3). Other parameters $\Delta t = 0.1, \gamma_0 = 1.0, D = 0.1, c = 0.001$ . . . . .  | 164 |
| 5.10 | Distributions of $v$ (upper plot) and $e$ (lower plot) for particles immediately before & after switching with varying values of $q_0$ at $d_0 = 10.0$ (Cases E1-E3). Other parameters $\Delta t = 0.1, \gamma_0 = 1.0, D = 0.1, c = 0.001$ . . . . . | 165 |
| 5.11 | Least-square line fits for short and long timescale data (Cases A1, A2, A3). $d_0 = 0.1, c = 0.001, D = 0.1, \gamma_0 = 1.0$ . . . . .  | 175 |
| 5.12 | Least-square line fits for short and long timescale data (Cases B1, B2, B3). $d_0 = 1.0, c = 0.001, D = 0.1, \gamma_0 = 1.0$ . . . . .  | 176 |
| 5.13 | Least-square line fits for short and long timescale data (Cases C1, C2, C3). $d_0 = 2.0, c = 0.001, D = 0.1, \gamma_0 = 1.0$ . . . . .  | 177 |
| 5.14 | Least-square line fits for short and long timescale data (Cases D1, D2, D3). $d_0 = 6.0, c = 0.001, D = 0.1, \gamma_0 = 1.0$ . . . . .  | 178 |
| 5.15 | Least-square line fits for short and long timescale data (Cases E1, E2, E3). $d_0 = 10.0, c = 0.001, D = 0.1, \gamma_0 = 1.0$ . . . . .   | 179 |
| 5.16 | Velocity autocorrelation plot for an OU particle over lag time range $\Delta\tau[0, 100]$ . $D = 0.1, \gamma_0 = 1.0$ . . . . .   | 186 |
| 5.17 | Comparisons of $v$ and $e$ autocorrelation for varying $q_0$ values over lag times $\Delta\tau[0, 100]$ (Cases A1-A4). Other parameters $d_0 = 0.1, c = 0.001, D = 0.1, \gamma_0 = 1.0$ . . . . .   | 187 |
| 5.18 | Comparisons of $v$ and $e$ Autocorrelation for varying $q_0$ values over lag times $\Delta\tau[0, 100]$ (Cases B1-B4). Other parameters $d_0 = 1.0, c = 0.001, D = 0.1, \gamma_0 = 1.0$ . . . . .   | 188 |
| 5.19 | Comparisons of $v$ and $e$ Autocorrelation for varying $q_0$ values over lag times $\Delta\tau[0, 100]$ (Cases C1-C4). Other parameters $d_0 = 2.0, c = 0.001, D = 0.1, \gamma_0 = 1.0$ . . . . .   | 189 |
| 5.20 | Comparisons of $v$ and $e$ Autocorrelation for varying $q_0$ values over lag times $\Delta\tau[0, 100]$ (Cases D1-D4). Other parameters $d_0 = 6.0, c = 0.001, D = 0.1, \gamma_0 = 1.0$ . . . . .   | 190 |
| 5.21 | Comparisons of $v$ and $e$ Autocorrelation for varying $q_0$ values over lag times $\Delta\tau[0, 100]$ (Cases E1-E4). Other parameters $d_0 = 10.0, c = 0.001, D = 0.1, \gamma_0 = 1.0$ . . . . .  | 191 |
| 7.1  | Scatter plot of particle velocity and energy at intervals of $\Delta t = 0.1$ for a single particle trajectory of length $t_{\text{end}} = 30000.0$ . Other parameters $d_0 = 0.1, \gamma_0 = 1.0, D = 0.1, c = 0.001$ . . . . .                      | 223 |
| 7.2  | Scatter plot of particle velocity and energy at intervals of $\Delta t = 0.1$ for a single particle trajectory of length $t_{\text{end}} = 30000.0$ . Other parameters $d_0 = 1.0, \gamma_0 = 1.0, D = 0.1, c = 0.001$ . . . . .                      | 224 |
| 7.3  | Scatter plot of particle velocity and energy at intervals of $\Delta t = 0.1$ for a single particle trajectory of length $t_{\text{end}} = 30000.0$ . Other parameters $d_0 = 2.0, \gamma_0 = 1.0, D = 0.1, c = 0.001$ . . . . .                      | 225 |
| 7.4  | Scatter plot of particle velocity and energy at intervals of $\Delta t = 0.1$ for a single particle trajectory of length $t_{\text{end}} = 30000.0$ . Other parameters $d_0 = 6.0, \gamma_0 = 1.0, D = 0.1, c = 0.001$ . . . . .                      | 226 |
| 7.5  | Scatter plot of particle velocity and energy at intervals of $\Delta t = 0.1$ for a single particle trajectory of length $t_{\text{end}} = 30000.0$ . Other parameters $d_0 = 10.0, \gamma_0 = 1.0, D = 0.1, c = 0.001$ . . . . .                     | 227 |

---

## Glossary of Symbols

**Table 1:** Reference table for mathematical symbols used throughout the thesis presented with dimensions  $\mathcal{L}$  (length),  $\tau$  (time),  $\mathcal{M}$  (mass),  $\mathcal{T}$  (temperature).

| Symbol               | Description                                 | Dimensions or Units                                 |
|----------------------|---|---|
| $\beta$              | Bifurcation point ( $v_0^2$ )               | $\mathcal{L}^2\tau^{-2}$                            |
| $\mathbf{x}i(t)$     | Gaussian white noise                        | -   |
| $\chi^2$             | Chi-squared statistic for least-squares fit | -   |
| $\Delta t$           | Simulation time step                        | $\tau$  |
| $D_{\text{eff}}$     | Effective diffusion constant                | $\mathcal{L}^2\tau^{-2}$                            |
| $\eta$               | Hydrodynamic viscosity                      | $\mathcal{M}\tau^{-1}\mathcal{L}^{-1}$              |
| $\eta(t)$            | Delta-correlated Gaussian white noise       | -   |
| $\gamma_0$           | Static Friction                             | $\tau^{-1}$   |
| $\kappa$             | Discrete autocorrelation lag                | -   |
| $\lambda$            | Power law fitted decay rate                 | $\tau$  |
| $\mathbf{I}$         | Identity matrix                             | -   |
| $\mathcal{N}$        | Normalisation function                      | -   |
| $\mu$                | Arithmetic mean value                       | -   |
| $\rho$               | Autocorrelation                             | -   |
| $\sigma$             | Standard deviation                          | -   |
| $\chi_{\text{OU}}^2$ | Fitting error                               | -   |
| $\tau$               | Switching time                              | $\tau$  |
| $\tau_0$             | Power law fitted reference time             | $\tau$  |
| $\tau_s$             | Switching time                              | $\tau$  |
| $c$                  | Energy depot dissipation rate               | $\tau^{-1}$   |
| $D$                  | Diffusion constant                          | $\mathcal{L}^2\tau^{-2}$                            |
| $d(\mathbf{v})$      | Depot energy conversion function            | $\tau^{-1}$   |
| $d_0$                | Depot conversion coefficient                | $\tau\mathcal{L}^{-2}$                              |
| $e_0(v)$             | Adiabatic energy                            | $\mathcal{M}\mathcal{L}^2\tau^{-2}$                 |
| $e_p$                | Pumping energy                              | $\mathcal{M}\mathcal{L}^2\tau^{-2}$                 |
| $h(\tau_s)$          | First hitting time probability              | -   |
| $h_0$                | Power law scaling factor                    | -   |
| $k_B$                | Boltzmann constant                          | $\mathcal{M}\mathcal{L}^2\tau^{-2}\mathcal{T}^{-1}$ |
| $n$                  | Number of dimensions                        | -   |
| $q(t)$               | Depot energy uptake rate                    | $\mathcal{L}^2\tau^{-3}$                            |
| $q_0$                | Depot constant Uptake Rate                  | $\mathcal{L}^2\tau^{-3}$                            |
| $R_H$                | Hydrodynamic radius                         | $\mathcal{L}$                                       |
| $T$                  | Temperature                                 | $\mathcal{T}$                                       |
| $t$                  | Simulation time                             | $\tau$  |
| $U(\mathbf{r})$      | Potential                                   | $\mathcal{M}\mathcal{L}^2\tau^{-2}$                 |
| $v_0$                | Stationary velocity                         | $\mathcal{L}\tau^{-1}$                              |

---

---

## Glossary of Abbreviations

**Table 2:** Reference table for abbreviations used throughout the thesis.

| Abbreviation | Full Name                    |
|--------------|------------------------------|
| ABM          | Active Brownian motion       |
| ABP          | Active Brownian particle     |
| BC           | Boundary condition           |
| BP           | Brownian particle            |
| CKE          | Chapman-Kolmogorov equation  |
| ED           | Energy depot                 |
| FPE          | Fokker-Planck equation       |
| LE           | Langevin equation            |
| MC           | Monte Carlo                  |
| MNM          | Micro/nanomotor              |
| MSD          | Mean-squared displacement    |
| OU           | Ornstein-Uhlenbeck           |
| PDF          | Probability density function |

# Chapter 1

## Introduction

This thesis uses computational methods to study a model of active Brownian particle (ABP) transport, inspired in part by previous experimental results with driven nano particles [1]. In particular, we focus on small (nano scale) particles where translational diffusive effects are dominant and utilise the Energy Depot (ED) model to simulate active components of particle motion in agent based simulations.

Active Brownian Motion (ABM) has been the subject of increased studies over the past two decades, as reviewed in detail in Chapter 2, due at least partly to interest in how living examples such as bacteria, viruses, and motor proteins achieve transport — and how artificial engineered versions of these active particles might be designed.

### 1.1 Thesis Overview

In Chapter 2 we present a comprehensive literature review of ABM and ABPs. A review of historical and ongoing research across the multiple areas of interest within this field — such as hydrodynamic

approaches, purely statistical approaches, multi-particle approaches — is presented. Empirical laboratory experiments which give the field a real-world grounding are discussed, and the translation of these results into computational models are presented.

Special attention is then given to the ED model on which much of the work in this thesis is based. We present an overview of the work carried out by the original authors of the model and the follow-on research since this point. We highlight the adiabatic assumption of energy relaxation and postulate on whether a more rigorous description of when this does and does not apply can be presented. The results of multiple studies in both 1- and multiple- dimensions are explored in order to provide context to the results which are presented in chapters 4 and 5.

Chapter 3 will explore the theory discussed in the literature review in more depth, explaining in detail the theoretical concepts and equations used in the field of ABPs throughout this work. The base equations of motion and their statistical roots are explained, along with the partial differential (Fokker-Planck) equations which govern the probability distributions for these systems. A detailed explanation of the theory of the ED model along with the key fixed points in the model, possible parameter regimes and time-scales which may arise are explored.

The computational simulation methods used and the resulting numerical implementation of the aforementioned equations are presented. A summary of the statistical and analytical methods used

to process the results from these computational simulations are also given.

In Chapter 4 non-adiabatic ABPs with EDs are simulated in 1-D. The initial conditions of systems starting from rest, average velocity distributions, and ensemble average behaviour in  $v - e$  phase-space are simulated. We compare the results against the adiabatic model. These numerical results are compared with the analytical solutions at steady-state where applicable and conclusions are drawn as to the different dynamics which occur in the adiabatic and non-adiabatic regimes. The velocity distributions are used to gain an insight into the canonical behaviour of the particles over long trajectories, whilst the distribution of the energy against the velocity is used to show the spread of the energy away from the value of  $e_0(v)$  (the adiabatic fixed point) as well as the regions of velocity space where this occurs for different simulation parameters.

In Chapter 5 the transition of particles between their stationary velocity limits in one-dimension is investigated. We highlight that there are characteristic times for directional switching in the two different regimes of motion — pumping at low  $v$  in the low-activity phase-space, and depot depletion at higher  $v$  near to the stationary velocity  $v_0$ . We present this as an alternative way to quantify the propensity of the particles to switch direction and suggest that this methodology is applied to existing research in multiple dynamics to describe behaviour in multiple dimensions. We look at the auto-correlation for both velocity and depot energy and draw conclusions

on how these analysis techniques can be used alongside the switching time distributions to understand the dynamics of particles in different regimes of motion.

Chapter 6 concludes this thesis by summarising all of the above results and comparing them in the context of the literature which we have explored. The simulations we carried out are given comparison with other systems seen elsewhere. We present further research ideas to take our current results further, as well as finally exploring ideas for using our framework and analysis techniques to enrich the results of other ED studies in non-adiabatic regimes or to extend our framework to alternative models of active motion.

## Chapter 2

# Literature review

### 2.1 Introduction

#### 2.1.1 Brownian Motion

Particles immersed in fluids on very small length scales undergo large numbers of highly chaotic collisions with the molecules in the surrounding fluid causing for a random motion. Robert Brown, the Scottish botanist and namesake of the motion, was one of the first to publish detailed investigations of the phenomenon from his experimental observations through a microscope[2]. Small particles of pollen in water were not at rest but were in fact moving in a seemingly random fashion within the fluid — as if agitated by some invisible force. Later, in one of the seminal papers from his *Annus Mirabilis*, Einstein laid out a statistical theory[3] that this motion occurred as the result of collisions with surrounding molecules and offered a thermodynamic as well as mechanical explanation. Soon thereafter, Langevin [4] presented a description of this motion which confirmed Einstein's work. Perrin then proved this theory experimentally[5] by physically measuring Brownian particles and confirming that their behaviour matched the predictions made by

Einstein. Through this early work, the diffusivity of a Brownian particle was well defined based on the fluid (viscosity, temperature) and particle (hydrodynamic radius, mass) properties.

The movement of small particles through a fluid as a result of Brownian motion is referred to as *translational* Brownian motion[6, 7]. The same forces from the surrounding fluid on a particle also cause for a random *rotational* Brownian motion[6, 7].

Pure Brownian systems exist in a thermodynamic equilibrium — fluctuations in the particle kinetic energy gained through collisions are cancelled out by the dissipation of this energy back into the surrounding fluid as heat (this is referred to as the Fluctuation-Dissipation theorem[8]).

### 2.1.2 Active Brownian Motion

Active Brownian Particles (ABPs) refer to a subset of Brownian particles which undergo additional motion as a result of internal or external forces, this motion is called Active Brownian Motion (ABM)[9].

Interest in the field of ABM was initially sparked by Feynman and Smoluchowski's thought experiment of the *Brownian Ratchet* — an engine on a molecular scale which would perpetually harvest energy by utilising the asymmetrical motion of individual Brownian particles[8]. Whilst this conjecture was proven to be thermodynamically impossible, it has inspired many functioning active Brownian machines and particles with real world applications.

### 2.1.2.1 Natural Active Brownian Particles

Micron-scale microbes such as e-coli *swim* through fluids by exerting a force on the surroundings using their appendages[10]. They can undergo periods of forward motion called *runs* where the physical force exerted by the flagella on the fluid drives the particle as the flagella work together (moving towards food-rich areas), when these flagella begin to rotate in different directions the particle enters the *tumble* phase — moving around the region of space (harvesting food)[11, 12]. This type of active motion is thus often referred to as *run and tumble*. These run and tumble dynamics occur on the order of magnitude of the length scale of the microbes themselves.

The motion can be governed by a process called *chemotaxis*[10, 13], where the swimmers sense the areas of higher food concentration by a chemical gradient and are attracted to that area. Living cells may use this phenomenon to move towards or away from areas of higher concentration — for example towards a food source or away from toxins.

Protein molecules such as kinesins and dyneins exhibit an active motion where hydrolysis of adenosine triphosphate (ATP) molecules causes them to *walk* along a protein track. The resultant biased force in one direction manifests an active motion where the stochastic Brownian force is overcome[14, 15, 16].

Other authors have focused on active motion through the process of cells binding to external substratum[17], cell migration with directional bias (taxis)[17, 18].

Rotational forces can still be prevalent, and in the case of bacteria such as e-coli asymmetric motion is seen as the microbe twists its tail to move forward[19, 10], taking a random trajectory dictated by its orientation. The asymmetry in this case is caused by the chirality of the swimming tail. Other swimmers may use flagella on their surface to paddle forward[20]. The back-stroke of these flagella is different to the forward motion and thus the broken symmetry of this motion allows for a net-displacement of the particle within a single cycle of swimming. Symmetry breaking (and thus irreversibility) is a key component in active motion such that the final net force on a particle over a cycle of motion is non-zero. For these swimmers the source of energy for this motion will normally be from chemical energy stored within the cell which is metabolised as needed.

#### **2.1.2.2 Micro/Nanomotors (MNMs)**

In other cases, synthetic particles are manufactured to act as engines or motors and drive motion as a result of their inherent properties. The energy source can come from within the particle assembly itself, or from the surrounding fluids. These particles are often called micro/nanomotors (MNMs)[21].

Conical micro-rockets (or microtubes) on the micron-scale are one such example[22, 21]. These were created by manufacturing nano-scrolls of a platinum coated material and placing them into different concentrations of hydrogen peroxide. The platinum surface catalyses the decomposition of the  $H_2O_2$  into water and oxygen. The resultant oxygen bubbles inside the scrolls protruded from the end

of the scroll when a critical volume is reached. The pressure of the emergence of the bubble causes an acceleration of the scroll through the liquid and a visible rocket trail. The rotational Brownian effects on these scrolls alters the trajectory as the particles move through the liquid. Tadpoles & boomerangs are another two examples of manufactured ABP swimmers which have been studied (on the scale of  $< 100nm$ )[23].

Another similar mechanism has been seen in microscopic Janus particles[24, 25, 26, 21, 27]. So called because of their two diametrically opposite faces, these particles are manufactured from microbeads of plastic or similar materials where one face of the particle is coated with a catalytic material such as platinum. In the case of bubble propulsion, this coating catalyses the decomposition of hydrogen peroxide just as with the micro scrolls.

Other configurations of catalytic coating on spheres such as *Saturn* swimmers and *three-slice* swimmers have also been investigated [26], with different geometries of coatings as illustrated in figure 2.1. Different configurations of the particles are shown with the chemical activity  $\alpha$  and resultant motility  $\mu$  in each region as a result of these designs also labelled. Design of different motility behaviours is possible by configuration of the particle surface chemistry. The asymmetry of the coatings (e.g. Janus coatings on opposite sides) is responsible for the active directed motion, as opposed to simply increasing the magnitude of the random force.

Ikezoe et al.[28] created micro-chemical motors in metal-organic

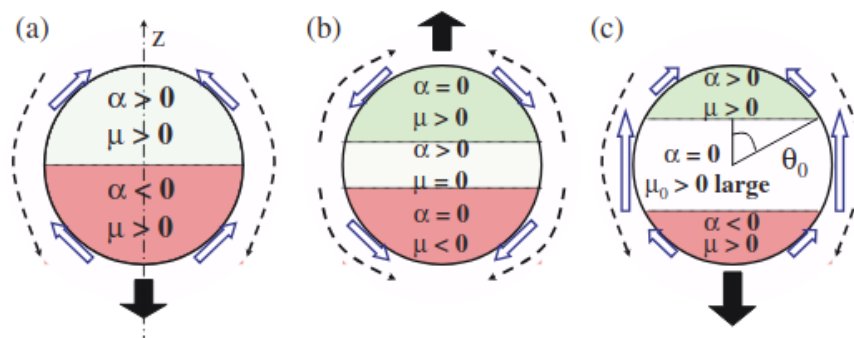


**Figure 2.1:** Examples of different theoretical synthetic spherical active Brownian particles outlined by Golestanian et al. [26] — (a) Janus swimmer (b) Saturn swimmer with an *equatorial belt* (c) *Three-Slice Design* (as Saturn but with a wider equator). These three designs for different spherical swimmers exhibit swimming behaviour.  $\mu$  is the mobility of the swimmer;  $\alpha$  is the chemical activity;  $\theta$  is the latitude angle (used with permission).

frameworks (MOFs) by utilising the self assembly of peptides. MOFs are highly porous organised structures. The self-assembly of the peptides at the surface interface between the MOF pores and the surrounding liquid created a strong surface tension gradient as a result of the peptide’s hydrophobic properties, accelerating the MOF’s transport through the fluid. The authors found that this motion was reliant on the peptides’ ability to form a self-assembled structure at the pore interface and that when non-assembling molecules were used the phenomenon did not occur. Addition of a soap-like solvent which reverted the self-assembly behaviour (and thus neutralised the surface-tension gradient) of the peptides was found to freeze the motion of the molecules, confirming that the motion was as a result of the surface tension gradient. Using this motor, the authors constructed a *boat*, a structure with a small 1mm region which could accommodate the motor. Using this construction they were able to observe the boat swimming in a fluid under the active force provided by the self-assembly.

For chemical motors, there are a variety of mechanisms which may drive the active force. The above examples show that chemical gradient, hydrodynamic pressure, surface tension and mechanical stress may all be factors in acceleration of chemically-driven ABPs on multiple different length scales.

Another example of manufactured ABPs are Pt-Au nano-rods as synthesised by Paxton et. al[29], micron-length cylinders 370 nm in diameter, with one half of the cylinder coated in Pt and the other in Au. The Pt end catalyses the formation of hydrogen from a  $\text{H}_2\text{O}_2$  solution, creating a concentration gradient of  $\text{O}_2$  in the solution which caused for acceleration. These swimmers along with the other examples of Janus swimmers and micro-rockets have achieved irreversible active motion through the decomposition of  $\text{H}_2\text{O}_2$  into water and oxygen[30].

Our group studied bio-catalytic self-assembly when amino-phosphatase enzymes attached to quantum dot particles (QD-AP particles of sizes from 2 nm–150 nm)[1, 31]. When placed in a micellular solution of *fuel* molecules, the enzymes catalysed the reaction and self-assembly of rod-like structures within the liquid causes an acceleration of the particles away from the rods. A key environmental factor which determined whether active motion was observed was the concentration of fuel molecules — at concentrations where the fuel formed micellular structures, active motion occurred via the formation of rod-like structures; whilst when the fuel was freely dissociated in solution there was no active motion. As shown in figure 2.2,

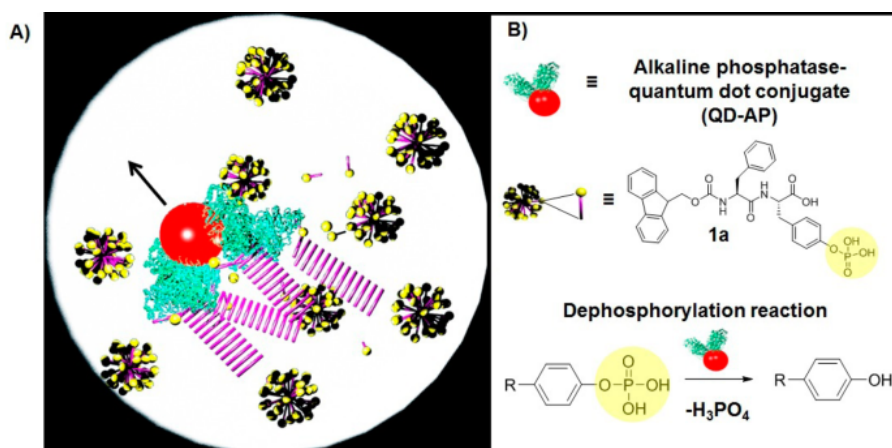


**Figure 2.2:** (A) Illustration of QD (red sphere) and AP (green molecules) conjugate producing self-assembled fibres (purple structures) from fuel micelles (black/yellow/purple) in the fluid. (B) Dephosphorylation reaction resulting in formation of fibres and resultant accelerated motion. [1].

the physical formation of these rods drives acceleration, in contrast to the chemical gradients formed in the other examples discussed here.

All of these examples of MNMs carry out active motion by consuming a fuel from the surroundings.

### 2.1.2.3 External Potential Fields

Another source of energy for active motion can be an external field. Additional energy in a targeted direction can be applied to particles to influence their motion. Magnetic [32, 33] potentials have been shown to exhibit control over the motion of BPs. Active motion can also be achieved through an external light source providing energy, known as phototaxis[34]. Research into these areas are motivated by goals of self assembly for manufacturing or non-intrusive targeted application of medicines.

### 2.1.3 Conclusions

ABPs are of great interest for their potential medicinal and manufacturing applications. The possibility of control or influence over the average behaviour of seemingly chaotic systems would be a game-changing discovery in the fields of nanotechnology and manufacturing. In non-physical systems, the mathematics describing these particles have already been applied successfully to predict canonical behaviour in unrelated fields such as the modelling of financial systems[35] and in models of opinion formation amongst human populations[36, 37, 38]; amongst others.

## 2.2 Active Brownian Particle Simulations

### 2.2.1 Introduction

This thesis focuses on the results of agent-based numerical simulations using a specific *Energy Depot* (ED) model developed for ABPs by Werner, Ebeling and Tilch[39]. The literature around this particular model will be discussed in detail in Section 2.4, with the theory covered in more depth in Chapter 3, however we will initially review a broad range of methodologies used throughout the field for simulation of ABPs.

Agent based models consider individual particles which self-describe their behaviour in the surrounding medium. Individual agents (i.e. particles) are simulated separately from each other and their effect on the surrounding fluid is encapsulated by the dynamics describing the particles themselves. Another method for simulating active particles is to consider the force balance on the particles from the surrounding fluid or *continuum*. These models look at the behaviour which particles exert on the fluid, and vice-versa. We consider agent based modelling for nano-scale particles where the transient effects of active motion on the surroundings will be negligible[40, 41].

### 2.3 Modelling Brownian Motion

Computational modelling and numerical simulation studies account for a large quantity of the investigative literature in the field of ABPs. The different mechanisms for the active motion discussed above, along with the varying length scales on which motion is ob-

served mean that many different approaches have been taken to model these particles. In this section a summary of these methodologies along with some of the results which were observed are presented.

As will be discussed in detail in Chapter 3, the motion of an ABP can be defined generally through the Langevin differential equation:

$$m\dot{\mathbf{v}} = -\mathcal{F}_{friction} + \mathcal{F}_{active} - \nabla U(\mathbf{v}, \mathbf{r}) + \mathcal{F}_{stoch} \quad (2.3.1)$$

The velocity and force components in this equation may be related to system conditions, neighbouring particles, hydrodynamic stresses, particle direction or a variety of other factors. The active force  $\mathcal{F}_{active}$  is therefore implemented in many different ways, some of which will be discussed in this section.

### 2.3.1 Agent Based Approaches

Active particles such as kinesin have also been modelled specifically as molecular combustion engines [42] which convert energy from the surroundings into motile energy. On these nano-scales, the viscous effects of the particles in the fluid are negligible compared to the Brownian force. This method predicts the motion of these particles along skeletal structures by calculating the Gibbs free energy of the reaction, however more phenomenological methods for modelling active particles over multiple length scales have also been suggested.

Simple reaction-diffusion systems on lattice grids were modelled [43] under which particles of component  $A$  could react to form a secondary component  $B$  at a point on the grid. The different diffusive

behaviours of these two particles and their effect on each other resulted in a concentration cluster on the lattice.

These numerical approaches do not tend to describe the behaviour of the system which surrounds the particles. The energy lost to friction is usually assumed to dissipate into the system and not to affect the particle's diffusion. This can make sense on smaller length scales or in single-particle systems without interaction, however in more clustered systems the model assumptions may fail.

Romanczuk et al [44] modelled the activity of a particle in 2-D by introducing a stochastic force in the direction of the particle orientation. Particles were simulated with three random forces - a purely stochastic diffusion force, a rotational diffusive force, and a force in the direction of particle orientation. Initially with a simple Gaussian approximation of noise, they saw the formation of a donut-like probability distribution of velocities in  $(v_x, v_y)$  which reverted to a classical Brownian-like Gaussian distribution with a more pointed peak at the origin as the active noise was increased. These donut-like distributions strongly resembled the stationary velocity distributions developed earlier by the same group[45].

The Viscek model is one way of simulating systems of multiple particles which involves a two-step motion[46, 47]. In the first *streaming step*, particle velocities are updated. The next *collision step* updates the orientations of the particles by taking a local space average of the particle direction and then updating individual particle direction with a stochastic deviation from this clus-

ter average. This method has been widely used for investigation of polar active matter as well as swarms and clusters of active particles[48, 49, 50, 51].

#### 2.3.1.1 Continuum Models

At low Reynolds numbers, the activity of particles can be modelled by effect which the particle motion has on the surrounding fluid (the continuum)[52]. As particles move through the fluid they exert a shear stress which causes for a motion which is well defined by classical fluid dynamics. ABPs of such a nature may also be referred to as micro-swimmers (or micro-motors in the case of manufactured particles) and will operate on a length scale of around 100nm - 100 $\mu$ m.

Yan et al. consider the average motion of an ensemble of active particles in a system contributing to an overall *swim pressure*[53]. They found that the overall pressure, in addition to the weight, on a system of this ensemble is the sum of individual particle pressures. For randomly oriented particles this results in a net-zero additional force. Particle-particle interactions causes for accumulation at boundaries of the system under additional external gradients (such as gravity or a potential field), leading to non-zero pressures[54]. In this viscous regime at low Reynolds numbers, the dynamics of motion are governed by these hydrodynamic forces exerted on the surrounding fluid from the particles and on each other. Takatori modelled the shear stress exerted on fluids by active particles, observing resultant both thickening and shear thinning regimes

as a result of the particle active force[55].

Alongside the stochastic motion exhibited by regular BPs, ABPs exert an additional force as a result of a separate mechanism. This additional force may be deterministic such as a uniform potential gradient; it may be somehow intelligently controlled by an organism such as the movement of a flagella or tail; or it may be in itself stochastic such as the force exerted by the spontaneous chemical reaction on the particle surface. To achieve net motion, the mechanism generating the active component must be irreversible[26, 56]. This means that moving backwards along the same trajectory leaves the particle in a different state to the original starting point. Examples of this asymmetrical hydrodynamic motion are the paths of flagella on microbial swimmers as discussed earlier — the drag for swimming is lower during the *backstroke* which breaks the symmetry of the motion; or the three-sphere Purcell swimmer where the configurations of the spheres and rods are asymmetrical[57, 58].

Continuum modelling offers a mechanism for simulating systems more efficiently by simplifying  $N$  particles into a single continuum approximation[59].

### **2.3.2 Group Motion of Active Brownian Particles**

One area of interest in the field of ABPs is collective active motion — individual interacting particles show emergent characteristics in larger groups as a result of the active component of motion[59]. The hydrodynamic effects of motion on the surrounding fluids of some of the earlier discussed particles may also affect nearby particles.

There is thus much ongoing research into the movement of clusters or groups of active particles, and the manifestation of swarm behaviour which may be seen[60, 61, 62].

Active nematic particles are active particles which align in the same direction under their active force[52]. The collective hydrodynamic effect of individual particles moving cause for these particles to swarm and move together as an individual body with a centre of mass and its own flow field. Another type of group behaviour which is observed with active particles is Motility-Induced Phase Separation (MIPS)[63, 64, 61]. This is a phenomenon where particles begin to behave like multi-phase evaporating systems. Singular *gaseous* ABPs move independent between larger *liquid* clusters which exhibit cluster motion.

Research into the grouped motion of these swimmers focuses mostly on complex matter such as cells at low Reynolds number. Such conditions emulate crowded systems which may be found in blood or inside living cells and so are useful in the understanding of medical applications of ABPs. On a more macroscopic scale, these clusters of active particles can be analogous to swarming mammals such as fish or birds[65, 43]. The rotational-Brownian component of the motion allows for a random reorientation of agents within these swarms.

## 2.4 Energy Depot Model

A model of active motion suggested by Ebeling, Schweitzer and Tilch [39] proposes that BPs contain an internal energy depot which is capable of storing energy which is gained from the surroundings. This energy can then be converted into useful work or dissipated to the surroundings. This Energy Depot (ED) model is the focus of much of the simulations and work carried out as part of this thesis.

The original work has been cited frequently since its original publication, with other works expanding or refining on the model. Its relative simplicity makes it easy to implement whilst it provides a strong analogue for systems of Brownian agents which can exhibit active motion. Much of the work was carried out by the research groups of the original authors, though some separate groups have utilised the model and enriched the literature by providing their own studies. In this section we review this existing research and literature and present our motivations and work within the context of this.

### 2.4.1 Parameters

Table 2.1 summarises the parameters used in the model, along with their descriptions as described in the literature [39, 40]. This table serves as a point of reference moving forward as the model is explained in more detail.

### 2.4.2 Theoretical Summary

This model at a basic level provides an elementary description of an active system by which a general approximation of the conversion of chemical energy into particle motion for both complex and less complex matter may be made. In the case of a biological swimmer this would be the metabolising of food.

Mathematically, the model introduces a balance on the depot energy of the particle,  $e$ :

$$\frac{de(\mathbf{v}, \mathbf{r}, t)}{dt} = q(\mathbf{r}, \mathbf{v}, t) - c e(\mathbf{v}, t) - d(\mathbf{v}, \mathbf{r}, t) \mathbf{v}^2(t) e(\mathbf{v}, t) \quad (2.4.1)$$

The first term  $q$  signifies the rate of energy accumulation in the depot which may depend on the particle position, velocity, or an external control defined by the time. The depot dissipates energy at a rate  $c$  proportional to the depot level. The final term signifies the conversion of depot energy into particle kinetic energy. The conversion of depot energy  $e$  into kinetic energy can be given by the ansatz:

$$d(\mathbf{v}) = d_0 \mathbf{v}^2 \quad (2.4.2)$$

In this generalised case  $d_0$  is a constant throughout  $v$  and  $r$ . Other more complex variants of this conversion rate have been studied, which will be discussed in the following paragraphs.

The total energy of the particle  $E(t)$  is given by the sum of the particle mechanical energy  $E_0(t)$  and depot energy  $e(t)$ . Thus the

mechanical energy of the particle as shown by Schweitzer[39] is:

$$\begin{aligned} E(t) &= E_0(t) + e(t) \\ E_0(t) &= \frac{1}{2}m\mathbf{v}^2(t) + U(\mathbf{r}) \end{aligned} \quad (2.4.3)$$

Given that  $E_0(t)$  is simply a balance between energy gained from depot conversion and dissipated due to friction, over an infinitesimally small timestep  $dt$ , the differential energy balance on  $E_0(t)$  is thus (implementing the ansatz eq. (2.4.2)):

$$\frac{d}{dt}E_0(t) = d_0\mathbf{v}^2e(t) - \gamma_0\mathbf{v}^2 \quad (2.4.4)$$

Where the energy dissipates from friction proportional to  $\mathbf{v}^2$ . With eq. (2.4.1) defined, solving the differential equation (2.4.4) using the definition for  $E_0(t)$  from eq. (2.4.3) the corresponding system of LEs for particles with EDs is given[39]:

$$\frac{d\mathbf{r}}{dt} = \mathbf{v} \quad (2.4.5a)$$

$$\frac{d\mathbf{v}}{dt} = -\gamma_0\mathbf{v} - \nabla U(\mathbf{r}) + e(\mathbf{v}, t)d_0\mathbf{v} + \sqrt{2D}\boldsymbol{\xi}(t) \quad (2.4.5b)$$

$$\frac{de}{dt} = q(\mathbf{r}, \mathbf{v}, t) - (c + d_0\mathbf{v}^2)e(\mathbf{v}, t) \quad (2.4.5c)$$

Where  $\nabla U(\mathbf{r})$  is the potential gradient, and  $\boldsymbol{\xi}(t)$  the  $\mathbf{n}$ -dimensional delta-correlated white noise such that for the identity matrix  $\mathbf{I}$ :

$$\langle \boldsymbol{\xi}(t) \rangle = 0 \quad \langle \boldsymbol{\xi}(t)\boldsymbol{\xi}(t') \rangle = \mathbf{I}\delta(t - t') \quad (2.4.6)$$

The noise  $\mathbf{x}\mathbf{i}(t)$  originates from the thermal fluctuations in the fluid — surrounding particles colliding with the active particle transfer momentum to and from the particle in an uncorrelated manner. The velocity of these particles is governed by their temperature — hotter

fluids exhibit more stochastic (noisy) behaviour, whilst cooler fluids exhibit the opposite, as is discussed further in Chapter 3.

### 2.4.3 Adiabatic Assumption Of Motion

As has been mentioned previously, often the assumption is made that particles with energy depots are adiabatic in energy. This means that the rate at which the depot level updates is much faster than that of the particle velocity, i.e.  $\dot{e} \approx 0$ . This results in an energy determined purely by the velocity of the particle:

$$e_0 = \frac{q_0}{c + d_0 \mathbf{v}^2} \quad (2.4.7)$$

The resultant LE for this approximation yields an active friction  $\gamma(\mathbf{v})$ :

$$\gamma(\mathbf{v}) = \gamma_0 - \frac{d_0 q_0}{c + d_0 \mathbf{v}^2} \quad (2.4.8)$$

The friction is thus equivalent to the static friction  $\gamma_0$  in the high velocity limit, and negative in the limit of low velocities. This negative friction allows for active motion or pumping of velocities as discussed previously[45]. It can thus be seen that the adiabatic approximation allows for a much simpler description of the different pumping behaviours of the particles based purely upon velocity, though as a result the model fails to describe possible fluctuations in the energy depot level at lower velocities and the resulting system dynamics.

In the initial work by Schweitzer, Ebeling and Tilch [39] the assumption of a *quasi-stationary* energy  $e_0$  was presented as a general model behaviour. In a separate work, Ebeling et al.[66] in-

roduced an adiabatic parameter  $\mu$  on the LHS of the  $\dot{e}$  equation in the LE 2.4.5c, where a value of between 0 and 1 could tune how adiabatic the particles were. They found that at limit cycles the energy within the depot did not change for deterministic particles at the given parameter ranges and presented all other results assuming  $\mu = 0$ .

Erdmann et al. [67] further modelled adiabatic particles with EDs in parabolic potential gradients where they found that particles formed left and right handed limit cycles, where the direction of the particle was dependent on the initial conditions. The justification given for using the energy depot in this case was that the relaxation of  $e$  was fast such that the value could be assumed as quasi-stationary - though no specific mention was made of the parameter regimes or timescales which would be responsible for this behaviour.

Erdmann et al. again [68] modelled these particles explicitly in the adiabatic regime. They assumed that the active friction was analogous to a Rayleigh friction [9] close to the stationary velocity  $v_0$  and modelled group motion of clusters of these particles in linear potentials. They noted that in the low translational noise limit these particle swarms moved in clusters rotating around a centre. The authors simply made the assumption that within the Rayleigh parameter regime which they chose, these particles would be adiabatic.

A description of the the thermodynamics of active systems has

been described [69]. They presented a steady state probability distribution of the entropy of ED particles in the adiabatic regime, where the distribution of entrees depends on the additional active parameters.

The quantifiable region of values of  $q_0$ ,  $c$  and  $d_0$  where the adiabatic assumption holds is not clear from our research in the literature — though it is valid when the energy updates much faster than the velocity [39, 70] (exact parameter regimes which create these timescale differences are not explained anywhere, to our knowledge). These three parameter values are all of importance, as is the instantaneous value of the velocity  $\mathbf{v}$  whose length and timescales are set by the diffusion constant  $D$ [39, 70, 9, 68, 71].

Despite presenting the model for all ranges of  $\mathbf{v}$  and not outlining any limitations on the constant values of  $q$  and  $c$  used, Zhang et. al[70] presented their results in the adiabatic regime.

At lower velocities these adiabatic particles can be seen to follow a Rayleigh-Helmholtz model [69]:

$$\gamma(v) = \gamma_1 + \gamma_2 v^2 \tag{2.4.9}$$

With parameters  $\gamma_1 = \frac{d_0 q_0}{c}$  and  $\gamma_2 = \frac{d_0^2 q_0}{c^2}$ . It can be seen that for small  $c$  the numerator of the second friction term is much diminished.

The cases where energy conversion occurs adiabatically may be commonplace in real systems, and so it is frequently seen throughout the literature that the assumption is at once presented and implemented. There is little attention given to the possible edge

cases of when this assumption may not hold, or even in some cases as to whether the differential equation for depot level was solved independently of the velocity at all as a trial.

#### 2.4.4 Other Models

Zhang et al. presented a *fourth-order* model for adiabatic energy depots, where the adjusted energy uptake rate  $d(v)$  is a function of  $\mathbf{v}^4$ :

$$d(\mathbf{v}) = a_{0,2}\mathbf{v}^2 + a_{0,4}\mathbf{v}^4 \quad (2.4.10)$$

Where  $a_{0,2}$  and  $a_{0,4}$  are the second- and fourth-order coefficients for energy conversion. They introduce a breaking mechanism such that the velocity tends to zero at a critical braking velocity  $v_c = \sqrt{a_{0,2}/|a_{0,4}|}$  as below[70]:

$$d(\mathbf{v}) = a_{0,4}\mathbf{v}^2 \left( 1 - \frac{\mathbf{v}^2}{v_c^2} \right) \quad (2.4.11)$$

This introduces a third behaviour outside the existing pumping and reduced-friction regimes, where for velocities  $v > v_c$  the particle has a friction  $\gamma(v) > \gamma_0$  and is dragged no-matter the value of  $e$  in the depot. They found that for deterministic and adiabatic particles in 1-D  $v - e$  phase-space, the particles would enter different limit cycles dependant on the activity constant  $a_{0,4}$  which could cause a constant forward momentum even in the absence of the potential field  $\nabla U$ .

Upon application of an external force-field particles were found to be driven even under the influence of the strong friction above the critical velocity and negative forces allowed for the particle to

switch directions. These particles underwent interesting trajectories around stationary fixed points and saddle points, even in the absence of stochastic forces. We draw attention to the fact that an external force was applied in order to switch the direction of these particles, though due to the constant direction of this field there was no presence of back-and-forth switching behaviour or mention of the periodicity of the limit cycles.

An alternative second order conversion rate has also been studied [72, 73]:

$$d(v) = a_1 |v| + a_2 v^2 \quad (2.4.12)$$

In this case the polynomial function  $d(v)$  varies with both the linear and quadratic degrees of  $v$ , representing an asymmetric conversion rate. This goes beyond the original ansatz (eq.(2.4.2)) made by Schweitzer [39] and allowed them to introduce a drift velocity term, thus treating the particles as overdamped. They applied this to a system of kinesin proteins consuming ATP, tweaking the external gradient and observing the bias between forward and reverse motion in weak Brownian regimes. These particles were non-adiabatic in one-dimension with the fuel uptake  $q(t)$  modelled as a pulse to simulate ATP on-loading from the kinesin molecules. The distribution of forward and backward discrete steps for the motors is presented by the authors. The *dwell time* defined by the amount of time spent at each discrete step before consumption of ATP causes for either a forwards or backwards motion offers a different view due to the time-dependent accumulation of ATP in the depot ( $q(t)$ ) varying as

a step function).

Zabicki used energy depots to model kinesin molecules converting ATP — performing a walk along a protein and exhibiting a forward-biased motion [16]. Lee et al. [74] again simulated kinesin with energy depots but used a time-dependent depot uptake rate  $q(t)$  which was constant for periods with a tunable frequency. Both groups were able to model the forward motion of the molecules, as well as the backwards motion if the activity increased beyond the *stall force*.

Other adaptations on the dynamics of depot energy uptake have been suggested and studied[75]:

$$\frac{de}{dt} = q\sqrt{e} - ce - d\mathbf{v}^2\sqrt{e}$$

The ED model is ideal for agent-based methodologies of simulation as these different dynamics of energy uptake can be easily implemented.

#### 2.4.5 External Fields

Other works observe one dimensional deterministic ED particles pushing against the gradient (an uphill motion)[76]. They varied the energy conversion rate  $d_0$  only in the presence of a linear sawtooth like potential in  $r$  space. Two critical conversion rates  $d_0 = d_{c,i}$  ( $0 < d_{c,1} < d_{c,2}$ ) were found. The first,  $d_{c,1}$ , above which particles moving backwards could overcome the shallower reverse-slope of the tooth, and a second,  $d_{c,2}$ , above which the particle could move in the forward direction over the steep forward face of the tooth. For

values  $d_0 < d_{c,1}$  below these two values, the particles would oscillate in  $v$  near to zero such that they would never *escape* from the region of space between the initial two teeth. The authors comment that the stochastic forces have no great effect on the dynamics in these 1-D systems with potential gradients, and so focused on varying the strength of  $d_0$ . Particle direction was entirely dependent on the initial conditions — deterministic motion of particles through  $v, e$  phase-space is entirely dependent on the values of  $(v_0, e_0)$ . The active pumping force was confined to a single value at any  $v$ .

#### 2.4.6 Multiple Particle Systems

Erdmann et al. studied multi-particle systems of particles with adiabatic EDs in 2-D[68]. They modelled single particles and again found the donut-shaped limit cycles as in the previous studies. For multiple particle systems, particle-particle interactions caused for the emergence of rotational swarm behaviours, which would randomly change rotational direction. Of interest in this study is the author's suggestion that the switching of direction is a chaotic process — the clusters unpredictably change direction as result of the collective random motion. Adiabatic ED particles were been used to model opinion formation in social situations for multi-agent systems, where flocking and clustering of agents with the same opinion was observed in certain system conditions, along with transitional behaviours between these behavioural clusters[77]. Abstract applications such as this show how relatively simple systems can be used as powerful analogues for real world physical, and in this case social,

problems.

Miranda et al. recently modelled adiabatic ED particles in 2-D as repulsive discs in a crowded environment[71]. They observed flocking behaviours similar to those discussed earlier in Viscek’s original work[46]. Whilst phenomena such as MIPS[61] were not observed, the emergence of density bands was observed. The adiabatic assumption was again made here, citing the rate of energy consumption being faster than the rate of acceleration, though the authors make no mention of the parameter regimes which are responsible for such behaviour.

#### 2.4.7 Conclusion

Particles with energy depots are well understood in both one and multiple dimensional systems in the literature. Particles in potential fields, multiple particle systems, and time and position dependence for energy uptake have all been investigated. Additional models for energy conversion  $d(v)$  have also been covered. These studies frequently assume an adiabatic uptake of energy to the depot. It is not clear from the literature under what scenarios this assumption holds, or if there is a formalisation of this. As such, many of these studies could potentially show additional interesting information when the energy in the depot was non-deterministic with  $v$ .

The adiabatic assumption reduces the computational cost of any simulations of these particles by reducing the degrees of freedom of the system greatly, and allows for the authors to investigate more

complicated dynamics in potential gradient systems.

In many cases of low relative diffusivity (i.e. larger particles) the Brownian velocity component is smaller and therefore a large energy uptake should indeed lead to adiabatic behaviour. For smaller particles it can be observed from the equations that a fluctuating velocity could have a larger effect on the value of  $e$ . In such a diffusion dominated regime, the active component of the particle motion will be heavily correlated to stochastic fluctuations in the particle velocity and therefore any assumption of instantaneous correction in the value of  $e$  may be less exact.

This offers an opportunity to explore the transitional behaviours in the regions where this assumption is not valid. At lower particle diameter (higher diffusion) and lower energy uptake and dissipation, it appears that there should be regions where  $e$  will be non-adiabatic. Throughout this thesis the behaviour of these particles in a non-explicitly-adiabatic regime is investigated.

In our work we look at 1-dimensional particles with energy depots using the classic description of the depot energy equation[39], though we rely on the random force and a system which is not explicitly adiabatic in energy consumption to study the transition between regions of the  $v - e$  space. We also aim to show how particles in non-adiabatic 1-D regimes switch direction due to the low- $v$  ED dynamics and study the emergence of non-adiabatic behaviours in these low velocity regimes.

We have reviewed studies which observed oscillatory limit cycle

behaviours in 2- and 3-dimensions for adiabatic particles. We will look to further understanding of these cycles by providing constant energy uptake throughout space in one-dimension for non-adiabatic particles with higher stochastic forces. We aim to observe under what regimes particles break out of 1-D cycles, and what the dynamics of the systems are in these transitional regions. It is of interest to understand how the activity affects this behaviour in the stochastic regime.

**Table 2.1:** Summary table of parameters for ED model and corresponding simulations.

| Parameter    | Name                         | Description  | Units                        | Dimensionless Group                        |
|--------------|------------------------------|--|------------------------------|--|
| $\mathbf{r}$ | Particle position            | Position of the particle at any time $t$ in $n$ dimensions.  | $[\mathcal{L}]$              | $\frac{\mathbf{r}\gamma_0^{3/2}}{D^{1/2}}$ |
| $\mathbf{v}$ | Particle velocity            | Velocity of the particle at any time $t$ in $n$ dimensions.  | $[\mathcal{L}][\tau]^{-1}$   | $\frac{\mathbf{v}\gamma_0^{1/2}}{D^{1/2}}$ |
| $e$          | Particle depot energy        | Amount of energy stored in the particle depot at time $t$ .  | $[\mathcal{L}]^2[\tau]^{-2}$ | $\frac{e\gamma_0}{D}$                      |
| $D$          | Particle diffusion constant  | Strength of the diffusive force $\xi(t)$ .   | $[\mathcal{L}]^2[\tau]^{-3}$ | 1  |
| $c$          | Depot dissipation rate       | Rate of internal dissipation of energy from depot, could be analogous to metabolism or simply internal energy losses.    | $[\tau]^{-1}$                | $\frac{c}{\gamma_0}$                       |
| $q_0$        | Depot energy uptake rate     | Uptake of energy from surroundings into the depot. Can be constant or a function of $\mathbf{v}$ , $\mathbf{r}$ or $t$ . | $[\mathcal{L}]^2[\tau]^{-3}$ | $\frac{q_0}{D}$                            |
| $d_0$        | Depot energy conversion rate | Constant controlling the rate of conversion of $e$ into $E_k$ of the particle.   | $[\tau][\mathcal{L}]^{-2}$   | $\frac{d_0 D}{\gamma_0^2}$                 |
| $\gamma_0$   | Static friction              | Drag on the particle from energy losses to surroundings through friction.  | $[\tau]^{-1}$                | 1  |
| $\Delta t$   | Simulation time step         | Time step between simulation steps   | $[\tau]$                     | $\Delta t \cdot \gamma_0$                  |

## 2.5 Conclusion

The field of ABM and ABPs are widely researched to this day, with many groups focusing on particles on the microscopic scale. Research is often motivated by medical or manufacturing use cases.

Experimentalists study manufactured ABPs such as Janus particles, nano-rods, or scrolls which exhibit active motion either due to chemical gradients in the solutions or other phoretic effects from external fields (such as light). They also look into ABM in the natural world of microbial swimmers or active motion on the cellular level.

Theoreticians model these real world phenomena using either agent-based (modelling each particle as an individual *agent* within the system) or continuum (modelling the effects of groups of individual particles on the system as a whole) methodologies.

We specifically focus on the Energy Depot (ED) model introduced by Schweitzer, Ebeling and Tilch[39]. In the 1-D case of this model, depot energy is constrained to consumption from a single dimension in  $v$ . When limit cycles were observed in higher dimensions in the literature, acceleration in all directions would consume depot energy  $e$ . In the special 1-D case (analogous to a higher dimensional case with discrete depots for each direction), the velocity in each cardinal direction is de-correlated from the others.

Given the preceding analysis of the existing literature, we thus aim to address the below questions for particles with EDs within this thesis:

1. By varying the energy uptake  $q_0$  and rate of consumption  $d_0$  for 1-D systems with low depot dissipation, how do the dynamics of the system in  $v - e$  space correspond with the adiabatic assumption and is there a clear onset of adiabatic behaviour in this parameter space?
2. How do the average behaviours of these 1-D particles vary throughout these different parameter regimes?
3. For individual non-adiabatic particle trajectories in 1-D what are the dynamics of the transitional behaviour between the limits, and what is the effect of the stochastic force in switching particles between these limits?
4. What are the characteristic timescale behaviours for particles outside of these limits, and is there a clear emergence of any patterns which are only exposed in the 1-D regime or any way in which to quantify the onset of these behaviours?

Our motivation is to add to the understanding of this particular assumption within the literature by modelling individual ED particles in 1-D using an agent-based approach. We also aim to apply additional methodologies of analysis of these particles within our computational simulations which have thus-far been discussed within the literature. This could help us also to understand the dynamics of particles escaping fixed trajectories in the real world.

## Chapter 3

# Theory and Methodologies

This chapter aims to outline the theoretical background of Brownian particles (BPs) and active Brownian particles (ABPs), as well as the supporting theory for the which were used in the completion of this thesis.

Brownian motion is introduced, explained and discussed before a more detailed analysis of the mathematics behind BPs is carried out. The mathematical concepts on which this theory is constructed are introduced and explained. These equations and theories are then put into the context of ABPs, followed by a more detailed discussion of the relevant equations of motion and theories for the Energy Depot model within the context of this thesis. Finally, we explore the methodologies for simulation and analysis of these active particles which were used in completion of this work.

### 3.1 Brownian Motion

Brownian motion refers to the random movement of particles on the micro to nano scale caused by collisions with surrounding matter. Particles within systems which exhibit this type of motion can be

referred to as Brownian particles. The chaotic nature of the high number of collisions over short timescales and the correlations between these events makes prediction of the ballistic motion of these particles impossible. Thus the kinetics of BPs are modelled using statistical mechanics which take into account average behaviours across ensembles or the random expected behaviour of the system on an individual particle.

This section introduces the theory for these particles and the mathematical methods of calculating average behaviour. The governing equations of motion for these particles are then introduced and discussed, followed by the background theory of the different types of motion. Finally, equations governing probability distributions for Brownian particles are introduced.

### **3.1.1 Langevin Equations & the Ornstein-Uhlenbeck Process**

Due to the additional stochastic forces exerted on particles at small length scales, classical Newtonian dynamics do not give a feasible representation of the motion of these particles. As such, an additional stochastic force element is required in order to model this random element.

The equations of motion for particles with random forces, or Langevin Equations (LEs), are used to represent these systems by considering both the classical Newtonian ballistic forces alongside the stochastic force. The ballistic forces are deterministic. As mentioned earlier, it is not possible to calculate the exact deterministic values of the random force, and so instead these are represented by

stochastic terms which represent the expected statistical behaviour of the system.

In underdamped regimes (i.e. where the timescale of the velocity relaxing and the timescale of the stochastic force are on similar order of magnitudes), the Ornstein-Uhlenbeck (OU) process models a Brownian particle with friction and is described by the LEs[78, 79, 40]:

$$\frac{d\mathbf{r}}{dt} = \mathbf{v} \quad (3.1.1a)$$

$$\frac{d\mathbf{v}}{dt} = -\gamma_0\mathbf{v} - \nabla U(\mathbf{r}) + \sqrt{2D}\boldsymbol{\xi}(t) \quad (3.1.1b)$$

Where  $U(\mathbf{r})$  represents a potential gradient and  $D$  is the diffusion constant, which is related to the temperature of the system through[79, 40]:

$$D = \frac{(k_B T)^2}{6\pi\eta R_H} \quad (3.1.2)$$

From Stokes' law[80]:

$$\gamma_0 = 6\pi\eta R_H \quad (3.1.3)$$

$T$  is the system temperature and  $k_B$  is the Boltzmann constant.  $\eta$  is the dynamic viscosity of the fluid which governs the friction exerted on the particle by the fluid[80].

Recalling the definition from eq. (2.4.6) that  $\boldsymbol{\xi}(t)$  in eq. (3.1.1b) is an  $\mathbf{n}$ -dimensional delta-correlated Gaussian white noise such that:

$$\langle \boldsymbol{\xi}(t) \rangle = 0 \quad \langle \boldsymbol{\xi}(t)\boldsymbol{\xi}(t') \rangle = \mathbf{I}\delta(t - t') \quad (3.1.4)$$

$\mathbf{I}$  is the identity matrix.

The first term on the RHS of eq. (3.1.1b) represents the frictional drag forces experienced by a particle in a viscous fluid. The final

term represents the stochastic Brownian force; which is the net effect of all collisions of surrounding matter with the particle such that across the entire system the net effect is zero, as per eq. (3.1.4).

This description is rigorous so long as the fluctuation dissipation theorem holds — the overall system is at a thermodynamic equilibrium as energy lost by the particle to the fluid is on average the same as that absorbed from Brownian collisions[3, 78, 79, 80, 81].

### 3.1.2 Underdamped & Overdamped Motion

#### 3.1.2.1 Overdamped Motion

When the timescale of particle motion  $\tau$  is high compared with the frictional forces, i.e.  $\tau \gg \gamma_0^{-1}$ , then the particle is said to be in the overdamped limit. In this limit, the particle velocity is adiabatic as  $\mathbf{v}$  changes on a much shorter characteristic timescale than  $\mathbf{r}$ . Changes in particle velocity as a result of the Brownian force are quickly corrected by the loss of energy to the fluid, and the particle behaves in a purely Markovian manner[40, 80]. As such, an overdamped Brownian particle is said to be *memory-less*. This means that the velocity and position of the particle are independent on its history, and are purely a result of the Brownian force[78, 40, 80]. Eqs. (3.1.1) become (in the absence of any potential gradient):

$$\frac{d\mathbf{r}(t)}{dt} = \mathbf{v}(t) = \sqrt{2S}\boldsymbol{\xi}(t) \quad (3.1.5)$$

$S$  is the positional diffusion constant which governs the strength of the stochastic motion.

When a potential gradient  $\nabla U(\mathbf{r})$  is considered, eqs. (3.1.1) sim-

plify instead to:

$$\frac{d\mathbf{r}}{dt} = \frac{-1}{\gamma_0} \nabla U(\mathbf{r}) + \sqrt{2S} \boldsymbol{\xi}(t) \quad (3.1.6)$$

### 3.1.2.2 Underdamped Motion

The alternative case, where the value of  $\gamma_0$  is low such that particle behaves in a non-Markovian manner is known as the underdamped limit. In this case, the LEs (3.1.1) provide a description of the system dynamics.

### 3.1.3 Fokker-Planck Equation

The solution to probability density function (PDF) for the LEs of a random process is the Fokker-Planck Equation (FPE), which gives a probability distribution in  $n$ -dimensional phase space[78].

#### 3.1.3.1 Ornstein-Uhlenbeck Process

The FPE for the OU process described in eqs.(3.1.1) is[79]:

$$\frac{\partial P(\mathbf{v}, \mathbf{r}, t)}{\partial t} = - \frac{\partial (\mathbf{v}P(\mathbf{v}, \mathbf{r}, t))}{\partial \mathbf{r}} + \gamma_0 \frac{\partial (\mathbf{v}P(\mathbf{v}, \mathbf{r}, t))}{\partial \mathbf{v}} + D \frac{\partial^2 P(\mathbf{v}, \mathbf{r}, t)}{\partial \mathbf{v}^2} \quad (3.1.7)$$

This describes the evolution of the PDF through time —  $P(t)$ . The first term on the RHS corresponds to the drift of the probability through  $\mathbf{r}$ -space, with the second term corresponding to the same concept but in  $v$ . The final term on the RHS is the diffusion of probability as a result of the stochastic force — with the diffusion coefficient  $D$  corresponding to the strength of this diffusion.

This derivation of this equation is shown in Section 7.3.

### 3.1.3.2 Overdamped Process

In the overdamped limit, a FPE in the phase space of  $\mathbf{r}$  can also be formed from eq. (3.1.5):

$$\frac{\partial P(\mathbf{r}, t)}{\partial t} = S \frac{\partial^2 P(\mathbf{r}, t)}{\partial \mathbf{r}^2} \quad (3.1.8)$$

This is the classic diffusion equation[80].

### 3.1.3.3 Time Dependent Solution

The position-independent solution  $P(\mathbf{v}, t)$  to eq. (3.1.7) is an  $n$ -dimensional Gaussian for the velocity distribution of a particle:

$$P(\mathbf{v}, t) = \left( \frac{2\pi}{\sigma^2(t)} \right)^{1/2} \exp \left[ \frac{-(\mathbf{v} + \mu(\mathbf{v}_0, t))^2}{2\sigma^2(t)} \right] \quad (3.1.9)$$

With variance  $\sigma^2(t)$  and mean  $\mu(\mathbf{v}_0, t)$  defined as:

$$\sigma^2(t) = \frac{D}{\gamma_0} (1 - e^{-2\gamma_0 t}) \quad (3.1.10a)$$

$$\mu(\mathbf{v}_0, t) = \mathbf{v}_0 e^{-\gamma_0 t} \quad (3.1.10b)$$

This is derived using a Fourier transform methodology in Appendix 7.4.

## 3.1.4 Deterministic Limits of Particles in 1D

### 3.1.4.1 Stationary Solution

The stationary velocity distribution of an OU particle in the absence of any potential gradient is given by the solution to the FPE at equilibrium i.e.  $\frac{\partial P(\mathbf{v}, t)}{\partial t} \rightarrow 0$ :

$$P_{SS}(\mathbf{v}) = \mathcal{N} \exp \left( -\frac{\gamma_0}{2D} \mathbf{v}^2 \right) \quad (3.1.11)$$

Where  $\mathcal{N}$  is the relevant normalisation function based upon the boundary conditions of the system. The methodology for numer-

ically approximating this normalisation function is discussed for other particles in Section 3.4.

In the time limit where  $t \gg \gamma_0^{-1}$ , eqs. (3.1.9) and (3.1.11) are equivalent.

### 3.1.5 Survival Probability and First Passage Time in 1-D

Given an OU particle with initial velocity  $v(t = 0) = v_{t_0}$  in one dimension, the direction of travel of the particle is  $d = \frac{v_{t_0}}{|v|}$  and may be either positive or negative.

eq. (3.1.9) represents the Green's function for the particle based upon the initial velocity  $v_{t_0}$  at  $t_0 = 0$ .

It is possible to calculate the probability that after some time  $\tau$  the particle is still travelling in the direction  $d$  by calculating the survival time probability of the PDF of the particle with boundary conditions at  $v = 0$ . The survival time probability may be defined as the probability that a particle is still travelling in the same direction at time  $\tau = t - t_0$  as it was travelling at time  $t_0$ , without ever having changed direction up until that point. This can be represented mathematically by an absorbing boundary conditions at  $v = 0$  and  $v = \infty$ . Applying this boundary condition to eq. (3.1.9), the Green's function thus becomes:

$$G(v, \tau | v_{t_0}) = P(v, \tau | v_{t_0}) - P(v, \tau | -v_{t_0}) \quad (3.1.12)$$

Thus the probability function for a particle being at velocity  $v$  in direction  $d$  at time  $\tau$  is the difference between the probability functions for a particle moving in the same direction and the probability that

the particle started in the other direction and has already switched direction at time  $\tau$ .

Taking the convention that  $d(t_0)$  is positive (i.e.  $v_{t_0} > 0$ ), then the survival probability  $S(\tau)$  is found by integrating the Green's function over all positive velocities:

$$S(\tau, v_{t_0}) = \int_0^{\infty} dv G(v, \tau | v_{t_0}) \quad (3.1.13)$$

The survival probability is the proportion of all particles which have yet to change direction. The probability of a particle crossing the boundary between some time  $\tau$  and  $\tau + d\tau$  is given by the first passage time probability  $h_0(\tau)$ :

$$h_0(\tau, v_{t_0}) = -\frac{dS(\tau)}{d\tau} = -\frac{d}{d\tau} \left[ \int_0^{\infty} dv G(v, \tau | v_{t_0}) \right] \quad (3.1.14)$$

In order to generalise the first passage time for all possible  $v_{t_0} > 0$  eq. (3.1.14) becomes:

$$\begin{aligned} h(\tau) &= \int_0^{\infty} dv_{t_0} P(v_{t_0}, t_0) h_0(\tau, v_{t_0}) \\ &= -\frac{d}{d\tau} \left[ \int_0^{\infty} dv_{t_0} P(v_{t_0}, t_0) \int_0^{\infty} dv G(v, \tau | v_{t_0}) \right] \end{aligned} \quad (3.1.15)$$

### 3.1.5.1 Survival Time Distribution for an OU Particle

Combining the generalised form of Green's function eq. (3.1.12) with an absorbing boundary at  $v = 0$  for an OU particle using eq. (3.1.9);

the survival time distribution  $S(\tau)$  may be written as:

$$S(\tau) = \frac{1}{2} \left( \operatorname{erf} \left( \left( \frac{\gamma_0}{2D(1 - e^{-2\gamma_0\tau})} \right)^{1/2} v_{t_0} e^{-\gamma_0\tau} \right) - \operatorname{erf} \left( - \left( \frac{\gamma_0}{2D(1 - e^{-2\gamma_0\tau})} \right)^{1/2} v_{t_0} e^{-\gamma_0\tau} \right) \right) \quad (3.1.16)$$

Some example solutions to eq. (3.1.16) are shown in fig. 3.1.

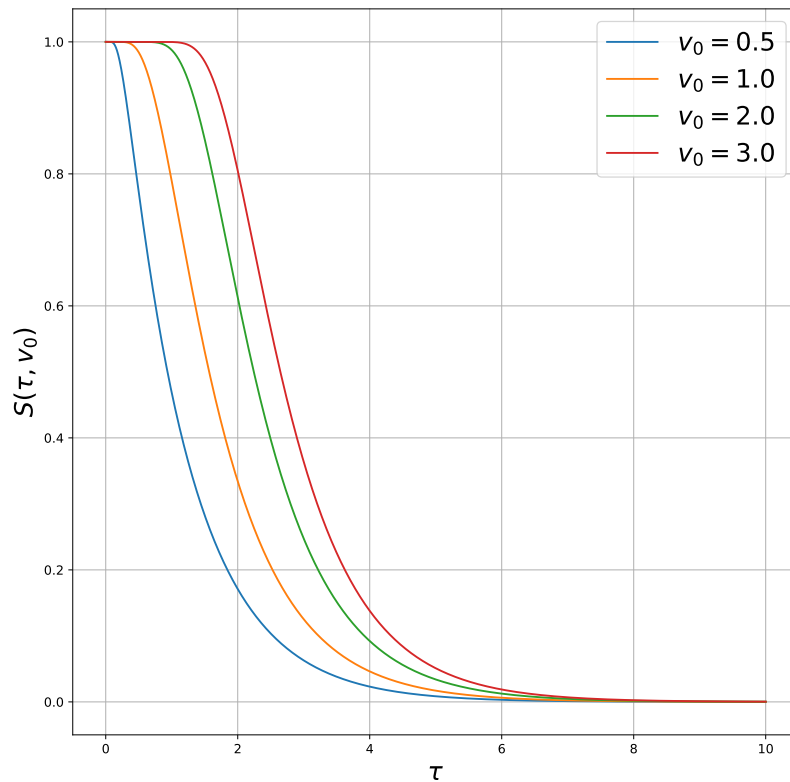


**Figure 3.1:** Solution to particle survival distribution from eq. (3.1.16) for an absorbing boundary at  $v_c = 0$  for different positive starting velocities  $v_{t_0}$ . Particles starting at higher velocities are less likely to reverse direction quickly than those starting slower.  $\gamma_0 = 1.0$ ,  $D = 0.1$ .

### 3.1.5.2 First Passage Time Probability for an OU Particle

The first passage time probability as a function of a single value of  $v_{t_0}$  for an OU particle in the underdamped regime is given by the

solution to eq. (3.1.14) for eq. (3.1.16):

$$h_0(\tau|v_{t_0}) = \left(\frac{2v_{t_0}^2\gamma_0^3}{\pi D}\right)^{1/2} \left(\frac{e^{-\gamma_0\tau}}{(1 - e^{-2\gamma_0\tau})^{1/2}} + \frac{e^{-3\gamma_0\tau}}{(1 - e^{-2\gamma_0\tau})^{3/2}}\right) \exp\left(-\frac{\gamma_0v_{t_0}^2}{2D} \frac{e^{-2\gamma_0\tau}}{(1 - e^{-2\gamma_0\tau})}\right) \quad (3.1.17)$$

Dependent on the form of the initial PDF  $P(v_{t_0})$ , this equation may be integrated as per eq. (3.1.15) for an exact solution in terms of  $\tau$  only. Example solutions to eq. (3.1.17) for varying  $v_{t_0}$  values are shown in fig. 3.2. The full derivation is outlined in Appendix 7.6.

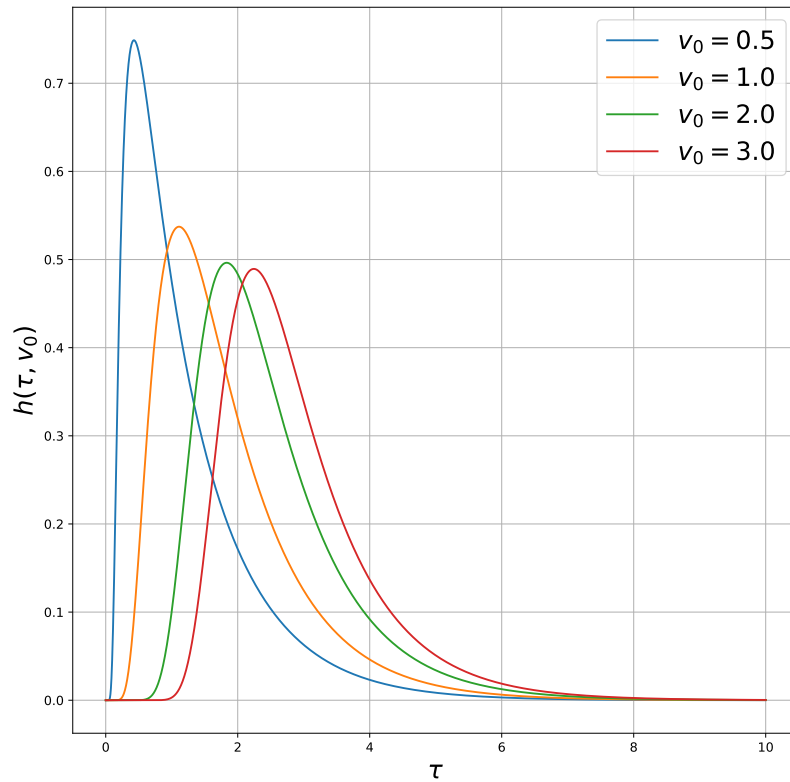


**Figure 3.2:** Solution to particle survival distribution from eq. (3.1.17) for an absorbing boundary at  $v_c = 0$  for different positive starting velocities  $v_{t_0}$ . Slower initial velocities lead to a higher probability of changing directions at lower values of survival time  $\tau$ .  $\gamma_0 = 1.0$ ,  $D = 0.1$ .

## 3.2 Statistical Theory of Random Motion

The previous section contained an introduction to Brownian particles and a discussion of the specific equations and models covering the OU process.

In this section, some of the concepts which were previously touched upon are explained in more detail.

### 3.2.1 Markov Processes

A Markov process is a random process which is memory-less on long timescales, such that the state of the process is only dependent on the most recent state of the system[80, 78] and is defined by the Markov assumption:

$$P(\mathbf{x}_n, t_n | \mathbf{x}_{n-1}, t_{n-1}; \mathbf{x}_{n-2}, t_{n-2} \cdots \mathbf{x}_1, t_1; \mathbf{x}_0, t_0) = P(\mathbf{x}_n, t_n | \mathbf{x}_{n-1}, t_{n-1}) \quad (3.2.1)$$

Where  $t_n > t_{n-1} > \cdots > t_0$ . This states that the state of a truly random system is only dependent on its most recent state, and that it has no “memory” of its further history

#### 3.2.1.1 Chapman-Kolmogorov Equation

The Chapman-Kolmogorov equation (CKE) gives a rigorous mathematical definition linking the joint probability distribution of a Markov system moving from one state to another:

$$P(\mathbf{z}, t | \mathbf{y}, t') = \int_{\Omega} d\mathbf{x} P(\mathbf{z}, t | \mathbf{x}, \tau) P(\mathbf{x}, \tau | \mathbf{y}, t') \quad (3.2.2)$$

That is to say that the probability of the system existing at state  $\mathbf{z}$  at time  $t$  given that at some previous time  $t'$  it existed at state

$\mathbf{y}$  is the sum of the probability of arriving at this state through all intermediate states  $\mathbf{x}$  at intermediate times  $\tau$ , and independent of each state ( $t \geq \tau \geq t'$ )[78]. This allows for the ensemble average behaviours to be calculated without consideration of intermediate states. The reader is directed towards Gardiner (1983)[78] for a complete background on the theory of the CKE, the master equation, and the Fokker-Planck equations for stochastic systems.

### 3.2.2 Statistical Mean Values

Given a particle or a system of particles, it is often of interest to measure the average or statistically expected behaviour.

For a Markov system, the statistical mean of a single particle's velocity across all times is equivalent to the mean of a population of particles at a single time step.

We therefore define two different averages when working with systems of particles.

#### 3.2.2.1 Ensemble Average

The ensemble average is the mean value of a particle state  $x$  (velocity, position, energy etc.) at a specific time  $t$  over  $n$  particle trajectories in a population. For  $i$ , any individual particle trajectory:

$$\langle x(t) \rangle_c = \sum_i^n \frac{x_i(t)}{n} \quad (3.2.3)$$

### 3.2.2.2 Trajectory Average

The trajectory average is defined as the mean value of velocity or energy over a range of a single trajectory. For  $j \in (0, 1, \dots, N)$  for  $t_j = j\Delta t$ :

$$\langle x_j \rangle_t = \sum_j^N \frac{x(t_j)}{n} \quad (3.2.4)$$

### 3.2.2.3 Combined Ensemble & Trajectory Average

It is possible to take a complete system average across all particles  $i$  at all time steps  $j$ :

$$\langle x \rangle = \sum_i^n \sum_j^N \frac{x_i(t_j)}{nN} \quad (3.2.5)$$

This technique will describe well the mean system behaviour in the case of a Brownian particle (Markovian), for example, where it is known that all data points are uncorrelated.

### 3.3 Active Brownian Motion

The main research presented in this thesis focuses on active Brownian motion, which is a subset of Brownian motion where the particles themselves exhibit some activity outside of the random force. This may be generalised as an additional force which may or may not be correlated with the other states of the particles within the system. This force may take different forms, some of which are discussed here. A mathematical generalisation is introduced which then serves as a basis for the continued development of different active particle models.

#### 3.3.1 The Active Force

For ABPs, we may split the contribution to the balance of forces on the particle into active and inactive components. That is to say that, in general, there will be some additional forces acting upon the particle which cause for a deviation away from pure Brownian motion and towards some increased motility or control.

A modification may be made to the LEs (3.1.1) for a single OU particle, introducing a generalised active force:

$$\frac{d\mathbf{r}}{dt} = \mathbf{v} \tag{3.3.1}$$

$$\frac{d\mathbf{v}}{dt} = -\gamma_0\mathbf{v} - \nabla U(\mathbf{r}) + \mathcal{F}_{\text{active}}(\mathbf{v}, \mathbf{r}, \boldsymbol{\kappa}, t) + \sqrt{2D}\boldsymbol{\xi}(t) \tag{3.3.2}$$

Where  $\boldsymbol{\kappa}$  represents any set of parameters which may control the dynamics of the active force.

### 3.3.2 Multiple Particle Interactions

In systems with multiple particles, there may be a resultant force due to the interactions between these particles. The Brownian force itself is independent of these particle interactions, but any active force may be caused or affected by the motion of a particle or particles in the surrounding vicinity. This additional force may be derived and added to a unique set of LEs for each particle, with some form of correlation between these equations depending on the model used. In this study we will focus on the theory and development of a single particle with activity in underdamped regimes. The reader is directed towards[52] for a comprehensive review on the theory of multi-particle systems of active Brownian particles.

### 3.3.3 The Energy Depot Model

Particles with internal energy depots which contribute to the activity of the particle by converting this internal energy into kinetic energy have been discussed[39, 40]. The active force  $\mathcal{F}_{active}$  in this case is a function of the model parameters and the quantity of energy stored within the depot.

The mathematical theory of this model is discussed in further detail in the next Section 3.4.

### 3.4 Energy Depot Model

The energy depot (ED) model developed by Schweitzer, Ebeling and Tilch[39] is a model for an active particle where the activity derives from an internal depot which stores and transfers energy into kinetic energy for particle motion. The literature and introduction to the theory was covered extensively in Section 2.4.

In this section the theory of the model itself is explained in more detail, beginning with a description of the model parameters and their meanings alongside the LEs for the system and the FPEs for the probability distributions.

#### 3.4.1 Model Description

The ED model considers particles of size  $R_H$  with an internal energy storage depot. The quantity of energy within the depot at any time  $t$  is denoted by  $e(t)$ . The depot is capable of absorbing energy from the surroundings at a rate  $q(\mathbf{r}, \mathbf{v}, t)$ . This energy may then be dissipated proportionally to the amount of energy within the depot with rate  $-c e(t)$  or converted into kinetic energy with rate  $d(\mathbf{v}, t) e(t)$ .

Though many other relationships for energy conversion have been discussed in the literature (see Section 2.4.4), in this study we focus on the below relationship for the depot energy conversion  $d(\mathbf{v}, t)$ :

$$d(\mathbf{v}, t) = d_0 \mathbf{v}^2 \quad (3.4.1)$$

Where  $d_0$  is the energy conversion rate constant. i

### 3.4.2 Langevin Equations

A set of coupled LEs exist for  $e$ ,  $\mathbf{r}$  and  $\mathbf{v}$ [39]. Taking into account the conversion relationship from eq. (3.4.1), the resulting LEs for the ED model are thus:

$$\frac{d\mathbf{r}}{dt} = \mathbf{v} \quad (3.4.2a)$$

$$\frac{d\mathbf{v}}{dt} = -\gamma_0\mathbf{v} - \nabla U(\mathbf{r}) + e(\mathbf{v}, t)d_0\mathbf{v} + \sqrt{2D}\boldsymbol{\xi}(t) \quad (3.4.2b)$$

$$\frac{de}{dt} = q(\mathbf{r}, \mathbf{v}, t) - (c + d_0\mathbf{v}^2)e(\mathbf{v}, t) \quad (3.4.2c)$$

For  $e(\mathbf{v}, t) = 0$  — these equations correspond to that of an OU particle.

As with the case of an OU particle, the Brownian motion is modelled by the diffusion constant  $D$ , where  $\boldsymbol{\xi}(t)$  is an  $n$ -dimensional array of independent Gaussian random variables as per eq. (3.1.4). The energy uptake  $q(\mathbf{r}, \mathbf{v}, t)$  may be a constant value  $q_0$ . In this case, eq. (3.4.2c) becomes:

$$\frac{de}{dt} = q_0 - (c + d_0\mathbf{v}^2)e(\mathbf{v}, t) \quad (3.4.3)$$

### 3.4.3 Adiabatic Assumption

In some parameter spaces the characteristic timescale for the update of  $e$  is much faster than that of  $\mathbf{v}$  — in such cases the particles are said to be adiabatic in  $e$  (the adiabatic assumption). Though this does not directly relate to the classical thermodynamic definition of an adiabatic process, where no heat is exchanged with the surrounding system, it keeps with the more abstract definition where changes in  $\mathbf{v}$  are slow relative to the changes in  $e$  such that  $e$  does not

deviate from its *equilibrium* value ( $e_0(\mathbf{v})$ ). As such,  $e$  resolves to a deterministic value  $e_0(\mathbf{v})$  as  $\dot{e} \rightarrow 0$ . From eq. (3.4.3):

$$e_0 = \frac{q_0}{c + d_0 \mathbf{v}^2} \quad (3.4.4)$$

The LE (3.4.2b) becomes:

$$\frac{d\mathbf{v}}{dt} = -\gamma_0 \mathbf{v} - \nabla U(\mathbf{r}) + \frac{q_0}{(c/d_0) + \mathbf{v}^2} \mathbf{v} + \sqrt{2D} \boldsymbol{\xi}(t) \quad (3.4.5)$$

#### 3.4.4 Active Friction

The friction term in the LE (3.4.2b) may be combined with the active coefficient to the velocity on the RHS in order to represent an effective active friction  $\gamma(\mathbf{v})$ :

$$\gamma(\mathbf{v}) = \gamma_0 - d_0 e(\mathbf{v}, t) \quad (3.4.6)$$

It may be seen from this equation that in the region where  $e(\mathbf{v}) > \frac{\gamma_0}{d_0}$ , the active friction is negative and so the particle will accelerate due to the active force. When  $e(\mathbf{v}) < \frac{\gamma_0}{d_0}$ ; the particles loss of energy to friction will be less as a result of the active force, but there will be no active pumping of the particle[40].

If both  $\gamma_0$  and  $d_0$  are constant for a system, then we may define a pumping energy  $e_p$  which defines the stationary value of energy at which the switch between positive and negative friction occurs:

$$e_p = \frac{\gamma_0}{d_0} \quad (3.4.7)$$

For adiabatic particles, the friction function from eq.(3.4.6) simplifies to:

$$\gamma(\mathbf{v}) = \gamma_0 - \frac{q_0 d_0}{c + d_0 \mathbf{v}^2} \quad (3.4.8)$$

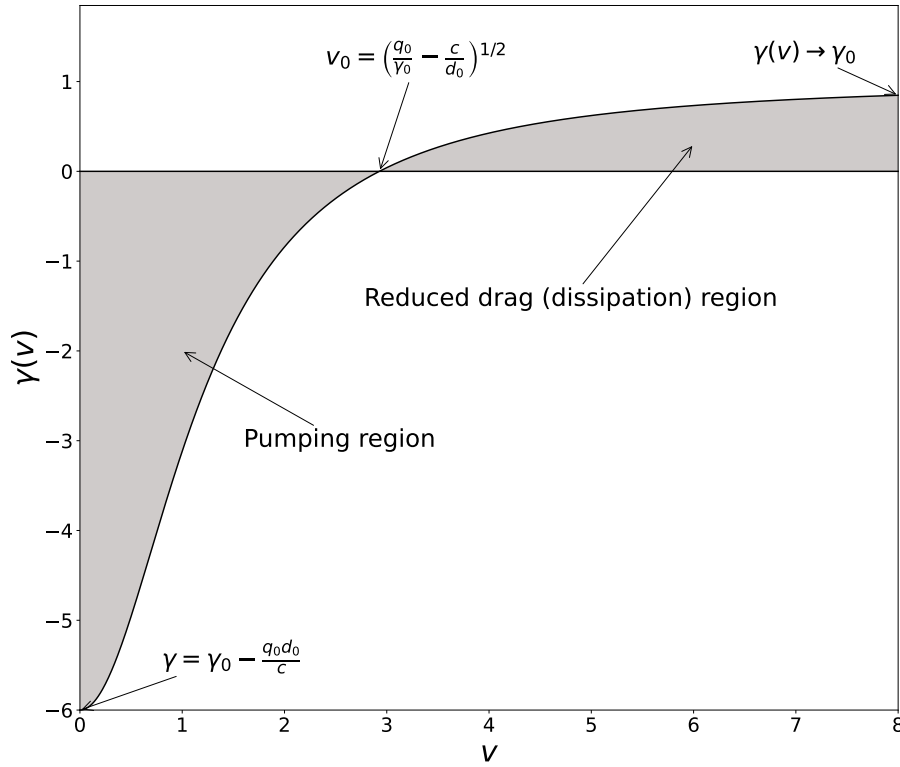


**Figure 3.3:** Graphical representation of the active friction eq.(3.4.8) for adiabatic particles. For values of  $\gamma(v) < 0$  (the pumping region) the particle is “pumped” and the velocity increases, depleting the internal depot. For values of  $\gamma(v) > 0$  (the reduced drag, or dissipation region) the particle is dragged as with static friction, however the active motion reduces this drag force. At the stationary velocity  $v_0$  (eq. (3.4.9)), the active and static friction components are balanced and the particle maintains a steady velocity. Adapted from[67]. Sample values  $\gamma_0 = 1.0$ ,  $d_0 = 0.7$ ,  $q_0 = 10.0$ ,  $c = 1.0$ .

Equation (3.4.8) is plotted for a 1-D particle in fig.3.3 which has been adapted from Erdmann [67]. It can be seen that there are two distinctive regions of friction dependent on the model parameters with a fixed point corresponding to the stationary velocity at  $v_0$ . At higher velocities the active friction asymptotically tends towards the static friction  $\gamma_0$  as a result of the ever increasing  $v^2$  term on the denominator of the equation.

In the more complex case of non-adiabatic particles there will also be additional dynamics related to the relevant timescales set by the model parameters ( $q_0$ ,  $d_0$ ,  $c$  and  $\gamma_0$ ), as will be investigated

in Section 4.4. We present in fig. 3.4 the  $v - e$  phase space streamlines plot for a deterministic particle which we will present later in Chapter 4, where these fixed points and the deterministic motion of particles through the phase space is shown.

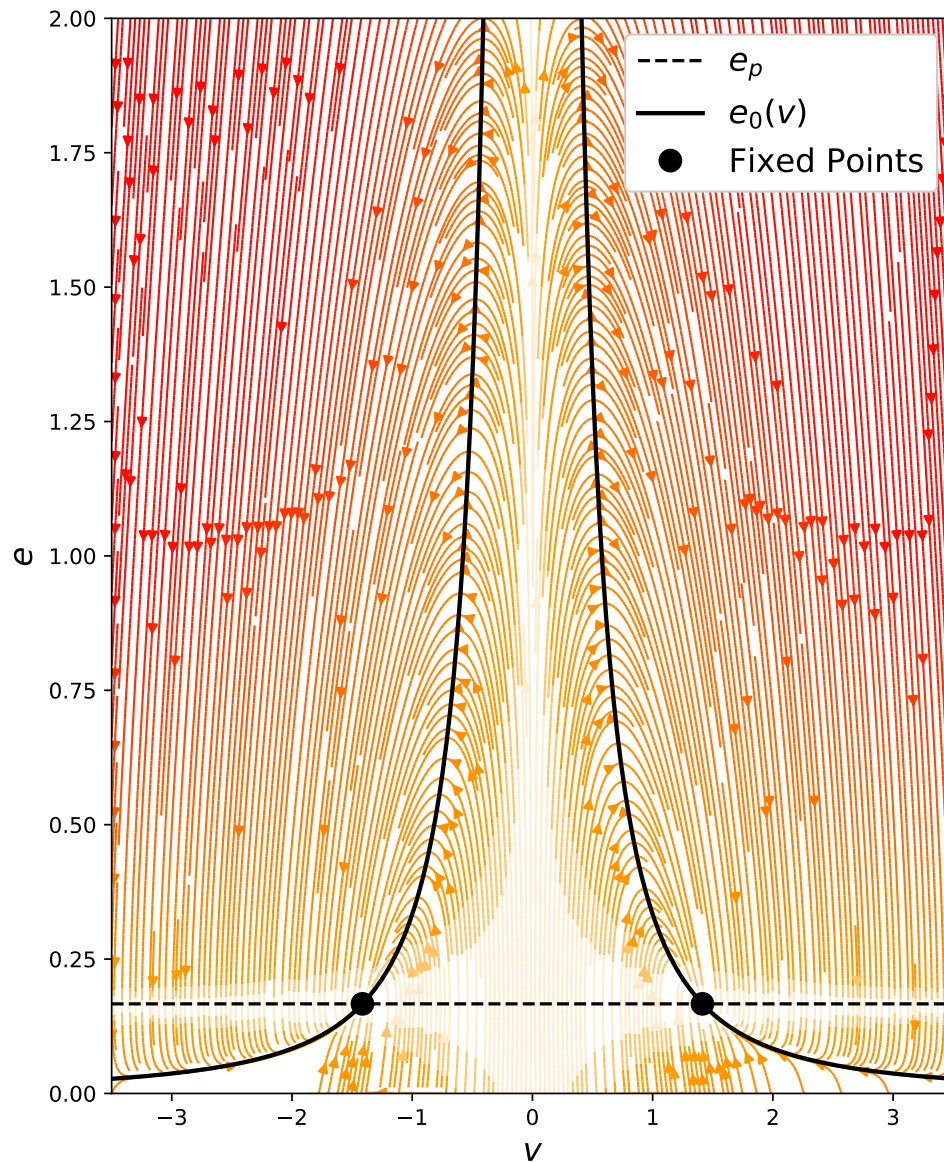


**Figure 3.4:** Velocity and energy streamlines for a deterministic particle with ED. The lines show the particle motion in  $(v, e)$ -space always tending towards the stationary points at  $(v_0, e_p)$  — darker red lines correspond to a higher gradient of motion through the phase space, with lighter orange corresponding to a lesser gradient. Example values:  $q_0 = 2.0$ ,  $c = 0.001$ ,  $d_0 = 6.0$ ,  $\gamma_0 = 1.0$ .

### 3.4.5 Stationary Velocity & Bifurcation Point

For deterministic particles ( $D = 0$ ) in the absence of any gradient  $U$ , the velocity and energy of the particles will tend towards their stationary points  $e_0$  and  $\mathbf{v}_0$ . In the adiabatic limit, the solution to eq.(3.4.5) is:

$$v_0 = \beta^{1/2} = \left( \frac{q_0}{\gamma_0} - \frac{c}{d_0} \right)^{1/2} \quad (3.4.9)$$

The bifurcation parameter  $\beta = \mathbf{v}_0^2$  signals whether there are any roots to the stationary velocity of the particle. There are thus three types of solution to eq. (3.4.9) depending on the system parameters  $q_0$ ,  $d_0$ ,  $c$  and  $\gamma_0$ :

1.  $\frac{q_0}{\gamma_0} = \frac{c}{d_0}$ :  $\beta = 0$  and  $v_0 = 0$ .
2.  $\frac{q_0}{\gamma_0} > \frac{c}{d_0}$ :  $\beta > 0$ ,  $v_0$  has a positive and negative conjugated real value.
3.  $\frac{q_0}{\gamma_0} < \frac{c}{d_0}$ :  $\beta < 0$  and no real roots exist.

In a deterministic system, if  $\beta \geq 0$  (i.e cases 1 and 2) the particle will tend towards the steady state value of  $v^2 = \beta$ . For case 2 it will depend on the initial velocity  $v(t = 0)$  whether or not the particle will end up in the positive or negative direction. In parameter regimes of type 3 the ED model does not represent real systems of which we are interested in modelling.

For deterministic particles, the points  $(\pm v_0, e_0)$  correspond to the intersection of the  $e_0$  curve (eq. (3.4.4)) with the pumping line  $e_p$  (eq. (3.4.7)) as shown in fig. 3.5.

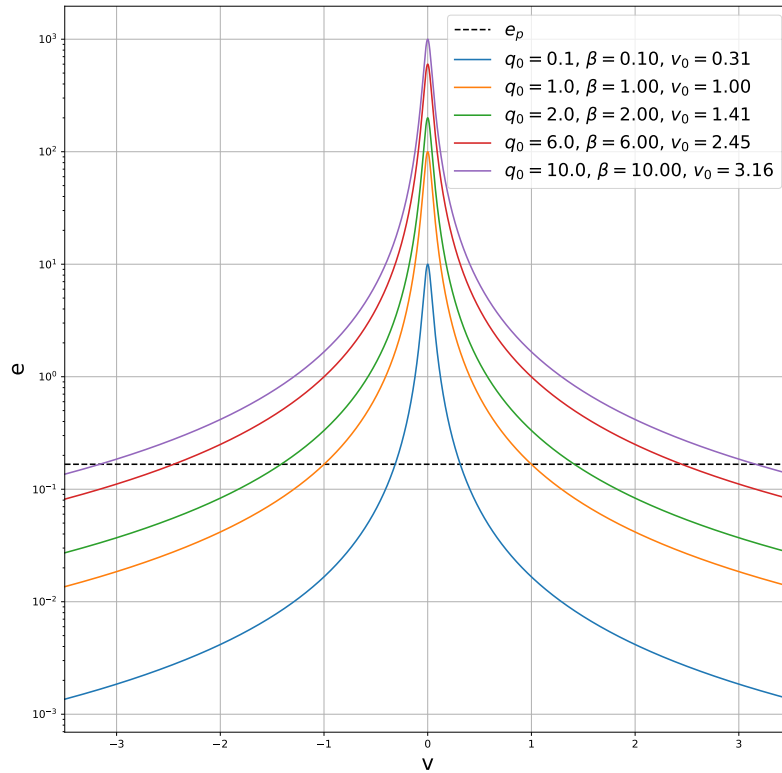


**Figure 3.5:** Plot showing  $e_0$  curves vs.  $v$  for varying values of constant energy uptake rate  $q_0$ . The black dashed line shows  $e_p$ , the threshold for pumping behaviour defined in eq. (3.4.7). The points where  $e_0 = e_p$  is the stationary velocity  $v_0$ . For  $\beta < 0$  the  $e_0$  line never meets  $e_p$ . If  $\beta = 0$  then the lines intersect at  $v = 0$  only.  $d_0 = 4.0$ ,  $c = 0.01$ ,  $\gamma_0 = 1.0$ .

### 3.4.6 Fokker-Planck Equation

As the system is modelled by a system of LEs, a FPE exists which shows the solution to the probability distribution and its evolution for this system.

### 3.4.6.1 General Form of FPE

From the system of LEs eqs. (3.4.2), the complete FPE for the ED model is thus[78]:

$$\begin{aligned} \frac{\partial P(\mathbf{v}, \mathbf{r}, e, t)}{\partial t} = & - \frac{\partial}{\partial \mathbf{r}} [\mathbf{v}P] - \frac{\partial}{\partial \mathbf{v}} \left[ (-\gamma_0 + d_0 e) \mathbf{v}P + D \frac{\partial P}{\partial \mathbf{v}} \right] \\ & - \frac{\partial}{\partial e} [(q(\mathbf{r}) - e \cdot (c + d_0 \mathbf{v}^2)) P] \end{aligned} \quad (3.4.10)$$

This derivation can be found in Appendix 7.2.

### 3.4.6.2 Adiabatic Form of FPE

When the particle energy is adiabatic eq. (3.4.5) may be applied to eq. (7.2.2). The resultant FPE is:

$$\begin{aligned} \frac{\partial P(\mathbf{v}, \mathbf{r}, t)}{\partial t} = & - \frac{\partial}{\partial \mathbf{r}} [\mathbf{v}P] \\ & - \frac{\partial}{\partial \mathbf{v}} \left[ \left( -\gamma_0 + \frac{d_0 q(\mathbf{v}, \mathbf{r}, t)}{c + d_0 \mathbf{v}^2} \right) \mathbf{v}P + D \frac{\partial P}{\partial \mathbf{v}} \right] \end{aligned} \quad (3.4.11)$$

A stationary solution to this equation exists in  $\mathbf{v}$ , giving the steady-state probability distribution of velocity for an ED particle:

$$P_{ss} = \mathcal{N} \left( 1 + \frac{d_0}{c} \mathbf{v}^2 \right)^{\frac{q_0}{2D}} \exp \left[ -\frac{\gamma_0}{2D} \mathbf{v}^2 \right] \quad (3.4.12)$$

Where  $\mathcal{N}$  is a normalisation function dependent on the boundary conditions and  $q_0$  is the constant energy uptake independent of  $\mathbf{r}$ ,  $\mathbf{v}$  and  $t$  (derived in Appendix 7.7).

A simple rearrangement of this equation prevents any issues due to large exponent values of  $\frac{q_0}{2D}$  causing memory overflow errors when carrying out this calculation in simulations:

$$P_{SS}(v) = \mathcal{N} \exp \left( \frac{1}{2D} \left( q_0 \ln \left( 1 + \frac{d_0}{c} v^2 \right) - \gamma_0 v^2 \right) \right) \quad (3.4.13)$$

The normalisation condition for a 1-D distribution over all  $v$  stipulates that cumulative probability densities over all velocities is 1, therefore  $\mathcal{N}$  is a scaling function such that:

$$\mathcal{N} = \left( \int_{-\infty}^{\infty} dv P(v) \right)^{-1} \quad (3.4.14)$$

In discrete form:

$$\mathcal{N} = \left[ \sum_{i=0}^M P(v_i) \cdot (v_i - v_{i-1}) \right]^{-1} \quad (3.4.15)$$

Fig. 3.6 shows this steady state distribution for underdamped Brownian particles with EDs with varying values of  $q_0$ .

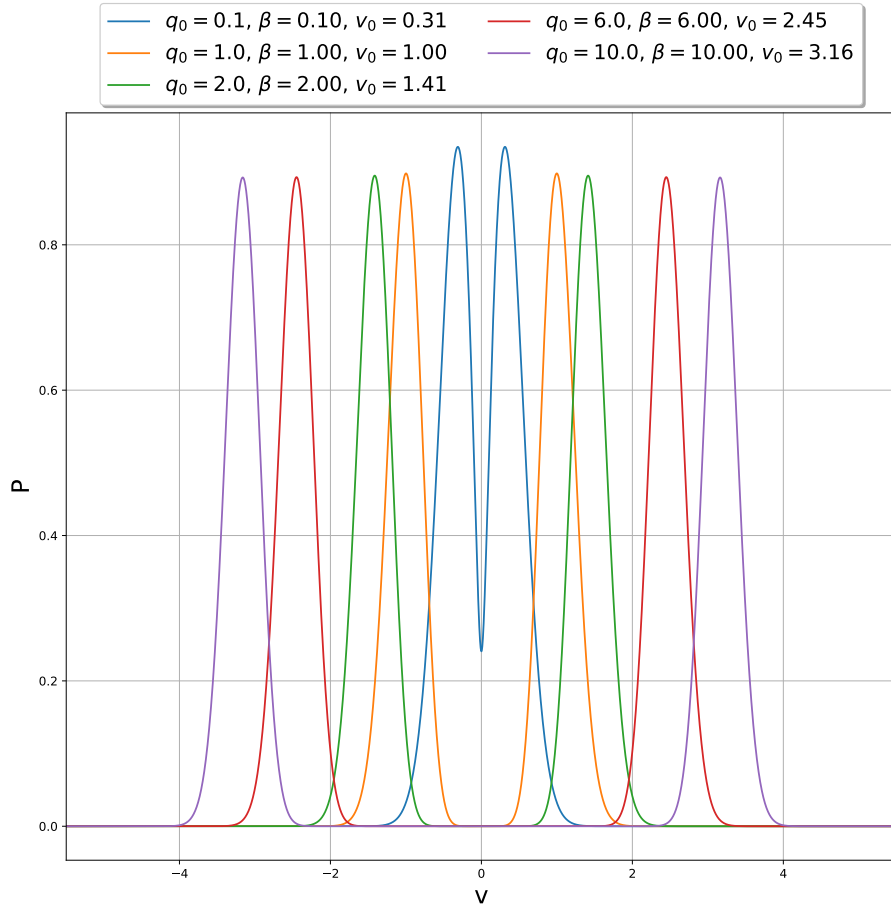


**Figure 3.6:** Normalised steady-state velocity distribution for particles with energy depots for different values of  $q_0$ . There is an emergence of bimodal distribution for particles with  $\beta > 0$ . As  $q_0$  is increasing, the stationary velocity value also increases and the distributions move apart. There is no large effect on the variance of the velocities. The bimodal distribution gives an interesting case where  $\langle v \rangle = 0$  but  $\langle v^2 \rangle = \beta$ .  $D$  has no effect on the value of  $\beta$ .  $D = 0.1$ ,  $d_0 = 4.0$ ,  $c = 0.01$ ,  $\gamma_0 = 1.0$ .

We present here the solutions to the PDF for adiabatic particles, trajectories for non-adiabatic particles which still contain a degree of freedom for the parameter  $e(\mathbf{v})$  may be simulated in order to observe the corresponding ensemble behaviours for the adiabatic steady-state FPEs presented here.

### 3.5 Stochastic Calculus

We provide here a summary of the numerical methods used to solve the preceding LEs for particles with EDs, as well as the numerical method for resolving inactive (OU) particles.

#### 3.5.1 Heun Method

The Heun methodology provides a predictor-corrector numerical approximation to the solution of SDEs. This involves a forward time step and a backwards correction[82]. For each time dependent variable  $\phi_i$  in a set of LEs:

$$\tilde{\phi}_i(t) = \phi_i(t) + f_i(\phi(t))\Delta t + g_{ij}(\phi(t))\xi_j(t) \quad (3.5.1)$$

$$\begin{aligned} \phi_i(t + \Delta t) = & \phi_i(t) + \frac{1}{2} \left( f_i(\phi(t)) + f_i(\tilde{\phi}(t)) \right) \Delta t \\ & + \frac{1}{2} \sum_j \left( g_{ij}(\phi(t)) + g_{ij}(\tilde{\phi}(t)) \right) \xi_j(t) \end{aligned} \quad (3.5.2)$$

For  $\xi_j(t)$  as a delta-correlated white noise variable as defined in eq. (3.1.4).  $f_i$  is the non-stochastic component of the RHS of the LE, and  $g_i$  is the stochastic coefficient.

The algorithm approximates the solution to the differential equations by first calculating the candidate value of a variable  $\tilde{\phi}_i(t)$  from the system state at time  $t$ , as per eq. (3.5.1). In eq. (3.5.2) the value at the next time stamp  $\tilde{\phi}_i(t + \Delta t)$  is then calculated using the arithmetic mean between the two calculated values of  $\phi_i$ .

This predictor-corrector approach ensures that changes in the values of  $\phi_i$  during extrapolation which would affect the next calculated value are taken into account. Even over small time steps  $\Delta t$  for

stochastic equations, there can be sensitivities in the system which this method helps to more accurately calculate.

In the case where the calculated value of a parameter  $\phi_i(t + \Delta t)$  crossed a limit during our simulations, for example when the energy was calculated to be negative, the calculation was re-executed with a smaller time-step. In these cases the most simple approach was to divide the time-stamp into two pieces and then follow the path of calculating  $\phi(t + \frac{\Delta t}{2})$  and  $\phi(t + \Delta t)$  from this. By executing this algorithm in a loop with the goal of a non-zero value of  $\phi_i$ , it was possible to handle these edge cases by continually halving the time-step until it was small enough to capture dynamics that did not generate negative numbers.

### 3.5.1.1 Numerical Solution to OU Process

Gillespie[79, 83] outlined a numerical solution to the OU LEs eqs. (3.1.1). We use this to compare the inactive case ( $d_0 = 0$ ) for ED particles and benchmark the implementation of our software. The time evolution of an OU process with friction  $\gamma_0$  and diffusion constant  $D$  is:

$$\mathbf{r}(t + \Delta t) = \mu \mathbf{r}(t) + \sigma_r \boldsymbol{\xi}_1(t + \Delta t) \tag{3.5.3a}$$

$$\begin{aligned} \mathbf{v}(t + \Delta t) = & \mathbf{v}(t) + \frac{\mathbf{r}}{\gamma_0}(t)(1 - \mu) + \left( \sigma_v^2 - \frac{\kappa_{rv}^2}{\sigma_r^2} \right)^{1/2} \boldsymbol{\xi}_2(t + \Delta t) \\ & + \frac{\kappa_{rv}}{\sigma_r} \boldsymbol{\xi}_1(t + \Delta t) \end{aligned} \tag{3.5.3b}$$

Where:

$$\mu = e^{-\gamma_0 \Delta t} \quad (3.5.4a)$$

$$\sigma_r^2 = \frac{D}{\gamma_0} (1 - \mu^2) \quad (3.5.4b)$$

$$\sigma_v^2 = \frac{2D}{\gamma_0^3} \left( \gamma_0 \Delta t - 2(1 - \mu) + \frac{(1 - \mu^2)}{2} \right) \quad (3.5.4c)$$

$$\kappa_{rv} = \left( \frac{D}{\gamma_0^2} \right) (1 - \mu)^2 \quad (3.5.4d)$$

$\xi_1$  and  $\xi_2$  are statistically independent unit normally distributed random vectors as per eq. (3.1.4).

### 3.5.2 Autocorrelation

For a time-series of data, the autocorrelation function represents how correlated a point of data is with itself after a certain number of data points  $\kappa$ , referred to as a *lag*. For the example of the velocity of a Brownian or OU particle, the velocity autocorrelation shows the relationship between the velocity at time  $t$  ( $v(t)$ ) and the velocity at time  $t + \tau$  ( $v(t + \tau)$ ) — where  $\tau = \kappa \Delta t$ . The autocorrelation function for variable  $X$  at a lag of  $\kappa$  is denoted as  $\rho_X(\kappa)$ . A value of  $\rho_x(\kappa) = 1.0$  means that the two values are completely correlated, i.e. there is a fully deterministic relationship. A value of 0 represents completely uncorrelated data. A negative auto-correlation value shows an inverse relationship — where a value at one time signals a tendency for a negative value at a later time, or vice-versa.

$\rho(\kappa)$  is mathematically defined as the relationship between the auto-

covariance of  $X$  and its variance  $\sigma_X^2(t)$ [84]:

$$\rho_X(\kappa) = \frac{\text{Cov}(X_t, X_{t+\kappa})}{\sigma_X^2(t)\sigma_X^2(t+\kappa)} \quad (3.5.5)$$

The auto-covariance for a discrete set of events is given as[84]:

$$\text{Cov}(X_t, X_{t+\kappa}) = \frac{1}{N} \sum_{t=0}^N [(X_t - \mu_X)(X_{t+\kappa} - \mu_X)] \quad (3.5.6)$$

Where  $\mu_X$  is the mean value of variable  $X$  and  $N$  is the total number of data points.

The calculation of the autocorrelation for time-series data is done using the *statsmodels* ([85]) python library which uses a Fast-Fourier-Transform (FFT) implementation.

### 3.5.3 Switching Time Distribution

For an OU particle, the survival time distribution for a particle with an absorbing boundary at  $v = 0$  is described analytically in eq. (3.1.16). In the case of a particle with an energy depot the solution to the FPE (3.4.10) in time is not elementary. As such, the switching times for particles were calculated using a monte-carlo (MC) method.

#### 3.5.3.1 Definition of a Switch

A switch is defined as the point at which a particle (in one dimension) changes velocity from positive/negative to negative/positive, respectively.

#### 3.5.3.2 Numerically Measuring the Switching Time

The switching time for particles was measured by initiating a trajectory and continuing until the particle switched directions as defined

above. At this point, the time taken  $\tau_s$  is noted and is defined as the switching time — the time a particle takes when travelling in one direction to switch to the reverse.

These times were compiled using a normalised histogram in order to show the overall probabilistic behaviour of the system switching time distribution. These numerically gathered results represent analogous solution to eq. (3.1.13) for the Green's function solution to(3.4.10) for values of  $v$  and  $e$  at  $t = 0$ .

#### 3.5.4 Power Law Fit For Switching Time

In the case of long time-scales for switching, a heavy-tailed distribution is more sensible for fitting the switching-time distribution due to the large span between possible events described by similar behaviours[86]. A power law is thus presented in order to fit these distributions at longer characteristic time-scales:

$$h(\tau_s) = h_0(1 - h_0)^{\frac{\tau_s - \tau_0}{\lambda}} \quad (3.5.7)$$

$\tau_0$  is the reference time. This parameter corresponding to the timescale at which power law behaviour becomes prevalent.  $\lambda$  is the decay time constant, in this context it describes the rate of decay of switching probability as  $\tau_s$  increases. Smaller  $\lambda$  values will decay more quickly, whilst higher values will decay at a slower rate.  $h_0$  is the scaling factor which determines the magnitude of the value  $P(\tau_s)$ .

#### 3.5.5 Chi-Squared Testing

The Chi-Squared test is used to signify the fit error for a data sample[87]. Given a sample population of  $n$  independent data points

$O_i$  (the observed value) and the corresponding expected value for each point given by a fit  $E_i$ , the value of  $\chi^2$  is defined as:

$$\chi^2 = \sum_{i=0}^n \frac{(O_i - E_i)^2}{E_i} \quad (3.5.8)$$

A value of  $\chi^2 = 0$  indicates a perfect fit between the data set and the fitted model. Estimated values  $E_i$  which are further away from the observed values are punished more severely due to the squaring of the difference.

## Chapter 4

# Ensemble Average Behaviour of Particles with Energy Depots in 1-D

## 4.1 Introduction

In this chapter, we investigate the ensemble average behaviours of simulated non-adiabatic particles with energy depots (EDs) in 1-Dimension using an agent-based approach. The adiabatic assumption of depot relaxation (Section 3.4.3) assumes that the relaxation of the depot energy is much faster than the rate of acceleration of the particles, such that the energy becomes a fixed function of velocity  $e_0(\mathbf{v})$ . Here, the particle depot energy will be calculated at each step irrespective of the velocity in order to understand regimes where this assumption may not apply.

We begin by investigating particle behaviours when starting from rest with empty depots, and observe the dynamics of arrival at steady-state across different parameter regimes.

The velocity distributions across long trajectories are then observed and compared with the expected analytical results.

In order to understand the deviation from these analytical adiabatic results, we investigate the ensemble average energies at different velocity values in order to give a picture of the particle behaviour in  $v - e$  phase-space. We then compare these results to the literature and explain the dynamics of the particles as they move around this phase-space in the presence of noise.

### 4.1.1 Simulation Motivation and Experimental Outline

Individual Ornstein-Uhlenbeck particles (the agents) with EDs (ED particles) were simulated in 1-D. The aim of these simulations was

to observe how changing the rate of energy conversion  $d_0$  and the rate of uptake of energy  $q_0$  affected different observed particle behaviours. One main motivation was to determine the characteristics and the region of parameter space under which these particles show adiabatic behaviour in  $e$ .

We choose to investigate the one-dimensional case where energy consumption from depots is isolated to motion in a single direction. Higher dimensional studies have been focused on particles in adiabatic parameter regimes, though to our knowledge, there is no consistent description in the literature of particles away from these regimes. Though our work could expand to higher dimensions, we choose to focus on the special emergent behaviour of particles driving in a single direction and the observed non-adiabatic behaviour which differs to the cyclical motion of adiabatic particles which is observed in higher dimensional studies[76].

In the field of ABPs, it is common to present the results of simulations in the form of calculated mean-squared displacement (MSD) values across different time steps from the simulation result set which can be mapped back to an effective diffusion constant. We chose not to pursue this analysis in this section as we were motivated to make a direct observation of how the velocity distributions compared to those expected from the analytical solutions to the Langevin equations for adiabatic particles. Similarly, due to the bimodal distribution of the velocity distributions expected in some parameter regimes from the literature and observed in our results,

the effective diffusion constant would not be a sensible parameter to adjust the data to as it would limit the system to a Gaussian distribution of velocities.

This chapter discusses the simulations which were carried out along with an analysis of their results. At each stage of analysis, observed behaviours are used as a motivation for the subsequent analysis.

Initially, the unsteady state canonical time evolution of systems starting from rest are discussed. These lead on to an analysis of the overall steady-state velocity and energy distributions of the particles, with the aim of understanding how well stochastic modelled particles in different parameter regimes adhere to any assumptions made in the model. The emergence of distinct particle behaviours is observed, ranging from almost Brownian behaviour to particles which are completely adiabatic in  $e$ .

In between these two extremes, particles are observed which exist adiabatically (with depot energies dictated by their velocity) for long periods of time before undergoing directional switches in low velocity regions, in the process deviating from adiabatic behaviour. An analysis of the frequency of these switching events as well as their relationship with the decorrelation times of the particle velocities and energy and the timescales for particles to reach steady-state is then presented.

### 4.1.2 Model Parameters

The theoretical background of the model along with a more detailed explanation of how each parameter effects the deterministic system behaviour is outlined in Chapter 3. Table 4.1 presents a summary of each parameter used in the model along with a description.

**Table 4.1:** Summary table of parameters for ED model

| Parameter       | Name                         | Description   | Units                        | Dimensionless Scaling Factor |
|-----------------|------------------------------|---|------------------------------|------------------------------|
| $\mathbf{r}(t)$ | Particle position            | Position of the particle at any time $t$ in $n$ -dimensions.                                  | $[\mathcal{L}]$              | $D^{1/2}\gamma_0^{-3/2}$     |
| $\mathbf{v}(t)$ | Particle velocity            | Velocity of the particle at any time $t$ in $n$ -dimensions.                                  | $[\mathcal{L}][\tau]^{-1}$   | $D^{1/2}\gamma_0^{-1/2}$     |
| $e(t)$          | Particle depot energy        | Amount of energy stored in the particle depot at time $t$ .                                   | $[\mathcal{L}]^2[\tau]^{-2}$ | $D\gamma_0^{-1}$             |
| $D$             | Particle diffusion constant  | Strength of the stochastic force.   | $[\mathcal{L}]^2[\tau]^{-3}$ | $D$                          |
| $c$             | Depot dissipation rate       | Rate of internal dissipation of energy from depot.  | $[\tau]^{-1}$                | $\gamma_0$                   |
| $q_0$           | Depot energy uptake rate     | Uptake of energy from surroundings into the depot. Constant throughout any single simulation. | $[\mathcal{L}]^2[\tau]^{-3}$ | $D$                          |
| $d_0$           | Depot energy conversion rate | Constant controlling the rate of conversion of $e$ into particle kinetic energy $E_k$ .       | $[\tau][\mathcal{L}]^{-2}$   | $D^{-1}\gamma_0^2$           |
| $\gamma_0$      | Static friction              | Frictional drag coefficient for particle from energy losses to surroundings.                  | $[\tau]^{-1}$                | $\gamma_0$                   |
| $\Delta t$      | Simulation time step         | Time step between points on simulation output trajectory.                                     | $[\tau]$                     | $\gamma_0^{-1}$              |

### 4.1.3 Simulation Parameters and Assumptions

Stochastic simulations were carried out over a range of values of  $d_0$  and  $q_0$ . The other simulation parameters were kept constant and are summarised in table 4.2 alongside the relevant dimensionally scaled values.

**Table 4.2:** Summary of simulation parameters kept constant throughout experiments.

| Parameter  | Input Value | Dimensionless Value |
|------------|-------------|---------------------|
| $D$        | 0.1         | $0.1^{1/2}$         |
| $\gamma_0$ | 1.0         | 1.0                 |
| $c$        | 0.01        | 0.01                |
| $\Delta t$ | 0.01        | 0.01                |

#### 4.1.3.1 Constant Parameter Selection

The ratio of the diffusion constant  $D$  and static friction  $\gamma_0$  was chosen to represent overdamped non-active Brownian particles on the 15–20nm scale in water at 298K. This length scale was initially chosen as it corresponds to the nano-scale active particles from which the original work was based. At this length scale, the stochastic dynamics can be dominant which offered an opportunity to investigate parameter configurations for the ED model in both noise and activity dominated regimes and to compare them and observe emergent behaviour.

The ratio of  $\frac{D}{\gamma_0}$  as a function of hydrodynamic radius is found by combining the Stokes-Einstein equation (3.1.2) with Stokes' Law eq. (3.1.3):

$$\frac{D}{\gamma_0} = \frac{K_B T}{(6\pi\eta R_H)^2} \quad (4.1.1)$$

Fig. 4.1 shows an example curve of this ratio against hydrodynamic radius for real system of small particles in water. For particles of a constant radius, increasing the ratio  $D/\gamma_0$  is analogous to an increase in system temperature (as per (3.1.2)).

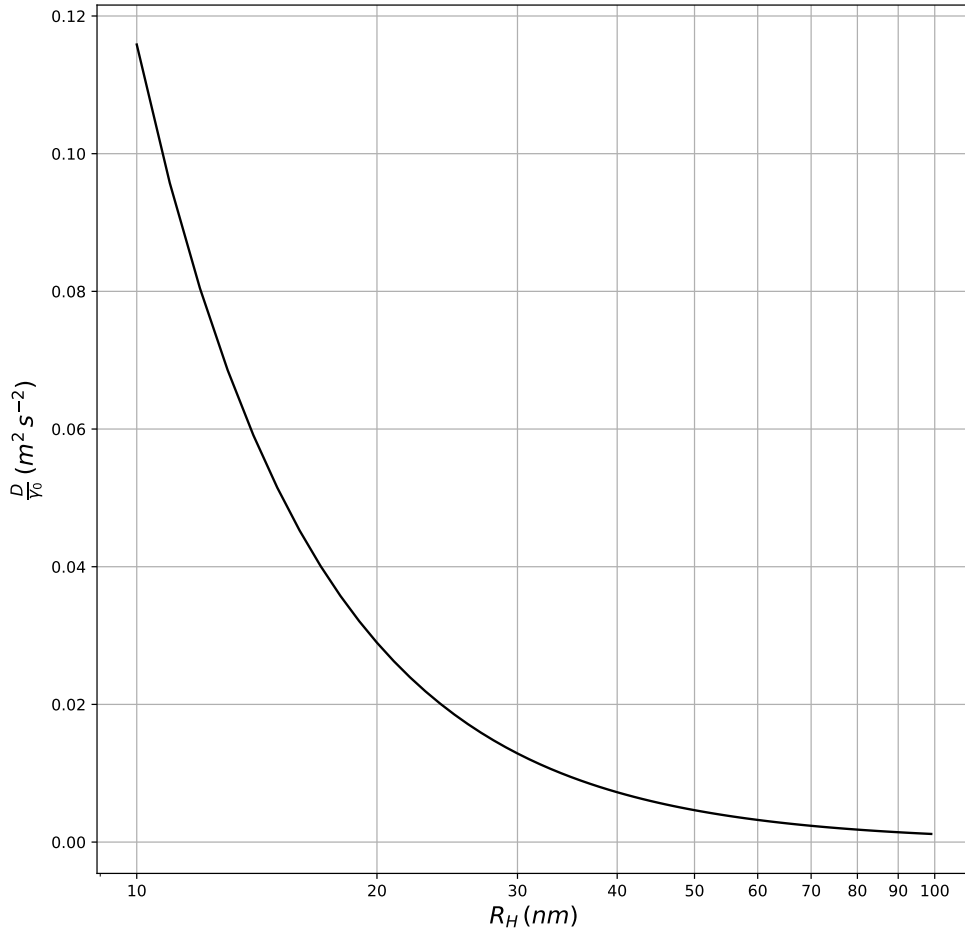


**Figure 4.1:** Ratio of  $D/\gamma_0$  for spherical Brownian particles in water. The line shows the expected value of this ratio for a constant temperature system of real particles over a range of possible radii.  $T = 298.15 K$ ,  $\eta = 0.001 Pa s$ .

#### 4.1.3.2 Dimensionless Groups

The dimensions of the particles were simplified by setting the reference units to unity or to scale with simulation parameters. This allows for simulation equations to be simplified by eliminating mass, and for different parameter sets to be scaled against each other

through these dimensionless groups, rather than relying on real-world length/time scales which may become more difficult to contextualise when simulating. There are also computational advantages to this methodology, as the numbers which are used can be more manageable in terms of data entry, result processing, and the computational power required.

The unit of mass  $[\mathcal{M}]$  was set to unity as the mass of a single particle. The length-scale  $[\mathcal{L}]$  and time-scale  $[\tau]$  were set based upon the values of  $D$  and  $\gamma_0$  such that their dimensionless values are unity as per tab. 4.1.

$$[\tau] = \gamma_0^{-1} \tag{4.1.2}$$

$$[\mathcal{L}] = \left(\frac{D}{\gamma_0^3}\right)^{1/2} \tag{4.1.3}$$

The dimensional groups are presented below in table 4.3. Substitu-

**Table 4.3:** Dimensionless groups used without simulations and calculations.

| Dimension | Unit            | Dimensional Scaling              |
|-----------|-----------------|----------------------------------|
| Length    | $[\mathcal{L}]$ | $(D \times \gamma_0^{-3})^{1/2}$ |
| Time      | $[\tau]$        | $\gamma_0^{-1}$                  |
| Mass      | $[\mathcal{M}]$ | 1                                |

tion of the relevant dimensions for the units in table 4.1 gives the dimensional scaling for each parameter or value in the simulations. These definitions are then substituted for the dimension units in table 4.1 in order to give the corresponding dimensionless scaling factor also presented in the table. A value is converted to its corresponding dimensionless number by dividing by the dimensionless scaling factor.

The graphs in this chapter are presented in dimensionless form, meaning that values have been scaled by the appropriate factor for the values being shown.

By setting the values of  $D$  and  $\gamma_0$  as in tab. 4.2 the effective dimensionless simulation temperature  $k_B T = 0.1$  was chosen as per the Stokes-Einstein Equation (see eq. (3.1.2)). This physically represents the velocity of the particles in the simulated medium — a higher  $k_B T$  value corresponds to a higher temperature fluid where surrounding particles are colliding with higher thermal energy and thus momentum[78]. As we are simulating individual particles as agents, the forces which these surrounding particles exert on the ABPs are represented by the stochastic elements of the LEs through the diffusion constant  $D$ .

$$D = \frac{k_B T}{\gamma_0} \tag{4.1.4}$$

$$0.1 = \frac{k_B T}{\gamma_0} \tag{4.1.5}$$

$$k_B T = 0.1 \tag{4.1.6}$$

Values of energy and velocity were dimensionally scaled throughout. Other parameters are presented as entered into the simulations with dimensions. Where appropriate to present these in dimensionless form they are appended with a superscript  $D$ , e.g  $c^D = \frac{c}{\gamma_0}$ . The dimensions of each parameter are listed in table 4.1.

Rotational diffusion was ignored in the model. Acceleration from the depot is applied in the current direction of motion. In order to switch direction, a particle must pass through the  $v = 0$  boundary.

#### 4.1.3.3 Variable Simulation Parameters

A total of 20 different combinations of  $q_0$  and  $d_0$  were simulated comprising of 4 variations of  $q_0$  and 5 variations of  $d_0$ . The nomenclature used herein for referencing each simulation parameter set is summarised in table 4.4. The simulation with, for example, values of 6.0 and 0.1 for  $d_0$  and  $q_0$ , respectively, is referred to as simulation or case D1.

**Table 4.4:** Reference table for dimensionless simulation parameter sets used.

| $d_0^D \downarrow q_0^D \rightarrow$ | 0.1 | 1.0 | 2.0 | 10.0 |
|--------------------------------------|-----|-----|-----|------|
| 0.1                                  | A1  | A2  | A3  | A4   |
| 1.0                                  | B1  | B2  | B3  | B4   |
| 2.0                                  | C1  | C2  | C3  | C4   |
| 6.0                                  | D1  | D2  | D3  | D4   |
| 10.0                                 | E1  | E2  | E3  | E4   |

The choice of these values was motivated by the previous investigations into existing results in the literature. The low value of  $c$  chosen meant that the bifurcation point  $\beta$  and thus the stationary velocities  $\pm v_0$  (eq. (4.1.7)), were only weakly affected by changes in  $d_0$ . This value of  $c$  also ensures that the depletion of energy in the depot is a stronger function of the velocity. Thus, increasing the value of  $q_0$  would almost proportionally increase the value of  $\beta$ . Similarly, the adiabatic energy value was not greatly affected by the dissipation term  $c$ .

$$\beta = v_0^2 = \frac{q}{\gamma_0} - \frac{c}{d_0} \tag{4.1.7}$$

Based upon existing comments in the literature, the most likely particles to exhibit adiabatic behaviour would be in case E4, with case A1 the least likely as being the least active.

#### 4.1.4 Simulation Methodology

A computational numerical integrator was constructed using the Stochastic Heun method (Section 3.5.1) to solve the LEs for the ED model in the absence of any potential gradient. Recalling the LEs which have previously been declared in Section 3.4.2:

$$\frac{dr}{dt} = v \quad (4.1.8a)$$

$$\frac{dv}{dt} = -\gamma_0 v + e(v, t)d_0 v + \sqrt{2D}\xi(t) \quad (4.1.8b)$$

$$\frac{de}{dt} = q_0 - (c + d_0 v^2)e(v, t) \quad (4.1.8c)$$

This program was fed parameter input data along with information for the required time-step  $\Delta t$ , end time  $t_{end}$ , and initial conditions for the simulation:

$$e(t = 0) = 0 \quad (4.1.9)$$

$$v(t = 0) = 0 \quad (4.1.10)$$

$$r(t = 0) = 0 \quad (4.1.11)$$

At each time step, the particle ID, velocity  $v$ , position  $r$ , and energy  $e$  of a single simulated particle were output to a data file.

In order to minimise the error over any measurement step in the integration, a separate internal simulation time step was also provided to the programme which was set to be at least an order of magnitude lower than the smallest timescale in the system set by the parameters. When  $q_0$ ,  $d_0$ ,  $\gamma_0$  or  $c$  are particularly high, the simulation step must be made much smaller in order to ensure the dynamics are captured.

#### 4.1.4.1 Simulation Bench-Marking

In order to show that the software was correctly configured, a single particle benchmark test was carried out to compare the captured value of the depot energy at a simulation step  $i$  ( $e_{\text{sim},i}$ ) against the calculated value ( $e_0(v_i)$ ) based off of the analytical solution to the Langevin equations at the velocity captured at the same time step (eq. (3.4.4)).

Fig. 4.2 graphically shows the energy trajectory of a particle in a short simulation (2000 time steps) where the simulation parameters were chosen for near-adiabatic relaxation of the depot energy (i.e.  $e_{\text{sim},i} \approx e_0(v_i)$  (3.4.4)). The distribution of the ratio of the simulated and calculated energies shows mean value of 1.0 (i.e. equivalence) with a standard deviation of 2%. Later in the chapter (sec. 4.4), we will analyse the differences between the simulated and adiabatic energies, this simulation serves as a benchmark for that analysis.

Multiple simulations were completed for each parameter set, dependent on the type of data required. Where a single long trajectory was required, one particle would be simulated as necessary. For canonical averages over large samples of particles at shorter time-scales, a separate simulation was run with these conditions applied across multiple particles.

Large samples and long trajectories were required to ensure that the statistical data collected was representative of the expected behaviour of the system. Data was generated to output text files which were post-processed by separate programs.

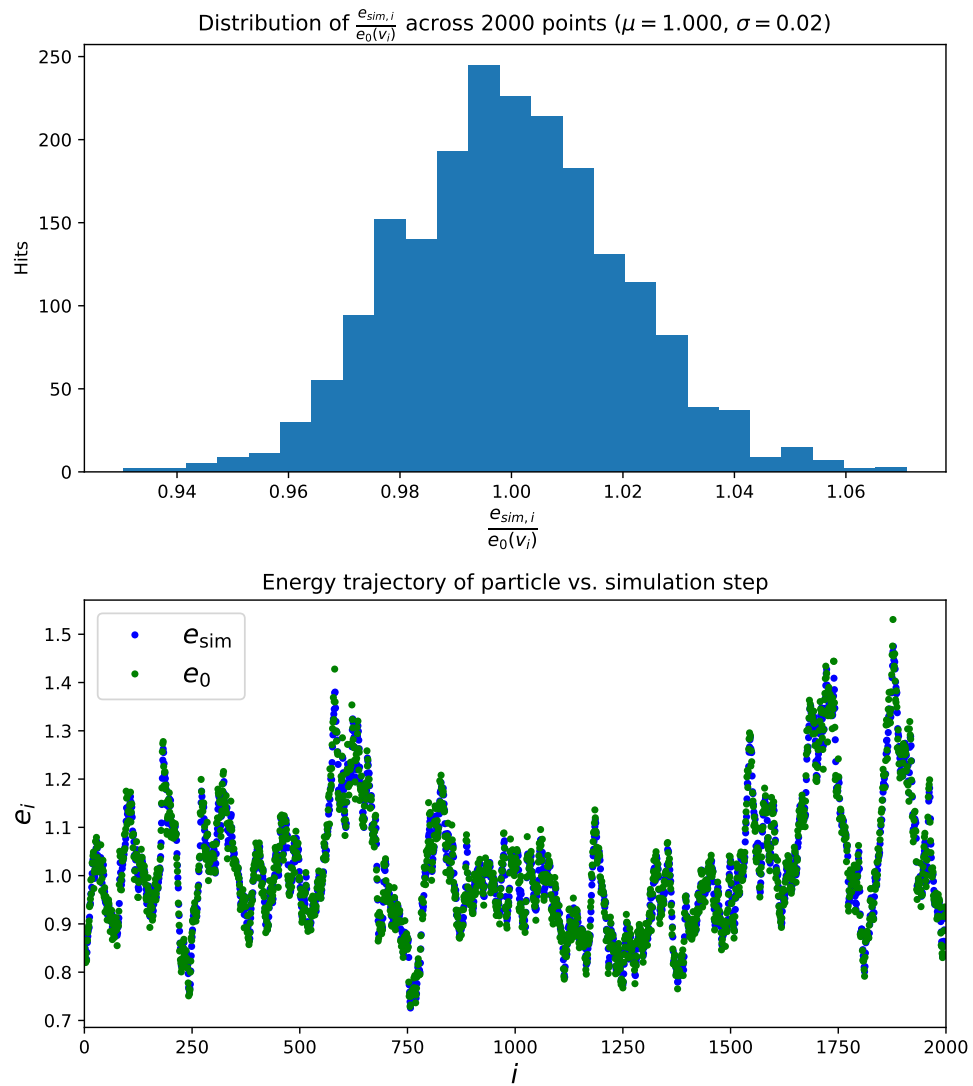


**Figure 4.2:** Top: Distribution of ratio of simulated energy  $e_{sim}$  to calculated adiabatic energy  $e_0(v_i)$ . Bottom:  $e_i$  for both simulated and calculated energies over a 20 time-unit trajectory. Parameters:  $D = 0.1, \gamma_0 = 1.0, c = 0.001, d_0 = 10.0, q_0 = 10.0, \Delta t = 0.01$ .

## 4.2 Time Evolution of 1-D ED Particles Starting From Rest

### 4.2.1 Introduction

Multiple single particle simulations were carried out over short trajectory lengths. The ensemble average behaviours in velocity and energy at each simulation time  $t$  for these particles was observed.

The two motivations for this analysis were to determine the time-frame with which particles starting from rest would come to a stationary state and to observe the average dynamics of particles starting from rest and how they varied as the parameters  $d_0$  and  $q_0$  were varied.

In Chapter 5 an analysis of stochastic particles switching between their 1-D limits is carried out. This switching behaviour requires a velocity transition through the origin ( $v = 0$ ) and so understanding these dynamics will also assist in future discussions.

The deterministic stationary limit of ED particles was previously discussed in Section 3.1.4. In the absence of the stochastic force, a particle in motion will not move from the stationary velocity ( $v = 0$ ) whilst  $e$  moves to  $e_0(v = 0) = \frac{q_0}{c}$ .

The addition of the stochastic force causes for particles to randomly drift between these  $v - e$  streamlines dependent on the diffusion constant  $D$ . When the particles move to the stationary points  $(\pm v_0, e_p)$  (if these exist) they are unlikely to remain there. The drift motion of the particles through the  $v - e$  plane is still governed by the deterministic elements in the Langevin Equations (LEs), with

the stochastic force adding a diffusive element to this behaviour.

As per eq. (3.4.9) and the mathematical behaviours outlined in eqs. (3.4.5); the values of  $d_0$  and  $q_0$  were chosen for these simulations in order to ensure that the stationary points always exist (i.e.the bifurcation parameter  $\beta$  is always a positive real number, there is no imaginary component of  $v_0$ ).

## 4.2.2 Methodology

### 4.2.2.1 Simulation Parameters

Brownian Particles starting from rest with empty energy depots were simulated in 1-D with initial conditions:

$$v(t = 0) = 0$$

$$e(t = 0) = 0$$

The total number of particles simulated was  $n = 400,000$  per data set. All parameters other than  $d_0$  and  $q_0$  were kept constant —  $D = 0.1$ ,  $\gamma_0 = 1$ ,  $c = 0.001$ .

The software program simulated these trajectories for each particle and captured the values of  $v$  and  $e$  at every time  $t$ . Time steps were separated by  $\Delta t = 0.001$ .

The ensemble average values  $\langle |v(t)| \rangle$  and  $\langle e(t) \rangle$  were calculated after each time step in the simulation using eq. (3.2.3) as per the methodology outlined in Section 3.2.2. This data was written to an output file. The average value of the absolute velocity  $|v(t)|$  was taken due to the symmetry in  $v$  causing for  $\langle v(t) \rangle = 0$ .

Case A1 was simulated first to benchmark the maximum required

time to reach steady-state. Once this result was available, the remaining simulations were run for the same amount of time. The end time of simulation  $t_{\text{end}} = 156$  which corresponds to  $1.56 \times 10^5$  data points per plotted line.

### 4.2.3 Results

The results are presented in graphical form grouped by values of  $q_0$  using the alpha-numerical index nomenclature (i.e. A1-E4) outlined in table 4.4.

Each line on the graphs represents results for a different value of  $d_0$  at constant  $q_0$ . A1-E1 are presented in the top-left; A2-E2 are presented in the top right; A3-E3 are presented in the bottom left; and A4-E4 are presented in the bottom right hand sub-plots in each grouping.

The values of  $\beta$ , and thus the steady-state velocity, are on the same order of magnitude in each sub-plot (see table 4.5). As per eq. (4.2.1) it is expected that particles with lower  $d_0$  values at constant  $q_0$  will have higher values of  $\langle e \rangle_{SS}$  due to a slower consumption rate.

#### 4.2.3.1 Particle Velocity

The output velocities  $v$  from the simulations were used to calculate the ensemble average value of the absolute velocity  $\langle |v| \rangle_{SS}$ , given the particles started from rest with empty depots. Fig. 4.3 shows the results of these simulations for the different cases listed in table 4.4. Fig. 4.4 presents the same results with logarithmic axes for easier

observation of low timescale behaviour. Subplots are grouped by values of  $q_0$ .

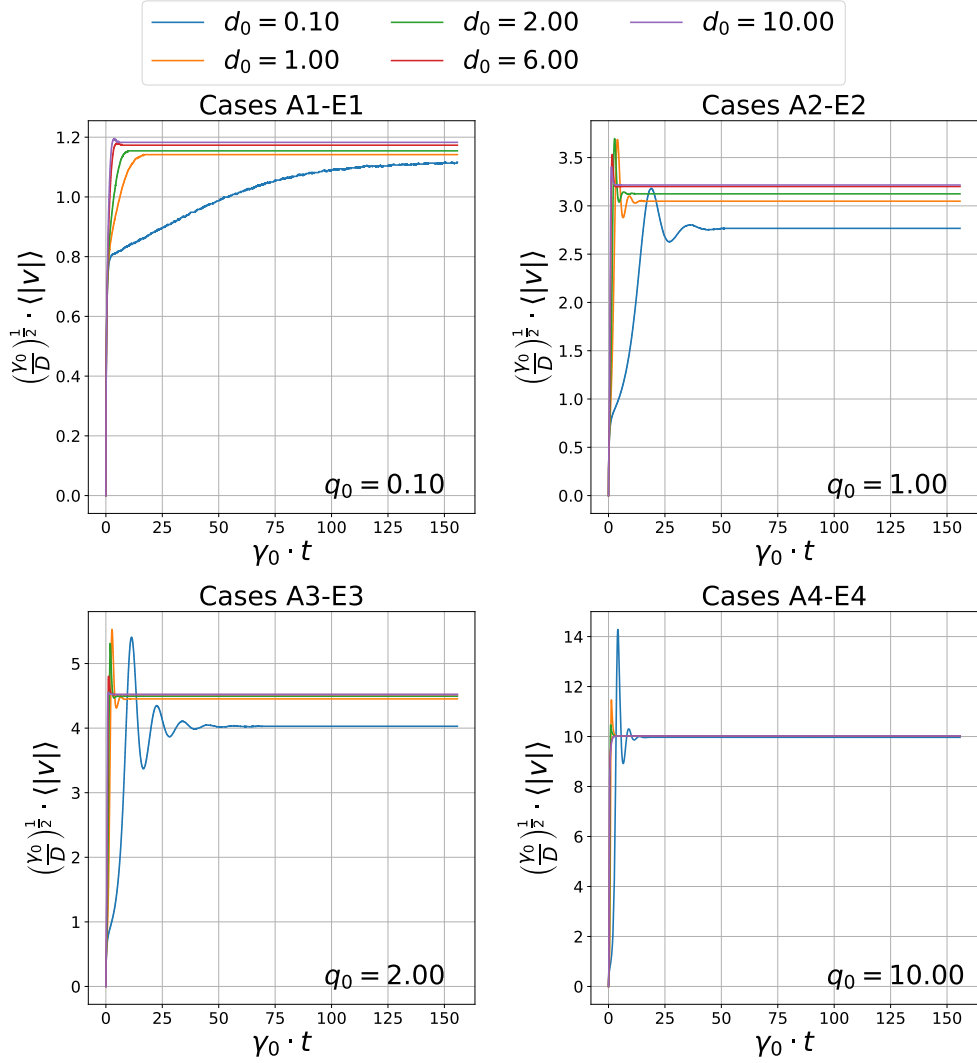


**Figure 4.3:** Average values  $\langle |v| \rangle_{SS}$  for particles starting from rest with empty energy depots ( $v(0) = 0$ ,  $e(0) = 0$ ) for all cases A1-E4. Simulations of varying  $d_0$  values are grouped with the same  $q_0$  values in each subplot. Other parameters  $\gamma_0 = 1.0$ ,  $D = 0.1$ ,  $c = 0.001$ ,  $\Delta t = 0.001$ .

#### 4.2.3.2 Particle Energy

In a similar manner as the velocity, the value of the dimensionless ensemble average steady-state depot energy  $\langle e \rangle_{SS}$  was calculated. The graphical results are shown in fig. 4.5, and on logarithmic scales in 4.6.

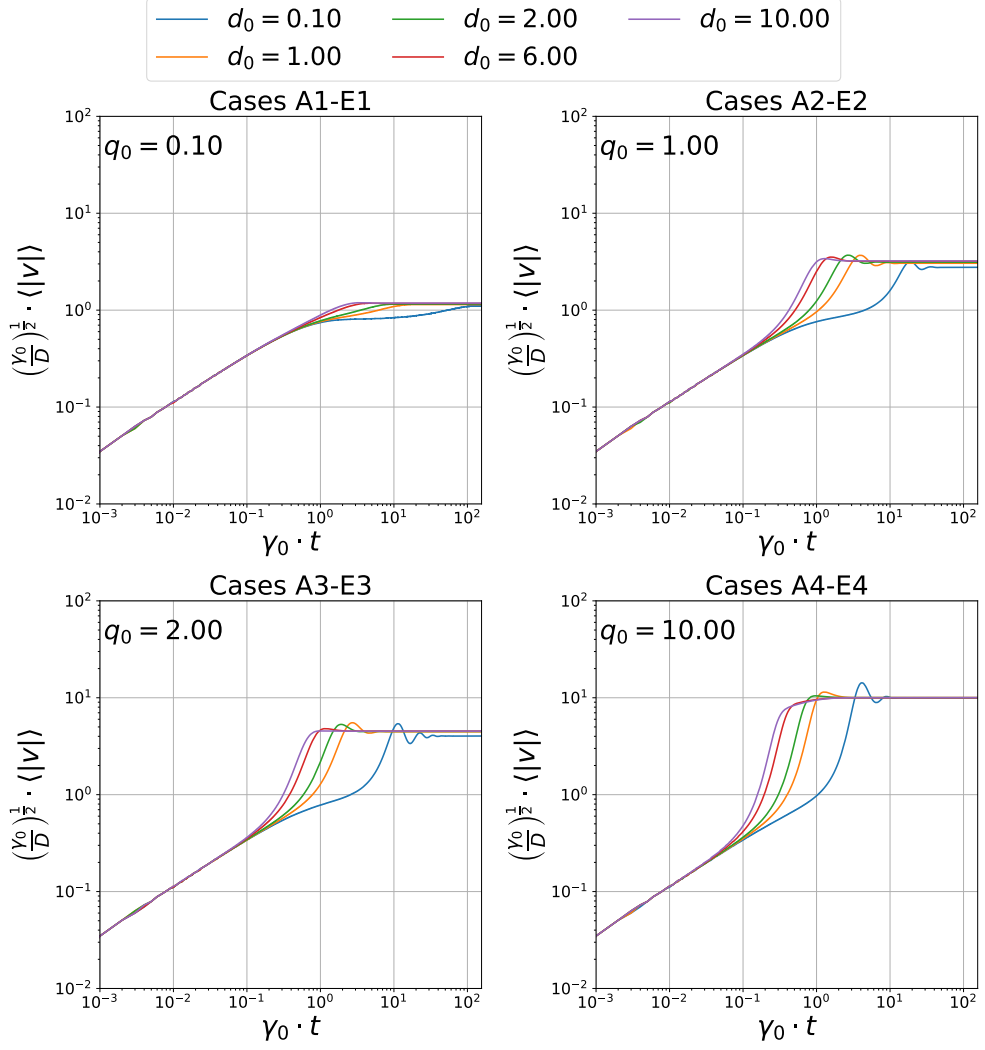


**Figure 4.4:** Average values of  $|v(t)|$  for particles starting from rest with empty energy depots ( $v(0) = 0$ ,  $e(0) = 0$ ) for all cases A1-E4 presented with log – log axes. Simulations of varying  $d_0$  values are grouped with similar  $q_0$  values in each subplot. Other parameters  $\gamma_0 = 1.0$ ,  $D = 0.1$ ,  $c = 0.001$ ,  $\Delta t = 0.001$ .

The adiabatic energy  $e_0$  for simulated  $\langle |v| \rangle_{SS}$  was also calculated using equation (4.2.1).

$$e_0(\langle |v| \rangle_{SS}) = \frac{q_0}{c + d_0 \langle |v| \rangle_{SS}^2} \quad (4.2.1)$$

#### 4.2.3.3 Ensemble Averages

The ensemble average energy and velocity at steady state were calculated from the final data point in the time series from the simu-

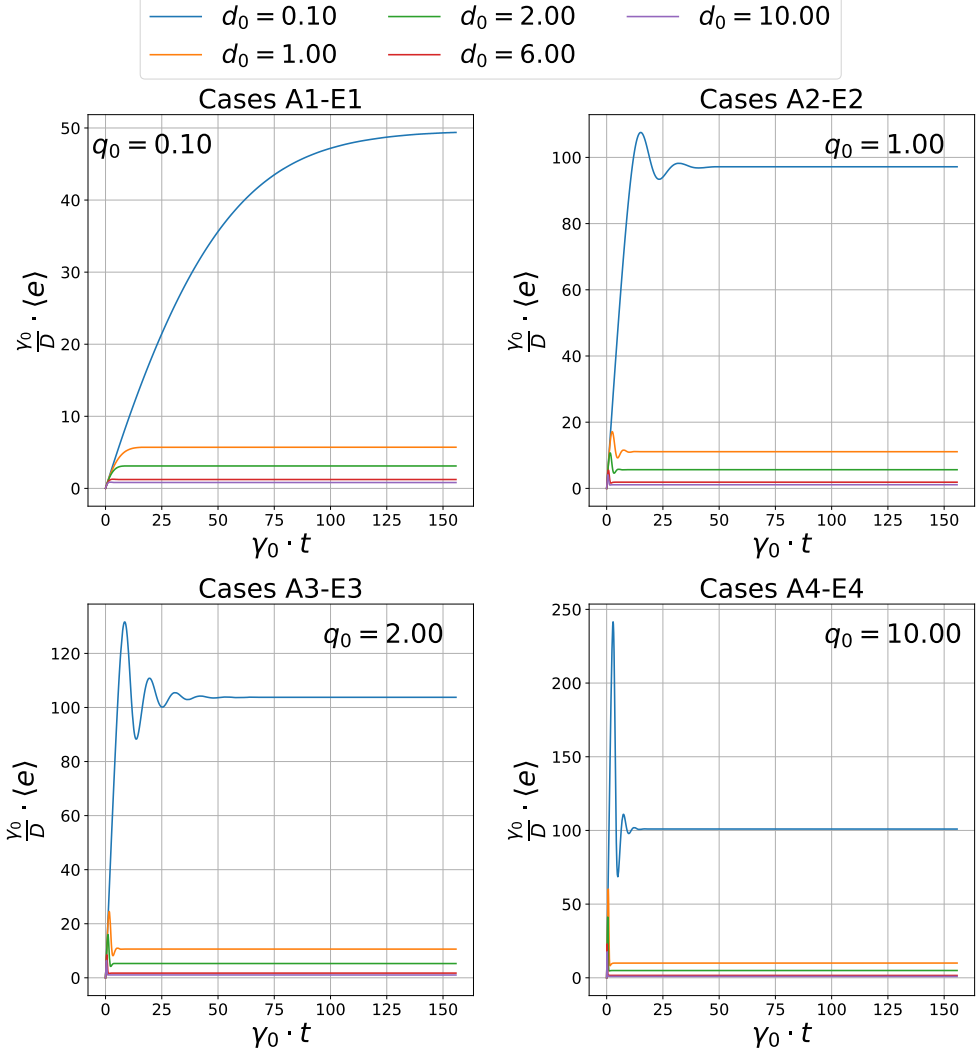


**Figure 4.5:** Average value of  $e(t)$  for particles starting from rest with empty energy depots ( $v(0) = 0$ ,  $e(0) = 0$ ) for all cases A1-E4. Other parameters  $\gamma_0 = 1.0$ ,  $D = 0.1$ ,  $c = 0.001$ ,  $\Delta t = 0.001$ .

lations. The values are presented in table 4.5.

## 4.2.4 Discussion of Results

### 4.2.4.1 A1-E1 — Cases of Slowest Energy Uptake ( $q_0 = 0.1$ )

The initial velocity is governed almost entirely by Brownian motion, as seen by the fact that the different cases all behave similarly on the short time scale. The logarithmic scaling in fig. 4.4 shows more clearly that across all data sets the particles reach  $\langle |v(t)| \rangle = 0.1$  at approximately  $t = 0.07$  before a dependence on  $d_0$  becomes ap-

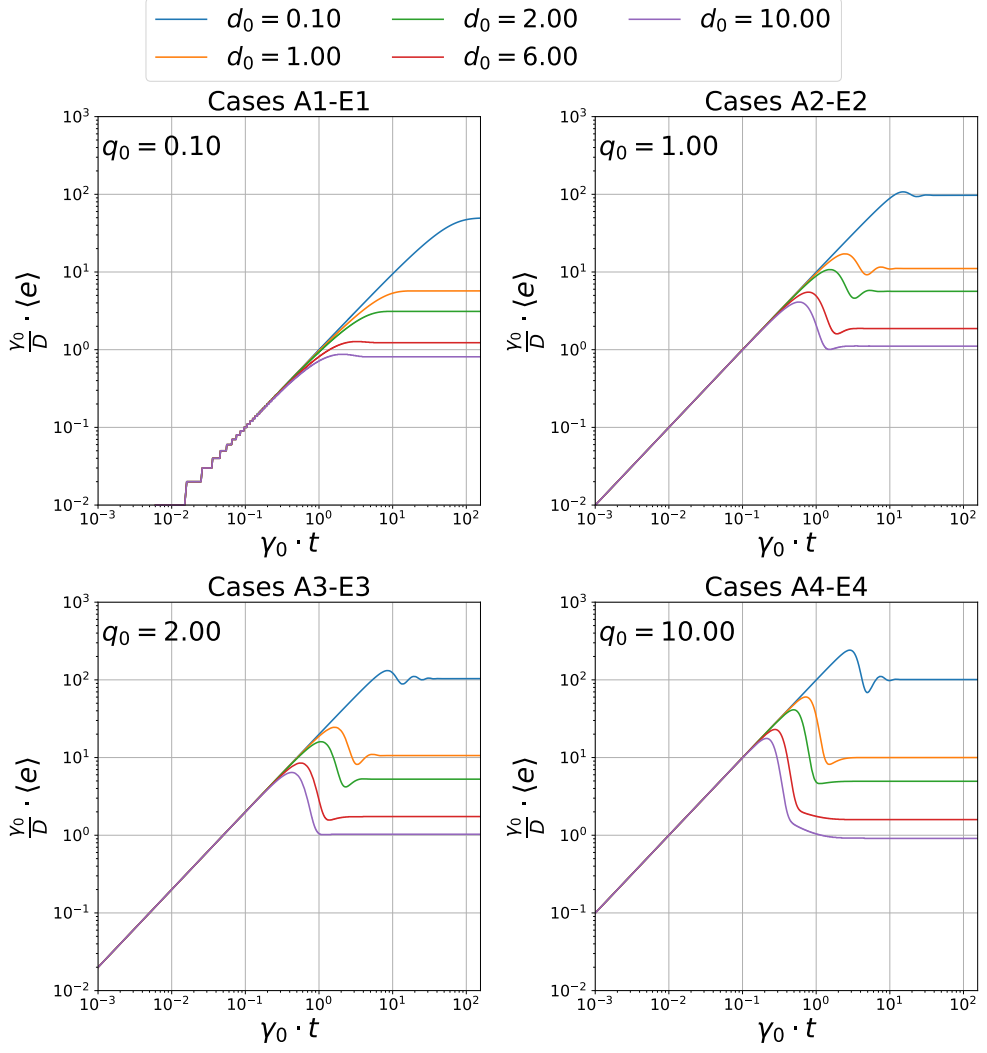


**Figure 4.6:** Average value of  $e(t)$  for particles starting from rest with empty energy depots ( $v(0) = 0$ ,  $e(0) = 0$ ) for all cases A1-E4. Other parameters  $\gamma_0 = 1.0$ ,  $D = 0.1$ ,  $c = 0.001$ ,  $\Delta t = 0.001$ .

parent. At low values of  $e$  the stochastic force contribution to the velocity is dominant. As  $q_0$  is increased, the characteristic time at which the active behaviour emerges reduces due to the depot filling up quicker. Before this characteristic time particles are stochastic rather than driven as they don't yet have enough energy to be active. This is apparent in cases A1-E1 ( $q_0 = 0.1$ ) where the  $d_0$  value begins to affect behaviour at  $t \approx 0.6$ . For A4-E4 ( $q_0 = 10.0$ ) this occurs much sooner at  $t \approx 0.07$ .

**Table 4.5:** Summary of simulation results for ensemble average dimensionless energy and ensemble average dimensionless velocity at steady-state (taken as  $t = 100.0$  for all simulations). Deterministic adiabatic energy fixed point  $e_0(\beta)$  and velocity bifurcation point  $\beta = (v_0^2)$  are also listed for reference.

| Case | $\langle  v  \rangle_{SS}$ | $\beta$ | $\langle e \rangle_{SS}$ | $e_0(\langle  v  \rangle_{SS})$ | $e_0(\beta) = e_p$ |
|------|----------------------------|---------|--------------------------|---------------------------------|--------------------|
| B1   | 1.981                      | 0.990   | 5.706                    | 5.022                           | 10.000             |
| C1   | 1.985                      | 0.995   | 3.105                    | 2.513                           | 5.000              |
| D1   | 2.005                      | 0.998   | 1.231                    | 0.830                           | 1.667              |
| E1   | 1.969                      | 0.999   | 0.819                    | 0.508                           | 1.000              |
| A2   | 11.033                     | 9.900   | 97.203                   | 89.822                          | 100.000            |
| B2   | 11.028                     | 9.990   | 11.126                   | 9.060                           | 10.000             |
| C2   | 10.967                     | 9.995   | 5.650                    | 4.557                           | 5.000              |
| D2   | 10.922                     | 9.998   | 1.893                    | 1.526                           | 1.667              |
| E2   | 11.025                     | 9.999   | 1.120                    | 0.907                           | 1.000              |
| A3   | 20.913                     | 19.900  | 104.098                  | 95.177                          | 100.000            |
| B3   | 21.030                     | 19.990  | 10.641                   | 9.506                           | 10.000             |
| C3   | 20.916                     | 19.995  | 5.311                    | 4.780                           | 5.000              |
| D3   | 21.046                     | 19.998  | 1.751                    | 1.584                           | 1.667              |
| E3   | 20.970                     | 19.999  | 1.054                    | 0.954                           | 1.000              |
| A4   | 100.768                    | 99.900  | 101.164                  | 99.139                          | 100.000            |
| B4   | 100.850                    | 99.990  | 10.117                   | 9.915                           | 10.000             |
| C4   | 101.067                    | 99.995  | 5.044                    | 4.947                           | 5.000              |
| D4   | 100.924                    | 99.998  | 1.685                    | 1.651                           | 1.667              |
| E4   | 101.082                    | 99.999  | 1.009                    | 0.989                           | 1.000              |

The cases A1-E1 show a different response in both the velocity and energy from the other cases with higher  $q_0$  values. The  $\langle |v(t)| \rangle$  value for A1 is seen to rise quickly to the approximate value of 1.0 before rising towards the final steady-state value; which it does not reach within the timescale. Increasing  $d_0$  reduces the time taken to reach the steady-state value of the velocity. The early behaviour of the cases B1-E1 is similar to that of A1 as previously mentioned — governed by the stochastic behaviour. The time taken to reach the steady-state velocity decreases moving from B1 to E1 as  $d_0$  is increased. The overshoot of the final value of  $\langle |v| \rangle_{SS}$  is more pronounced for higher values of  $d_0$  with E1 being the most pronounced. The overshoot of the steady-state value in cases B1 and C1 is less visible.

For case-A1 and case-B1, the steady-state energy value is approached in an overdamped manner as evidenced by the lack of overshoot when compared with the other cases at this value of  $q_0$ , which show a small overshoot and relaxation to the final steady-state value (underdamped behaviour). The time taken for the energy to reach steady-state is similar to that for the velocity. Due to the low  $d_0$  value, case A1 takes the longest to reach its steady-state value.

#### 4.2.4.2 A4-E4 — Cases of Highest Energy Uptake ( $q_0 = 10.0$ )

For D4 and E4 (the most active cases) the  $\langle |v(t)| \rangle$  value reaches a steady-state quickly in an overdamped manner — not overshooting the steady-state value. The other three cases with lower conversion rates also quickly approach steady-state (in less than 10 time units), though overshoot the value and oscillate back to the steady-state value. The timescale to reach the steady-state was similar for both  $e$  and  $v$  for these cases.

The least active case A4 shows two behaviours which are distinct from the others in this batch. Initially there is a more delayed onset of the acceleration from the depot seen clearly in fig. 4.4, where the rate of acceleration increases at  $t \approx 1$ . The particles then rapidly accelerate and overshoot the final steady-state value by more than 40%. The velocity then enters a cycle of oscillatory decay in an underdamped fashion around the expected steady-state value before settling.

This oscillatory behaviour arises from the active component of the force on the velocity. At lower velocities and fixed lower values

of  $d_0$ , the particles cannot convert the large quantities of depot energy quickly into kinetic energy. As they eventually accelerate, there is a surplus of energy in the depot (constant  $q_0$  has caused for an accumulation) which is quickly converted and pushes the value of  $v$  still higher such that it overshoots the steady-state value. This overshoot in turn consumes any surplus energy in the depot, reducing the value of  $e$  below the steady-state value. This deficit combined with the static friction causes for the particles to slow below  $\langle |v| \rangle_{SS}$ . This behaviour repeats again with ever decreasing amplitude, eventually arriving at a steady-state in both  $v$  and  $e$ .

The intermediate cases B4 & C4 overshoot in velocity, resulting in an over-consumption of energy away from the steady-state. The magnitude of the overshoot decreases as  $d_0$  increases. Both of these show an overdamped response after overshoot, returning to the steady-state value without any oscillation. Though there is an increase in the acceleration due to the early accumulation in the depot whilst the particles were moving slowly, the rate of energy conversion is such that the depot can be depleted before any accumulation which would cause oscillation.

The values of  $\langle |v| \rangle_{SS}$  for all of these cases closely matched the calculated values of  $\beta$ , as shown in table 4.5, and correspond to the stationary velocities discussed earlier in Section 3.1.4.

#### 4.2.4.3 A2-E2, A3-E3 — Cases of Intermediate Energy Uptake ( $q_0 = 1.0, q_0 = 2.0$ )

In the intermediate sets of data A2-E2 and A3-E3 the initial velocity response was the same as in the other cases — a short non-active ac-

celeration where the dynamics are governed by the stochastic force. Once the active component of the motion begins to dictate the dynamics, particles with a higher  $d_0$  accelerate faster in  $v$  and consume their depot energies at a higher rate. Case E2 shows a slight overshoot of the steady state value, with an overly damped relaxation to steady-state. This is less visible in case E3 — at this value of  $q_0$  the particles are close to the threshold between changing from the overshooting behaviour seen in E1/E2 to the behaviour of E4 (which behaves more like a classic critically damped response).

With a lower  $q_0$  value, there is less of an accumulation of energy in the depots for cases A2 and A3 causing for a smaller overshoot proportional to the  $\langle |v| \rangle_{SS}$  value. An underdamped oscillatory response is still seen in the relaxation phase.

Cases B2, B3 and C2 also exhibit this underdamped response and oscillations around  $\langle |v| \rangle_{SS}$ . C3 is seen to overshoot and relax in an overdamped manner to the steady-state value. The energy in all cases overshoots  $\langle e \rangle_{SS}$ . The behaviour of  $\langle e(t) \rangle$  is more similar in these intermediate sets to the high-uptake set A4-E4 and high conversion-low uptake case E1 in that it overshoots steady state severely in the initial stochastic phase before relaxing to steady-state in an underdamped fashion.

#### 4.2.4.4 Overall Behaviour

The data shows that particles with higher  $d_0$  values reach steady state quicker. This time is also reduced by increasing the uptake of energy  $q_0$ .

Particles showing overdamped dynamics do not overshoot the steady-state value. Underdamped particles, however, overshoot the steady-state values and then relax to the final steady-state value by oscillating around it.

In case A4 it was seen that even with a large amount of energy available, there was still an underdamped oscillatory response in both energy and velocity. The particles take longer to reach steady-state as the consumption of energy is affected more by  $v$  than  $d_0$  as per eq. (3.4.2c).

#### 4.2.5 Conclusions

Active Brownian particles with empty energy depots were simulated over short trajectories from rest. By looking at the ensemble averages of the velocity  $v$  and energy  $e$  the dynamics of these particles in this scenario were observed.

One of the questions posed by this thesis is under what circumstances the adiabatic assumption that the timescale of depot energy relaxation is much quicker than that of the acceleration holds true.

The cases may be classified as adiabatic or non-adiabatic based on whether or not the above assumption on energy assimilation holds true.

For cases A4-E4, the  $\beta$  value is higher (100), however it is seen that within the low velocity regime there is no adiabatic relaxation of the energy. The energy oscillates as a result of the velocity increasing and decreases once the velocity reaches a high enough level to consume energy faster than it is accumulated. Once this energy

is consumed, the drag force is greater than the active acceleration and the velocity tends back towards the stationary point. A lag between the uptake of energy and the acceleration of the particles was seen in the intermediate and non-adiabatic cases.

The energy conversion formula is:

$$\dot{e} = q_0 - ce(t) - d_0v(t)^2e(t) \quad (4.2.2)$$

Across the data sets, comparing (referencing table 4.5) the resulting values of  $\langle |v| \rangle_{SS}$  and  $\langle e \rangle_{SS}$  from the simulations with the analytical values  $\beta$  and the corresponding calculated values of energy using  $\beta$  it can be seen that the simulation average values are not equivalent under the adiabatic assumption and that therefore the adiabatic assumption does not apply in this parameter space. For low values of  $q_0$ , there is not enough energy in the depot at any time for the rate of energy uptake to be independent of  $e$ . When  $q_0$  is high but  $d_0$  is low, the effect of  $v$  on the energy in the depot is minor compared to the decay from dissipation and the passive uptake. In the most active case E4 it is seen that the particle behaves adiabatically because the velocity will be high enough from the active component of the force such that it quickly depletes any energy added to the depot.

Because cases A1-A4 have values of  $d_0$  which are so low, the particles are frequently governed by the Brownian forces and moving at low velocities around about 0. The depletion of the energy depot in these cases is thus more governed by the quantity  $e$  than the value of the velocity and the particles are less likely to enter the adiabatic limit.

As a reference, the value of dimensionless  $\langle |v(t)| \rangle$  and  $\langle e(t) \rangle$  were taken at the end of these trajectories ( $\gamma_0 t = 100.0$ ). These values are close to the simulated steady-state values  $\langle e \rangle_{SS}$  and  $\langle |v| \rangle_{SS}$  within a reasonable statistical variance as an artefact of simulating a finite population.

Case A1 has been discounted from the summary of these values in table 4.5 as this case did not reach the steady-state within the time frame. The value of  $\beta$  was calculated for the particles in each case along with the adiabatic energy found at both the calculated mean  $\langle |v| \rangle_{SS}$  value and also that of the pumping energy  $e_p$ , which is the adiabatic energy at the stationary point  $v_0 = \beta^{1/2}$ .

The energies listed in the table show that for the less active and more fuel-starved cases there is no correlation between  $\langle e \rangle_{SS}$  and  $e_0(\langle |v| \rangle_{SS})$  (calculated adiabatic energy from velocity stationary point). As  $q_0$  is increased with  $d_0$  the differences between  $\langle e \rangle_{SS}$  and  $e_p$  reduce. In cases E3 and B4-E4 these values are almost the same. This indicates that these particles are behaving more adiabatically.

It was seen that with the exception of case A1, all simulations arrived at steady-state by  $t = 100$ . It was concluded that for  $t > 100$  the system is no longer influenced by the initial conditions — this point will be used in the next section to analyse particles after they have arrived in the steady-state region; and observe their non-equilibrium dynamics near these fixed points.

Particles were driven towards their steady-state fixed points at different rates and with different dynamics — either overdamped or

underdamped. In Section 4.4 the dynamics of how particles move towards these fixed points in  $v - e$  phase-space will be discussed.

The consumption and depletion of the energy within the depot causes for the particles to accelerate towards the stationary point in  $v - e$  space  $(v_0, e_p)$ , above which point the static friction on the particle is higher than the active component of the active friction  $\gamma(v)$ . From the data, it is not possible to determine which cases can be classified as adiabatic as the systems were started from a fixed point and allowed to transition to their stationary states within this time. In the subsequent sections, analysis on steady-state particle systems will be carried out in order to investigate this adiabatic assumption more fully.

This behaviour may not be evident in parameter regimes with high values of  $c$  where the rate of depot depletion at lower velocities (the  $-ce$  term in the update formula) is of a similar order of magnitude to the velocity-dependent conversion term.

This analysis of initial behaviour has shown that the particle behaviours reach a stationary state and that there are different dynamics governing the arrival at that state depending on the varied simulation parameters.

## 4.3 Steady-State Particle Velocity Distributions

### 4.3.1 Introduction

In the previous section, it was seen that most of the particle ensembles arrived at a steady-state by 100 time units. The dynamics of this approach varied, but in the higher energy uptake (higher values of  $q_0$ ) cases and the more active (higher  $d_0$ ) cases it was seen that there was a quicker response in the depot energy level and its conversion into kinetic energy.

In this section, simulation results are presented in the form of 1-D velocity distributions for all parameter sets. A discussion of the behaviours observed in each case is then presented. The behaviours are generalised into separate cases depending upon their shapes and adherence with the adiabatic energy approximation.

### 4.3.2 Simulation Parameters

For each parameter set (table 4.4) a single particle trajectory was simulated starting from rest with an empty depot ( $e(t = 0) = 0$ ,  $v(t = 0) = 0$ ) for a total simulation time of  $t_{end} = 5000$  with a time step of  $\Delta t = 0.01$ . Bias from the initial conditions were filtered from the results by introducing a *measurement start time* of  $t = 200$  — chosen based off of the times to reach steady state from Section 4.2 — before which the data points were discarded. Each simulation was repeated 5000 times with the same conditions. This resulted in  $\approx 2.4 \times 10^9$  unique data points for  $v(t)$  per simulation.

The mean value of the velocity  $\mu_v$ , the standard deviation of the

velocity  $\sigma_v$ , and the corresponding values for the absolute velocities  $\mu_{|v|}$  and  $\sigma_{|v|}$  were calculated from the results. ED particles form bimodal distributions in velocity in 1-D, and due to their symmetrical behaviour (as discussed in Section 3.4) are expected to have a mean value  $\mu_v = 0$ . Taking the absolute value of  $v$  before averaging gives more of an insight into the average behaviour of the particles in motion.

The velocity distributions of the results are visualised in this section using histograms which show the probabilistic behaviour of the particle velocity for each case. Each histogram initially contains 200 bins of equal width between the origin and the maximum observed value of  $|v|$ . The points plotted on the graphs represent the centre of each bin. The number of values in each bin was normalised by twice the total number of  $v$  values and reflected around the y-axis (the factor of 2 is required due to the number of total points plotted doubling to 400). This means that twice as much statistical data is generated due to the symmetry of the velocity distributions.

Alongside the stochastic calculated distribution curves, the analytical solution to the steady-state FPE for an adiabatic particle is also plotted (eq. (3.4.12)) for each case. The conformity of the stochastic results with this analytical solution may be observed graphically.

### 4.3.3 Results

#### 4.3.3.1 Inactive Velocity Distributions

The stochastic velocity distributions for an OU particle calculated using the numerical method outlined by Gillespie[79] (Section 3.5.1.1) as well as that of an inactive particle with an ED ( $d_0 = 0$ ) are presented alongside the analytical solution to the OU FPE (eq. (3.1.11)) in fig. 4.7. All curves are normalised for  $\int_{-\infty}^{\infty} dv P(v) = 1$ .

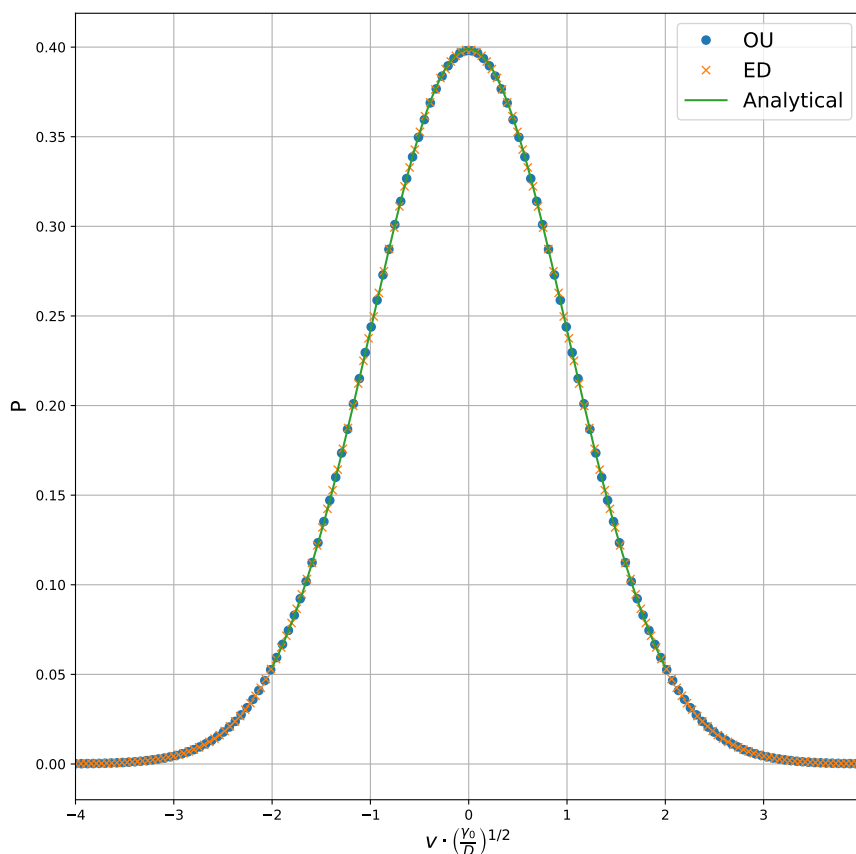


**Figure 4.7:** Velocity distributions of underdamped Brownian particles showing analytical solution to OU FPE (green line), Gillespie methodology[79] for an exact numerical solution to the OU process (blue circles) and normalised histogram of stochastic simulation for an inactive ED particle (orange crosses).

All three of the results are consistent with each other. The normal

(Gaussian) distributions are centred around  $v = 0$  which is consistent with the expected behaviour from the theory and also serves as a benchmark for the simulation methodology and implementation. The values of  $\sigma_v$  and  $\mu_v$  were calculated from both sets of data as 1.0 and 0.0, respectively. From eqs. (3.1.10) these can be seen at steady state to be consistent with the dimensionless expected values for this distribution.

#### 4.3.3.2 Active Velocity Distributions

Figures 4.8, 4.9, 4.10, 4.11 and 4.12 show the velocity distributions for all 20 of the parameter cases A1-E4 plotted against the analytical solution to the FPE for an adiabatic particle for each set of parameters.

The plots are presented in groups of constant  $d_0$  values with the subplots showing the different  $q_0$  values. For each subplot, the calculated value of the dimensionless stationary velocity  $v_0^D = \pm\sqrt{\beta}\left(\frac{\gamma_0}{D}\right)^{1/2}$  is labelled with a grid line on the  $v$ -axis for reference. The calculated statistical data for the particles is summarised in table 4.6.

Each result is discussed in detail in order to identify trends and behaviours across the parameter range and to observe the relationship which increasing  $d_0$  and  $q_0$  has on the behaviour of the particles.

As previously discussed, the analytical solution to the FPE makes the assumption that the particle is adiabatic in  $e$  ( $\dot{e} = 0$ ).

The degree of agreement with the adiabatic assumption can be seen by comparing the expected value of  $P(v)$  on the plots. Further

**Table 4.6:** Summary of statistical means and standard deviations for simulations over all 20 parameter pairings. The mean and standard deviation of the absolute values of the velocity are also shown, as they are more useful in analysing bimodal distributions.

| Case | $\beta^D$ | $ v_0 ^D$ | $\sigma_v$ | $\sigma_{ v }$ | $\mu_v$ | $\mu_{ v }$ |
|------|-----------|-----------|------------|----------------|---------|-------------|
| A1   | 0.90      | 0.949     | 1.396      | 0.839          | 0.000   | 1.116       |
| A2   | 9.90      | 3.15      | 3.302      | 1.809          | -0.004  | 2.763       |
| A3   | 19.90     | 4.46      | 4.571      | 2.169          | -0.006  | 4.024       |
| A4   | 99.90     | 10.0      | 10.045     | 1.255          | 0.120   | 9.967       |
| B1   | 0.99      | 0.995     | 1.412      | 0.830          | 0.002   | 1.143       |
| B2   | 9.99      | 3.16      | 3.315      | 1.308          | 0.006   | 3.046       |
| B3   | 19.99     | 4.47      | 4.582      | 1.085          | 0.017   | 4.451       |
| B4   | 99.99     | 10.0      | 10.054     | 0.777          | 0.101   | 10.025      |
| C1   | 0.995     | 0.997     | 1.413      | 0.817          | -0.000  | 1.153       |
| C2   | 9.995     | 3.16      | 3.316      | 1.107          | 0.006   | 3.126       |
| C3   | 19.995    | 4.47      | 4.581      | 0.906          | 0.143   | 4.493       |
| C4   | 99.995    | 10.0      | 10.059     | 0.742          | 0.060   | 10.032      |
| D1   | 0.998     | 0.999     | 1.413      | 0.789          | -0.001  | 1.173       |
| D2   | 9.998     | 3.16      | 3.318      | 0.871          | -0.012  | 3.201       |
| D3   | 19.998    | 4.47      | 4.584      | 0.773          | 0.089   | 4.519       |
| D4   | 99.998    | 10.0      | 10.078     | 0.717          | -0.141  | 10.053      |
| E1   | 0.999     | 0.999     | 1.414      | 0.774          | 0.001   | 1.183       |
| E2   | 9.999     | 3.16      | 3.318      | 0.806          | -0.025  | 3.219       |
| E3   | 19.999    | 4.47      | 4.569      | 0.745          | -0.418  | 4.527       |
| E4   | 99.999    | 10.0      | 10.083     | 0.703          | 0.020   | 10.058      |

information can be obtained from the energy distribution, which will be examined in a later section.

It is initially of interest to observe the behaviours in the least-active/least-fuelled case (A1) and most-active- most-fuelled case (E4). The subsequent analysis of intermediate parameter values may then be put into context by the results from these extremes.

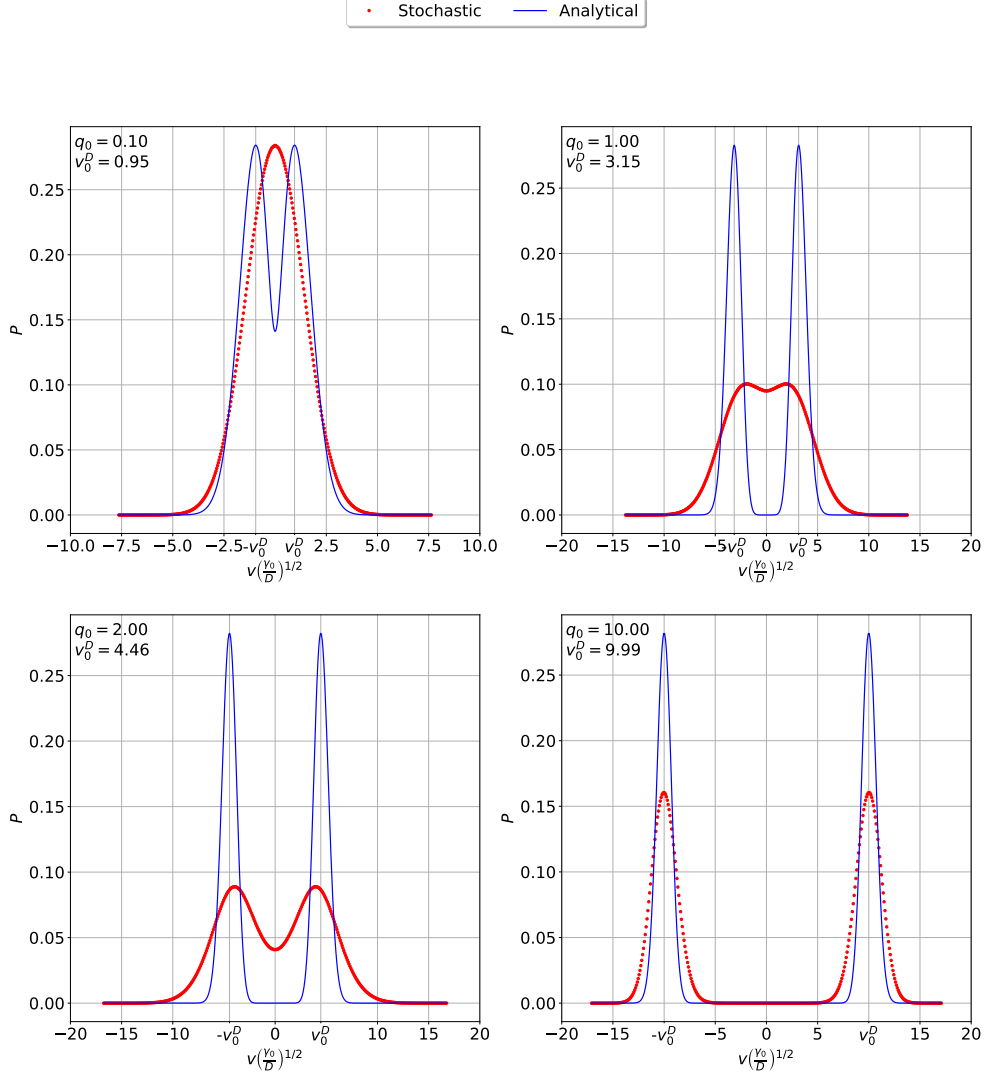


**Figure 4.8:** Stochastic and analytical dimensionless velocity distributions for  $d_0 = 0.1$  with varying  $q_0$  (top-left: A1, top-right: A2, bottom-left: A3, bottom-right: A4). Other parameters  $\gamma_0 = 1.0$ ,  $D = 0.1$ ,  $c = 0.001$ .

In case A1 (top-left fig. 4.8), it is clear that there is a stark difference between the stochastic behaviour and that of the analytical adiabatic solution; and so it may be said that the particle is non-adiabatic. The velocity distribution resembles that of the inactive OU process and the mean  $\mu_v = 0.0$  as seen in table 4.6. The standard deviation  $\sigma_v$  was measured as 1.396 which is greater than the value for the inactive OU case, showing that the distribution of velocities

itself is wider and that in the active case the particle is being accelerated. Even with such a low level of activity and access to fuel, a marked increase in the expected velocity of the particle can be seen, though the shape of the distribution appears to be the same.

There is no bifurcation of the velocity stationary points, instead the distribution is that of a flattened Gaussian. Particles are driven towards the stationary points by the active component of the force (depot consumption), but this component is overwhelmed by the stochastic force. The depot consumption thus simply accelerates the particle forward with no clear dynamics of acceleration towards a fixed point. The direction is dependent on whether the stochastic force causes for a switch across the  $v = 0$  boundary.

Case E4 (bottom-right fig. 4.12), appears completely adiabatic — with the calculated velocity distribution perfectly matching the analytical solution of the adiabatic FPE (3.4.12). The distribution is bimodal and symmetrical around the y-axis. The calculated mean is seen to be close to 0.0. The value of  $\sigma_v$  is 10.083. The value of  $\mu_{|v|}$  is 10.058 — the particle on average is located at the fixed points at  $\pm v_0$ . The  $\sigma_{|v|}$  value of 0.703 is lower than the standard deviation of the inactive OU case, indicating that the active particles are being driven to a narrower band of velocities by the active force (i.e. towards the fixed velocity  $v_0$ ). From the previously phase-space diagram (fig 3.4) it can be seen that active particles are indeed expected to be driven towards the fixed points in space at  $(v_0, e_p)$ .

If the particles are behaving adiabatically as the matching of the

velocity curves suggest, then the depot energy will be fixed along the  $e_0$  line in  $v - e$  space. It is also seen that  $P(v = 0) \approx 0$ , which suggests that there is a barrier to particles moving at this lower velocity and even switching directions. This is shown in the phase-space diagram as well, with  $e$  being at a maximum at  $v = 0$ . This behaviour will be discussed in more detail in the following section.

These observations of the least and most active cases have highlighted the emergence of two different behaviours. In case A1 there appears to be an OU-like distribution of velocities with an increased variance on account of the active contribution to the force, as if this was added on to the existing stochastic force. In case E4 the particles behave adiabatically, and the well understood bifurcation of the velocities around the two stationary points  $(\pm v_0, e_p)$  emerges; with no probability of the particle existing at low velocities.

The remaining distributions will now be discussed in this context, in order to try and understand the dynamics of these particles when they are not adiabatic but exhibit more complex active behaviour than case A1.

None of the cases A2 – A4 (top-right, bottom-left, bottom-right fig. 4.8, respectively) are behaving adiabatically as the stochastic and analytical distributions differ. In cases A2 and A3 the peaks of the emergent bimodal distributions are not located at the stationary velocities  $\pm v_0$  but are instead located at lower values of  $|v|$ .

Both of these cases also show a clearly non-zero value of  $P(v = 0)$ , which is in contrast with case A4 where the high value of  $|v_0|$

prevents the stochastic force and static friction from slowing the particles down enough for them to transition through this region and change directions.

In all three cases the value  $\mu_{|v|}$  is lower than the value  $|v|_0^D$ , however the emergent distributions have a wider deviation which leads to the possibility of particles accelerating to a higher maximum velocity. This suggests that there must be excess energies in the depot in some cases, allowing for additional acceleration.

In the adiabatic case, this would not be possible — as the depot would relax to its expected value  $e_0(v)$ . This could be made possible in this case by periods of time spent travelling at lower velocities. As  $\dot{e}(v)$  is a function of  $v^2$ , less energy from the depot would be used immediately at these slow speeds. Once the particle enters a phase of acceleration, it would be turbo-charged by a value of  $e > e_0$  and accelerate over a longer period of time to a higher final velocity. The particles are behaving in a similar manner as when starting from rest with an empty depot, as outlined in figs. 4.5 and 4.5

For case A4 this is seen by a standard deviation for each of the peaks on the distribution of  $\sigma_{|v|} = 1.224$ , higher than that seen from both a pure OU particle and the adiabatic case E4.

None of these parameter sets exhibit the behaviours seen in the extreme cases A1 and E4. The slow conversion of energy from the low  $d_0$  value suggests that the depot energy can fluctuate widely for any given value of velocity, and this manifests in all three cases by a non-adiabatic and less of a tendency to drive straight towards the

stationary velocity.

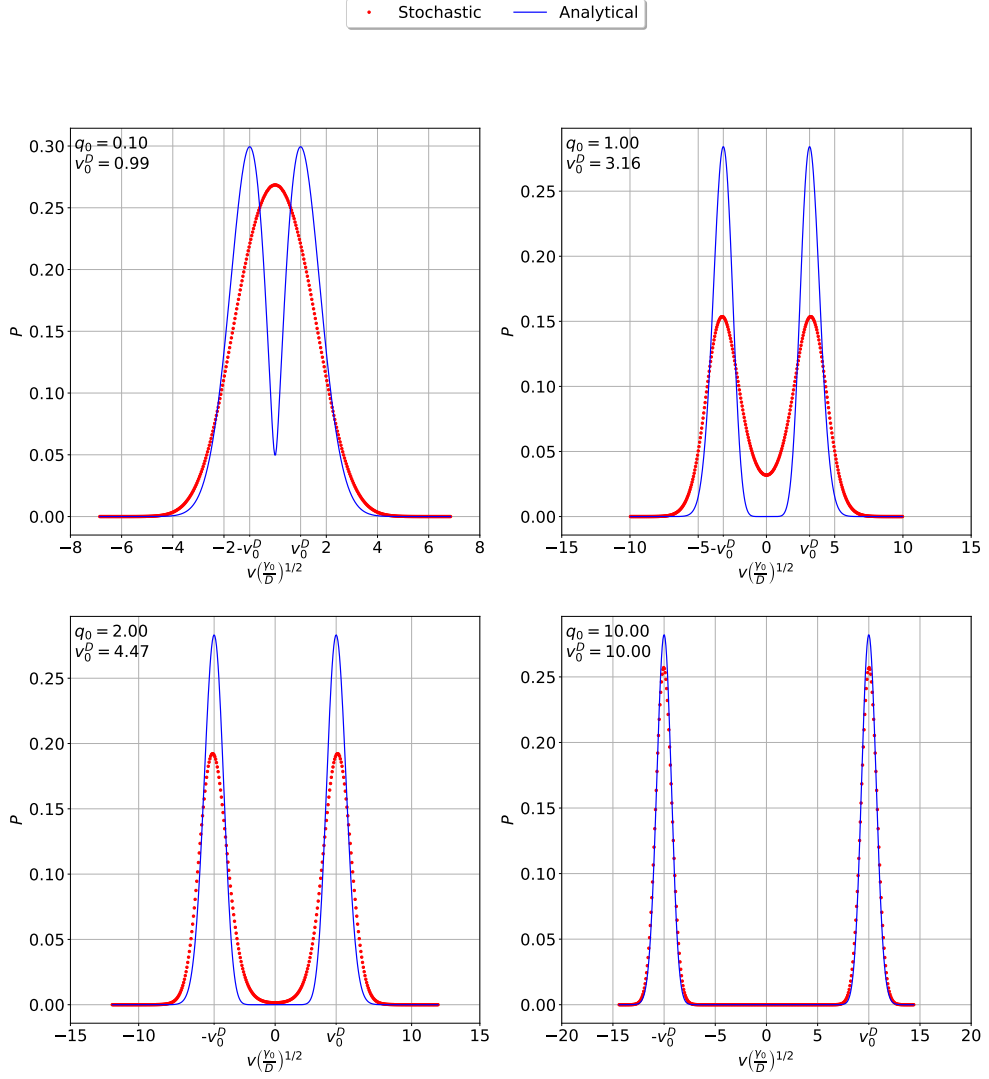


**Figure 4.9:** Stochastic and analytical dimensionless velocity distributions for  $d_0 = 1.0$  with varying  $q_0$  (top-left: B1, top-right: B2, bottom-left: B3, bottom-right: B4). Other parameters  $\gamma_0 = 1.0$ ,  $D = 0.1$ ,  $c = 0.001$ .

When  $d_0$  is slightly higher, as with cases B1-B4 (fig. 4.9), the rate of depot energy conversion into kinetic energy is increased. The results show that this increase from cases A1-A4 to B1-B4 is not enough to cause the particles to behave adiabatically on its own.

The behaviour of case B4 close to adiabatic, but there are still differences in the analytical and stochastic results. Particles velocities

were recorded more frequently further away from the stationary velocity than would be the case if the behaviour was adiabatic, which corresponds to more time spent further away from the fixed points. This is the same behaviour but less pronounced than that in case A4 (fig. 4.8).

In case B1 (low energy uptake  $q_0 = 0.1$ ) the particle behaves similarly to case A1 — with a wider deviation  $\sigma_v = 1.412$  for B1 whereas for A1  $\sigma_v = 1.396$ . The higher  $d_0$  value results in a higher stationary velocity  $v_0$ . This slightly conversion rate leads to higher velocities which widens the distribution. For the absolute values of velocity the deviation from  $\mu_{|v|}$  is marginally lower for B1 ( $\sigma_{|v|} = 0.839$ ) compared to A1 ( $\sigma_{|v|} = 0.830$ ). This shows that particles are being more driven towards non-zero  $v$  (i.e.  $v_0$ ) and precludes the emergence of the bimodal distributions seen in B2 and B3.

Particles moving at lower velocities are accelerated slightly towards the stationary velocity  $v_0$ . There is then a lower probability of the particle being stationary than in a pure OU case, but no emergence of the double-peaked bimodal behaviour of particles with access to more energy.

Cases B2 and B3 are other examples of situations where the particles are transitioning between these stochastic and depot dominated regimes. The value of  $P(0)$  for case B2 is clearly non-zero, whilst B3 has a finite but small probability of being stationary. The increase in activity for cases B2-B4 shows a narrowing of the distribution as  $\sigma_{|v|}$  is smaller than for the first set of parameters A1–4. As activity

is increasing, the particles propensity to return to the stationary velocity  $v_0$  also increases due to the  $v^2$  relationship with  $e(v)$ . As the active force overtakes the stochastic force by orders of magnitude, deviations away from these fixed points become more limited in magnitude as particles deplete energy quicker.

It can therefore be concluded that an the increased rate of conversion reduces the likelihood of a buildup of energy in the depot. The particles will be confined to narrower areas in  $v - e$  phase-space. This increase in  $d_0$  compared with the first set of parameters has shown that increasing  $d_0$  has more of an effect on limiting the distribution of the values of  $v$ , as compared with  $q_0$  which determined the exact position of the stationary point.

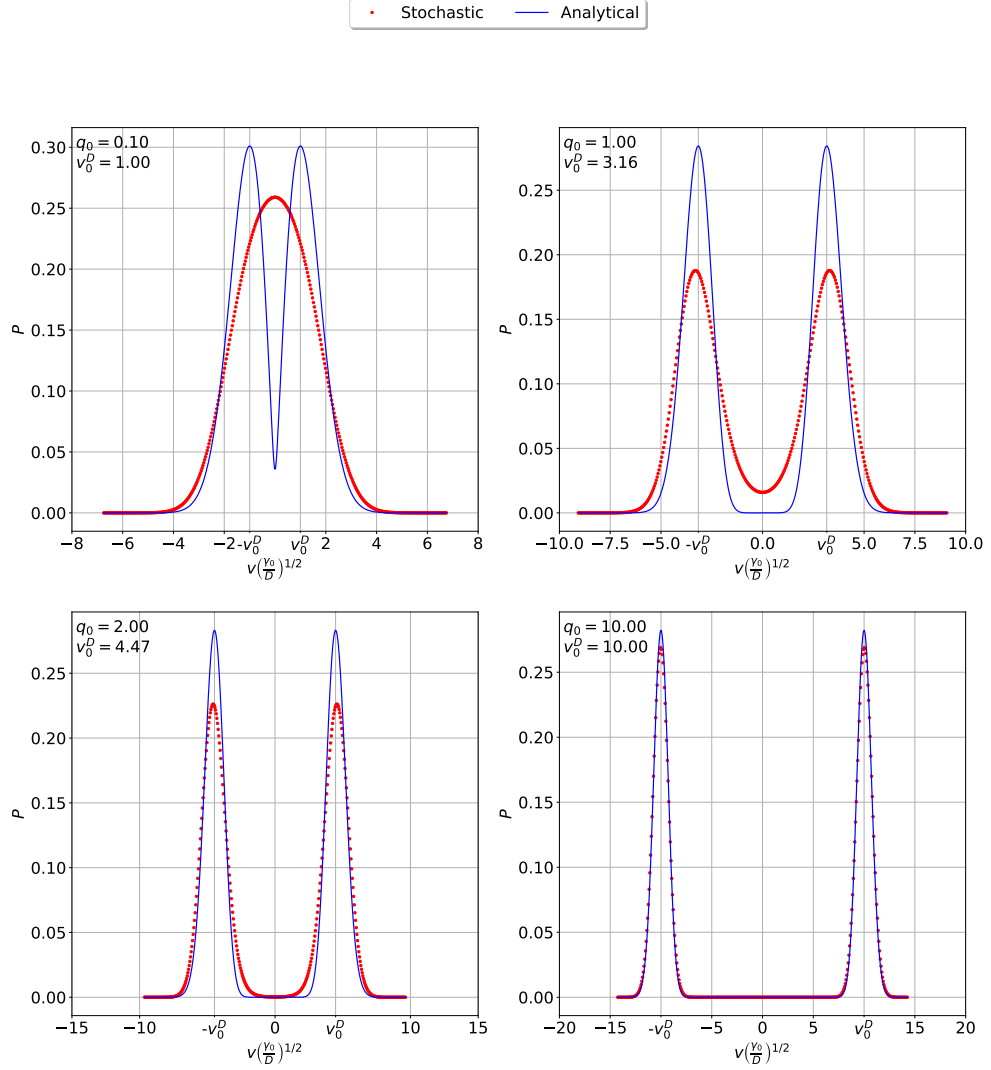


**Figure 4.10:** Stochastic and analytical dimensionless velocity distributions for  $d_0 = 2.0$  with varying  $q_0$  (top-left: C1, top-right: C2, bottom-left: C3, bottom-right: C4). Other parameters  $\gamma_0 = 1.0$ ,  $D = 0.1$ ,  $c = 0.001$ .

In cases C1–4 (fig. 4.10) a similar pattern to the previous cases is seen. Case C1 is much like A1 & B1, the value of  $\sigma_v = 1.413$  is also very close to the previously calculated values for this value of  $q_0$ . The distribution shape has changed with particles more likely to be found at non-zero velocities than before, again suggesting driving towards the stationary velocities but showing that the stochastic force is still the main driver of motion. None of the cases fit well

with the analytical adiabatic curve. As with case B4, case C4 is a much closer fit than any previous case has been. The overall trend is again that the increase in energy conversion is narrowing the distribution of the velocities around about the stationary points which are determined primarily by the uptake rate. As with before, for the lower  $q_0$  cases of B2 and C2 the value of  $v_0$  is close enough to the origin that the distributions on either side overlap and a non-zero  $P(0)$  is seen. It may also be seen that in in case C4, much like all of the high  $q_0$  cases, the  $v_0$  value is many orders of magnitude of  $D$  away from the origin. This means that the active force will always overcome the stochastic attempt to change the particle direction and force the particle back to the stationary points.

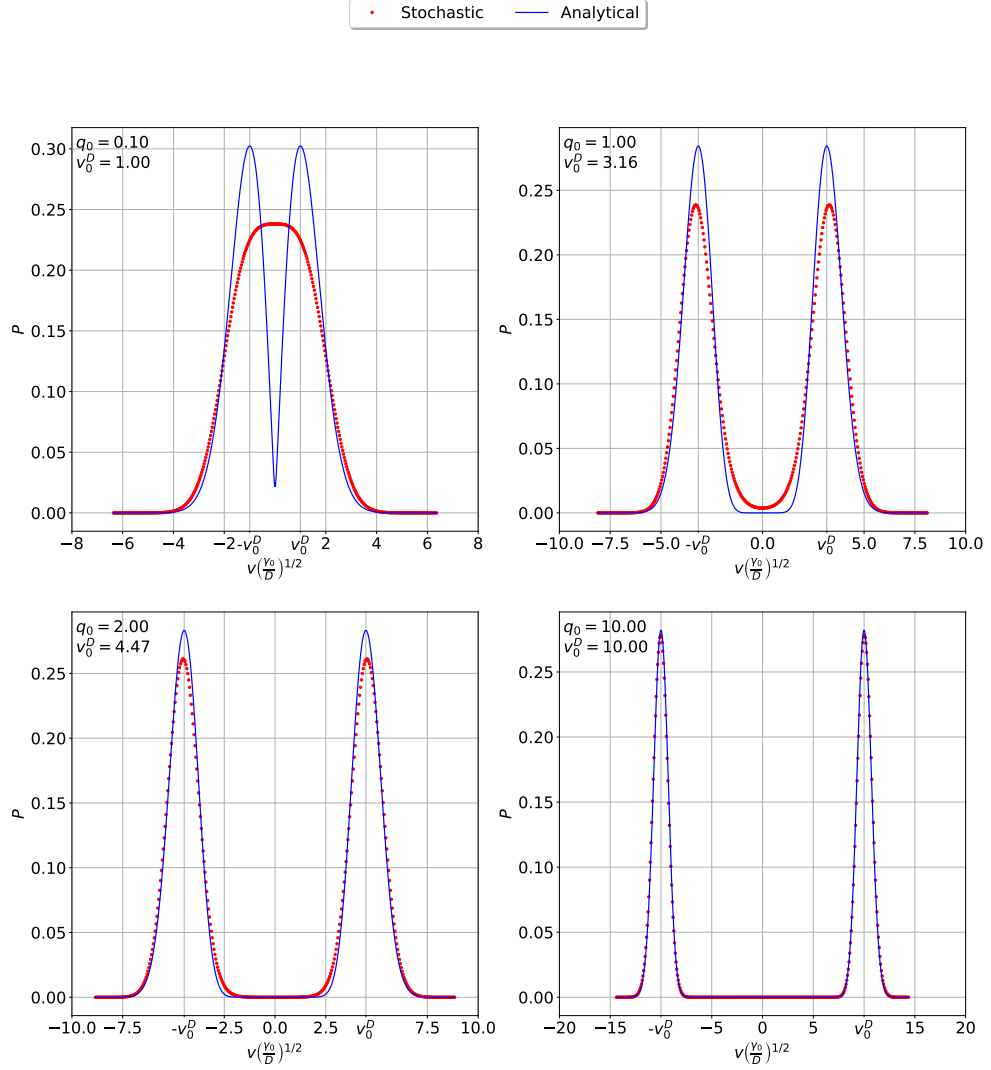


**Figure 4.11:** Stochastic and analytical dimensionless velocity distributions for  $d_0 = 6.0$  with varying  $q_0$  (top-left: D1, top-right: D2, bottom-left: D3, bottom-right: D4). Other parameters  $\gamma_0 = 1.0$ ,  $D = 0.1$ ,  $c = 0.001$ .

Increasing the rate of depot consumption  $d_0$  further in cases D1–4 (fig 4.11) shows the same trend again. Case D1 is once more a “flattened” Gaussian, with a standard deviation of  $\sigma_v = 1.413$ . Like in the previous  $q_0 = 0.1$  cases, the energy in the depot is too small to completely change the dynamics of the motion, however the particle is accelerated slightly away from the origin at low velocities. It can again be noted that the stochastic force is the main driving

force here and there is no development of a bifurcated distribution, though the peak of the distribution is flattening.

In case D2 the width of the individual peaks of the bimodal distributions are narrower than in case C2, with the standard deviation of the absolute velocities reducing to  $\sigma_{|v|} = 0.871$  from  $\sigma_{|v|} = 1.107$ . There is still a non-zero value of  $P(0)$ , so the particles are not confined to motion in one direction.

D3 shows a behaviour very similar to the previous near-adiabatic cases in that the stochastic and adiabatic-analytical curves almost match. There is a very low probability of a switch in this case as  $P(0) \approx 0$ , though the distribution of velocities around about the stationary point is wider than for an adiabatic particle. D3 and D4 thus show very similar behaviours, with particles driven towards the stationary velocity. The large differences in the stationary velocity however mean that whilst D3 may be able to switch sometimes, D4 never can. Though the D4 distribution is close to the adiabatic case, there is a slight deviation. The higher activity and energy available confines the energy to values closer to the theorised adiabatic energy  $e_0$ , but the differences in the distribution show slight deviations away from this value.

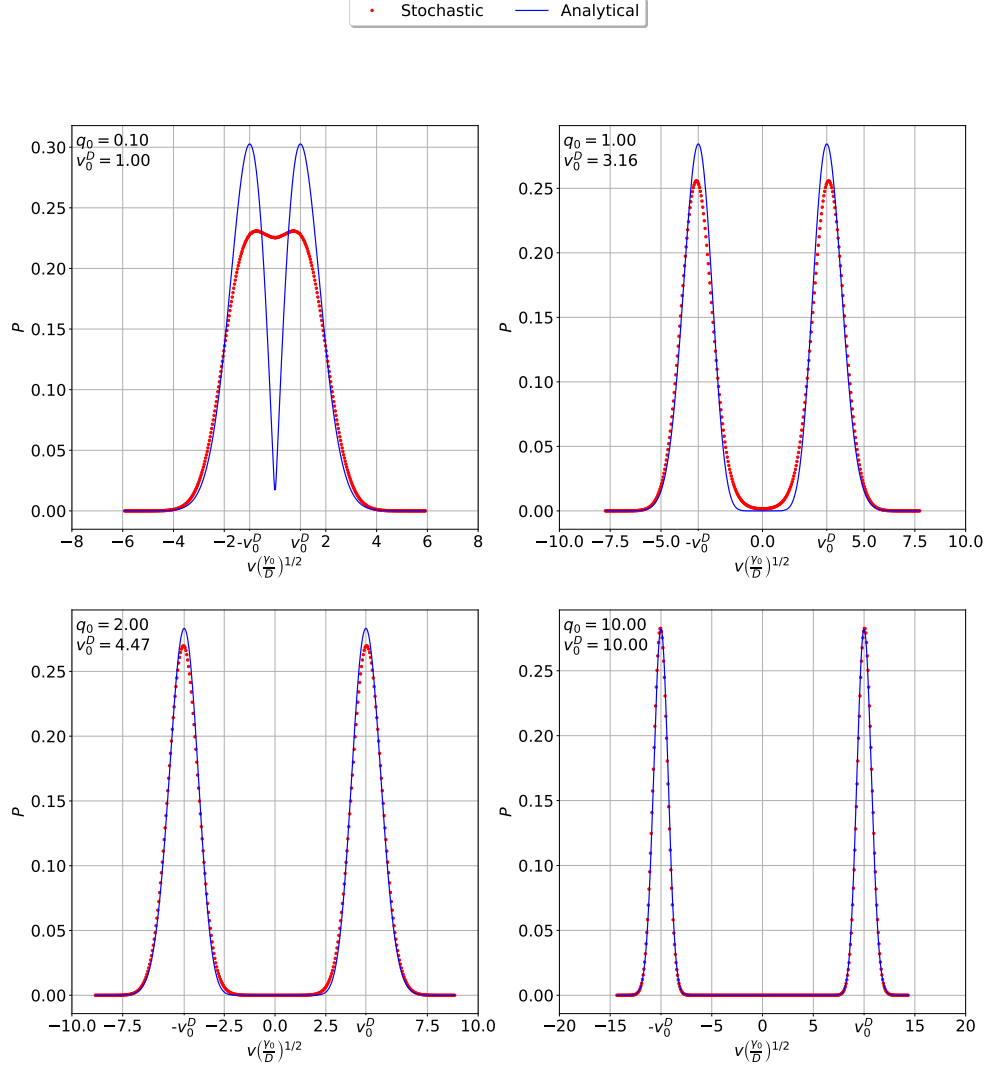


**Figure 4.12:** Stochastic and analytical dimensionless velocity distributions for  $d_0 = 1.0$  with varying  $q_0$  (top-left: E1, top-right: E2, bottom-left: E3, bottom-right: E4). Other parameters  $\gamma_0 = 1.0$ ,  $D = 0.1$ ,  $c = 0.001$ .

Finally, the velocity distributions for the highest values of  $d_0$  (cases E1-E4) are shown in fig. 4.12. E1 is an interesting case as the standard deviation of the points is very close to the values from all of the other simulations for this value of  $q_0$  at  $\sigma_v = 1.414$ , yet the twin peak of the bimodal distribution is emerging. Table 4.7 shows the ratio of the  $\sigma_v$ ,  $\sigma_{|v|}$  and  $\mu_{|v|}$  values to  $|v_0|^D$  for all cases. It is seen that the low  $d_0$  cases all have a  $|v_0|^D$  on the same order of

**Table 4.7:** Ratios of standard deviations and mean to the absolute stationary velocity  $|v_0|^D$  for all cases.

| Case | $\sigma_v /  v_0 ^D$ | $\sigma_{ v } /  v_0 ^D$ | $\mu_{ v } /  v_0 ^D$ |
|------|----------------------|--------------------------|-----------------------|
| A1   | 1.471                | 0.884                    | 1.176                 |
| A2   | 1.048                | 0.574                    | 0.877                 |
| A3   | 1.025                | 0.486                    | 0.902                 |
| A4   | 1.004                | 0.126                    | 0.997                 |
| B1   | 1.419                | 0.834                    | 1.149                 |
| B2   | 1.049                | 0.414                    | 0.964                 |
| B3   | 1.025                | 0.243                    | 0.996                 |
| B4   | 1.005                | 0.078                    | 1.002                 |
| C1   | 1.417                | 0.819                    | 1.156                 |
| C2   | 1.049                | 0.350                    | 0.989                 |
| C3   | 1.025                | 0.203                    | 1.005                 |
| C4   | 1.006                | 0.074                    | 1.003                 |
| D1   | 1.414                | 0.790                    | 1.174                 |
| D2   | 1.050                | 0.276                    | 1.013                 |
| D3   | 1.026                | 0.173                    | 1.011                 |
| D4   | 1.008                | 0.072                    | 1.005                 |
| E1   | 1.415                | 0.775                    | 1.184                 |
| E2   | 1.050                | 0.255                    | 1.019                 |
| E3   | 1.022                | 0.167                    | 1.013                 |
| E4   | 1.008                | 0.070                    | 1.006                 |

magnitude as  $\sigma_{|v|}$  (i.e. the ratio is close to 1). In other words, the particles are not driven to regions of  $v$  where the active force dwarfs the stochastic force. The particles spend parts of their trajectory at lower  $v$  where the active contributions — though present — are very weak. Once  $d_0$  is suitably high (as in case E1) the particles will accelerate and consume energy during times at higher  $v$ , but behave similarly to the other cases A1-D1 at lower  $v$ . As with all other cases A1-D1, the adiabatic assumption does not hold for these parameters.

The intermediate cases E2 and E3 behave similarly to the prior cases D2 and D3. The distribution of velocities around the stationary points is again narrowing. This is seen by the lower value of  $\sigma_{|v|}$  for these cases. It can be seen that with such a large increase in  $d_0$ ,

the relative reduction in the width of the distribution is minor, as the particles near complete adiabatic behaviour. Nevertheless, both distributions fail to match the analytical solution for an adiabatic particle. In case E2 the probability of the particle being stationary  $P(v = 0)$  is still non-zero, though the value is very small.

Whether or not a particle can change direction (i.e. travel through  $v = 0$ ) is dependent on both  $q_0$  and  $d_0$ . For the chosen parameters  $c$  and  $\gamma_0$ , the value of  $q_0$  has a much larger effect on the value of  $v_0$  than  $d_0$  does. Because the value of  $D$  is kept the same in all cases, as the  $q_0$  value is increased from case B2 to B3, the velocity of the particle relative to the velocity of a purely OU particle and the probability of a stochastic event slowing the particle down enough for a switch to be made reduces. This is complimented by an increase in  $d_0$ , which forces for the particle to react quickly to any changes in its internal depot and move faster towards its fixed points. The combined effect of a higher  $d_0$  and  $q_0$  values is to push particles towards adiabatic analytical behaviour. Large enough values of  $q_0$  and  $d_0$  (i.e. E4) confine the depot energy to values on the  $e_0(v)$  line at and around the stationary velocity  $v_0$ . In this case the active force will be orders of magnitude greater than the stochastic force and so the particle can never switch direction.

For particles at or around the stationary velocity  $v_0$  in all non-adiabatic cases, the fact that the velocity does not react instantly to fluctuations in the depot level means that stochastic events may push the particle horizontally in  $v - e$  phase space. The velocity

of the particle may increase as a result of such an event, leaving the depot level above the  $e_0$  curve until the system has a chance to correct itself. The earlier discussed phase-space diagram (fig. 3.4) and streamline plot helps to show how the particle velocity will then be driven from this higher value back towards the stationary point via the  $e_0$  line. When both the  $d_0$  and  $q_0$  values are large enough, the depot level can update quickly due to the  $v^2$  relationship (the value of the stationary velocity is higher) and the larger  $d_0$  coefficient. This will be investigated in more depth in Section 4.4.

This analysis of the particle velocity distributions in different parameter regimes has highlighted four different particle behaviours. This lays the foundations for the subsequent analysis of these particles in non-adiabatic regimes with a view towards defining these behaviours in 1-D. These four behaviours are:

1. OU-like behaviour with a wider distribution. Particle motion is accelerated by consumption of energy in the depot. Lower values of  $|v_0|^D$  (from lower  $q_0$ ) mean that particles are found frequently in low  $v$  regions where the active force (even with higher  $d_0$ ) is less dominant than the stochastic force. Particles are likely to be changing direction with a peak probability at  $P(v) = 0$  in most cases. Seen in all cases with low  $q_0 = 0.1$  (A1-E1).
2. The distribution of velocities is bimodal, with two peaks near to the stationary velocities  $\pm v_0$ . The magnitude of the stochastic force is enough to have some influence over the particles' direc-

tion. Changes in the depot energy are not instantly converted into changes in velocity so the particle may exist at low velocities and high depot energy without necessarily being driven quickly back towards  $|v_0|^D$ . particles are thus able to switch direction. The stationary velocity is low enough that the positive and negative velocity distributions overlap.

3. A more defined bimodal distribution of the particles is seen with larger  $v_0$  and close agreement to adiabatic behaviour. There is still a delay between the energy depot gaining energy and this being converted into kinetic energy, thus the particle can move through regions of  $v - e$  phase space which are not on the  $e_0$  line. Fluctuations in the velocity due to the stochastic force are offset quickly by the more dominant active force which drives the particles strongly back towards the stationary points. It is unlikely for the particle to change directions due to its preference to remain near the stationary points. As  $P(v = 0) \neq 0$ , particles are able to change direction, however the frequency of this is low.
4. The particle behaves completely adiabatically as expected from the theory. The large uptake of energy (and thus higher value of  $|v_0|$ ) coupled with a high conversion rate mean that the particle quickly responds to any deviations in depot energy by updating the velocity — moving through  $v - e$  phase space strictly along the  $e_0$  line. There is no possibility of the particle changing directions once it has begun moving in 1-D.

**Table 4.8:** Summary of observed behaviour types based upon definitions for all parameter variation cases.

| Case | Distribution Type | Case | Distribution Type |
|------|-------------------|------|-------------------|
| A1   | 1                 | C3   | 2                 |
| A2   | 2                 | C4   | 3                 |
| A3   | 2                 | D1   | 1                 |
| A4   | 3                 | D2   | 2                 |
| B1   | 1                 | D3   | 3                 |
| B2   | 2                 | D4   | 4                 |
| B3   | 2                 | E1   | 2                 |
| B4   | 3                 | E2   | 3                 |
| C1   | 1                 | E3   | 3                 |
| C2   | 2                 | E4   | 4                 |

In table 4.8, the data sets are referenced against their observed behaviours according to these defined types. Moving forward, this serves as a reference point when describing and explaining other observed behaviours.

#### 4.3.4 Low Activity Particles

In the cases A1-E1 (Distribution Type-1 particles as per the classification) where  $q_0$  was set to its lowest value, a unique behaviour was seen. The close values of  $\sigma_v$  show that the standard deviation of the particle velocities were all very similar. It was also seen that the distributions were centred around the origin. OU particles have Gaussian distributions in velocity with a  $\sigma_v$  related to the diffusion constant and a mean  $\mu_v = 0$  (eq. (3.1.10)). In order to see more clearly the differences between these curves, they are plotted against each other in fig. 4.13. Alongside these curves, the analytical solution for an OU particle with  $D = 0.1$ ,  $\gamma_0 = 1.0$  is shown. Similarly, a Gaussian distribution with a standard deviation of  $\sigma_v = 1.41$  is shown as a reference to a theoretical OU particle

with a similar standard deviation to the active particles. Case A1

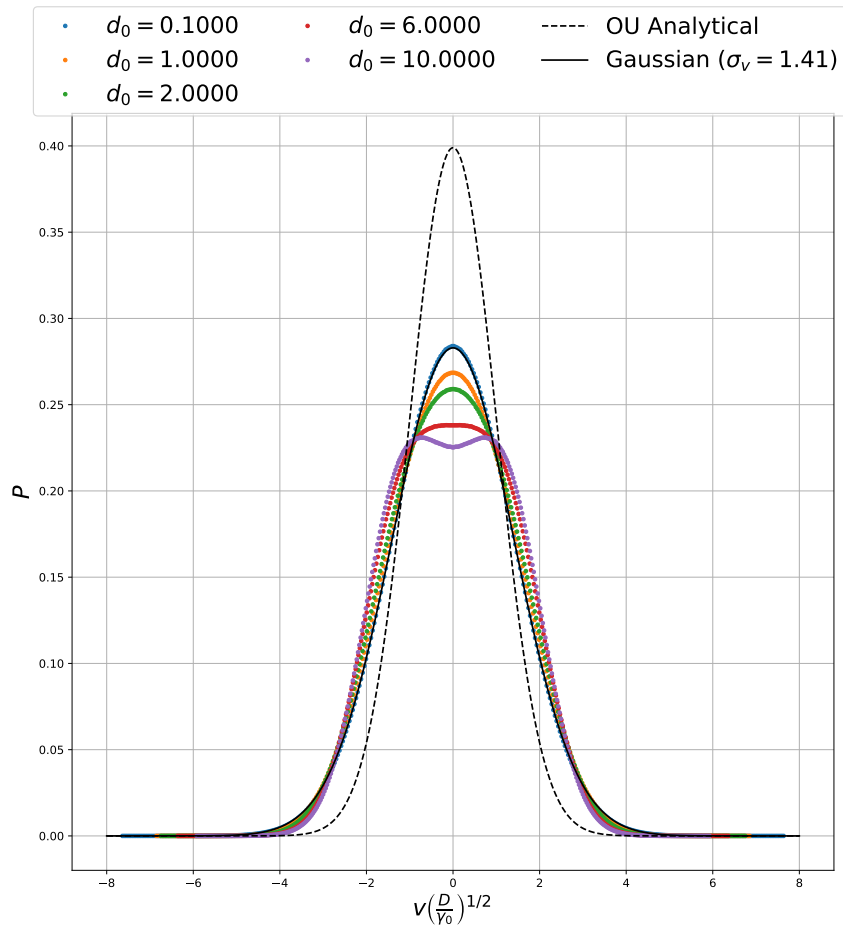


**Figure 4.13:** Dimensionless velocity distributions for particles with  $q_0 = 0.1$  shown alongside an inactive OU distribution and an inactive OU distribution with  $\sigma_v = 1.41$ .

is unique in that it is the only distribution that follows the Gaussian curve. The other cases are stretched wider — the probability of finding particles moving at intermediate velocities is higher but there is a lower probability of the highest values of  $v$  and decreased probability of  $P(v \rightarrow 0)$ . For this low value of  $q_0$  there is not much energy available in the particle depots. The static friction is not easily overcome by the active force (because of low  $e$  and  $d_0$ ) and the motion is mostly dominated by the stochastic force. Figs. 4.4

and 4.6 showed a mostly overdamped response to these particles approaching equilibrium when starting from rest. Individual particles which have depleted their depots and slow down due to friction will display a similar response as they spend time at lower velocities and re-accumulate energy slowly in their depots. Thus the unimodal distribution is seen with a maximum at  $P(v = 0)$ , except for in case E1 where a bimodal distribution is just beginning to appear.

#### 4.3.5 Conclusions

Particle trajectories were simulated for a variety of  $d_0$  and  $q_0$  values. It was seen that increasing the value of  $q_0$  increased the value of the stationary velocity  $v_0$ . Four behaviours emerged from the different parameter sets. The first behaviour showed OU-like distribution of velocity with a mean at  $v_0$  and no emergence of bifurcation of velocities. This was seen in parameter regimes where the rate of energy uptake  $q_0$  was at its lowest and the resultant bifurcation parameter was  $\beta = v_0^2 > \frac{D}{\gamma_0}$ . At low values of both  $d_0$  and  $q_0$  as in case A1, this behaviour was Gaussian with an increased value of  $\sigma_v$ .

Increasing the energy conversion rate  $d_0$  saw the probability at intermediate  $v$  increase with the reduction of  $P(v \rightarrow 0)$  due to the particles expending depot energy to accelerate more quickly. At higher velocities, particles quickly deplete their depots, after which point static friction drives them back towards the  $|v_0|^D$ .

Type-2 distributions exhibit a clear bimodal distribution with the peaks near to the stationary velocity  $v_0$ , but with a clearly non-zero value at  $P(v \rightarrow 0)$ . Particles are able to move through this bound-

ary and spend parts of their trajectories moving at low velocity. These were observed when the particle had a higher uptake of energy  $q_0$ , resulting in a higher level of energy in the depot. The  $|v_0|^D$  value is far enough away from  $v = 0$  that the active dynamics begin to dominate the stochastic events, however particles still find themselves in the low-velocity region and are able to change direction. Increasing  $d_0$  in these cases narrows the width of the distribution near to the stationary velocities, as the correction in the depot energy to fluctuations in velocity becomes quicker the particles are driven to the stationary points more.

Type-3 distributions were defined where  $P(v \rightarrow 0) \approx 0$  such that particles could not switch direction once in motion. Secondly, the particles in this category did not show adiabatic behaviour in terms of the velocity distributions around the stationary velocities. They differ from type-2 particles in that they are unable to switch, and from type-4 particles because they are non-adiabatic. The two bimodal regions of velocity space was not possible but the particles did not behave adiabatically in energy. These particles had high enough values of  $\beta$  that the stochastic motion could not cause the particle to switch direction or the energy conversion rate  $d_0$  was high such that the particle responded quickly to stochastic decreases in velocity and was forced back towards the stationary point. This was seen by the value of  $P(0) = 0$ .

The type-4 particles exhibited adiabatic behaviour in  $e$ . It was seen that these particles had no probability of changing direction or

moving at low  $v$ .

By looking at a range of values of  $d_0$  and  $q_0$  for OU particles with EDs in 1-D, the trends of how particle velocity distributions change as these parameters change have been identified. It is apparent that the value of  $\beta$  on its own does not define the adiabatic behaviour. Similarly, the low value of  $c$  does not make adiabatic behaviour impossible. It was seen that increasing  $d_0$  narrowed the distribution of velocities around the stationary velocities  $\pm v_0$ . Due to the values of  $\gamma_0$  and  $c$  which were chosen, the position of this stationary point was almost entirely controlled by the value of  $q_0$ . Stationary velocities which were large relative to the stochastic forces on the particle showed particles which had no probability of moving at low velocities and thus no probability of changing direction.

It is of interest to understand how the energy behaves over the range of velocities. For non-adiabatic particles a particle moving at a given velocity may have a range of values of depot energy. An adiabatic particles is defined to have an energy which responds instantly to changes in the velocity. The following sections will investigate further how the energy behaves in order to add more resolution to the four classifications made here and the reasons behind these behaviours.

The one-dimensional case is unique in that the pathways through low-velocity spaces are reduced.in 2- and 3-dimensions, other dimensional velocity components can consume energy from the depot and thus the different velocity components are correlated with each

other. The simulations and results within this section help to understand this special case where energy in the depot can only be consumed in a fixed dimension.

## 4.4 Particle Motion in Velocity-Energy Phase-Space

### 4.4.1 Introduction

In the previous section, particles with energy depots were investigated arriving at steady-state in velocity and energy from rest. The velocity distributions of the particles at steady-state were also investigated.

It was seen that by varying the rate of energy uptake  $q_0$  and the energy conversion rate  $d_0$  independently, the particle behaviour both prior to and at steady-state was changed. Particles with a higher  $q_0$  and higher conversion rate  $d_0$  arrived at their steady-state faster and fluctuated less around the steady-state values.

In total, four different behavioural types were observed from the velocity distributions.

In the adiabatic case (D4, E4) the stochastic velocity distribution agreed completely with the theoretical prediction. In some of the other cases, there was a strong similarity though minor differences showed that the particles were not behaving adiabatically. The classifications of all of these cases are summarised in table 4.8.

This section examines the behaviour of particle depot energy in order to investigate further the relationship between the parameters chosen in the model and the emergent adiabatic, OU-like or transitional behaviours outlined in the previous section.

The adiabatic assumption defines the energy as fixed as a function of  $v$  (eq. (3.4.4)) as outlined in Section 3.4.3. This is seen as a line  $e_0(v)$  within  $v - e$  phase-space. When the particles in intermediate

parameter regimes are exhibiting non adiabatic behaviour, it is of interest to know exactly where and by how much the energy is deviating from this line and in what manner.

#### 4.4.2 Simulation Parameters

OU particles with EDs were simulated in 1-dimension starting from rest with empty depots ( $v(t = 0) = 0$ ,  $e(t = 0) = 0$ ) for the same range of parameters which have been covered previously (tab. 4.4). A single particle was simulated over a trajectory length of  $t_{\text{end}} = 30000$  with a time-step  $\Delta t = 0.1$ . The first 200 units of time were ignored for each simulation. In total each simulation therefore contained 298,000 data points. This allowed for the movement of the particle through  $v - e$  phase-space over consecutive time steps to be observed. All other simulation parameters were identical to the previous simulations (as per table 4.2).

#### 4.4.3 Methodology

The value of  $v$  and  $e$  at each point in a trajectory was recorded as an output from the simulation. In order to see the regions of  $v - e$  phase-space through which the particle travels when starting from rest, these were then displayed as individual points on a scatter plot.

The mean behaviour over a trajectory at each velocity was found by splitting the velocity range into 400 bins of equal width. The value of the energy for each point in the velocity trajectory was attributed to the corresponding velocity bin. The arithmetic mean value of energy in each bin was then calculated based upon the

number of data points in each bin.

The theoretical adiabatic energy  $e_0(v)$  for the particles was also calculated and plotted as a line on the graph using eq. (4.4.1). Adiabatic particles have depot energy values fixed to this line for a given velocity, as any fluctuations in  $e$  are assumed to instantly adjust the velocity. For non-adiabatic particles it will be observed how close to this line the mean value of energy lies and for what values of velocity there is agreement.

$$e_0(v) = \frac{q_0}{c + d_0 v^2} \quad (4.4.1)$$

Another important value within the context of these simulations is the pumping energy  $e_p$  (eq. (4.4.2)) which was previously discussed in more detail in Section 3.4.3. This defines the transitional energy value above which particles will undergo pumping — a negative friction term causes a positive contribution to the velocity from the depot. Below this value the particle will be slowed — the static friction is reduced by the active component but the overall friction is still positive.

$$e_p = \frac{\gamma_0}{d_0} \quad (4.4.2)$$

In sections 4.2 and 4.3 the absolute value of the velocity was analysed and distributions were mirrored around the axes. In the following section, the data was analysed in a raw directional format in order to highlight any trajectories which switched direction during the simulations.

#### 4.4.4 Particle Motion through $v - e$ Phase-Space

The dynamics of the active friction  $\gamma(\mathbf{v})$  for an adiabatic particle were discussed in 3.4.4. It was seen that the particles exhibited either pumping or dissipative characteristics depending on the instantaneous velocity, and that the friction drove the particles towards the stationary velocity  $v_0$ .

For non-adiabatic particles, the active friction is dependent on the dynamics of both the depot energy  $e$  and the velocity  $v$ . Again using the concept of an active friction, the particles may now be thought to be driven towards the stationary points within a two-dimensional phase-space  $(v, e)$ . The dynamics of this phase-space are again governed by the set of LEs for the ED model (eqs. (4.1.8)) in the absence of any adiabatic assumptions, as is shown in fig. 4.14.

For deterministic particles, the direction and *velocity* of motion through this space is exactly defined for a set of parameters by the solution to the LEs (eqs. (4.1.8)) where  $\xi(t) = 0$ . For stochastic particles, the deterministic (drift) particle motion through the phase-space is the same — though there is now an additional diffusive component of the motion away from the flow lines as a result of the stochastic force. As a result, at the next discrete time-step the drift motion of the particle through the space will then be dictated by the streamline at the new value of  $(v, e)$  and the stochastic force will continue to cause particle diffusion to other streamlines.

It was previously seen that all of these streamlines in phase-space lead towards the stationary points at  $(\pm v_0, e_p)$ . At these points

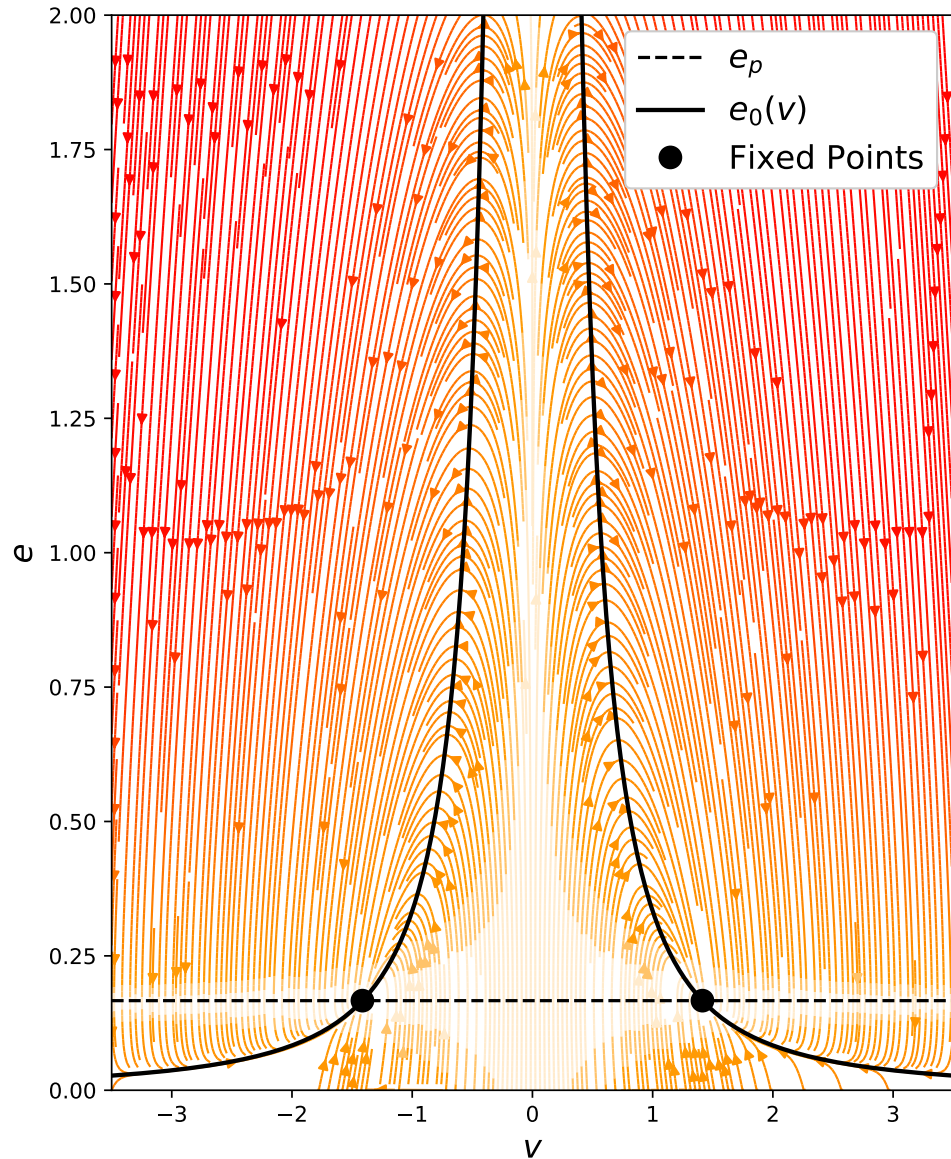


**Figure 4.14:** Velocity and energy streamlines for a deterministic particle with ED. The lines show the particle motion in  $(v, e)$ -space always tending towards the stationary points at  $(v_0, e_p)$ . Example values:  $q_0 = 2.0$ ,  $c = 0.001$ ,  $d_0 = 6.0$ ,  $\gamma_0 = 1.0$ .

$e_p = e_0(v_0)$ , where  $e_p$  is the pumping energy which separates the behavioural regions of the phase-space. Values of  $e$  above  $e_p$  have an effective negative frictional coefficient, where values below have an effectively reduced static friction value. The third stationary point at  $(0, \frac{q_0}{c})$  will not be reached in stochastic systems, as any non-zero particle velocity drives them towards the other stationary

points and the probability of remaining stationary at  $v = 0$  for long enough to gather enough energy to reach this stationary point is extremely small.

The way in which the system reacts to the stochastic force on the particles for different values of  $d_0$  and  $q_0$  will be investigated. These parameters were shown previously to control the position of the stationary points and the distributions of velocities which particles may take. The distribution of energy values and the mean energy values are now investigated.

#### 4.4.5 Scatter Plot of Trajectories ( $d_0 = 0.1$ )

An initial investigation into the behaviour of the energy in  $v - e$  phase-space for simulated particles was conducted.

A full scatter of the particle velocities and corresponding depot energies across all points in a trajectory are shown in fig. 4.15 for all cases A1-A4. These particular cases were chosen to show the variability in the depot energy which may occur for any given velocity in very non-adiabatic regimes.

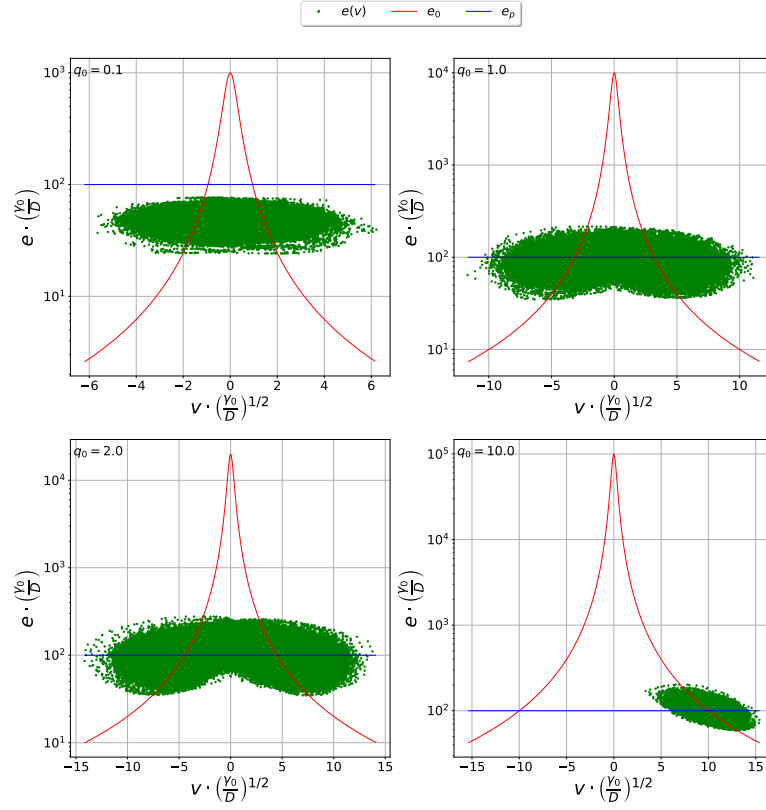


**Figure 4.15:** Scatter plot of particle velocity and energy at intervals of  $\Delta t = 0.1$  (top-left: A1, top-right: A2, bottom-left: A3, bottom-left: A4). Each green point shows the depot energy to an instance where a particle was found at velocity  $v$  throughout the trajectory. The lines show the adiabatic energy  $e_0(v)$  (red) and the pumping energy  $e_p$  (blue). The stationary points are found at the intersections of these two lines. Trajectory length  $t_{\text{end}} = 30000.0$ . Other parameters  $d_0 = 0.1$ ,  $\gamma_0 = 1.0$ ,  $D = 0.1$ ,  $c = 0.001$

Every tenth data point in the trajectory was plotted ( $\Delta t = 0.1$  between points). It can be seen that the energies are spread over a large region and take multiple values for each velocity. Scatters for all other cases may be found in Appendix 7.5.

The plot shows that for all four cases that the particles spread around certain points of the  $v - e$  space, and thus confirms the non-adiabatic nature of the particles discussed earlier. In the most active case seen here, A4, this *cloud* of points is centred around the positive stationary point. The lack of a cloud at the negative point shows

that over this specific trajectory length the particle did not change direction. The spread of  $e$  and  $v$  around this deterministic point is the result of the stochastic force. As the particle drifts through this phase-space along the streamlines from fig. 4.14 there is also a diffusive motion. There is thus a probability that it may exist at points nearby, as opposed to a definite value at each velocity. This probability is set in part by the diffusion constant  $D$ , though the energy-velocity correlation means that other simulation parameters will also affect it. This was seen in the previous sections where an increase in conversion rate  $d_0$  narrowed the distribution of the velocity distributions at a constant value of  $D$ . In the lower activity regimes, the spread is wider as the active force drives the particles less towards the stationary point and the stationary point itself is at lower  $v$  (there is a lower magnitude of the active force at this point).

In the least active case A1, all points in the trajectory exist at energies below the  $e_p$  line. The depot energy never reaches  $e_p$  and so the pumping effect of negative friction is never present.

In cases A2 and A3, particle energies are on the order of  $e_p$ . The distribution of points resembles two clouds around the stationary points which merge in the centre. It was seen earlier (fig. 4.8) that two peaks began to form on the velocity distribution near to the stationary velocity  $v_0$  for these cases. The overlap of the two clouds of points forming near to the stationary points in cases A2 and A3 show that when a particle exists within the region of phase-

space where this overlap occurs, it is able to continue towards either stationary point. These regimes allow for the particle to switch direction.

In A4 only one cloud is seen, which is focused around the positive stationary point. It can be seen that the particle is not adiabatic as there is a spread of energy points about the  $e_0$  line. It can also be seen that the particle has no route to switch directions as  $v$  is never at a low enough value where the stochastic fluctuations could cause direction change.

Each case was attributed to one of 4 types of behaviour in table 4.8. These plots add further resolution to these definitions. The scatters of  $v$  and  $e$  in  $v - e$  phase-space overlap almost completely in type-1; in type-2 are centred around the stationary points though overlap at  $v_0$  in some way; in type-3 are centred around the stationary points though for a single particle do not overlap. The value of  $e$  for type-3 particles is not bound to  $e_0(v)$  — with values seen above and below this value. Though none of the cases A1-A4 exhibited type-4, by definition the distribution of energies should be centred around the stationary point with a value of  $e(v) = e_0(v)$  (i.e. all values are on the  $e_0$  line).

The cloud of points in all of A1-A4 show that none of these particles are behaving adiabatically, as the trajectories took multiple values for any given  $v$  away from the  $e_0$  line.

The large quantity of data points presented in the plot for this initial investigation makes the frequency of each value of depot en-

ergy difficult to observe. This will be addressed in the full analysis of the results.

#### 4.4.6 Results

To show the expected behaviour of the particle energy with velocity more clearly, the mean value of  $e$  within small bins of velocity space  $v_i$ ,  $\langle e(v_i) \rangle$ , was calculated for all cases A1-E4. The graphical results are presented in figures 4.16, 4.17, 4.18, 4.19 and 4.20. The values of both  $e$  and  $v$  were made dimensionless through the previously defined length and timescales.

4.4.6.1 Cases A1-A4 ( $d_0 = 0.1$ )

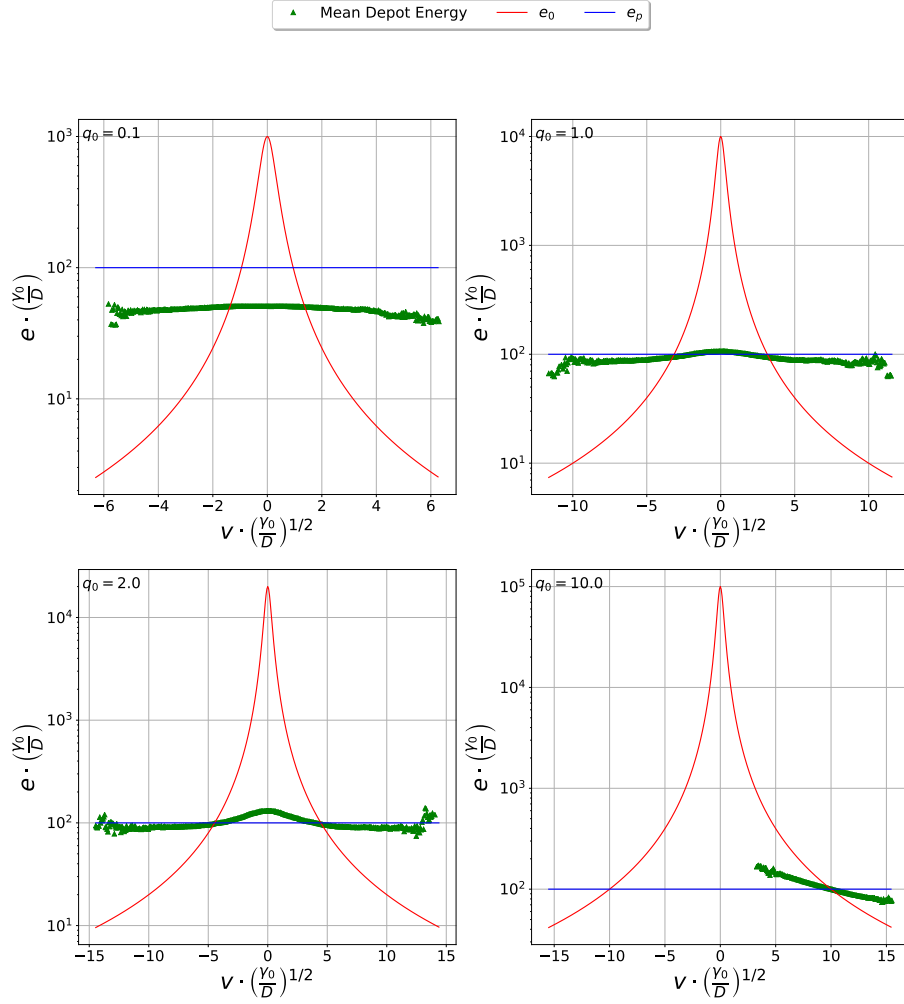


**Figure 4.16:** Energy-velocity scatter from trajectories of varying values of  $q_0$ ,  $d_0 = 0.1$  (top-left: A1, top-right: A2, bottom-left: A3, bottom-left: A4). Other parameters  $t_{\text{end}} = 30000.0$ ,  $n_p = 1$ ,  $\gamma_0 = 1.0$ ,  $D = 0.1$ ,  $c = 0.001$ .

The mean values of energy in case A1 all exist below the blue line, indicating as expected that the energy depot does not pump the particle but instead reduces the effect of the static friction. The values of energy show no relationship with the adiabatic  $e_0$  line and there is little variation across the range of  $v$ . Earlier, a velocity distribution with a Gaussian like shape and an increased value of  $\sigma_v$  was seen (table 4.6) for this case. This is explained by the near-constant

mean energy, the depot level is more or less the same across the entire velocity range meaning that the active friction term becomes constant also with velocity (as with an OU particle):

$$\langle \gamma(v) \rangle = \gamma_0 - d_0 \langle e(v) \rangle \quad (4.4.3)$$

In case A2 all values of  $\langle e(v) \rangle$  are within the region  $e_p > e > e_0$  when  $|v| > v_0$ . The deterministic motion of the particles in this region of  $v - e$  space is driven towards the stationary point along the  $e_0$  line, however it seems that the low value of  $d_0$  means that the particles cannot deplete the energy depot quick enough to ever reach this line and so instead hover just below the  $e_p$  line. At the stationary velocities the mean energy lies close to the adiabatic value. Velocities just below  $v_0$  show energies below the  $e_p$  line, while particles at lower velocities have energies greater than  $e_p$ . This behaviour is consistent with the earlier observation that particles moving around at low velocities accumulate energy in their depots, so that when a stochastic event moves them to a higher velocity they can stay there for a longer time due to their sustained activity countering the passive friction.

Case A3 shows similar behaviours to A2, though there is a clearly higher energy at velocities close to 0. At high values of  $|v|$  the mean energy is seen to spike above the  $e_p$  line. Due to the fact that  $P(v) \rightarrow 0$  at this velocity (bottom-left of fig. 4.8) the statistics at these points are not likely to be fully accurate within this population. It is nevertheless interesting to note that for both positive and negative velocities this behaviour was observed. It is possible that

because this is the upper limit of velocities reached, all data points correspond to particles which have accelerated *into* this region of the phase-space. There is no data for the particle slowing from a higher  $v$ , which would be expected to approach with a reduced depot energy (as per flow-lines in 4.14). These outliers in depot energy at the upper limits of velocity merit further investigation.

Outliers are seen at high values of  $|v|$  which are likely due to the unlikely stochastic events which move particles with large  $e$  values quickly from low to high velocities. The similarities in the  $v - e$  behaviour of cases A2 and A3 reinforce the similarities seen in the velocity distributions previously, where particles can exist at low velocities for periods of time collecting energy in their depots so that when they accelerate to higher velocity regions where this energy is expended, they can move in either direction. Hence particles can switch direction.

In A4, a single straight line of points is seen around the positive stationary point. This shows that the  $v - e$  behaviour here is much more well defined than in the other cases. The high rate of uptake of energy increases the depot level such that even for a low activity the particle is actively driven towards the stationary points, and even strong stochastic events are not enough to slow the particle down. The particle is non-adiabatic as previously observed, but is most likely to take the value of  $e_0$  at the stationary point. No particle measurements were seen at low  $v$ , as seen by the lack of points in this region. When fluctuations happen to reduce the particle velocity,

the conversion rate of energy  $y$  is so low that the particle depot energy increases rapidly (similar to as in figs. 4.5, 4.6) which forces the particle to accelerate (in the current direction) before it has the chance to slow down enough for fluctuations to change its direction.

#### 4.4.6.2 Cases B1-B4 ( $d_0 = 1.0$ )

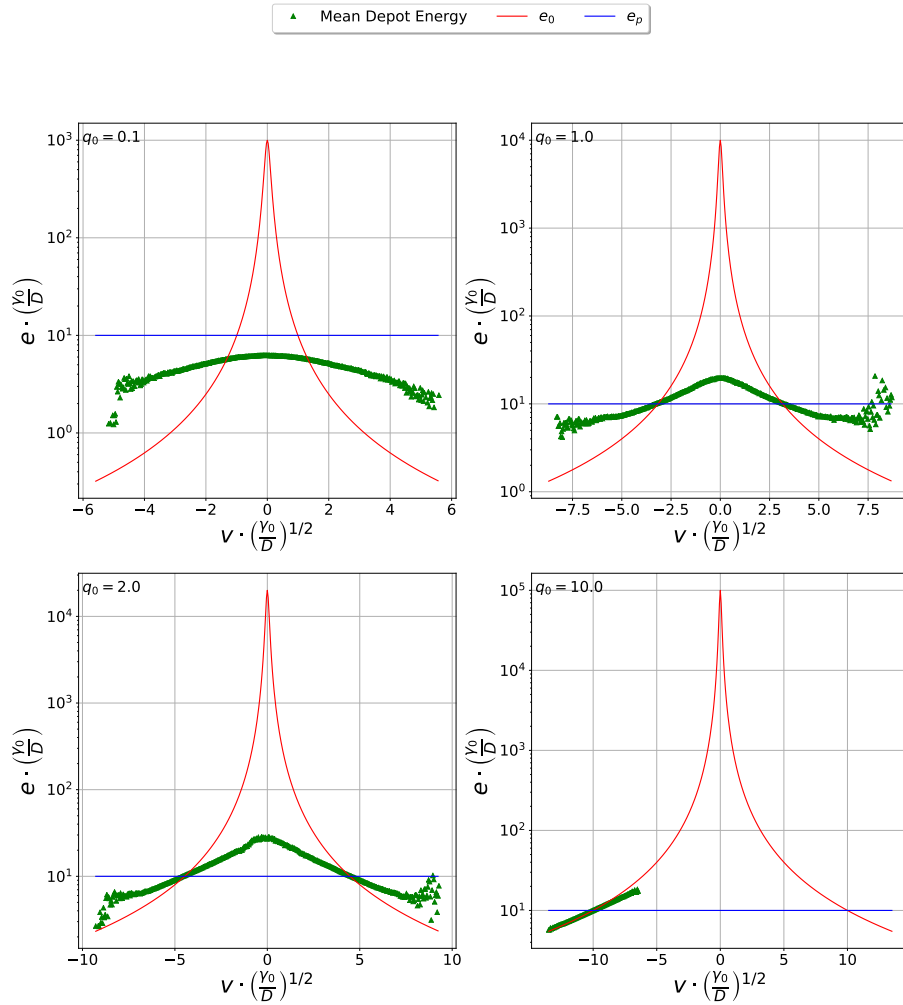


**Figure 4.17:** Energy-velocity scatter from trajectories of varying values of  $q_0$ ,  $d_0 = 1.0$  (top-left: B1, top-right: B2, bottom-left: B3, bottom-left: B4). Other parameters  $t_{\text{end}} = 30000.0$ ,  $n_p = 1$ ,  $\gamma_0 = 1.0$ ,  $D = 0.1$ ,  $c = 0.001$ .

Fig. 4.17 shows the energy-velocity graph for cases B1-B4. B1 shows a similar trend to case A1, though the energy value is notably higher at lower values of  $|v|$  than at higher values. While case A1 had an

approximately constant active friction  $\langle\gamma(v)\rangle$  (eq. (4.4.3)), in the case of B1  $\langle\gamma(v)\rangle$  is in fact slightly lower at higher velocities. This explains why the velocity distribution is not Gaussian as seen in fig. 4.13.

Cases B2 and B3 show very similar behaviours to one another. Particles at low velocities have a much higher value of  $\langle e(v)\rangle$  than those at higher velocities. The low activity ensures that at low velocities particles do not consume their depot reserves. Increasing the activity increases the value of this stationary energy  $\langle e(0)\rangle$ . In both of these cases it can be seen at the stationary point that  $\langle e(v_0)\rangle \approx e_0(v_0) \approx e_p$  — i.e. it is equal to the energy at the stationary point  $v_0$ . For  $|v| > v_0$ , it is seen that  $e_p > e > e_0$  as in cases A2-A4 (fig. 4.16). This again shows that particles are being driven back towards the stationary points as seen in the streamline plots, though the conversion rate  $d_0$  is not high enough to quickly convert excess energies.

The highest energy case B4 again shows the particles being trapped on one side of velocity space and fluctuating around the stationary point. At the highest  $|v|$ , the mean energy lies very close to the  $e_0(v)$  line, while at lower  $|v|$ , the mean energy is below  $e_0(v)$ . Therefore, this case shows a mixture of adiabatic behaviour (at higher  $|v|$ ) and non-adiabatic behaviour (at lower values of  $|v|$ ). Due to the high value of  $|v_0|$ , the stochastic force is again not enough to overcome the large active force component and change the particle direction.

#### 4.4.6.3 Cases C1-C4 ( $d_0 = 2.0$ )

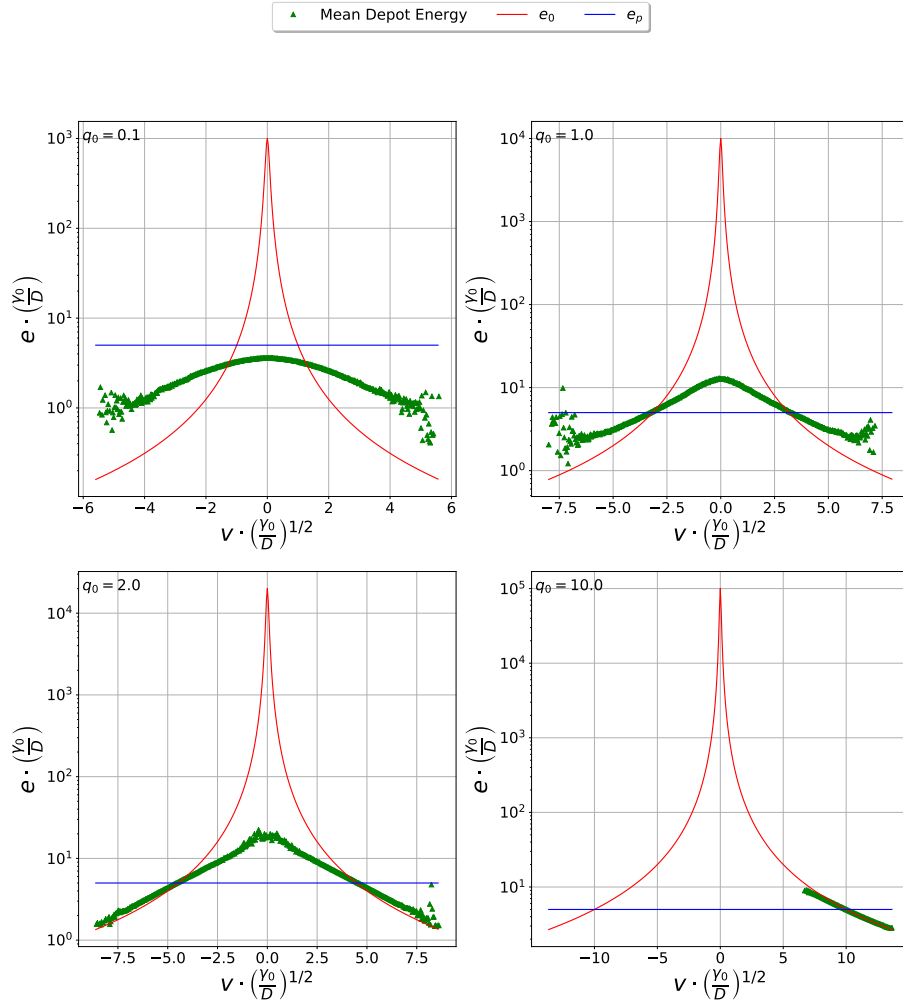


**Figure 4.18:** Energy-velocity scatter from trajectories of varying values of  $q_0$ ,  $d_0 = 2.0$  (top-left: C1, top-right: C2, bottom-left: C3, bottom-left: C4). Other parameters  $t_{\text{end}} = 30000.0$ ,  $n_p = 1$ ,  $\gamma_0 = 1.0$ ,  $D = 0.1$ ,  $c = 0.001$ .

The trend seen in the previous cases is also seen in fig. 4.18 for cases C1-C4. The distribution of energies for C1 is more arched than in case B1, though still completely below the  $e_p$  line. This further enforces the idea that these particles are being accelerated at higher velocities with the energy accumulated from low velocities.

For cases C2 and C3, both of which were previously defined as type-2 distributions in table 4.8, we see similar behaviour. This is

consistent with the other type-2 cases B2 and B3 (fig. 4.17). The depot energy at low  $|v|$  and when the particle is nearly stationary is higher as the particle gathers up energy in the depot but is unable to convert it in to kinetic energy. At higher velocities the particle is driven towards the stationary point. Case C3 shows values of  $\langle e(v) \rangle$  much closer to  $e_0(v)$  at higher velocities than in the previous cases. Though the points do not all overlap, there is a clear trend towards behaviour closer to adiabatic in this case. Case C4 again shows near-adiabatic behaviour, though at velocities below the stationary point there is a deviation from adiabatic behaviour. As the energy conversion rate has increased, the particle energies at higher velocities have become more likely to reside closer to the  $e_0$  line.

#### 4.4.6.4 Cases D1-D4 ( $d_0 = 6.0$ )

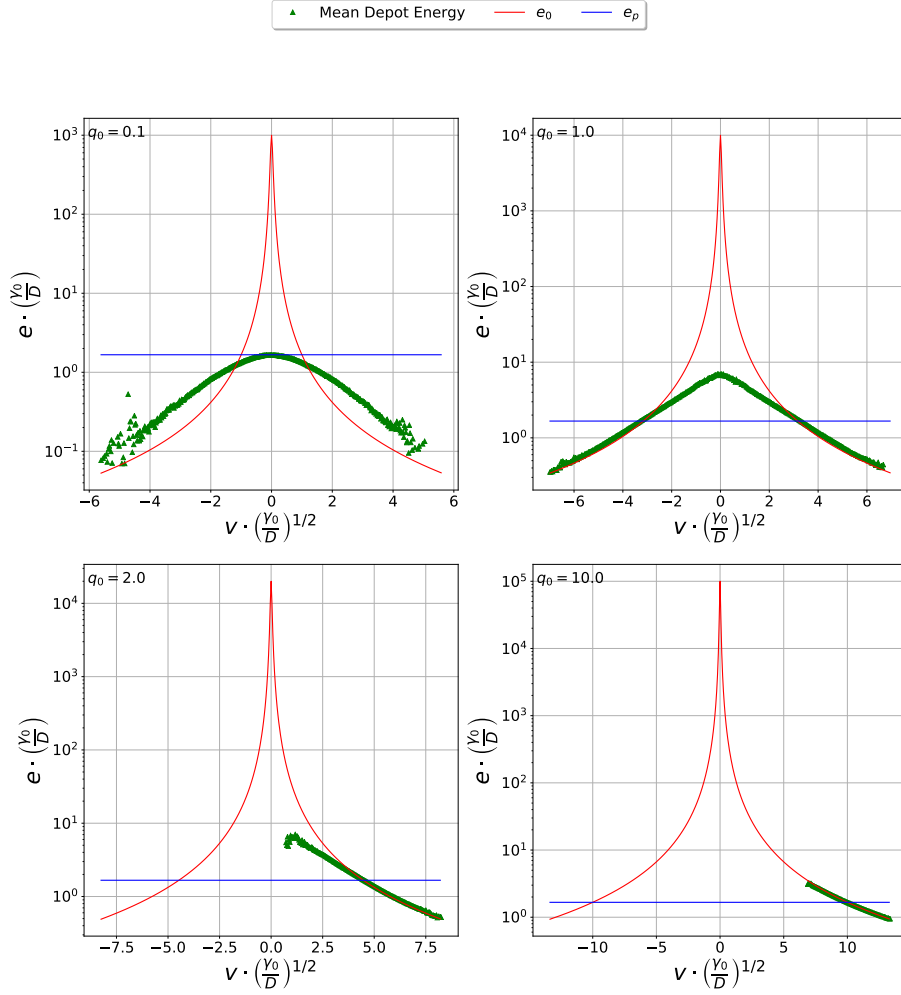


**Figure 4.19:** Energy-velocity scatter from trajectories of varying values of  $q_0$ ,  $d_0 = 6.0$  (top-left: D1, top-right: D2, bottom-left: D3, bottom-left: D4). Other parameters  $t_{\text{end}} = 30000.0$ ,  $n_p = 1$ ,  $\gamma_0 = 1.0$ ,  $D = 0.1$ ,  $c = 0.001$ .

The plots for cases D1-D4 (fig. 4.19) continue to show the trends which have been seen developing over the cases discussed so far for smaller values of  $d_0$ . As the  $d_0$  value is increased even further, the difference between the energy at low velocities and at higher velocities in case D1 is far greater than was seen in the previous type-1 cases. The value of  $\langle e(v_i) \rangle$  in the centre of the plot is close to the  $e_p$  line. In the velocity distribution (figs. 4.11, 4.13) for this case the

rounded peak which was previously seen had begun to flatten out as the distribution widened and moved towards the double peaked bimodal distribution seen in the more active cases. At higher velocities, the energy is much closer to the  $e_0$  line than in the previous cases.

Case D2 shows a strong resemblance to the previous type-2 distributions seen in earlier figures, with a large energy level for immobile particles and particles moving faster than  $v_0$  on average behaving in an adiabatic manner. Increasing  $d_0$  from case C3 to case D3 shows the energies at high velocities adhering more to the adiabatic line, while particles now appear never to reach the  $v \rightarrow 0$  area of the phase-space — the particle does not change direction. It is not possible from this trajectory length to conclude that the particle would never switch direction. A closer look at the probability of particles switching directions will be seen in the following section.

The final case D4 shows the average value of energy lying along the adiabatic line for all  $v$  — i.e.  $\langle e(v) \rangle = e(v)$ . The velocity distribution for this curve (fig. 4.11) showed very minor differences between the adiabatic distribution and the stochastic result, though it is clear from both of these results that these particles are forced towards the stationary points where the motion is completely controlled by the active force.

4.4.6.5 Cases E1-E4 ( $d_0 = 10.0$ )

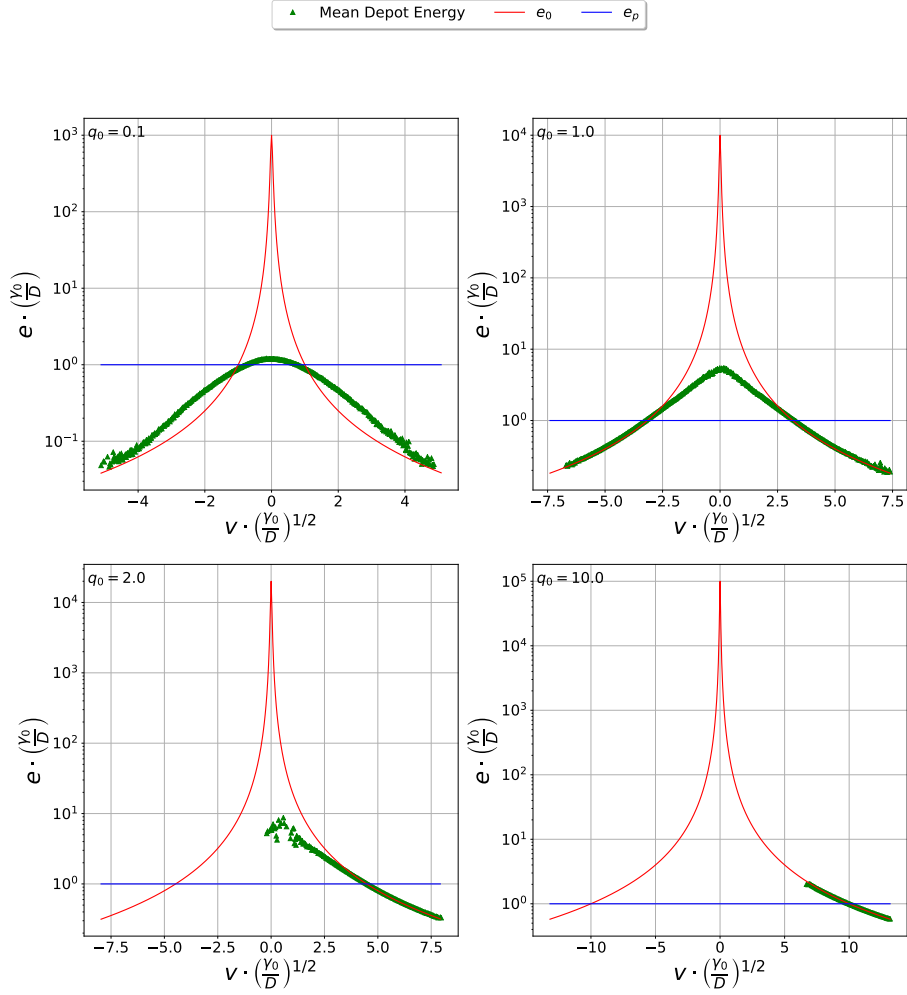


**Figure 4.20:** Energy-velocity scatter from trajectories of varying values of  $q_0$ ,  $d_0 = 10.0$  (top-left: E1, top-right: E2, bottom-left: E3, bottom-left: E4). Other parameters  $t_{\text{end}} = 30000.0$ ,  $n_p = 1$ ,  $\gamma_0 = 1.0$ ,  $D = 0.1$ ,  $c = 0.001$ .

The final set of results in fig. 4.20 help to conclude the analysis of the behaviours which have so far been seen to be emerging, particularly in cases E1 and E3.

Case E1 is the first of the particles with this value of  $q_0$  to show a value of  $\langle e(v_i) \rangle$  at any point in the distribution above the  $e_p$  line. It is also the only one of these five cases where the velocity distribution contained two separate peaks (fig. 4.13). At much higher

velocities the energy is almost adiabatic on average, inferring that in this case the particle is non-adiabatic due to the low value of energy in the depot and resulting preference to remain in low-velocity areas of phase-space. The particle builds up its energy at a low velocity where it is then moved towards either stationary point by the stochastic force. Due to the low level of energy available in the depot, the particle depletes its depot quickly and so the particle cannot accelerate to extreme velocities. As the depot energy conversion rate is high, any stochastic event can move the particle quickly away from low velocities. Low- $v$  particles have values of  $e(v) > e_p$  so they are quickly accelerated to higher  $v$  where  $e(v) < e_p$ . This quickly depletes the depots and they slow down again as the net friction is still a drag. The emergence of bimodal distribution in figs. 4.12 and 4.13 is caused by  $\langle e(v = 0) \rangle > e_p$ .

Case E2 behaves in a very similar manner to case D2, though the values of the energy at higher velocities indicate a more adiabatic behaviour in this part of phase-space. At lower velocities ( $|v| < |v_0|$ ), the energies of the particles lie above the  $e_p$  line but below the  $e_0$  line, the particle energy is driven upwards until it can move into a region of velocity space where it can deplete its depot. This is a good example of these type-2 particles which show a combination of adiabatic-like (type-4) active motion at high velocities, and slightly active OU (type-1) behaviour at low velocities.

Case E3 again shows the mean energy of these particles almost perfectly agreeing with the adiabatic energy  $e_0$  though there are de-

viations and outliers seen at lower velocities. The behaviour around the stationary points is similar to that for other type-2 and type-3 particles, where particles above  $v_0$  deplete their depots before being slowed along the  $e_0$  line towards the stationary point and particles moving slower than  $v_0$  accrue energy in their depots which they then use to accelerate towards this point.

It is also seen that there are some points with negative  $v$  throughout this trajectory, the erratic distribution suggests that these are outliers with poor statistics. This is confirmed by the scatter plot shown in Appendix 7.5 in fig. 7.5. Though the particle did change direction, it did not then transition towards the negative stationary point  $-v_0$ . As the particle is memoryless, it is likely that a stochastic event sent the particle back to positive  $v$  space from this point. The trajectory length in negative  $v$  was therefore short compared to that in positive  $v$ . It is not possible to see from the graph whether this happened multiple times, though attention is drawn to this event prior to the upcoming discussion of the particle switching time distributions in the following sections. The presence of data in the low-negative- $v$  region of the phase-space without a corresponding trajectory finishing at the negative fixed point shows that for type-2 particles at low velocity particles do not automatically drive towards the stationary point with the same sign (direction) as their current velocity. Fluctuations can still make them change direction again while  $v$  is low.

The adiabatic case E4 shows the mean energy lying along the

$e_0$  line at all  $v$ . Though there are some small deviations from this value, this is most likely due to the resolution of the simulation time step. The previous benchmark calculations carried out for this case (fig. 4.2) showed a small error between  $e$  and  $e_0$  which would account for these small fluctuations. In this case, the particle fluctuates along the  $e_0$  line around the stationary velocity as a result of the stochastic force, but is driven back towards this point from either side due to the pumping of energy from the depot into the particle (lower  $v - e > e_p$ ) or the increased static friction on the particle (higher  $v - e < e_p$ ).

#### 4.4.7 Conclusions

By looking at the mean value of energy across the range of velocities a deeper understanding of the four previously described behaviours was seen. The type-1 particles showed a single cloud of points, with the mean values of the energy similar across the range. This meant that in low energy cases the active friction was a constant positive value less than the static friction as  $\langle e \rangle$  was on average always below the  $e_p$  line. This gave the particles an “effective diffusion constant” greater than  $D$ , which was seen previously. For more active cases, these type-1 particles had lower mean energies at higher velocities but were overall seen to not show any preference for bifurcation towards the stationary points. This correlates with the velocity distributions where more active particles deviate from a Gaussian distribution of velocities and instead are more likely to exist at intermediate velocities whilst still maintaining the same overall variance.

The most active type-1 case E1 was the first case of this  $q_0$  value where the mean velocity energy reached the pumping line at low  $v$ . This was also the first type-1 case where the velocity distribution began transitioning to a double-peaked distribution. It was seen that particles at lower velocities would readily store energy in higher quantities which would then be used to accelerate the particles at the higher velocities, where the conversion rate was high enough to maintain an active motion. This particle appeared on the transition between the classified type-1 and type-2 behaviours.

For type-2 particles at low  $v$ , the mean energy was always above the pumping line indicating a low rate of depot depletion at these velocities. At velocities higher than the stationary velocity  $v_0$ , the mean particle energy depot level was higher than the adiabatic energy  $e_0(v)$ . The lower conversion rates and lower value of  $v$  relative to adiabatic particles means that the timescale of energy conversion in these cases is comparable with the timescale of the stochastic force. The large amount of statistical data gathered at low velocities and the slow reaction of the energy depot confirms that particles fixed in 1-dimension in these parameter regimes may switch readily between the positive and negative directions.

Type-3 particles never existed at low velocities and were not seen to change direction frequently within the trajectories. They showed similar behaviour to type-2 particles at intermediate velocities, where  $e_0 > \langle e \rangle > e_p$ . At the stationary velocity and values above it these particles took energy values of  $\langle e \rangle \approx e_0$ . This sug-

gests that at lower velocities the particles are clearly non-adiabatic but as the velocity of the particle increases the  $v^2$  term in the energy update formula becomes more powerful and drives the particle energy more towards  $e_0$ .

Case E4 showed all points lying within a narrow band of  $v$  on the  $e_0$  line. This shows that for high stationary velocity  $v_0$  when the depot-energy available is also large; if the conversion rate  $d_0$  is suitably high the particles behave in an adiabatic manner.

This analysis has shown the emergence of the transition between the adiabatic and non-adiabatic behaviour more clearly. The particle begins to drive itself towards the stationary points and overcome the stochastic force when the velocity is high relative to the diffusion constant and the conversion rate is also high. Simply increasing the value of the parameters to increase  $\beta$  does not make the particle adiabatic, as the conversion rate must also be high enough to convert the energy quickly. In non-adiabatic cases the energy is distributed more widely at lower velocities. In cases where the value of  $d_0$  is very high, the particle still behaves non-adiabatically at low velocities.

It was seen that particles which are adiabatic do not change direction, moving in the same direction as the initial velocity for the entire trajectory. Type-3 particles also maintained this direction, though they did not behave adiabatically. Type-2 particles were seen to move around the stationary velocities frequently but also were seen to exist at low velocities for times long enough that

stochastic fluctuations could cause a change in direction.

## 4.5 Chapter Conclusions

In this chapter we investigated ED particles in 1-D starting from rest, and at steady-state. It was seen that in higher  $d_0$  and  $q_0$  regimes, particle behaviour was closer to that of an adiabatic particle. For lower *activity* systems — discrepancies were seen between the distributions of energy  $e(v)$  and the expected adiabatic energy  $e_0$ . Simulated velocity distributions found through a stochastic methodology also differed from the analytical steady-state velocity distribution  $P_{SS}(v)$ , as expected due to the analytical solution being calculated using the adiabatic assumption.

We have shown that particles exhibit non-adiabatic behaviour at low velocities when the rate of consumption of the depot energy is diminished. Thus we can say that this assumption only holds when particles do not transition through low-velocity regions of space. In 1-D (or a potential special case of separate depots for each cardinal direction of motion), this is simply the particle velocity. In higher dimensions this means the magnitude of the velocity vector.

In the following Chapter 5, we will study the switching behaviour between the two stationary regions of  $v$  in order to further understand the directional switching behaviour of these particles in 1-D which was observed in Section 4.4.

## Chapter 5

# Directional Switching of 1-D Active Brownian Particles With Energy Depots

## 5.1 Introduction

The behaviour of single trajectories of Ornstein-Uhlenbeck (OU) particles with energy depots (EDs) is investigated. Particles in the different parameter regimes introduced in Chapter 4 were simulated in time until they switched direction. This process was repeated to generate a population of switching events with which the overall characteristic time distributions for the survival time a particle would move in the same direction was found. We present these results as switching time distributions.

The  $v$  and  $e$  behaviours just before and just after these switches were then observed to investigate relevant patterns and further categorise the parameter regimes.

The two characteristic timescales which emerge — corresponding to the fast-switching of OU-like trajectories and the slower-switching driven behaviour near to the stationary points — are fitted to curves. In this way, we are able to quantify these timescales and compare them with each other.

Finally, the auto-correlation of the velocity and depot energy in these regimes is investigated and compared. We investigate the result and tie the auto-correlation, switching time-scales and the results from Chapter 4 together to better understand the transitions that OU particles in 1-D with EDs make between the higher  $v$  and lower  $v$  regions of velocity space.

## 5.2 Particle Switching Time Distributions

### 5.2.1 Introduction

In Chapter 4 we carried out agent-based simulations of OU particles with EDs (ED particles) in 1-D and saw that in certain parameter regimes (lower  $d_0$  and  $q_0$ ) the particles were non-adiabatic — they go through periods of motion close to that of an adiabatic particle at high  $v$ , but also move at lower velocities where the particle may behave in a more OU-like (inactive) manner. By varying the  $q_0$  and  $d_0$  values, particles show varying levels of the mixture of these two behaviours. In Section 4.4, the velocity and energy trajectory of a single particle and the average depot energy over the entire range of velocity were observed and it was seen that particles which are able to reside at low velocities remain there for a time, building up a store of energy before they return toward the stationary point regions of  $v - e$  phase-space. This is also observed analytically by considering the active friction  $\gamma(v)$  which was previously introduced:

$$\gamma(v) = \gamma_0 - d_0 e(v) \tag{5.2.1}$$

These mixed behaviour systems correspond to type-1 and type-2 classification outlined in Section 4.3.3.

At values of  $0 < e < e_p$  (below the pumping energy defined in eq. (3.4.7)) the static friction on the particles is reduced, however the positive friction value still results in a dragging force. The particles behave like OU particles with reduced friction (i.e.  $\gamma_0 > \gamma(v) > 0$ ). Particles are likely to remain at low velocities in this case as there

is no pumping action from excess depot energy.

Therefore it may be said that at in the low velocity region, these particles are behaving similarly to OU particles, whilst at higher velocities their behaviour is closer to that of adiabatic particles, whilst still not being in the adiabatic regime. Purely adiabatic particles (type-4) will always remain on the  $e_0$  line and so never cross the threshold of  $v = 0$  (i.e. switch direction). This would require the accumulation of  $e_0(v = 0)$  energy in the depot which is very high for any adiabatic conditions so will never be observed.

Conversely, OU-like active particles (type-1) are primarily governed by the stochastic force. In these cases the stationary velocity is at a low enough value that the distribution of velocities around these points overlap greatly, making the particle more likely to exist in between the two values of  $\pm v_0$ .

In this section we measure the length of time a particle spent travelling in the same direction. Upon switching direction, the timer was reset and the length of the subsequent trajectory was then recorded. Histograms of these results were generated in order to measure the probability distribution of switching times over a single long trajectory for each particle (i.e. parameter configuration).

### 5.2.2 Simulation Parameters

The same values of  $\gamma_0$ ,  $D$ ,  $c$  and  $\Delta t$  were used as outlined in table 4.2. A single particle starting from rest with an empty depot ( $v(0) = 0$ ,  $e(0) = 0$ ) over a trajectory of length  $t_{\text{end}} = 2 \times 10^7$  was simulated. This corresponded to  $2 \times 10^9$  data points with  $\Delta t = 0.01$ .

### 5.2.3 Methodology

The initial 200.0 units of time were discounted from each simulation as before to ensure that the simulation started from steady-state.

The time that the particle had been travelling in the same direction before switching was recorded from immediately after the previous direction change, until the time step immediately after the next direction change. For particles which never change direction (the type-4 near-adiabatic case), no results were ever recorded. It is also noted that for some type-3 particles, the time taken to switch direction is so large for the corresponding time the simulations run, that not enough switches were recorded in order to observe statistically meaningful results, even though type-3 particles are able to switch. The duration of each *switch* trajectory was continually recorded until the particle switched directions again.

Each switch was assigned to a bin in the histogram and the overall distribution of these times was plotted in a histogram. Due to the large number of switches when particles exhibit OU behaviour compared to those on a longer timescale, a logarithmic distribution of bin widths was used. The bins were normalised for the relevant width and the centre point of the bin was plotted against the probability of a particle trajectory length occurring within that period. The bins were selected heuristically such that there were 100 bins of width 0.01 in the range  $[0, 1]$ . For all values  $10^n$  above this the bin width was adjusted to  $n - 1$  for an exponentially increasing bin width as  $\tau_{\text{switch}}$  increased.

The resultant normalised distributions represent the hitting time distribution  $h(\tau_S)$  as defined in eq. (3.5.7) — the probability distribution for how long it takes for a particle to *hit* the absorbing boundary at  $v = 0$  (i.e. to switch directions).

One artefact of this methodology is that the particle initial velocity and energy were not constant. Due to the numerical methods employed, the minimum resolution is set by the value of  $\Delta t$  over how close or far away from the true value of the beginning or end time of the trajectory the recorded time is. It is also not possible to separate the switches of particles which switch with low depot energies from those which switch with higher depot energies by looking at the data in this way.

#### 5.2.4 Results

As with previous sections, the results are presented in sets of constant values of  $d_0$  with varying  $q_0$  corresponding to the parameter configuration cases defined in tab. 4.4. These are shown in figures 5.1, 5.2, 5.3,

As switching only occurs for type-1 and type-2 particles, results are only presented for the cases defined as these in tab. 4.8 in figs. 5.4 and 5.5.

##### 5.2.4.1 Cases A1-A3 ( $d_0 = 0.1$ )

In fig. 5.1 cases A1-A3 the number of switches over the entire trajectory length for all cases is high enough to guarantee good statistics. It is seen clearly that all three cases have an exponentially decaying

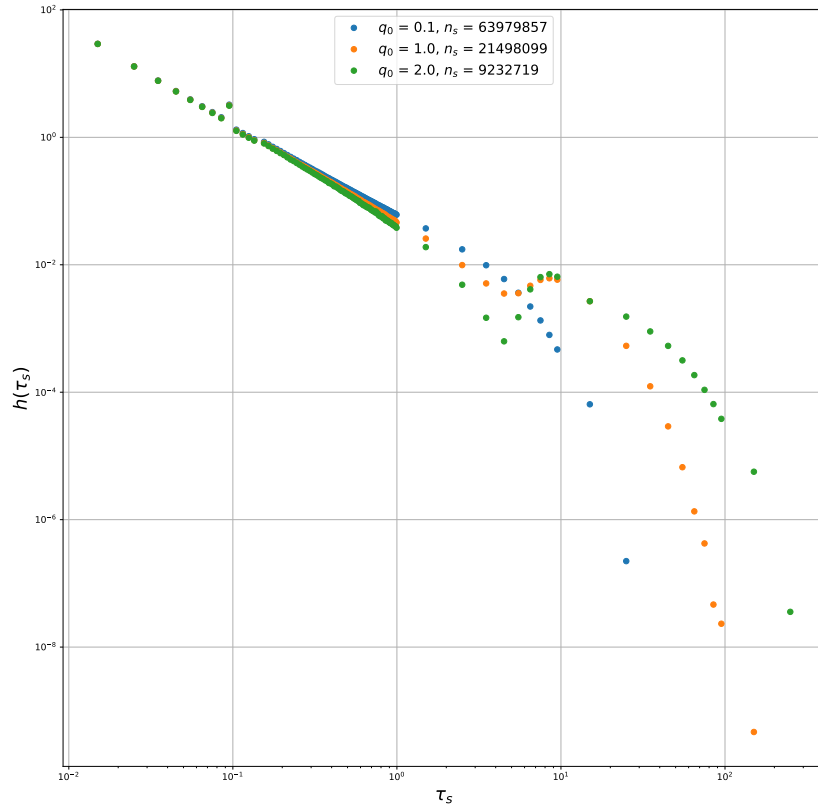


**Figure 5.1:** Switching time distributions for particles with varying  $q_0$  at  $d_0 = 0.1$  (cases A1-A3). Other parameters  $\Delta t = 0.1$ ,  $\gamma_0 = 1.0$ ,  $D = 0.1$ ,  $c = 0.001$

distribution of low values of  $\tau_s$  which a characteristic time which decreases slightly as the activity is increased. At around  $\tau_s = 5.0$ , an increase in the probability is seen for cases A2 and A3, where a hump-like decay then forms. In case A1, the tail of the distribution is much more similar to the pure OU case.

#### 5.2.4.2 Cases B1-B3 ( $d_0 = 1.0$ )

In fig. 5.2 for cases B1-3, the behaviour is much the same as in the first set of graphs, though now there is a much clearer difference between the initial decay and the second emergent timescale

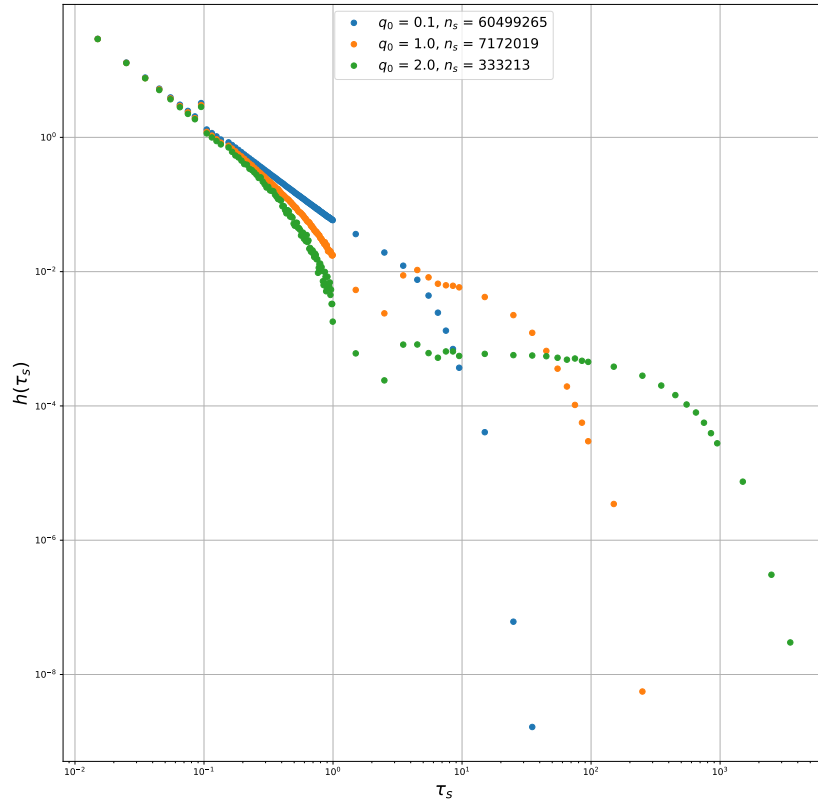


**Figure 5.2:** Switching time distributions for particles with varying  $q_0$  at  $d_0 = 1.0$  (Cases B1-B3). Other parameters  $\Delta t = 0.1$ ,  $\gamma_0 = 1.0$ ,  $D = 0.1$ ,  $c = 0.001$

for particle switching in cases B2 and B3. This is combined with a steeper initial decay, where cases B2 and B3 deviate from the OU like behaviour of case B1 much earlier. An emergence of two different timescales of switching is becoming apparent in the type-2 particles.

#### 5.2.4.3 Cases C1-C3 ( $d_0 = 2.0$ )

Cases C1-C3 (fig. 5.3) continue to show the trend of an increasing rate of decay of the short timescale as particles become more active. The type-2 particle cases C2 and C3 show once more the two

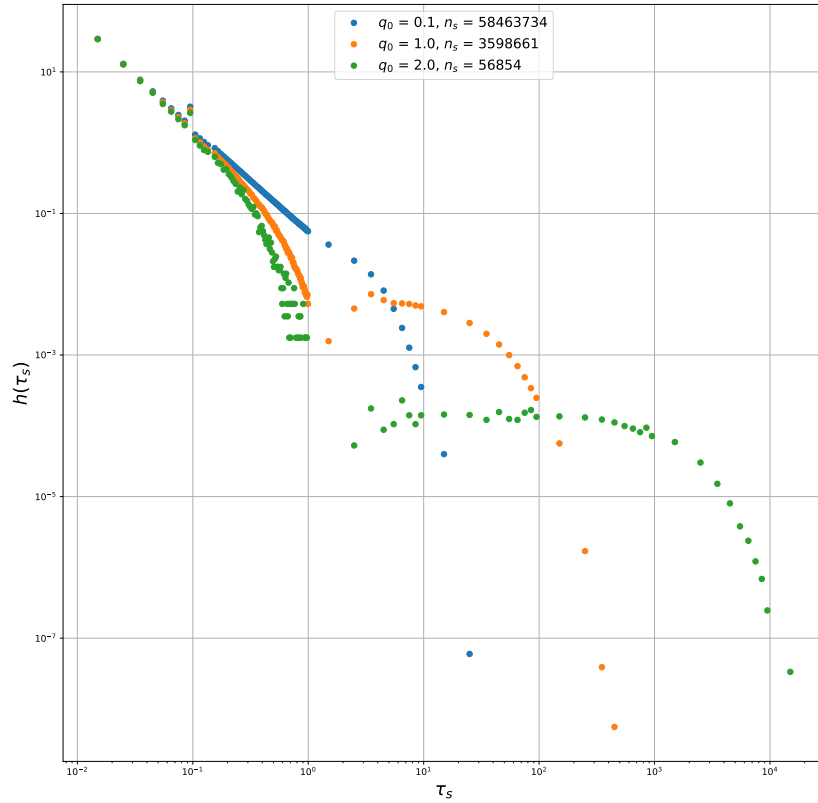


**Figure 5.3:** Switching time distributions for particles with varying  $q_0$  at  $d_0 = 2.0$  (Cases C1-C3). Other parameters  $\Delta t = 0.1$ ,  $\gamma_0 = 1.0$ ,  $D = 0.1$ ,  $c = 0.001$

different timescale behaviours, with an initial OU-like decay where most particles are likely to switch, followed by a longer timescale “hump”. The flat region shows there is a wide range of equally likely timescales of trajectories between switches.

#### 5.2.4.4 Cases D1-D3 ( $d_0 = 6.0$ ) & E1-E3 ( $d_0 = 10.0$ )

Cases D1–3 and E1–3 behave much like the first three sets of parameters, though as D3 and E3 begin to transition from type-2 into type-3 classifications of particles, the likelihood of switching directions decreases greatly and the statistical data available over these

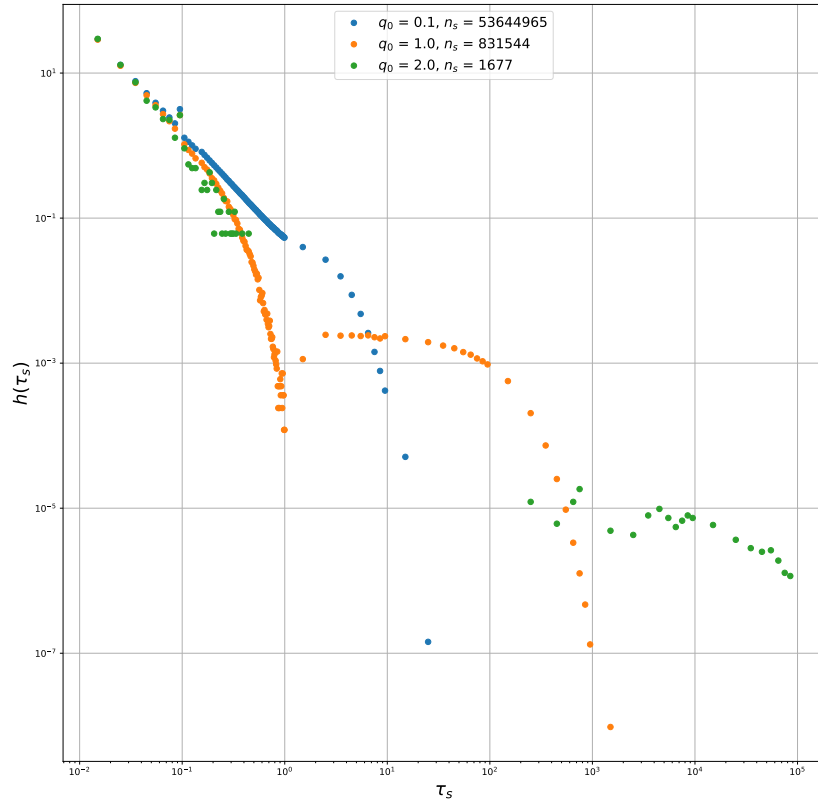


**Figure 5.4:** Switching time distributions for particles with varying  $q_0$  at  $d_0 = 6.0$  (Cases D1-D3). Other parameters  $\Delta t = 0.1$ ,  $\gamma_0 = 1.0$ ,  $D = 0.1$ ,  $c = 0.001$

long trajectories diminishes. All cases, no matter the classification of distribution or activity of the particle, have a very similar decay at very low values of  $\tau_s$ , with an increased likelihood of surviving for longer times once breaking past this initial limit. Only type-2 particles show the second, longer timescale tail to the distribution where particles continue in the same direction for a long time.

Case E1 shows the emergence of a transition into this type-2 behaviour as a slight bump in the distribution is seen at around  $\tau_s \approx 1.0$ .

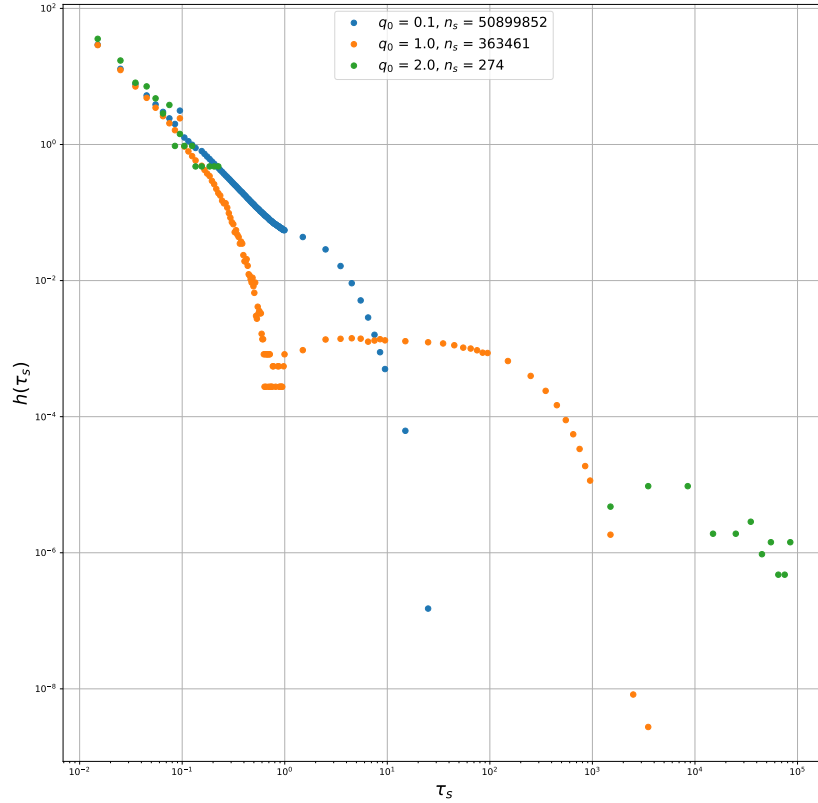


**Figure 5.5:** Switching time distributions for particles with varying  $q_0$  at  $d_0 = 10.0$  (Cases E1-E3). Other parameters  $\Delta t = 0.1$ ,  $\gamma_0 = 1.0$ ,  $D = 0.1$ ,  $c = 0.001$

For case E3 there are bins with no data for this case at intermediate  $\tau_s$ , showing a clear separation of timescales for short-switching trajectories (lower  $\tau_s$ ) and long-switching-trajectories (higher  $\tau_s$ ).

### 5.2.5 Conclusion

In the previous sections when the velocity and energy distributions of particles were observed, it was seen that all of the cases which exhibited switches could exist in some manner around the  $v = 0$  region, though in more active (higher  $d_0$ ) cases they are driven towards the stationary velocity  $\pm v_0$ . The energy scatter clouds showed an

overlap of the two clouds of points around each stationary point in  $v - e$  space in some cases at values of  $v = 0$  as well, and so there was a clear pathway through this phase-space for particles to switch directions in  $v$ .

These figures reinforce this behaviour. The type-1 particles exist much like OU particles, though the active force may drive them slightly in the direction of travel; which in the more active cases results in trajectories which take have a longer switching time  $\tau_s$ . The strength of the stochastic force relative to the active force means that eventually one of the more powerful stochastic events will change the particles' direction. This is seen by the similar decay rate with only a slightly delayed value of  $\tau_s$  before all particles have switched.

As the particles move towards bimodal behaviour this same phenomenon is seen (at lower  $v$ ); which is why the low  $\tau_s$  regions of all of the distributions are almost identical. At intermediate  $\tau_s$ , once the particle reaches the stationary velocity or higher regions of  $v$ -space in these more active cases, it takes a much less likely chain of stochastic events to overcome the active motion and move the particle back to the low velocity region where it can switch directions again. The timescale on which these rare stochastic events are most likely to occur is characterised by the second "hump" of the distributions in these type-2 particle cases. It can be seen that these events are less probable than the *OU switching*.

In summary, two timescales for switching were observed. The

first occurs at low velocities where the stochastic force is dominant. Particles are not driven far away from  $v \approx 0$  and so the stochastic force can overpower any active force to change the direction in the particles. The time between these switches is therefore low.

The second is the timescale of a particle to move away from the steady-state region around the stationary points. Infrequent chains of stochastic events combined with the correct conditions of depot-energy must first slow the particles to a lower  $v$  where they are able to switch direction

Both of these characteristic times for switching for the simulated data will be fitted in the Section 5.4.

## 5.3 Velocity and Energy Before and After Switches

### 5.3.1 Introduction

It was seen in Section 4.4 that for particles which switched directions, the energies around the origin  $v = 0$  varied and were on average higher than those at other velocities in the system. In the previous section two emergent timescales for switching were observed — very short, and long. As all particles must travel through the low  $v$  space in order to change direction, it was concluded that long time-scale switching was the result of particles reaching low  $v$  through a chain of stochastic events where they would behave as if they were on a short-time switching trajectory.

This section looks at the velocities and depot-energies of particles in the times around switching, i.e immediately before and immediately after a switch occurs. The aim is to gain an understanding of the dynamics which cause switches.

### 5.3.2 Methodology

The same simulation output data from the previous Section 4.3 was used to measure the values of  $e$  and  $v$  immediately before and after a switch occurred — i.e. the final point when a particle was moving in positive  $v$ , and the first point when it switched to negative  $v$  (and vice-versa).

These data are presented in histograms to show the distribution of the values and show how they compare to the fixed points  $v = 0$  for  $v$ , and  $e_p$  for  $e$ .

### 5.3.3 Results

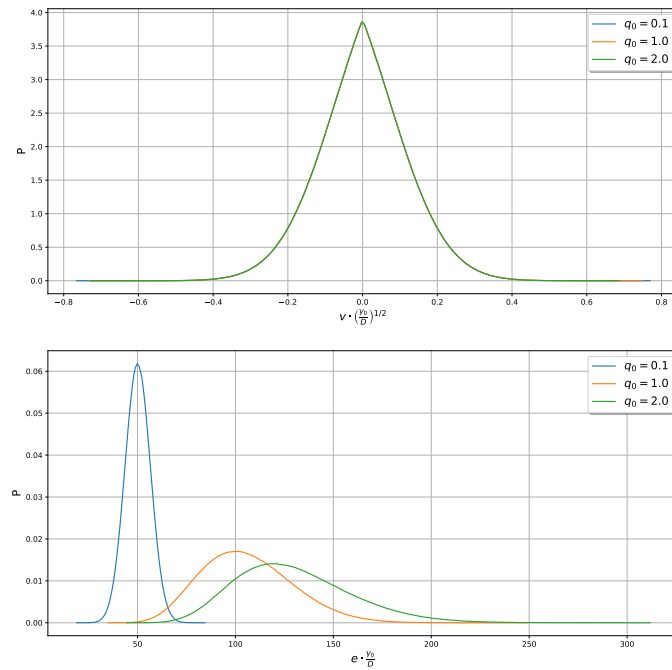


**Figure 5.6:** Distributions of  $v$  (upper plot) and  $e$  (lower plot) for particles immediately before & after switching with varying values of  $q_0$  at  $d_0 = 0.1$  (Cases A1-A3). Other parameters  $\Delta t = 0.1$ ,  $\gamma_0 = 1.0$ ,  $D = 0.1$ ,  $c = 0.001$

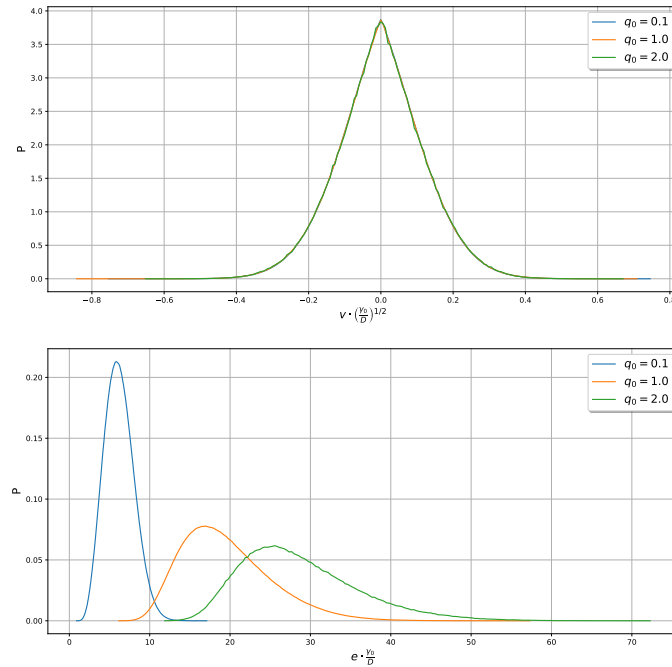


**Figure 5.7:** Distributions of  $v$  (upper plot) and  $e$  (lower plot) for particles immediately before & after switching with varying values of  $q_0$  at  $d_0 = 1.0$  (Cases B1-B3). Other parameters  $\Delta t = 0.1$ ,  $\gamma_0 = 1.0$ ,  $D = 0.1$ ,  $c = 0.001$

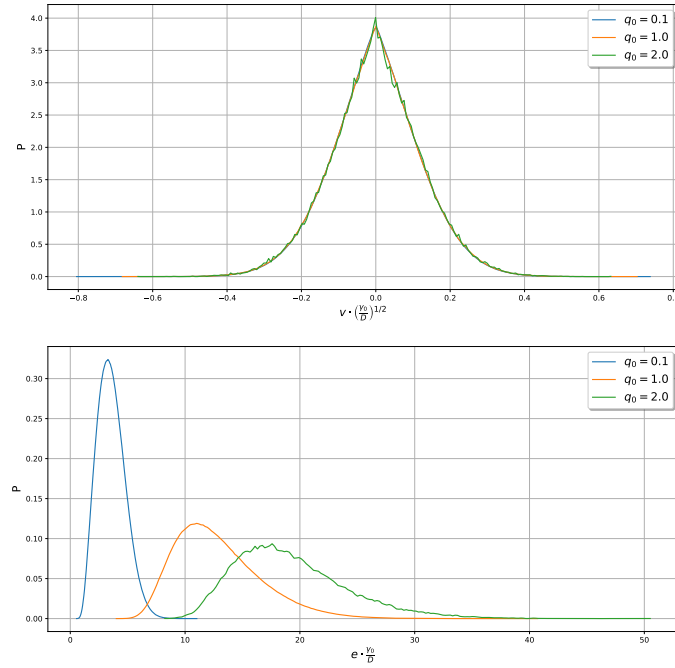


**Figure 5.8:** Distributions of  $v$  (upper plot) and  $e$  (lower plot) for particles immediately before & after switching with varying values of  $q_0$  at  $d_0 = 2.0$  (Cases C1-C3). Other parameters  $\Delta t = 0.1$ ,  $\gamma_0 = 1.0$ ,  $D = 0.1$ ,  $c = 0.001$

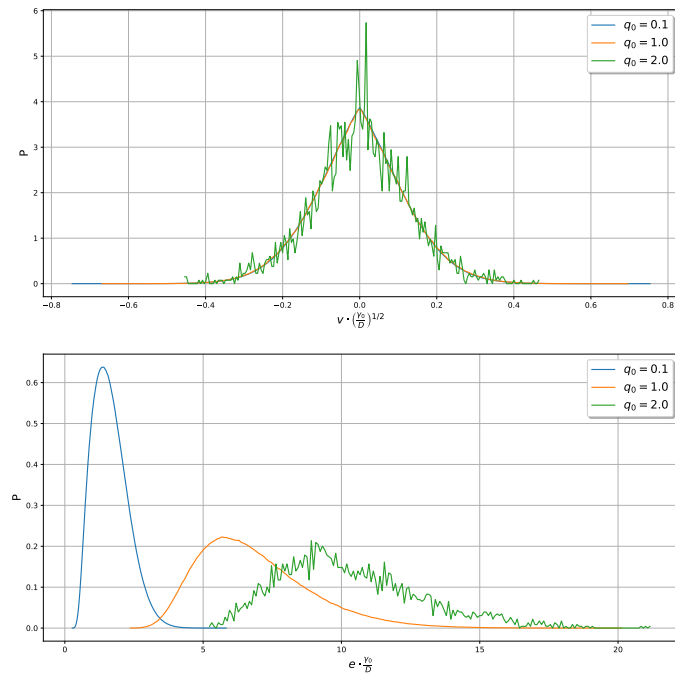


**Figure 5.9:** Distributions of  $v$  (upper plot) and  $e$  (lower plot) for particles immediately before & after switching with varying values of  $q_0$  at  $d_0 = 6.0$  (Cases D1-D3). Other parameters  $\Delta t = 0.1$ ,  $\gamma_0 = 1.0$ ,  $D = 0.1$ ,  $c = 0.001$

The results are presented in figs. 5.6, 5.7, 5.8, 5.9 and 5.10.

For all of the velocity distributions a Gaussian-like distribution

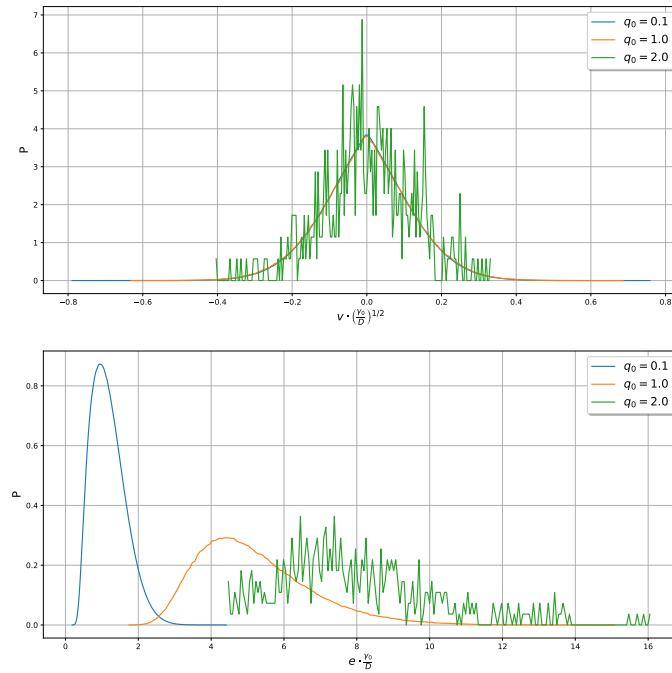


**Figure 5.10:** Distributions of  $v$  (upper plot) and  $e$  (lower plot) for particles immediately before & after switching with varying values of  $q_0$  at  $d_0 = 10.0$  (Cases E1-E3). Other parameters  $\Delta t = 0.1$ ,  $\gamma_0 = 1.0$ ,  $D = 0.1$ ,  $c = 0.001$

is seen centred at  $v = 0$ , the scale of this distribution is the same no matter the value of  $q_0$  or  $d_0$ . This conforms with the expectation from the theory (eqs. (4.1.8b)) that motion at low  $v$  is completely governed by stochastic dynamics. The statistics available for cases C3, D3 and E3 (figs. 5.8, 5.9 and 5.10) are poor due to the low number of switches recorded.

As  $d_0$  is increased and the value of  $e_p$  reduces it can be seen that larger portions of the distributions for  $e$  for cases A1-E1 sit on the right-hand-side of the line. This signifies that once the particles switch, they will have enough energy to undergo negative friction and accelerate towards the stationary velocity  $v_0$ . For case A1 in fig. 5.6 the entirety of the energy distribution is at values  $e(v) < e_p$ . This corresponds with the wide-Gaussian velocity distribution be-

haviour seen earlier (fig. 4.8) as well as with the lack of any high  $\tau_s$  switching times. Particles exist at lower  $v$  and are governed primarily by stochastic forces.

For cases C3, D3 and E3 the energy distributions exist for all values  $e(v) > e_p$ . This signifies that as soon as a particle switches direction it will begin to be pumped towards the opposite stationary point. The velocity is still too low for this to occur immediately (the depot has no effect on  $v$  at these low velocities) however once the particle is accelerated enough by the stochastic force it will drive towards the stationary velocity  $v_0$  as the active force takes precedent.

### 5.3.3.1 Conclusions

The energy distributions show a similar trend across all values of  $d_0$ , with the magnitude of the energy set by the value of  $q_0$ . Cases A-E1 ( $q_0 = 0.1$ ) show the most focused concentration of energy at lower values, with the distribution widening and as the value of  $q_0$  increases in the other cases. The values of  $\mu_e^D$ , the mean energy after switching (mean of the data from the plots), were calculated and are listed in tab. 5.1.

The values of  $\mu_e^D$  give an insight to the dynamics of these particles at low velocities and the relationship to the earlier discussed initial average ensemble behaviours (discussed in Section 4.2). Referencing the  $\langle e_{ss} \rangle_c$  data in table 4.5 and also the visual data in figs. 4.5 and 4.6, comparisons can be made.

For all of cases A1-E1, it can be seen that the value of  $\mu_e^D$  is

**Table 5.1:** Dimensionless standard deviation of velocity ( $\sigma_{vD}$ ) and mean value of the dimensionless absolute velocity ( $\mu_{|v|D}(t)$ ) and mean dimensionless energy ( $\mu_{eD}$ ) measured immediately before and after a directional switch for all parameter sets.

| Case | $\sigma_{vD}$ | $\mu_{ v D}$ | $\mu_{eD}$ |
|------|---------------|--------------|------------|
| A1   | 0.1211        | 0.1407       | 50.12      |
| A2   | 0.1213        | 0.1407       | 106.0      |
| A3   | 0.1214        | 0.1407       | 129.6      |
| B1   | 0.1211        | 0.1407       | 6.187      |
| B2   | 0.1217        | 0.1407       | 19.56      |
| B3   | 0.1220        | 0.1407       | 28.69      |
| C1   | 0.1212        | 0.1407       | 3.564      |
| C2   | 0.1220        | 0.1407       | 12.86      |
| C3   | 0.1230        | 0.1407       | 19.21      |
| D1   | 0.1213        | 0.1407       | 1.638      |
| D2   | 0.1227        | 0.1407       | 6.867      |
| D3   | 0.1251        | 0.1407       | 10.28      |
| E1   | 0.1214        | 0.1407       | 1.180      |
| E2   | 0.1235        | 0.1407       | 5.185      |
| E3   | 0.1226        | 0.1407       | 7.978      |

the same as the steady state energy  $\langle e_{SS} \rangle_c$  with the exception of E1 where the value is slightly higher. Case E1 was also the only case for these low  $q_0$  values where the particle velocity distribution was bimodal and where the behaviour was described as transitioning to type-2.

In all other cases the average energy after switching is equivalent to the value of energy of the first peak of the  $\langle e(t) \rangle_c$  graphs (figs. 4.8, 4.9, 4.10, 4.11 and 4.12).

This result goes further to show that the type-1 particles are behaving in an OU-like manner, where their canonical average of energy is the same at steady state as it is just before or after a switch. As this is the region of space which they most frequently occupy this distribution shows the mean behaviour of a large portion of their behaviour at steady state. The type-2 particles exist between two equilibria — near to the stationary velocity where their energies are

lower and velocities are higher; or near to the origin where their energy is higher and their velocity is the same as that for all other less active particles. The earlier observed peaks in the  $\langle e(t) \rangle_c$  line are thus seen to be as a result of the large influx of energy into particles on short timescales residing near to the origin at  $v = 0$  before they move into an area of velocity space where they accelerate towards the stationary points and deplete their depots.

The timescale with which the particles climb to their first peak of energy in these figures thus also shows the amount of time which particles will remain close to the origin, gaining energy and behaving like OU particles. After a particle changes direction it has been seen to have this same behaviour, as evidenced by the mean energy in v-e phase-space and also by the large proportion of switches which occurred on short timescales. The short time-scale for switching may also be thought of as a charging up time. Once the particle energy reaches this peak value, the probability of moving to the higher velocity limits increases. A proportion of particles do so, which was seen earlier by the initial decay of the mean energy after the first peak; which correlates with the observed increase in the particle velocity. The final mean value calculated earlier will be a weighted mean of the energy of the fraction of particles existing in the low velocity region ( $\mu_e^D$  calculated here) combined with that of the particles existing at the mean energies around the stationary point ( $mu_e(v_0) \approx e_P$ ).

These results show in a more detailed manner the dynamics of the

system when switches in velocity occur. Type-1 particles exist only in the OU-like limit where the average behaviour before and after switching is similar to the overall canonical behaviour. In the less active type-2 cases the particles more frequently exhibit this OU-like behaviour, though their overall average behaviour is also influenced by the longer spells spent near to the stationary velocities in a single region of  $v - e$  phase-space. The most active type-2 particles have longer trajectories in these regions which is seen by their higher period of switching as well as the wider velocity distributions seen earlier.

## 5.4 Fitting Parameters to Switching Time Distributions

### 5.4.1 Introduction

In Section 5.2 we saw that the distributions of switching times were of similar shape for all cases at low values of  $\tau_S$ , with the decay rate decreasing for more active type-2 particles. Type-2 particles also showed a second and longer characteristic timescale which showed a power law-like decay of probability at high  $\tau_S$ .

In this section, curve fitting techniques were used to attach a numerical value to the decay rate of characteristic time of these particles. The initial decay rate was seen to be similar to the analytical OU solution for the survival probability distribution. The distributions of velocities immediately after a switch (Section 5.3) also showed that when the particles were at low velocities they behaved in an OU-like manner regardless of the level of energy in their depots or their depot conversion rate  $d_0$ .

### 5.4.2 Methodology

The distributions were separated into two sets of data based upon the observed point at which the two time-scale behaviours separated from each other. In some cases, an overlap in the behaviours was seen which accounts for the increase in probability of switching at longer times than at shorter times.

#### 5.4.2.1 Shorter Timescale Fitting

In Section 3.1.5 the hitting time probability distribution was discussed (eq. (3.1.14)). This equation was used to fit the observed

value of the effective diffusion constant  $D_{\text{eff}}$  for the active particles. Making the assumption that at low velocities particles behave in a purely stochastic manner, the equation can be simplified with the value  $\gamma(v) \approx \gamma_0 = 1$ :

$$h(\tau|v_{t_0}) = \left(\frac{2v_{t_0}^2}{\pi D_{\text{eff}}}\right)^{1/2} \left( \frac{e^{-\tau}}{(1 - e^{-2\tau})^{1/2}} + \frac{e^{-3\tau}}{(1 - e^{-2\tau})^{3/2}} \right) \exp\left(-\frac{v_{t_0}^2}{2D_{\text{eff}}(1 - e^{-2\tau})}\right) \quad (5.4.1)$$

For the hitting time  $\tau$ , with initial velocity  $v_{t_0} = v(t = 0)$  (this is not related to the stationary velocity  $v_0$ ). For the case of a particle switching direction (i.e. hitting  $v = 0$ ), we refer to the hitting time as the switching time  $\tau_s$ .

The value of  $D_{\text{eff}}$  which fits the distribution to the curve was calculated. This makes the assumption that at low velocities  $\gamma(v) \approx \gamma_0$  and thus the activity simply results in an increase in the effective diffusion constant, which is the perceived increase in the strength of the stochastic force. This was seen to occur over all velocities for case A1,

Due to the simulation time-step, the minimum measurable  $\tau_s$  value for a particle is  $\tau_s = 2\Delta t$ , corresponding to a single measured simulation step in one direction before a switch to the reverse. As the likelihood of particles within the simulation ever actually being at an exact zero-value, the simulation results showed a majority of switching occurring at  $\tau_s = \Delta t$ . In order to correctly fit the data and compensate for this simulation artefact, a non-zero value of  $v_{t_0}$  was chosen. Because the velocity behaviour just before-and-after

switching was the same of all cases in Section 5.3, it was assumed that  $v_{t_0} = \mu_{|v|} \hat{D} = 0.1407$  for all cases. This is the value which was calculated and presented in table 5.1 for the mean absolute velocity after switching for all parameter sets.

Half of the probability of the particle surviving is lost when  $v_{t_0} = 0$ . In the simulations this was not seen due to the minimum time step  $\Delta t = 0.01$ . In order to compensate for this simulation artefact; the value of  $v_{t_0}$  for each curve was set as the value of  $|v|$  from the velocity before and after a switch data discussed in the previous section.

#### 5.4.2.2 Longer Timescale Fitting

The second, longer-timescale part of the results were fitted with a non-linear power law decay function using eq. (3.5.7) which was introduced in Section 3.5.4:

$$h(\tau_s) = h_0(1 - h_0)^{\frac{\tau_s - \tau_0}{\lambda}} \quad (5.4.2)$$

Where  $h_0$  is the probability of switching at the reference time  $\tau_0$  and  $\lambda$  is the decay time constant for the system. Descriptions of the fitting parameters  $\tau_0$  and  $\lambda$  and their effects on the dynamics of the function are provided in Section 3.5.4.

It is seen in some of the cases that the short timescale switching behaviour overlaps with the emergent longer timescale behaviour, as the probability of switching increases for longer times. If at these points the value of  $h(\tau)$  is some combination of the distribution functions of both of these behaviours, it is not possible to separate

this stochastic calculated value into its constituent parts.

The value  $\tau_0$  used for each fit was chosen from the graphical results in Section 5.2 as the point where there was a clear difference between the initial and long timescale switching distributions. The statistics of switches at long timescales for cases D3 and E3 were not sufficient to fit these curves.

The value  $\chi_{\text{OU}}^2$  shows the accuracy of the fit and is calculated using eq. (3.5.8) from Section 3.5.5.

### 5.4.3 Results

Figures 5.11, 5.12, 5.13, 5.14 and 5.15 show the calculated fits on log-log scales for the switching distributions. The subplots show the separate fits for the OU-like behaviour and the long time-scale power-law fit, as well as both plotted on the same axes. The values of  $D_{\text{eff}}$ ,  $h_0$ ,  $\lambda$ ,  $\tau_0$  and  $\chi_{\text{P}}^2$  (the chi-squared statistic for the power-law fit) for both fits are summarised in tables 5.2 and 5.3.

The values of  $D_{\text{eff}}$  measured for all cases were similar, with a very large error value. Due to the large error associated with calculating the proportion of particles which switch within the first time-step for OU particles, the least-squares method of fitting these data points to the  $h(\tau_s)$  distribution is ineffective. The analytical solution defines this exactly based upon the initial velocity  $v_{t_0}$ . The exact initial velocity of particles has to be estimated based off of the diffusion constant  $D$ . As seen in Section 5.3, particles behave in an OU manner just before and after switches, regardless of the level of activity or energy in their depots. Thus there is an equal chance

**Table 5.2:** Summary of fitted effective diffusion  $D_{\text{eff}}$  and fitting error  $\chi_{\text{OU}}^2$  for all cases for switching time fits at short timescales (lower  $\tau_s$  — where particles exhibit OU-like behaviour) calculated using the OU first hitting time distribution model eq. (5.4.1).

| Case | $D_{\text{eff}}$  | $\chi_{\text{OU}}^2$ |
|------|-------------------|----------------------|
| A1   | $0.264 \pm 0.075$ | 187.7                |
| A2   | $0.266 \pm 0.089$ | 184.7                |
| A3   | $0.266 \pm 0.089$ | 183.3                |
| B1   | $0.265 \pm 0.075$ | 187.2                |
| B2   | $0.269 \pm 0.090$ | 181.8                |
| B3   | $0.271 \pm 0.090$ | 178.8                |
| C1   | $0.265 \pm 0.075$ | 186.6                |
| C2   | $0.270 \pm 0.090$ | 178.4                |
| C3   | $0.274 \pm 0.091$ | 176.1                |
| D1   | $0.266 \pm 0.075$ | 185.3                |
| D2   | $0.276 \pm 0.091$ | 173.5                |
| D3   | $0.281 \pm 0.099$ | 197.9                |
| E1   | $0.266 \pm 0.091$ | 184.3                |
| E2   | $0.280 \pm 0.092$ | 171.6                |
| E3   | $0.263 \pm 0.140$ | 455.8                |

**Table 5.3:** Summary of fitted reference time ( $\tau_0$ ), decay rate ( $\lambda$ ) and scaling factor ( $h_0$ ) along with corresponding statistical errors for switching time fits at long-timescales using the power-law decay model eq. (5.4.2).

| Case | $\tau_0$ | $h_0$   | $\lambda$                         | $\chi_{\text{P}}^2$    |
|------|----------|---|-----------------------------------|------------------------|
| A2   | 8.5      | $6.37 \times 10^{-03} \pm 5.31 \times 10^{-05}$ | $0.0474 \pm 1.07 \times 10^{-03}$ | $1.55 \times 10^{-07}$ |
| A3   | 15.0     | $2.67 \times 10^{-03} \pm 4.17 \times 10^{-06}$ | $0.0494 \pm 1.21 \times 10^{-04}$ | $6.49 \times 10^{-10}$ |
| B2   | 4.5      | $8.95 \times 10^{-03} \pm 2.23 \times 10^{-04}$ | $0.113 \pm 7.07 \times 10^{-03}$  | $5.18 \times 10^{-06}$ |
| B3   | 4.5      | $6.30 \times 10^{-04} \pm 1.19 \times 10^{-05}$ | $0.187 \pm 1.21 \times 10^{-02}$  | $5.52 \times 10^{-08}$ |
| C2   | 3.5      | $6.27 \times 10^{-03} \pm 8.32 \times 10^{-05}$ | $0.168 \pm 5.70 \times 10^{-03}$  | $1.26 \times 10^{-06}$ |
| C3   | 3.5      | $1.44 \times 10^{-04} \pm 5.12 \times 10^{-06}$ | $0.231 \pm 3.66 \times 10^{-02}$  | $1.70 \times 10^{-08}$ |
| D2   | 3.5      | $2.41 \times 10^{-03} \pm 9.62 \times 10^{-06}$ | $0.240 \pm 2.75 \times 10^{-03}$  | $2.66 \times 10^{-08}$ |
| E1   | 1.5      | $4.45 \times 10^{-02} \pm 3.61 \times 10^{-04}$ | $0.0899 \pm 1.12 \times 10^{-03}$ | $6.28 \times 10^{-06}$ |
| E2   | 2.5      | $1.38 \times 10^{-03} \pm 6.67 \times 10^{-06}$ | $0.270 \pm 4.68 \times 10^{-03}$  | $1.79 \times 10^{-08}$ |

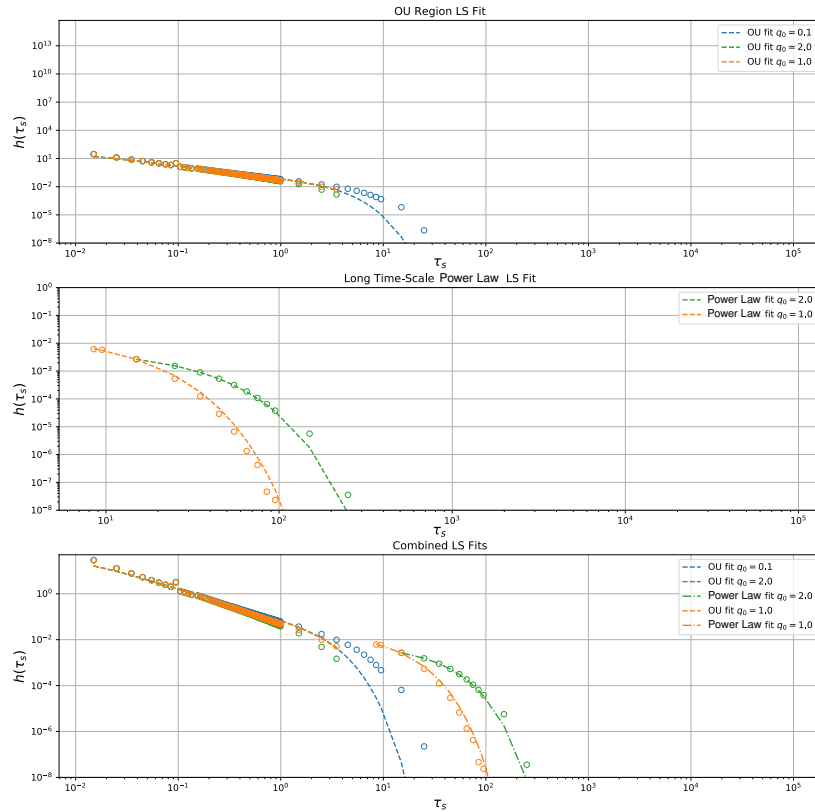


**Figure 5.11:** Least-square line fits for short and long timescale data (Cases A1, A2, A3).  $d_0 = 0.1$ ,  $c = 0.001$ ,  $D = 0.1$ ,  $\gamma_0 = 1.0$ .

of being moved in either direction and an immediate switch occurs approximately half of the time.

There is not much decay in the short-timescale section, and the longer-timescale part overlaps at quite an early  $\tau_s$ . This makes fitting eq. (5.4.1) quite difficult as the two data sets cannot be separated from each other. As the value of  $h(\tau_s)$  is so large at these low values of  $\tau_s$  compared with even slightly larger values, due to the large rate of decay, the least-squares method of fitting with this equation and the available data does not give an accurate fit.

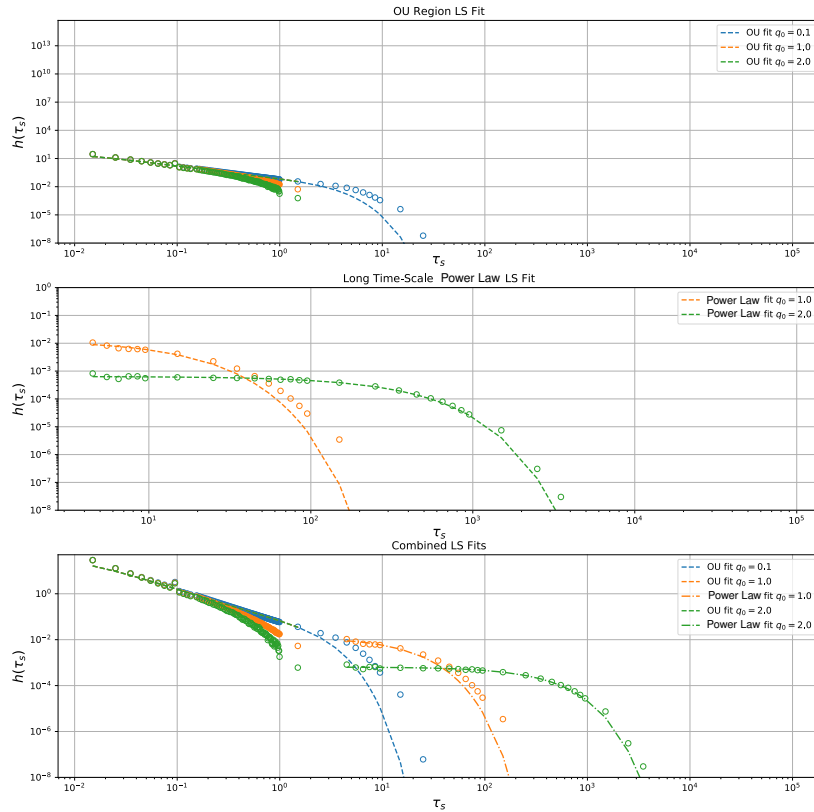


**Figure 5.12:** Least-square line fits for short and long timescale data (Cases B1, B2, B3).  $d_0 = 1.0$ ,  $c = 0.001$ ,  $D = 0.1$ ,  $\gamma_0 = 1.0$ .

The power law decay (eq. (5.4.2)) method of fitting the longer timescale data is much more accurate. It can be seen graphically that in all of the type-2 cases including the transitional case E1 the stochastic switching data fits very well with the calculated line fit. The calculated  $\chi^2_{\text{P}}$  values and the relative errors confirm this numerically.

It is seen that as the particles increase in activity  $d_0$ , the initial value of probability of switching  $h_0$  for this second behavioural region decreases. This is counterbalanced by an increase in the decay

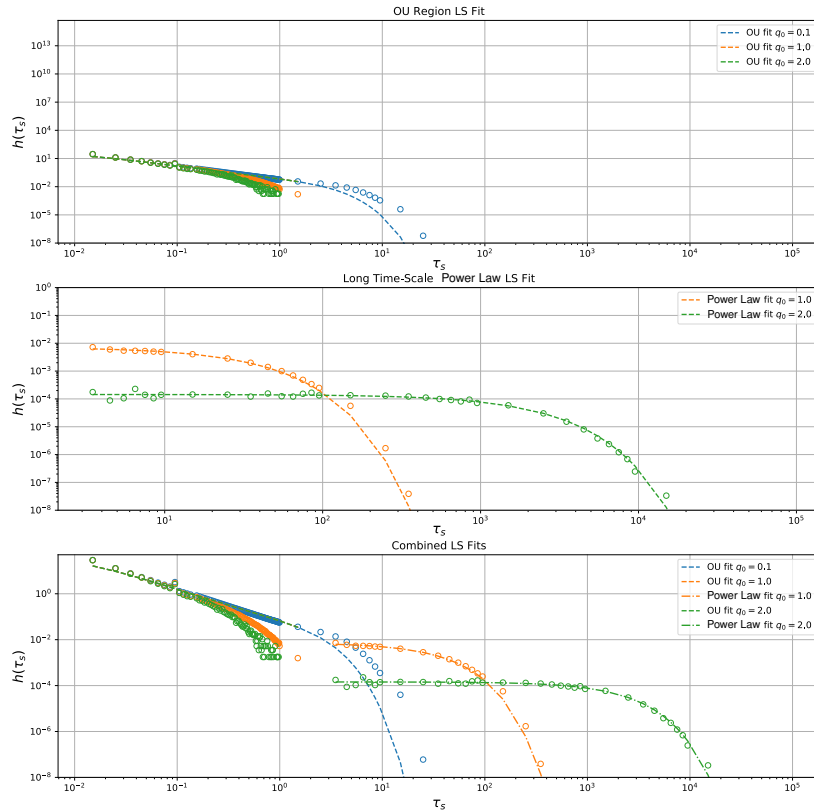


**Figure 5.13:** Least-square line fits for short and long timescale data (Cases C1, C2, C3).  $d_0 = 2.0$ ,  $c = 0.001$ ,  $D = 0.1$ ,  $\gamma_0 = 1.0$ .

time constant  $\lambda$ .

Case E1 is the only case for  $d_0 = 0.1$  which exhibited longer time-scale switching and has a very low value of  $\lambda = 0.0899$ . The onset time of this longer-timescale switching behaviour is seen to be on a similar order of magnitude to the short-timescale OU-like behaviour. This correlates with the earlier observation that the stochastic force for this case is always a similar order of magnitude to the active component (as discussed in Chapter 4).

This shows that even though these values are lower, the spread of

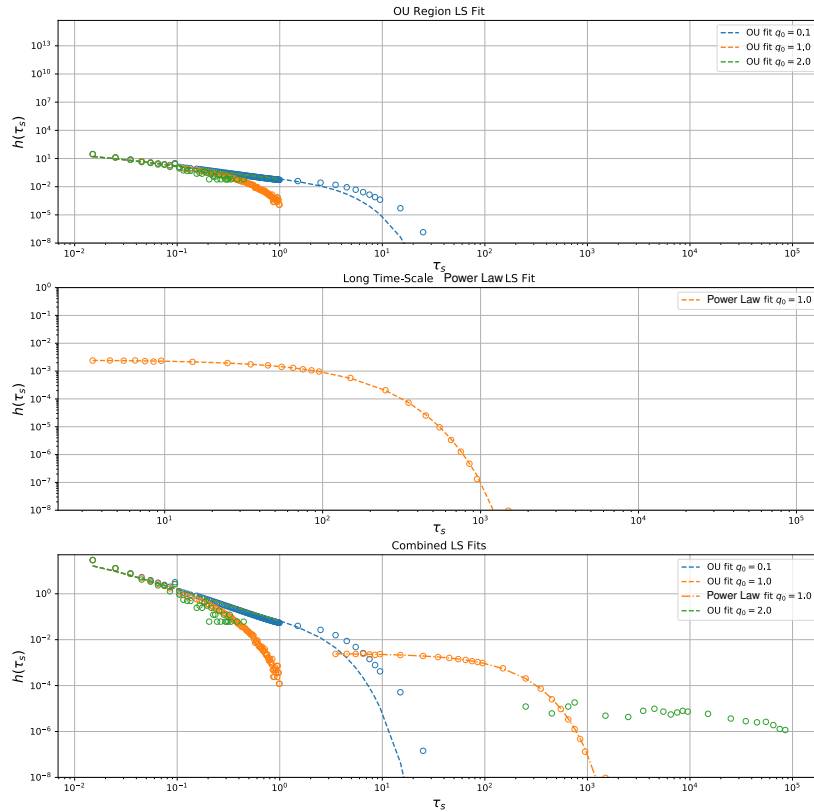


**Figure 5.14:** Least-square line fits for short and long timescale data (Cases D1, D2, D3).  $d_0 = 6.0$ ,  $c = 0.001$ ,  $D = 0.1$ ,  $\gamma_0 = 1.0$ .

switching times decays over a longer time period. The timescale of the decay of these long-time switches is many orders of magnitude larger than all of the other timescales in the system.

#### 5.4.3.1 Conclusions

It was seen that at higher  $q_0$  values, the *width* of the tail of the probability distribution for switching (i.e. the range of times over which the low-frequency switches occurred) was much wider. Particles are much less likely to reduce their velocity as the energy in the depot is much more quickly replenished when compared to the

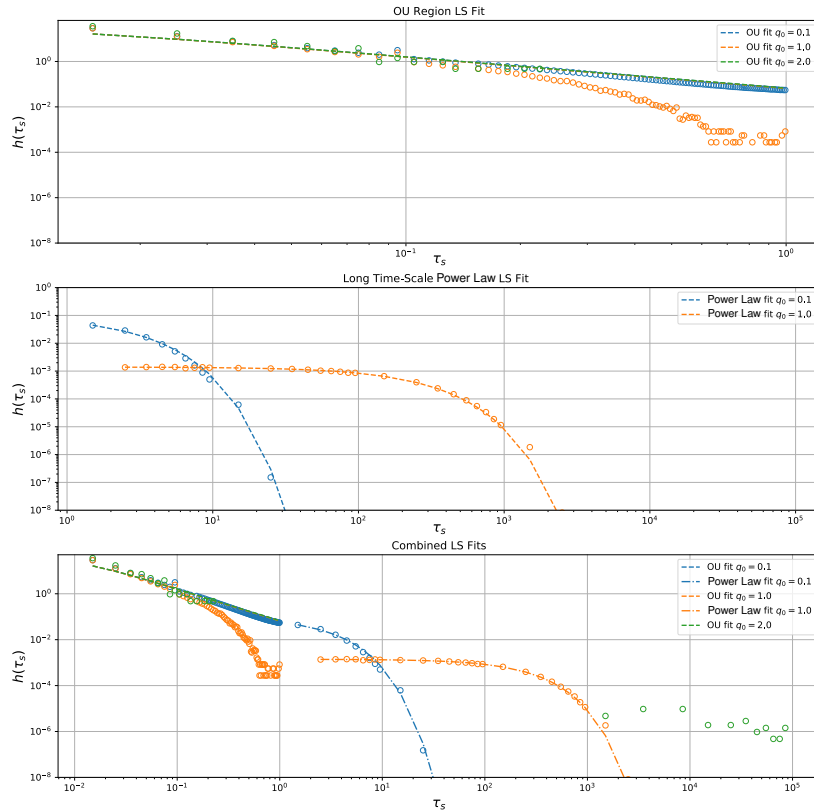


**Figure 5.15:** Least-square line fits for short and long timescale data (Cases E1, E2, E3).  $d_0 = 10.0$ ,  $c = 0.001$ ,  $D = 0.1$ ,  $\gamma_0 = 1.0$ .

lower  $q_0$  cases. This is also seen through the secondary effect of larger  $q_0$  values correspond to larger values of  $v_0$  — thus large chain of stochastic events is required to move from the typical stationary velocity  $v_0$  to the origin  $v = 0$ .

Increasing  $d_0$  also decreased the rate of switching at higher timescales, as the particle was more actively driven towards the stationary points. The long timescale thus represents the characteristic timescale of the “unlikely” chain of stochastic events required to force the particle from the stationary point back to  $v = 0$ .

The short time-scale switches occur chiefly as a result of stochastic forces at low velocities whilst the high  $\tau_s$  events occur due to the particle overcoming the active force. The scale of the active force is governed by the parameters  $q_0$  and  $d_0$ . When the stochastic force is small relative to the active force, as is the case for type-3 and type-4 particles or in the case where  $D$  is made small, the probability of a stochastic event which can overcome this force and switch diminishes until no switches are observed at all. This coincides with the region of  $q_0/d_0/D$  parameter space where the probability distribution in  $v - e$  space would have a value of  $P(v = 0) = 0$ .

The fits at shorter characteristic timescales were not of a good quality as shown by the high values of  $\chi_{\mathbf{P}}^2$ . This was partially as a result of the inability to model particles very close to the  $v = 0$  boundary at timescales below  $\Delta t$  — where a large quantity of the population of switches were lost in the simulations. The simulations could be adapted in order to use smaller timesteps at lower velocity in order to capture this behaviour as part of any future analysis.

At longer  $\tau_s$  a much better fit was found using the power-law method which is reflected in the low values of  $\chi_{\mathbf{P}}^2$  in Table 5.3. This shows that the data presented here can be modelled by a power law with the fitted parameters, however it may also be of interest to use methodologies such as those outlined by Clauset et al.[86] in order to confirm these findings.

These results could be improved with access to more computational resources. Simulations could be run which tracked only the

switching time of particles and did not remember the trajectory. The current simulations took days to run for each of the cases, so running for these longer periods may not be worthwhile. However, if left to run for long enough then more switches could be gathered for all parameter cases which would result in more accurate statistics. This would allow for more resolution over the behaviour at longer time-scales as the bin width could be reduced.

It may also be possible to run simulations which differentiated between switches in low velocity regions and the timescale of moving from the region near the stationary velocity to this low velocity regime so this meta-data could be used to explicitly fit the two behaviours separately. This would still require the additional computational resources to obtain good statistics.

## 5.5 Velocity & Energy Autocorrelation Functions

### 5.5.1 Introduction

In this section, the autocorrelation of the velocities and energies of particles with EDs are investigated. The autocorrelation function (described in Section 3.5.2) describes how related a value in a system is with itself at a time of  $\Delta\tau$  later (known as a lag). This function takes a value between 0 and 1. An autocorrelation of 1.0 means that the values at both times are perfectly correlated whilst a value of 0 means that the values are completely uncorrelated. Deterministic time evolution functions are perfectly auto-correlated as the future behaviour is directly as a result of a position in the past. OU particles and ED particles do not show this behaviour due to the random influence of the stochastic force.

In the previous sections particles defined as type-2 were shown to spend large periods of their trajectories travelling at velocities close to the stationary velocity  $v_0$  before moving to low- $v$  regions of space where they were able to switch direction. At low- $v$  these particles were seen to behave like purely OU particles (inactive) or particles with low activity. They spend time accumulating energy in the depot before accelerating to a higher region of velocity space by converting this energy into kinetic energy.

These particles therefore exist in two states, the first travelling at  $v$  near  $v_0$ , and the second moving slowly and undertaking switches. It was seen in the previous section that there are two distinct time scales over which the particles will exist in either state. By look-

ing at the autocorrelation of a particle velocity over a trajectory, it would be expected therefore that the particle would remain positively correlated whilst moving near to the stationary point, only becoming decorrelated when it moved to the switching region of velocity space or to the opposite stationary point. In other words, the autocorrelation for particles which switch may be another way to estimate the time scale over which they switch direction.

The second behaviour which may be seen by the autocorrelation of a particle is the similarity or difference in the decorrelation rate of the velocity and energy. In the adiabatic case, the velocity and energy must always decorrelate at the same rate as any change in depot energy is accompanied by a change in the  $v$ . For non-adiabatic particles this is not true, and the decorrelation of the particle energy may be slower or faster than the decorrelation of the velocity. It would be expected for the type-2 and type-3 particles that the relationship would be more similar to that of the adiabatic case, with differences accounted for by the non-adiabatic behaviours seen at low velocities. For the type-1 active-OU particles, it remains unclear to this stage whether the energy or the velocity would be expected to decorrelate faster.

The time scale of this decorrelation is also of interest. In Section 4.2 the time scale of particles moving from rest with empty depots to a system steady-state was considered. In Section 5.2 two distinctive time scales were observed, attributed to the switching time for particles at low velocities and the time scale for particles

moving at higher velocities to move into this low velocity region. It was seen that the initial time scale corresponded to particles moving at low velocities reaching a steady state energy within their depots before some of these particles moved towards the stationary point regions of velocity space. The observed switching time scales represented the fast velocity switching of particles at low velocities behaving like OU particles and the long time scale directional switching of particles which required rare stochastic events to overcome the active force and turn around.

In this section, the autocorrelation of both velocity and energy for active particles with EDs were measured over stochastic simulated trajectories.

### 5.5.2 Simulation Parameters

Data from the same single-particle trajectories used throughout this chapter were analysed. Values for  $t < 200$  were discarded as before, to ensure that the initial conditions were not having an effect on the results (as found in Section 4.2). The auto-correlation for the particle energy and velocity with lags in the range  $[\Delta\tau, 10^4 \times \Delta\tau]$  were calculated from the remainder of the data set.

### 5.5.3 Methodology

The autocorrelation of the velocity and energy at each point within the trajectory limits defined was found up to a maximum lag of  $10^4 \times \Delta\tau$ . For the simulation time-step  $\Delta t = 0.01$ , this corresponds to a maximum lag of  $\tau = 100.0$ . Software was written to calculate

these values using the methodology outlined in Section 3.5.2.

#### 5.5.4 Results

The velocity autocorrelation curve for OU particle with  $D = 0.1$ ,  $\gamma_0 = 1.0$ ,  $\Delta\tau = 0.01$  is presented in fig. 5.16.

From eq. (3.1.9) the velocity should de-correlate with its initial value  $v_0$  on a time scale governed by  $\gamma_0^{-1}$ . For underdamped OU particles, this time scale is finite and measurable relative to the time scale of the diffusion; unlike in the case of purely Brownian particles in the overdamped regime discussed earlier where the particle velocity would instantly decorrelate. This behaviour is seen in the results, with a sharp drop in the velocity correlation followed by a longer flat region. Fluctuations are present around  $v = 0$  due to statistical error, but it can be seen that the particle  $v$  becomes uncorrelated at very short time scales.

The results of the autocorrelation calculations for all cases are shown in figs. 5.17, 5.18, 5.19, 5.20 and 5.21.

It can be seen in case A1 (fig. 5.17) that the velocity quickly decorrelates over the first 10 time units, but that there is a much slower decay in the correlation of the energy. The velocity decorrelates much like the OU particle shown in fig. 5.16, though on a slightly longer time scale. As these particles exist at low velocities and have a low energy conversion rate  $d_0$ , the particle must find a way into a higher velocity space in order to deplete its depot reserves. It was seen earlier that the particles could exist at all velocity values with similar values of energy, and the fact that these particles take

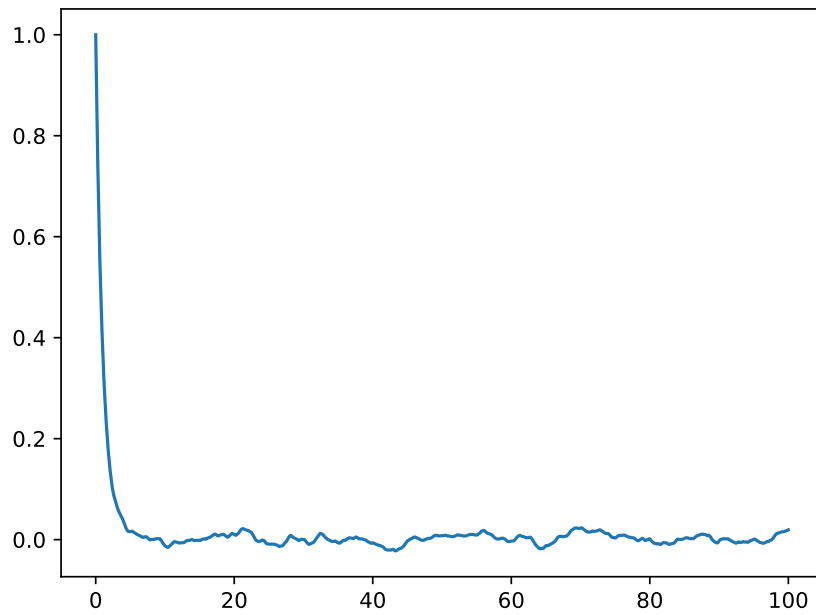


**Figure 5.16:** Velocity autocorrelation plot for an OU particle over lag time range  $\Delta\tau[0, 100]$ .  $D = 0.1$ ,  $\gamma_0 = 1.0$ .

a long time to use this energy up in general explains why the values decorrelate over a much longer time scale than the velocity.

Cases A2 and A3 show similar behaviour to each other. Both of these cases were classified as type-2 particles, where the particle may easily switch between directions and travel through the low velocity regions. These behaviours are seen again in the autocorrelation data. The velocity quickly decorrelates within the first few units of time, but then slows down and decays over a longer time scale. The first decay originates from particles in the low  $v$  OU-like region of space. These points quickly decorrelate due to the lack of memory of low velocity OU-like particles, where the history of the particle trajectory has little influence on its current position. The slower lag-time decay originates from particles which exist around either

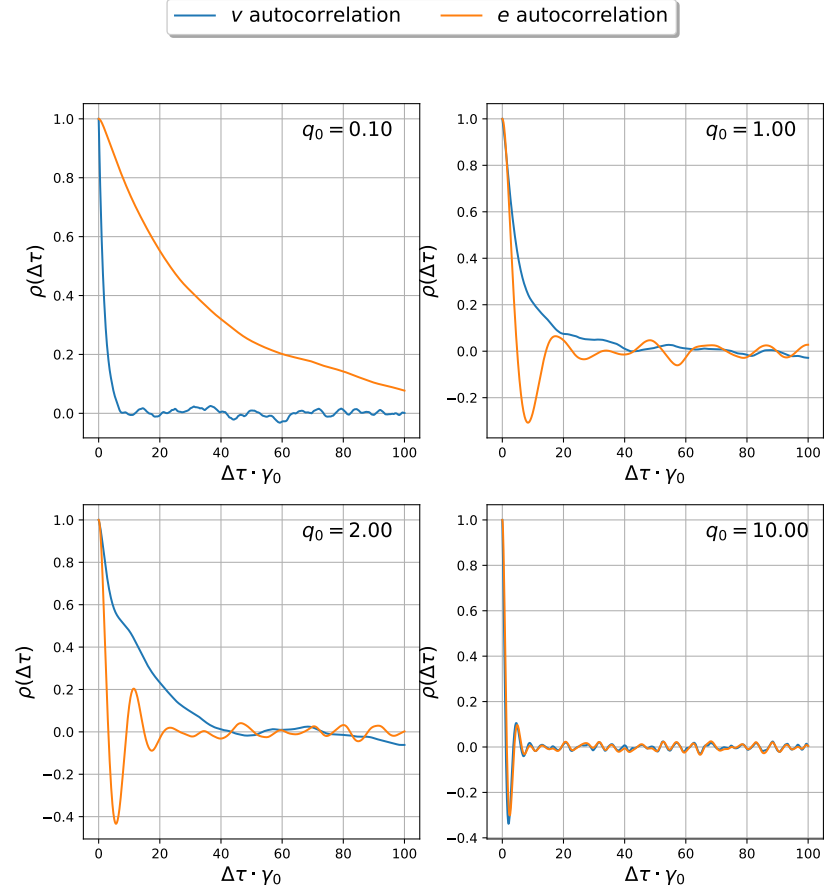


**Figure 5.17:** Comparisons of  $v$  and  $e$  autocorrelation for varying  $q_0$  values over lag times  $\Delta\tau[0, 100]$  (Cases A1-A4). Other parameters  $d_0 = 0.1$ ,  $c = 0.001$ ,  $D = 0.1$ ,  $\gamma_0 = 1.0$ .

stationary point  $\pm v_0$ . As shown in the previous sections, they may spend a longer time at these limits before switching, this is seen as the velocity remaining correlated as it rests in a certain region of velocity space. As a larger proportion of particles in case A3 take a longer time to switch direction, the decorrelation of the velocity is slower.

The autocorrelation of the energy also shows the existence of particles within the two velocity regions. The energy quickly decorrelates and then becomes negatively correlated. This can be explained by the oscillatory behaviour of the depot in these non-adiabatic regimes due to stochastic fluctuations deviating the particle from  $v_0$ .

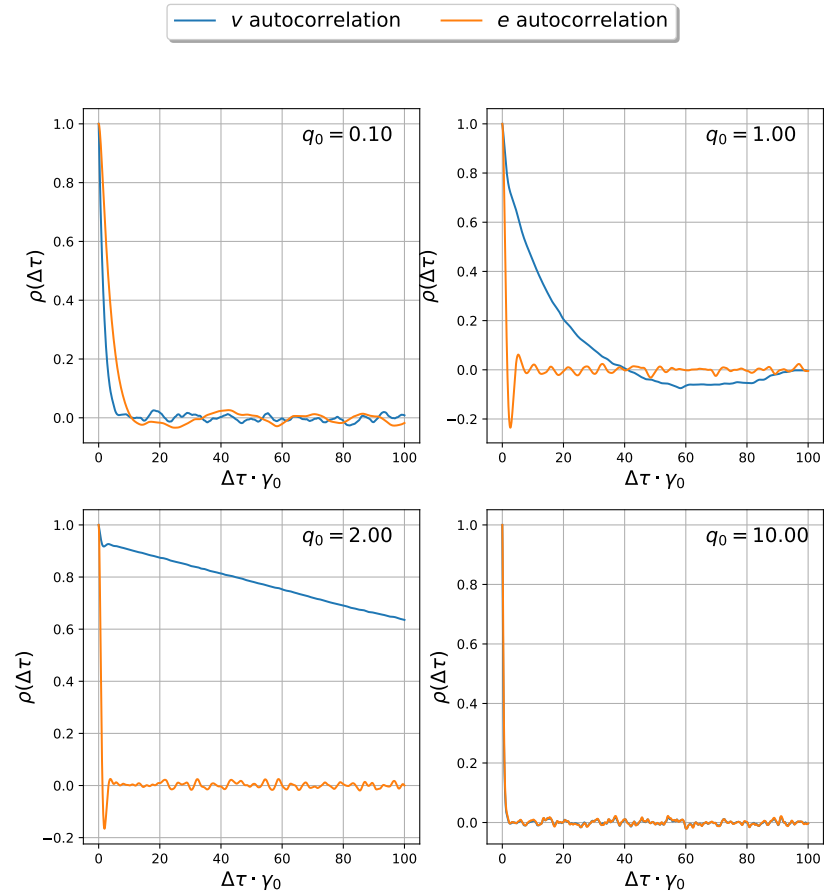


**Figure 5.18:** Comparisons of  $v$  and  $e$  Autocorrelation for varying  $q_0$  values over lag times  $\Delta\tau[0, 100]$  (Cases B1-B4). Other parameters  $d_0 = 1.0$ ,  $c = 0.001$ ,  $D = 0.1$ ,  $\gamma_0 = 1.0$ .

As with the  $v - e$  distributions in Section 4.4 (fig. 4.15), the depots fill up at lower  $v$  and then use this depot energy up to accelerate. Therefore on the time scale of a particle moving from the lower- $v$  energy accumulating mode in to the higher- $v$  depot-draining mode there is a negative correlation. It is seen that on a similar time scale particles will move back from this high- $v$  low- $e$  region and into the lower- $v$  high- $e$  region — so after this additional time the particles will be at similar values of  $e$  again and the correlation again becomes positive. There are “bumps” in the  $v$  correlation corresponding to the oscillations in  $e$ .

Case A4 shows an extremely fast decorrelation of both the ve-

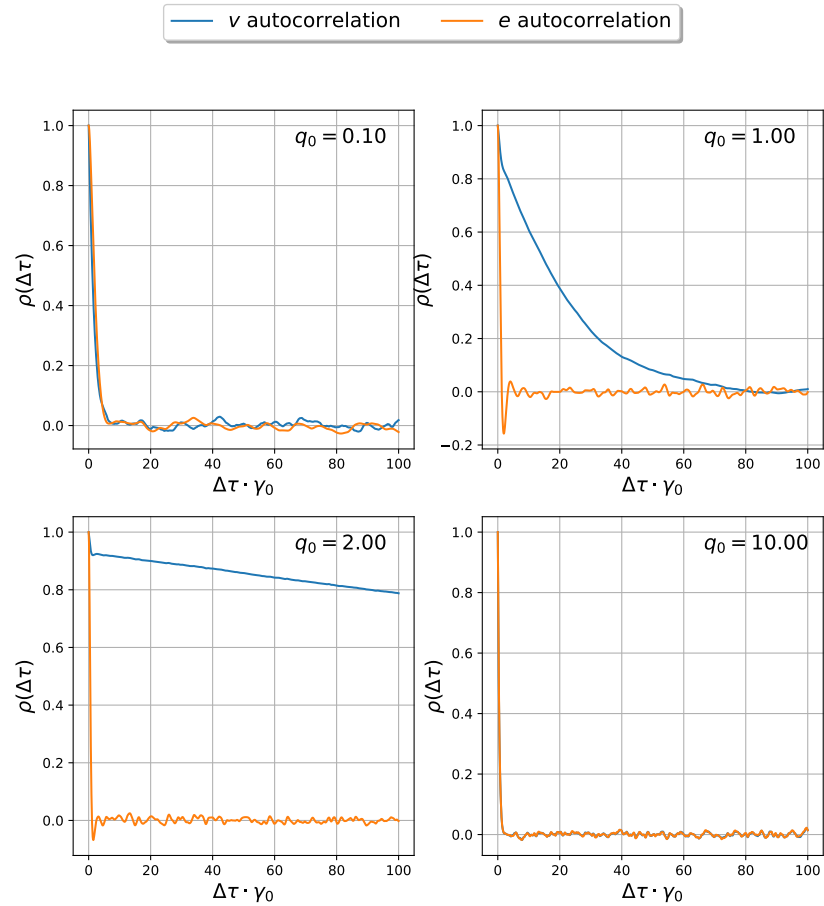


**Figure 5.19:** Comparisons of  $v$  and  $e$  Autocorrelation for varying  $q_0$  values over lag times  $\Delta\tau[0, 100]$  (Cases C1-C4). Other parameters  $d_0 = 2.0$ ,  $c = 0.001$ ,  $D = 0.1$ ,  $\gamma_0 = 1.0$ .

locity and the energy where both become negatively correlated before oscillating between positive and negative correlation. This fast decorrelation can be explained by the fact that the particle is always near to the stationary velocity  $v_0$  for these type-3 particles. The stochastic force was seen earlier to move the particle through a tightly constrained region of  $v - e$  phase space in this example. The negative correlation shows the data for particles on the opposite side of the distribution at the stationary velocity oscillating between the two allowed limits of this system.

Because there is only data for particles in one direction,  $v$  decor-

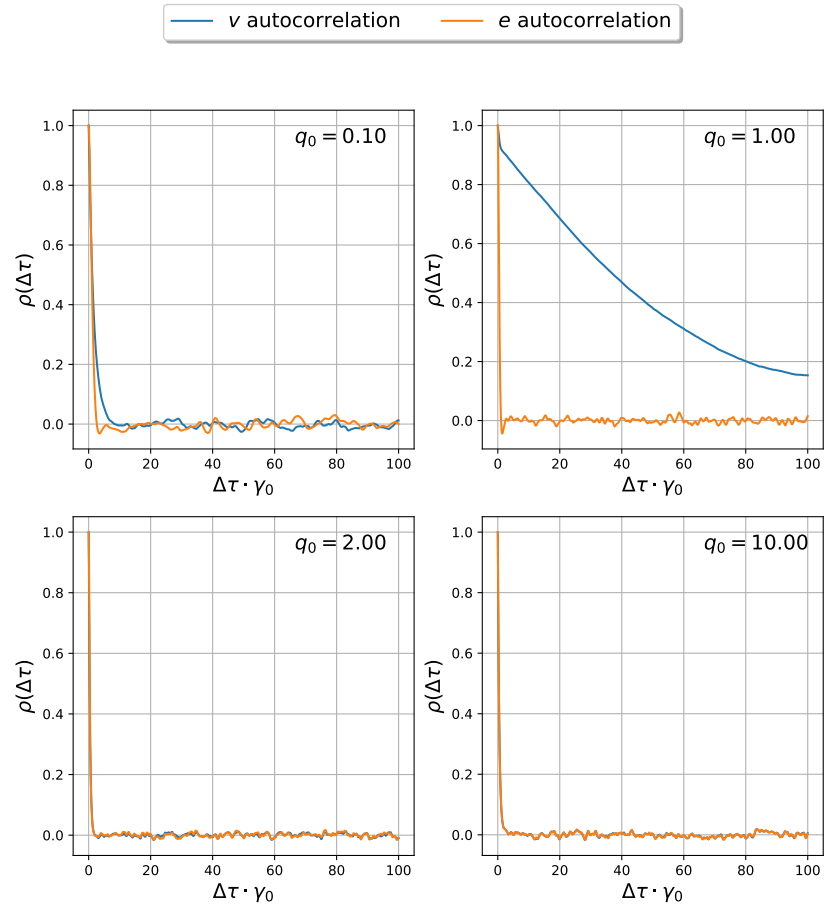


**Figure 5.20:** Comparisons of  $v$  and  $e$  Autocorrelation for varying  $q_0$  values over lag times  $\Delta\tau[0, 100]$  (Cases D1-D4). Other parameters  $d_0 = 6.0$ ,  $c = 0.001$ ,  $D = 0.1$ ,  $\gamma_0 = 1.0$ .

relates quickly over a shorter time scale. The longer time scale decorrelation seen for type-2 particles is not present as there is no concept of decorrelation through switching to the opposite region of  $v$  space near to  $v_0$ . The velocities therefore decorrelate as a result of fluctuations around a stationary point  $\pm v_0$  (recall fig. 4.8). The decorrelation behaviour is similar to that of an OU particle in that there is a fluctuation around a mean, showing that after a characteristic time the particle velocities are decorrelated (fluctuations are governed by the stochastic noise), however it is also reiterated that the dynamics are different as the active component of the force is

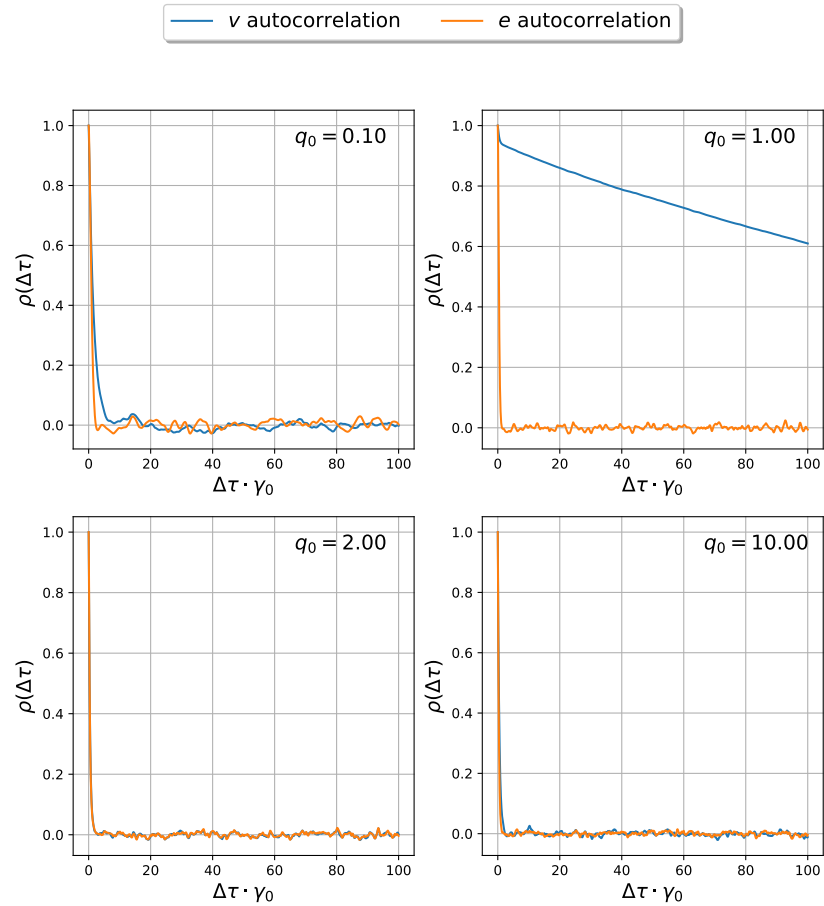


**Figure 5.21:** Comparisons of  $v$  and  $e$  Autocorrelation for varying  $q_0$  values over lag times  $\Delta\tau[0, 100]$  (Cases E1-E4). Other parameters  $d_0 = 10.0$ ,  $c = 0.001$ ,  $D = 0.1$ ,  $\gamma_0 = 1.0$ .

tightly coupled to  $v$ .

Increasing the value of  $d_0$  for type-1 particles greatly increases the decorrelation rate in energy. This is seen in cases B1-E1 — for B1  $v$  decorrelates faster than  $e$ , by case C1 both  $e$  and  $v$  are decorrelated on the same time scales, and by case D1  $e$  is decorrelating faster than  $v$ . It was previously noted that this increase of  $d_0$  also corresponded to how a change in the average energy depends velocity for these particles (Section 4.4). As the particles can convert their depot energy quicker and at lower velocities, the depot value is more affected by the stochastic force and so the energy itself decorrelates

quicker. This was seen by the average value of the energies at higher velocities getting closer to the value of  $e_0$  as  $d_0$  was increased.

For the A1-E1 cases where the particles are OU-like the  $v$  autocorrelation is similar. The velocity does not remain correlated even in case E1 where the particles transition towards a type-2 behaviour. This shows that the particles are completely governed by the stochastic force which decorrelates on the time scale set by the diffusion constant  $D$ .

The type-2 cases B2-D2 showed similar behaviour in  $v$  to the type-2 cases A2-A3 discussed above. There was a quick decorrelation on a very short time scale, followed by a slower decorrelation occurring within the 100 time units. This, again, indicates the two distinctive behaviours type-2 particles exhibit. The initial decorrelation is a result of the particles behaving like OU particles at low  $v$ . The longer time scale correlation shows particles remaining near to one of the stationary velocities  $\pm v_0$  for a time before switching to the other. When  $v$  is fluctuating around either the positive or negative  $v_0$ , the values are correlated in that region of  $v$ -space. Once a switch occurs, this correlation is lost. Thus the time scale of de-correlation and the time scale for switching ( $\tau_s$ ) for these particles are related. This will be discussed in more detail later.

Cases B3, C3 and E2 again showed similar behaviour in  $v$  to B2-D2. The reduced rate of switching manifested in the autocorrelation data as a very long time scale decorrelation after the initial fast decorrelation. The value of the initial decorrelation was also

much smaller, indicating that the total percentage of the particle trajectory spent in the OU-like region was much less than in the other cases. This again confirms what was seen in the previous switching time distributions. These particles spend much longer times moving at velocities near to the stationary points. The particle velocity therefore tends to remain correlated over longer periods of time.

A negative autocorrelation value of  $e$  is also seen for these particles at small time scales. This signifies particles moving between the limits in energy seen from the low, almost adiabatic values near to  $v_0$  and the higher values above  $e_p$  near to the origin in the OU-like region of velocity-space.

The remaining type-3 and the type-4 cases all show a quick decorrelation of both the velocity and the energy. This is expected as these particles do not switch direction and therefore fluctuations in  $e$  and  $v$  are purely from uncorrelated stochastic events. The non-adiabatic type-3 cases show energy and velocity decorrelating on similar time scales to each other.

### 5.5.5 Conclusions

Type-1 particles were seen to decorrelate in velocity over very short time scales due to their OU-like behaviour. The energy in case A1 decorrelated over a longer time scale as the rate of depot energy conversion  $d_0$  was low. As the conversion rate  $d_0$  increased in these cases, the rate of decorrelation of energy increased, eventually overtaking the rate of the velocity. The time scale of complete

decorrelation for the velocity was similar to the value of  $\tau_s$  for these particles where all of the particles had switched. The large initial rate of decorrelation also corresponded to the large probability of a switch at very low time scales.

Type-2 particles showed a quick decorrelation of energy which led to a negative correlation on short time scales. This was due to the particle energy being above the average when these particles are moving at low velocities and below the average when the particles are moving at higher velocities. These particles are defined by their transitional behaviour between this OU-like behaviour and the more adiabatic-like movement near to the stationary velocities  $\pm v_0$ . The negative correlations and oscillatory behaviour is caused by particles switching between these two regions over time. The velocity for all of these particles quickly partially decorrelated initially due to short time scale fluctuations, with a more gradual decorrelation over long time scales.

In the less active type-2 cases the time scale of this second decorrelation was shorter due to the larger probability of the particle switching. For more active type-2 particles the same behaviour is exhibited, though in these cases velocity decorrelates over a much longer time scale due to the switching period being much longer.

Case D3 appeared as an outlier to the other type-2 distributions. Across the simulation time-frame there were no switches seen for D3 due to its longer time scale for switching.

In order to improve the statistical quality of the data set, the

autocorrelation could be calculated over the entire trajectory with additional computational power — the auto-correlation calculation requires the full input data set (more data would introduce memory limitations) and has an algorithmic complexity which scales with  $n \times \log(n)$ [88] (for  $n$  the number of data points) for the number of data points  $n$ . This would also help to improve some of the statistics of the other plots and reduce the amount of statistical noise which is present in the plotted lines.

Negative correlation in case B2 and C3 are due to directional switching. The resultant  $v$  after a switch is on the other side of  $v = 0$ , nearer to the opposite  $v_0$  value. This results in negative value for autocorrelation in  $v$ .

The correlation of particles which exhibited switching could also be calculated over longer time scales with higher lag values. This would confirm that the long term velocity decorrelation time scale would be on the order of magnitude of the long time scale switching time.

The autocorrelation analysis of these particles has assisted in further clarifying the emergence of the two different behaviours for type-2 particles. The correlation between the velocities over long time scales adds more resolution to the emergent picture of the mixed behaviour. These particles show OU-like behaviour at lower velocities, where their depots fill up due to the lower activity and velocities reducing the rate of depot energy consumption. They then transition to higher velocities by depleting these depots. Once

at higher velocities, they are confined within a region of  $v - e$  space until the stochastic force slows them down and they return to the low velocity region.

# Chapter 6

## Conclusions

### 6.1 Conclusions of This Work

#### 6.1.1 This Work in Context

Since the initial studies of Schweitzer, Ebeling and Tilch[39] there have been many investigations into these ED particles in 1-,2- and 3- dimensions. We noted that a majority of these were carried out in regimes where the dynamics of the depot energy  $e_0$  were exactly coupled to the velocity  $v$  (the adiabatic assumption). We investigated particles in 1-D and found that by varying the model parameters  $q_0$  (fuel uptake) and  $d_0$  (conversion rate) at low  $v$  (depot dissipation) it was possible to observe particles in clearly non-adiabatic regimes, as evidenced by the decoupling of the  $e$  and  $v$  (especially at lower velocities).

From this work we have seen that the onset of adiabatic behaviour is not well defined in one parameter space, with only the highest  $d_0$  and  $q_0$  case E4 showing strong agreement with the assumption and similar behaviour to that seen in the literature[89].

When particles are travelling at low velocities, they accumulate a surplus of energy in their depots, which is rapidly consumed when

the correct sequence of stochastic events transitions them into areas of velocity space where they are able to consume the energy and accelerate towards, and beyond, the stationary points  $\pm v_0$ . The second behaviour was observed at the stationary points, where particles in our case travelled on trajectories through  $v - e$  phase-space above and below the  $e_0(v)$  line. In our simulations, stochastic events were able to slow particles from this region and into the low- $v$  region.

We quantified four separate behaviours in our system, three of which were non-adiabatic in  $e$ :

- Particles which behaved as with regular stochastic motion — an increased  $D_{\text{eff}}$  and a normal distribution in  $v$ .
- The emergence of a bimodal distribution in  $v$  and with a significant probability to exist at low  $v$  due to the stochastic force working on a similar order of magnitude to the active force.
- Bimodal distributions with non-adiabatic depots where  $v_0$  is a significantly non-zero value such that events which slow the particles and allow directional switching are rare.
- Adiabatic behaviour and fluctuation around stationary point  $v_0$ , with energy  $e(v) = e_0(v)$

Thus we have seen that the switching between these two behaviours is driven by the ability for the stochastic force to slow the particles down into the low- $v$  (the energy-accumulating region). At low- $v$  we saw in our simulations much larger deviations from  $e_0(v)$  in  $e$ . The low value of  $c = 0.001$  chosen for our simulations contributed to a

large difference between the stationary values  $e_0(v_0)$  and  $e_0(v = 0)$ . Thus if depot energy is unable to relax quickly as a result of  $v$  (i.e. consumption) and also  $c$  (i.e. dissipation), then particles cannot behave adiabatically.

We have analysed the distribution of the characteristic times for particles to exist at these regimes, and fit parameters to the two different characteristic timescales through the existing survival time distribution at low velocities, and a power law for particle survival time distributions near to the stationary points.

To the best of our knowledge, this form of analysis of switching times has not been used thus far in the literature for these particles. It would be of interest to apply this as a methodology for observing directional switching to limit cycles in 2-D.

### **6.1.2 1-D ED Particles in the Physical World**

Though our simulations were abstracted away from real systems in that they were purely numerical, it is important to consider how the work we have completed could be mapped back to the actual physical systems. Active motion of proteins such as Kinesin is a good example of a 1-D use-case in nature as they walk along a fixed path, we postulated that the catalysis of fuel by QD-AP conjugates which we observed in the laboratory could be modelled by the energy depot.

This use of the model may also be useful for multi-dimensional systems where motion is fixed to one-dimension an external field or gradient. In a system where a particle is confined to a single plane of

motion our research may be useful in understanding the time scales at which the particle could undergo directional switching behaviour. Particles at an interface of two fluids or running along the edge of a vessel may be found in similar states due to the effects of surface tension.

One artifact of the model, which is key to the results we present, is that the activity is low when the particle is near rest — the conversion term has a proportional dependence on the velocity of the particle. Though this may not be a common occurrence in nature, we could speculate that the model would fit well to systems where active motion only occurs once the particles (or organisms) are *warmed up*.

The parameters which we varied,  $q_0$  and  $d_0$ , find good analogues in the abundance of a fuel source and the rate of conversion of the fuel source in natural systems, respectively. In more fuel rich environments it is conceivable that there could be an increased rate of absorption of that fuel into the depot — the driving force behind such motion would on first assumption be a higher concentration gradient. Similarly, the rate of consumption of the fuel  $d_0$  may be an abstraction of a more complex process such as metabolism in cells or organisms — something which can vary depending on the organism itself or even between different sized organisms of the same type. For an inorganic object such as a Janus particle or the QD-AP aggregate which we discussed in Section 2.1.2.2, a good analogue could be the quantity of catalyst which bound with the

particle or even the physical configuration of the surface and thus the available rate of consumption of fuel.

The dissipation rate  $c$  was initially posited to be some form of *internal metabolism* for, say, a cell[39]. Whilst it perhaps fulfils a more important role in balancing the model equations to prevent an infinite accumulation of energy, this term does allow for the modelling of other losses of energy due to particle destruction or fuel decomposition which does not result in acceleration.

The abstract nature of the model as well as the particular dynamics of the depot consumption mean that it is difficult to map to exact real world scenarios, however we believe that it does offer a good framework. By introducing more particular dynamics relating to these physical (or even animal) systems into the key parameters it may be possible to adapt the model to more complex dynamics. A different form of the  $d(\mathbf{v}, \mathbf{r})$  ansatz could be utilised which would take into account distinct properties of the physical system — for example an animal’s rate of consumption of food; or photo-sensitivity of a cell that only consumes energy when exposed to light. More complex forms of the energy uptake  $q$  could also be introduced as mentioned earlier.

## 6.2 Future work

### 6.2.1 Extension to Present Work

In Section 4.2 we simulated particles starting from rest and observed ensemble average behaviour in  $v$  and  $e$ . We saw oscillatory responses

with different levels of damping across the values of  $d_0$  and  $q_0$  which we varied. We could go further by fitting these parameters of these *signal response curves* in the noisy ( $D \neq 0$ ) regime and comparing the damping factors against the theoretical values for non-noisy systems. It would be of interest to then compare these characteristic timescales against those observed in Section 5.4, where we observed the switching time distributions.

We have yet to numerically solve the first passage time distribution for ED particles, however it would be of interest to generate an analogous Green's function for eq. (3.1.12). Our results from Section 5.4 could then be compared against simulated results and we could better understand the two emergent switching characteristic timescales.

We observed particles at low  $c$ , allowing for accumulation of energy within the depots regardless of  $v$ . We would expect, in agreement with the literature, for the rate of depot relaxation to quicken with higher  $c$  (regardless of  $v$ ) which would bring particles more in line with the adiabatic assumption. It would be of interest to study where in the multi-parameter space of this model this onset would occur.

The type-3 particles behaved non-adiabatically, where we saw that  $e(v) \neq e_0$  (Section 4.4). There have been many studies in the literature for particles in 2-D where it would be of interest to compare our results. In 2-D, the additional directional motion allows for additional consumption of depot energy and could be the reason

why adiabatic behaviour is studied more frequently. In this case — it would also be of interest for us to compare the type-3 particles which were not able to switch direction, yet were also not adiabatic, and see whether these classifications would persist into 2-D and even 3-D velocity-space. The onset of adiabatic behaviour is a combination of the parameters which we varied, along with the dissipation  $c$  and strength of the active force  $D$ . We would look to use our extended 1-D study here to try and quantify this experimentally.

We have constructed a flexible simulation software which can be easily adapted to not only additional adaptations of the energy depot, but also to other models of particle activity.

It would be interesting to look further into the parameter fitting of switching time distributions in Section 5.4. As a first followup — additional analysis on the results of the fitting could be carried out to confirm that the tails of these distributions follow the heavy-tailed distribution pattern to which they were fitted. It was seen that the  $\chi^2_{\text{P}}$  values for the power-law fit presented in table 5.3 were low, indicating a good fit between the model and the raw data. Additional analysis on the quality of the fits as well as the suitability of the selected power law could be carried out using the methodologies outlined by Clauset[86] in order to further confirm that this was the correct model and that the fitted parameters could extrapolate to other simulation data sets.

A further research goal could be to investigate any way in which the parameters fitted in table 5.3 could be calculated from the sim-

ulation parameters  $D$ ,  $q_0$  and  $d_0$ . Whilst this may not initially be possible with a first principles approach, it would be of interest to attempt to use the fitted parameters from the multiple different cases to try and fit a relationship between the simulation parameters. This could then be tested by extrapolating to parameter regimes outside of the fitting population and seeing how the switching time distribution for simulation results compared with that expected from the power law fitting parameters which were estimated from the parameter values.

In real systems a particle confined to a single dimension may not necessarily only accelerate due to an active force in the forward direction. We could extend our model to take into account rotational Brownian motion on the agent particle, which would allow for switching of the direction-of-acceleration at non-zero values of  $v$ . In such a model, the active force component would be applied tangentially always in the same direction as the direction of motion. The active force could then act to slow a particle by applying a force against the present direction of motion.

### 6.2.2 Beyond the Present

The original authors of the ED model have looked in great depth at the 2-D and 3-D case. In these multi-dimensional systems the depot energy is consumed by the particle accelerating across all directional components of its velocity vector which moves the component velocity  $v_i$  into regions of  $v_i - e$  phase-space where switching is possible. It may be interesting to observe multi-dimensional particles with

depots reserved for dimensional consumption. At first, one would expect for  $v_i..v_j$  to become uncorrelated as the trajectories appear as independent 1-D cases.

Limit cycles and effects of external fields on these ED particles in 2-D and 3-D systems are broadly covered in the literature[70, 90, 91, 92, 91, 75], however there is still not a clear understanding of the onset of adiabatic behaviours within these cases. This work covered the dynamics of 1-D particles in depth where the dissipation parameter  $c$  was especially low. We carried out these observations in 1-D in the absence of external gradients in order to understand the difference between low and high velocity behaviours.

We did not cover external fields in this work, instead focusing on understanding the dynamics of non-adiabatic particles with random forces, and the unique dynamics which emerge in  $v, e$  phase space. Schweitzer's work in piece-wise linear potentials[76] showed interesting dynamics for particles where the conversion  $d_0$  was varied in the presence of an asymmetric saw-tooth-like gradient, as discussed in Section 2.4.5. Two critical conversion rates  $d_c$  were observed which governed a 1-D deterministic and adiabatic ED particle's ability to escape the potential well created by the gradient in  $v$  space. It would be interesting to revisit this work and compare the parameter regimes which we investigated here in order to understand if removing the two assumptions made in the original work (that the particles are purely adiabatic, and that the stochastic force has little effect on the system) could show more interesting dynamics. We

observed in Section 4.3 the type-2 and type-3 particles accumulating depot energy over longer periods at low  $v$ , and then consuming this to accelerate into higher  $v$  regions around the fixed points. It would be of interest to observe how particles would behave if they were confined to the minimum of the gradient (i.e. between two saw-teeth), and whether escape from this region of  $v$  space was linked to the characteristic switching time  $\tau$  which we calculated. In order to better contextualise these results within the literature, further work could carry out additional simulations in the presence of the different potential waves which have previously been studied (such as saw-tooth[76], ratchet[45]), and to add further resolution through application of the analytical techniques for how *adiabatic* the particles are (i.e. relationship between  $v$  and  $e$  in  $v - e$  phase-space) alongside the observations of the switching distributions.

We would similarly like to understand whether these transitional Brownian-like non-adiabatic behaviours observed in 1-D are present in multiple particle systems in higher dimensions. Models such as Vicsek's[46, 47] could be adapted for particles with energy depots in order to take account of particle direction and clustering due to particle-particle interactions. Czirok, along with Vicsek, in fact in the past studied self-propelled particles (SPP) in one-dimension and observed their organisational behaviours[93]. We could go beyond this work to observe how the transitional ED behaviour in non-adiabatic regimes, and the dynamics of depot accumulation and pumping would behave with studies such as this as a reference.

To our knowledge there are no studies of 1-D particles with either repulsive or attractive interactions — though one may conjecture that in the repulsive case these would space out *on a line* and cluster together in the attractive case for non-switching particles. In the parameter regimes where we saw switching, it may be of interest to observe the dynamics of particles and how these compare to classical oscillators. We are able to introduce additional forces and interactions to the software which we have created so these ideas may merit investigation.

It would be of interest to follow up on examples from the literature such as multi-particle systems in crowded environments[71].

Alternative ED models such as the fourth-order-conversion model (as in eq. (2.4.11))[70] or the asymmetric velocity conversion model (eq. (2.4.12)[72]); models where energy uptake  $q(\mathbf{r})$  or even conversion rate  $d(\mathbf{r})$  vary throughout space, models with time dependence on external fields  $\nabla U(t)$  or the depot uptake  $q(t)$  could be simulated and analysed in a similar way to the base model which was observed as part of this work.

### 6.3 Concluding Thoughts

Our analysis of 1-D Brownian particles with Energy Depots found that in certain parameter regimes for a fixed diffusion constant  $D$  particles tended closer to the adiabatic limit in depot energy  $e$  as the activity  $d_0$  and fuel accumulation  $q_0$  parameters were increased. We analysed the velocity distributions from numerical simulations to

compare to analytical solutions of the steady-state Fokker-Planck Equation (FPE) from which we identified 4 different behaviours approaching and within the adiabatic limit. For the non-adiabatic particles, running individual trajectories for longer times we were able to observe the dynamics of these particles switching direction and attempt to fit these using a power-law. Particles in low-velocity regions exhibited a more chaotic switching behaviour which was consistent with normal Brownian particles.

We utilised alternative methods to those commonly utilised within the literature in order to do our analysis, such as the observation of the switching time and also presented an auto-correlation analysis of both energy and velocity for particles. All of this analysis helped to enrich the understanding of the two different emergent behaviours at lower and higher (closer to the fixed points) velocities, and we have attempted to explain the dynamics of how particles accumulate energy at low  $v$  before expending it accelerating to near their fixed points where they are able to spend longer times before stochastic events slow them back down again.

The energy depot model represents a simple way of modelling ABPs which can offer rich dynamics and has the capacity to be expanded to more complex systems (multi-particle, potential gradients, different energy conversion models) as needs arise. Our study of this specific case of non-adiabatic particles offers more understanding of the specific parameter regimes we chose as well as the dynamics in 1-D which are not widely covered in the literature for

ABPs with EDs. This research could serve as a good foundation for future work adapting the aforementioned more complex systems to non-adiabatic systems and our methodologies for analysing characteristic timescales for different paths through switching time distributions could also find use elsewhere in the field.

# References

# Bibliography

- [1] Joy Leckie, Alexander Hope, Meghan Hughes, Sisir Debnath, Scott Fleming, Alastair W. Wark, Rein V. Ulijn, and Mark D. Haw. Nanopropulsion by biocatalytic self-assembly. *ACS Nano*, 8(9):9580–9589, 2014.
- [2] Robert Brown. A brief account of microscopical observations made in the months of june, july, and august 1827, on the particles contained in the pollen of plants; and on the general existence of active molecules in organic and inorganic bodies, 1827.
- [3] Albert Einstein. *Investigations on the Theory of The Brownian Movement*. Dover Publications, Inc., 1905/1956.
- [4] Don S. Lemons and Anthony Gythiel. Paul Langevin’s 1908 paper “On the Theory of Brownian Motion” [“Sur la théorie du mouvement brownien,” C. R. Acad. Sci. (Paris) 146, 530–533 (1908)]. *American Journal of Physics*, 65(11):1079–1081, 1997.
- [5] Jean Baptiste Perrin. Mouvement brownien et réalité moléculaire. *Annales de Chimie et de Physique*, 18:5–114, 1909.
- [6] Howard Brenner. Coupling between the translational and rotational brownian motions of rigid particles of arbitrary shape I. Helicoidally isotropic particles. *Journal of Colloid and Interface Science*, 22:104–122, 1965.
- [7] Howard Brenner. Coupling between the translational and rotational brownian motions of rigid particles of arbitrary shape: II. General theory. *Journal of Colloid and Interface Science*, 23:407–436, 1967.
- [8] Peter Reimann. Brownian motors: noisy transport far from equilibrium. *Physics Reports*, 361:57–265, 2002.
- [9] P. Romanczuk, M. Bär, Werner Ebeling, and B. Lindner. Active brownian particles. from individual to collective stochastic dynamics. *Eur. Phys. J. Special Topics*, 202:1–162, 2012.
- [10] M. S. Kumar and P. Philominathan. The Physics of flagellar motion of E. coli during chemotaxis. *Biophysical Reviews*, 2:13–20, 2010.
- [11] H. G. Othmer, S. R. Dunbar, and W. Alt. Models of dispersal in biological systems. *Journal of Mathematical Biology*, 26:263–298, 1988.
- [12] Rodrigo Soto and Ramin Golestanian. Run-and-tumble dynamics in a crowded environment: Persistent exclusion process for swimmers. *Physical Review E*, 89:012706, Jan 2014.
- [13] R. T. Tranquillo and D. A. Lauffenburger. Stochastic model of leukocyte chemosensory movement. *Journal of Mathematical Biology*, 25:229–262, 1987.
- [14] Nicolas J. Cordova, Bard Ermentrout, and George F. Oster. Dynamics of single-motor molecules: The thermal ratchet model. *Proceedings of the National Academy of Sciences of the United States of America*, 89:339–343, 1992.
- [15] Simon M. Sanford, Charles S. Peskin, and George F. Oster. What drives the translocation of proteins? *Proceedings of the National Academy of Sciences of the United States of America*, 89:3770–3774, 1992.
- [16] Michał Zabicki, Werner Ebeling, and Ewa Gudowska-Nowak. The thermodynamic cycle of an entropy-driven stepper motor walking hand-over-hand. *Chemical Physics*, 375:472–478, 2010.
- [17] Richard B. Dickinson and Robert T. Transquillo. A stochastic model for adhesion-mediated cell random motility and haptotaxis. *Journal of Mathematical Biology*, 31:563–600, 1993.
- [18] M. Schienbein and H. Gruler. Langevin equation, fokker-planck equation and cell migration. *Bulletin of Mathematical Biology*, 55:585–608, 1993.

- [19] Howard C. Berg and Douglass A. Brown. Chemotaxis in escherichia coli analysed by three-dimensional tracking. *Nature*, 239(1):500–504, 1972.
- [20] Guanglai Li, Lick-Kong Tam, and Jay X. Tang. Amplified effect of brownian motion in bacterial near-surface swimming. *Proceedings of the National Academy of Sciences*, 105(47):18355–18359, 2008.
- [21] Jia Sun, Haixin Tan, Shiyi Lan, Fei Peng, and Yingfeng Tu. Progress on the fabrication strategies of self-propelled micro/nanomotors. *JCIS Open*, 2:100011, 2021.
- [22] Jinxing Li, Wenjuan Liu, Jiyuan Wang, Isaac Rozen, Sha He, Chuanrui Chen, Hyun Gu Kim, Ha-Jin Lee, Han-Bo-Ram Lee, Se-Hun Kwon, Tianlong Li, Longqiu Li, Joseph Wang, and Yongfeng Mei. Nanoconfined atomic layer deposition of tio<sub>2</sub>/pt nanotubes: Toward ultrasmall highly efficient catalytic nanorockets. *Advanced Functional Materials*, 24:1700598, 2017.
- [23] Zhiheng Lyu, Lehan Yao, Zhisheng Wang, Chang Qian, Zuochen Wang, Jiahui Li, Chang Liu, Yufeng Wang, and Qian Chen. Nanoscopic imaging of self-propelled ultrasmall catalytic nanomotors. *ACS Nano*, 18:14231–14243, 2024.
- [24] S. Ebbens, D. A. Gregory, G. Dunderdale, J. R. Howse, Y. Ibrahim, T. B. Liverpool, and R. Golestanian. Electrokinetic effects in catalytic platinum-insulator janus swimmers. *Europhysics Letters*, 106(5):58003, jun 2014.
- [25] Stephen Ebbens, Mei-Hsien Tu, Jonathan R. Howse, and Ramin Golestanian. Size dependence of the propulsion velocity for catalytic Janus-sphere swimmers. *Physical review. E, Statistical, nonlinear, and soft matter physics*, 85:020401, 2012.
- [26] R. Golestanian, T. B. Liverpool, and A. Ajdari. Designing phoretic micro- and nano-swimmers. *New Journal of Physics*, 9:126, 2007.
- [27] Jonathan R. Howse, Richard A. L. Jones, Anthony J. Ryan, Tim Gough, Reza Vafabakhsh, and Ramin Golestanian. Self-motile colloidal particles: From directed propulsion to random walk. *Phys. Rev. Lett.*, 99:048102, Jul 2007.
- [28] Yasuhiro Ikezoe, Gosuke Washino, Takashi Uemura, Susumu Kitagawa, and Hiroshi Matsui. Autonomous motors of a metal–organic framework powered by reorganization of self-assembled peptides at interfaces. *Nature Materials*, 11:1081, 2012.
- [29] Walter F. Paxton, Kevin C. Kistler, Christine C. Olmeda, Senm Ayusman, Sarah K. St. Angelo, Yanyan Cao, Thomas E. Mallouk, Paul E. Lammert, and Vincent H. Crespi. Catalytic Nanomotors: Autonomous Movement of Striped Nanorods. *J. Am. Chem. Soc.*, 126:13424–13431, 2004.
- [30] S.J. Ebbens. Active colloids: Progress and challenges towards realising autonomous applications. *Current Opinion in Colloid & Interface Science*, 21:14–23, 2016.
- [31] Joy Susan Leckie. *Nanopropulsion by biocatalytic self-assembly*. PhD thesis, University of Strathclyde, 2015.
- [32] Joshua K. Hamilton, Peter G. Petrov, C. Peter Winlove, Andrew D. Gilbert, Matthew T. Bryan, and Feodor Y. Ogrin. Magnetically controlled ferromagnetic swimmers. *Scientific Reports*, 7:2045–2322, 2017.
- [33] V. Serreli, Chin-Fa Lee, Euan R. Kay, and David A. Leigh. A molecular information ratchet. *Nature*, 445:523–527, 2007.
- [34] Xiaoli He, Huaide Jiang, Jianjie Li, Yanmei Ma, Bi Fu, and Chengzhi Hu. Dipole-moment induced phototaxis and fuel-free propulsion of zno/pt janus micromotors. *Small*, 17(31):e2101388, 2021.
- [35] Fischer Black and Myron Scholes. The pricing of options and corporate liabilities. *Journal of Political Economy*, 81(3):637–654, 1973.
- [36] Janusz A Hołyst, Krzysztof Kacperski, and Frank Schweitzer. Social impact models of opinion dynamics. *Annual Reviews Of Computational Physics IX*, pages 253–273, 2001.
- [37] Janusz A Hołyst, Krzysztof Kacperski, and Frank Schweitzer. Phase transitions in social impact models of opinion formation. *Physica A: Statistical Mechanics and its Applications*, 285(1-2):199–210, 2000.
- [38] Frank Schweitzer and JA Hołyst. Modelling collective opinion formation by means of active brownian particles. *The European Physical Journal B-Condensed Matter and Complex Systems*, 15(4):723–732, 2000.
- [39] Frank Schweitzer, Werner Ebeling, and Benno Tilch. Complex motion of brownian particles with energy depots. *Physical Review Letters*, 80(23):5044–5047, 1998.

- [40] Frank Schweitzer. *Brownian Agents and Active Particles*. Springer, first edition, 2003.
- [41] Frank Schweitzer. An agent-based framework of active matter with applications in biological and social systems. *European Journal of Physics*, 40(1):014003, nov 2018.
- [42] Marcelo O. Magnasco. . *Physical Review Letters*, 72(16):2656–2659, 1993.
- [43] Schweitzer, Frank and Schimansky-Geier, Lutz. Clustering of "active" walkers in a two-component system. *Physica A*, 206:359–379, 1994.
- [44] Pawel Romanczuk and Lutz Schimansky-Geier. Brownian Motion with Active Fluctuations. *Physical Review Letters*, 106:230601, 2011.
- [45] Benno Tilch, Frank Schweitzer, and Werner Ebeling. Directed Motion of Brownian Particles with Internal Energy Depot. *Physica A: Statistical Mechanics and its Applications*, 273(3-4):294–314, 1999.
- [46] T. Vicsek, A. Czirok, E. Ben-Jacob, I. Cohen, and O Shochet. Novel Type of Phase Transition in a System of Self-Driven Particles. *Physical Review Letters*, 75(6):1226, 1995.
- [47] T. Ihle. Towards a quantitative kinetic theory of polar active matter. *The European Physical Journal Special Topics*, 223:1293–1314, 2014.
- [48] Ezequiel V. Albano. Self-Organized Collective Displacements of Self-Driven Individuals. *Physical Review Letters*, 77(10):2129, 1996.
- [49] Dirk Helbing and Tamas Vicsek. Optimal self-organization. *New Journal of Physics*, 1:2129, 1999.
- [50] Czirok, Andras and Vicsek, Tamas. Collective behavior of interacting self-propelled particles. *Physica A: Statistical Mechanics and its Applications*, 281:17–29, 2000.
- [51] A. Czirók, M. Matsushita, and T. Vicsek. Theory of periodic swarming of bacteria: Application to proteus mirabilis. *Physical Review E*, 63:031915, Feb 2001.
- [52] M. Christina Marchetti, J. F. Joanny, S. Ramaswamy, T. B. Liverpool, J. Prost, Madan Rao, and R. Aditi Simha. Hydrodynamics of soft active matter. *Reviews of Modern Physics*, 85:1143–1189, 2013.
- [53] Wen Yan and John F. Brady. The swim force as a body force. *Soft Matter*, 11:6235, 2015.
- [54] Sho C. Takatori and John F. Brady. Swimstress, motion and deformation of active matter: effect of an active field. *Soft Matter*, 10:9433, 2014.
- [55] S. C. Takatori and Brady J. F. Superfluid Behavior of Active Suspensions from Diffusive Stretching. *Physical Review Letters*, 118:018003, 2017.
- [56]
- [57] L. Becker, S. A. Koehler, and H. A. Stone. On self-propulsion of micro-machines at low reynolds number: Purcell's three-link swimmer. *Journal of Fluid Mechanics*, 490:15 – 35, 09 2003.
- [58] Ali Najafi and Ramin Golestanian. Simple swimmer at low Reynolds number: Three linked spheres. *Physical Review E*, 69:062901, 2004.
- [59] Herbert Levine, Wouter-Jan Rappel, and Inon Cohen. Self-organization in systems of self-propelled particles. *Phys. Rev. E*, 63:017101, Dec 2000.
- [60] M. Christina Marchetti, Yaouen Fily, Silke Henkes, Adam Patch, and David Yllanes. Minimal model of active colloids highlights the role of mechanical interactions in controlling the emergent behaviour of active matter. *Current Opinion in Colloid & Interface Science*, 21:34–43, 2016.
- [61] Adam Patch, David Yllanes, and M. Cristina Marchetti. Kinetics of motility-induced phase separation and swim pressure. *Physical Review E*, 95(012601):1–8, 2017.
- [62] Sho C. Takatori, W. Yan, and John F. Brady. Swim pressure: Stress generation in active matter. *Phys. Rev. Lett.*, 113(028103):1–5, 2014.
- [63] Michael E. Cates and Julien Tailleur. Motility-induced phase separation. *Annual Review of Condensed Matter Physics*, 6:219–244, 2014.
- [64] Alexandre P. Solon, Joakim Stenhammar, Raphael Wittkowski, Mehran Kardar, Yariv Kafri, Michael E. Cates, and Julien Tailleur. Pressure and phase equilibria in interacting active brownian spheres. *Phys. Rev. Lett.*, 114:198301, May 2015.
- [65] Udo Erdmann and Werner Ebeling. Noise-induced transition from translational to rotational motion of swarms. *Physical Review E*, 71:051904, 2005.
- [66] Werner Ebeling, Frank Schweitzer, and Benno Tilch. Active brownian particles with energy depots modeling animal mobility. *Biosystems*, 49:17–29, 1999.

- 
- [67] U. Erdmann, W. Ebeling, L. Schimansky-Geir, and F. Schweitzer. Brownian particles far from equilibrium. *Eur. Phys. J.*, 15:105–113, 2000.
- [68] Udo Erdmann, Werner Ebeling, and Vadim S. Anishchenko. Excitation of rotational modes in two-dimensional systems of driven Brownian particles. *Physical Review E - Statistical, Nonlinear, and Soft Matter Physics*, 65(6):1–9, 2002.
- [69] Chandrima Ganguly and Debashish Chaudhari. Stochastic thermodynamics of active Brownian particles. *Physical Review E*, 88:032102, 2013.
- [70] Yong Zhang, Chul Koo Kim, and Kong-Ju-Bock Lee. Active motions of Brownian particles in a generalized energy-depot model. *New Journal of Physics*, 10:1–17, 2008.
- [71] Juan Pablo Miranda, Demian Levis, and Chantal Valeriani. Collective motion of energy depot active disks. *Soft Matter*, pages –, 2025.
- [72] Pyeong Jun Park and Kong-Ju-Bock Lee. A modified active Brownian dynamics model using asymmetric energy conversion and its application to the molecular motor system. *J Biol Phys*, 39:439–452, 2013.
- [73] Lin Guan, Yuwen Fang, Kongzhai Li, Chunhua Zeng, and Fengzao Yang. Transport properties of active Brownian particles in a modified energy-depot model driven by correlated noises. *Physica A*, 505:716–728, 2018.
- [74] Kong-Ju-Bock Lee, Chul Koo Kim, and Myung-Hoon Chung. Walking motion of an overdamped active particle in a ratchet potential. *J Biol Phys*, 38:305, 2012.
- [75] Werner Ebeling and Gerd Ropke. Statistical mechanics of confined systems with rotational excitations. *Physica D: Nonlinear Phenomena*, 187(1-4):268–280, 2004.
- [76] Frank Schweitzer, Benno Tilch, and Werner Ebeling. Uphill motion of active brownian particles in piecewise linear potentials. *The European Physical Journal B*, 14:157–168, 2000.
- [77] Frank Schweitzer and J. A. Holyst. Modelling collective opinion formation by means of active Brownian particles. *The European Physical Journal B*, 15:723–732, 2000.
- [78] Crispin W. Gardiner. *Handbook of Stochastic Methods for Physics, Chemistry and the Natural Sciences*. Springer, third edition, 1983.
- [79] Daniel T. Gillespie. The mathematics of Brownian motion and Johnson noise. *American Journal of Physics*, 64(3):225–240, 1996.
- [80] Robert M. Mazo. *Brownian Motion*. Oxford Science Publications, 2009.
- [81] Peter Mörters and Yuval Peres. *Brownian Motion*. Cambridge, first edition, 2010.
- [82] Garcia-Ojalvo, Jordi and Sancho, José M. *Noise in Spatially Extended Systems*. Springer, first edition, 1999.
- [83] Daniel T. Gillespie. Exact numerical simulation of the Ornstein-Uhlenbeck process and its integral. *Physical Review E*, 54:2084–2091, Aug 1996.
- [84] George E. P. Box and Gwilym M. Jenkins. *Time Series Analysis - Forecasting and Control*. Holden-Day, second edition, 1970.
- [85] Skipper Seabold and Josef Perktold. statsmodels: Econometric and statistical modeling with python. In *9th Python in Science Conference*, 2010.
- [86] Aaron Clauset, Cosma Rohilla Shalizi, and M. E. J Newman. Power-law distributions in empirical data. *SIAM Review*, 51:661–703, 2009.
- [87] N. Balakrishnan, Vassily Voinov, and M.S. Nikulin. *Chi-Squared Goodness of Fit Tests with Applications*. Elsevier, first edition, 2013.
- [88] Skipper Seabold and Josef Perktold. statsmodels: Econometric and statistical modeling with python. In *9th Python in Science Conference*, 2010.
- [89] Frank Schweitzer, Werner Ebeling, and Benno Tilch. Statistical mechanics of canonical-dissipative systems and applications to swarm dynamics. *Physical Review E - Statistical, Nonlinear, and Soft Matter Physics*, 64(2):211101–211112, 2001.
- [90] Werner Ebeling. Active Brownian motion of pairs and swarms of particles. *Acta Physica Polonica B*, 38(5):1657–1671, 2007.
- [91] W. Ebeling and L. Schimansky-Geier. Swarm dynamics, attractors and bifurcations of active Brownian motion. *Eur. Phys. J. Spec. Top.*, 157:17, 2008.

- [92] Werner Ebeling, Ewa Gudowska-Nowak, and Alessandro Fiasconaro. Statistical distributions for hamiltonian systems coupled to energy reservoirs and applications to molecular energy conversion. *Acta Physica Polonica B*, 39(5):1251–1272, 2008.
- [93] Andras Czirok, Albert-Laszlo Barabasi, and Tamas Vicsek. Collective Motion of Self-Propelled Particles: Kinetic Phase Transition in One Dimension. *Physical Review Letters*, 82:209–212, 1999.

## Chapter 7

# Appendices

### 7.1 Differential Chapman-Kolmogorov Equation

A differential form of eq. (3.2.2) showing the time evolution of the probability of a system exists under certain assumptions[78]. This takes the form of a master equation for a Markovian stochastic process and is given by:

$$\begin{aligned} \frac{\partial P(\mathbf{z}, t | \mathbf{y}, t')}{\partial t} = & - \sum_i \frac{\partial}{\partial z_i} [A_i(\mathbf{z}, t) P(\mathbf{z}, t | \mathbf{y}, t')] \\ & + \frac{1}{2} \sum_{i,j} \frac{\partial^2}{\partial z_i \partial z_j} [B_{ij}(\mathbf{z}, t) P(\mathbf{z}, t | \mathbf{y}, t')] \\ & + \int d\mathbf{x} \left[ W(\mathbf{z} | \mathbf{x}, t) P(\mathbf{x}, t | \mathbf{y}, t') \right. \\ & \left. - W(\mathbf{x} | \mathbf{z}, t) P(\mathbf{z}, t | \mathbf{y}, t') \right] \end{aligned} \quad (7.1.1)$$

Where:

$$W(\mathbf{x}|\mathbf{z}, t) = \lim_{\Delta t \rightarrow 0} \frac{1}{\Delta t} P(\mathbf{x}, t + \Delta t | \mathbf{z}, t) \quad (7.1.2a)$$

$$A_i(\mathbf{z}, t) = \lim_{\Delta t \rightarrow 0} \frac{1}{\Delta t} \int_{\mathbf{x}-\mathbf{z} < \varepsilon} d\mathbf{x} (x_i - z_i) P(\mathbf{x}, t + \Delta t | \mathbf{z}, t) + \mathcal{O}(\varepsilon) \quad (7.1.2b)$$

$$B_{ij}(\mathbf{z}, t) = \lim_{\Delta t \rightarrow 0} \frac{1}{\Delta t} \int_{\mathbf{x}-\mathbf{z} < \varepsilon} d\mathbf{x} (x_i - z_i)(x_j - z_j) P(\mathbf{x}, t + \Delta t | \mathbf{z}, t) + \mathcal{O}(\varepsilon) \quad (7.1.2c)$$

For all  $\varepsilon > 0$  and in the case that for eq. (7.1.2a)  $|\mathbf{x} - \mathbf{z}| \geq \varepsilon$ .

## 7.2 Fokker-Planck Equation

In the case where the final term of eq. (7.1.1) is zero (i.e.  $W(\mathbf{z}|\mathbf{x}, t) = 0$  — there are no jump processes in the system), the CKE reduces to the FPE for a stochastic system. The general form of the FPE is thus[78]:

$$\begin{aligned} \frac{\partial}{\partial t}P(\mathbf{z}, t|\mathbf{y}, t') &= - \sum_i \frac{\partial}{\partial z_i} [A_i(\mathbf{z}, t)P(\mathbf{z}, t|\mathbf{y}, t')] \\ &\quad + \frac{1}{2} \sum_{i,j} \frac{\partial^2}{\partial z_i \partial z_j} [B_{ij}(\mathbf{z}, t)P(\mathbf{z}, t|\mathbf{y}, t')] \end{aligned} \quad (7.2.1)$$

$\mathbf{A}(\mathbf{z}, t)$  is the drift vector and  $\mathbf{B}(\mathbf{z}, t)$  is the diffusion matrix. For small values of  $\Delta t$ , the derivatives of  $A_i(\mathbf{z}, t)$  and  $B_{ij}(\mathbf{z}, t)$  are negligible compared to those for  $P$  and so eq. (7.2.1) becomes:

$$\begin{aligned} \frac{\partial}{\partial t}P(\mathbf{z}, t|\mathbf{y}, t') &= - \sum_i A_i(\mathbf{y}, t) \frac{\partial P(\mathbf{z}, t|\mathbf{y}, t')}{\partial z_i} \\ &\quad + \sum_{i,j} \frac{1}{2} B_{ij}(\mathbf{y}, t) \frac{\partial^2 P(\mathbf{z}, t|\mathbf{y}, t')}{\partial z_i \partial z_j} \end{aligned} \quad (7.2.2)$$

This represents the solution to a general set of LEs:

$$\mathbf{y}(t + \Delta t) = \mathbf{y}(t) + \mathbf{A}(\mathbf{y}(t), t)\Delta t + \boldsymbol{\xi}(t)\Delta t^{1/2} \quad (7.2.3)$$

Where:

$$\langle \boldsymbol{\xi}(t) \rangle = 0 \quad \langle \boldsymbol{\xi}(t)\boldsymbol{\xi}(t') \rangle = 2\mathbf{S}\delta(t - t') \quad (7.2.4)$$

Where  $\mathbf{S}$  is an array of stochastic coefficients for the LEs.

### 7.3 Derivation of Ornstein-Uhlenbeck Fokker-Planck Equation

Recall the set of LEs for an OU particle[78]:

$$\frac{d\mathbf{r}}{dt} = \mathbf{v} \tag{7.3.1a}$$

$$\frac{d\mathbf{v}}{dt} = -\gamma_0\mathbf{v} + \sqrt{2D}\boldsymbol{\xi}(t) \tag{7.3.1b}$$

The differential CKE for a system with drift and diffusion gives the FPE:

$$\begin{aligned} \frac{\partial}{\partial t}P(\mathbf{z}, t|\mathbf{y}, t') &= - \sum_i \frac{\partial}{\partial z_i} [A_i(\mathbf{z}, t)P(\mathbf{z}, t|\mathbf{y}, t')] \\ &+ \frac{1}{2} \sum_{i,j} \frac{\partial^2}{\partial z_i \partial z_j} [B_{ij}(\mathbf{z}, t)P(\mathbf{z}, t|\mathbf{y}, t')] \end{aligned} \tag{7.3.2}$$

Applying the LEs (7.3.1) to eq. (7.3.2) yields the FPE for an underdamped OU particle:

$$\begin{aligned} \frac{\partial P(\mathbf{v}, \mathbf{r}, t)}{\partial t} &= - \frac{\partial (\mathbf{v}P(\mathbf{v}, \mathbf{r}, t))}{\partial \mathbf{r}} + \gamma_0 \frac{\partial (\mathbf{v}P(\mathbf{v}, \mathbf{r}, t))}{\partial \mathbf{v}} \\ &+ D \frac{\partial^2 P(\mathbf{v}, \mathbf{r}, t)}{\partial \mathbf{v}^2} \end{aligned} \tag{7.3.3}$$

## 7.4 Derivation of Solution to OU FPE

The Fokker-Planck equation for the OU Process is[83]:

$$\frac{\partial P(\mathbf{v}, t)}{\partial t} = \gamma_0 \frac{\partial(\mathbf{v}P(\mathbf{v}, t))}{\partial \mathbf{v}} + D \frac{\partial^2 P(\mathbf{v}, t)}{\partial \mathbf{v}^2} \quad (7.4.1)$$

The Fourier transforms for the RHS terms in eq. (7.4.1) are (taking positive Fourier transform):

$$\begin{aligned} \mathcal{F} \left[ \gamma_0 \frac{\partial(\mathbf{v}P(\mathbf{v}, t))}{\partial \mathbf{v}} \right] &= \gamma_0 \int_{-\infty}^{\infty} d\mathbf{v} \frac{\partial \mathbf{v}P(\mathbf{v}, t)}{\partial \mathbf{v}} e^{i\mathbf{k}\mathbf{v}} \\ &= -\gamma_0 k \frac{\partial \hat{P}(k, t)}{\partial k} \end{aligned} \quad (7.4.2)$$

$$\begin{aligned} \mathcal{F} \left[ D \frac{\partial^2 P(\mathbf{v}, t)}{\partial \mathbf{v}^2} \right] &= D \int_{-\infty}^{\infty} d\mathbf{v} \frac{\partial^2 P(\mathbf{v}, t)}{\partial \mathbf{v}^2} e^{i\mathbf{k}\mathbf{v}} \\ &= -Dk^2 \hat{P}(k, t) \end{aligned} \quad (7.4.3)$$

Therefore eq. (7.4.1) can be transformed to:

$$\frac{\partial \hat{P}(k, t)}{\partial t} + \gamma_0 k \frac{\partial \hat{P}(k, t)}{\partial k} = -Dk^2 \hat{P}(k, t) \quad (7.4.4)$$

Using the method of characteristics, a system of ordinary differential equations may be found from eq. (7.4.4):

$$dt = \frac{dk}{\gamma_0 k} = -\frac{d\hat{P}(k, t)}{Dk^2 \hat{P}(k, t)} \quad (7.4.5)$$

Resulting in two ODEs:

$$\frac{dk}{dt} = \gamma_0 k \quad (7.4.6a)$$

$$\frac{d\hat{P}(k, t)}{dt} = -Dk^2 \hat{P}(k, t) \quad (7.4.6b)$$

Solving eq. (7.4.6a):

$$k = k_0 e^{\gamma_0 t} \quad (7.4.7)$$

Substituting eq. (7.4.7) into eq. (7.4.6b):

$$\int_{\hat{P}_0}^{\hat{P}(k,t)} \frac{d\hat{P}'(k,t)}{\hat{P}'(k,t)} = -Dk_0^2 \int_0^t dt \exp\left[2\frac{t}{\tau}\right] \quad (7.4.8)$$

The solution to this equation yields the solution to eq. (7.4.1) in Fourier space for initial value  $\hat{P}_0$ :

$$\hat{P}(k,t) = \hat{P}_0 \exp\left(\frac{-D}{2\gamma_0} (k^2 - k_0^2)\right) \quad (7.4.9)$$

#### 7.4.0.1 Case 1 — Initial Delta Function

Consider a particle starting at velocity  $\mathbf{v}_0$ :

$$P(\mathbf{v}, t | \mathbf{v}_0, t_0) = \delta(\mathbf{v} - \mathbf{v}_0) \quad (7.4.10)$$

Transforming this into Fourier space:

$$\mathcal{F}[P(\mathbf{v}, t | \mathbf{v}_0, t_0)] = \hat{P}_0 = \int_{-\infty}^{\infty} d\mathbf{v} \delta(\mathbf{v} - \mathbf{v}_0) e^{i\mathbf{k}\mathbf{v}} = e^{i\mathbf{k}_0\mathbf{v}_0} \quad (7.4.11)$$

Substituting eq. (7.4.11) into eq. (7.4.9), using eq. (7.4.7), yields:

$$\hat{P}(k,t) = \exp\left[ik\mathbf{v}_0 e^{-\gamma_0 t} - \frac{Dk^2}{2\gamma_0} (1 - e^{-2\gamma_0 t})\right] \quad (7.4.12)$$

Let:

$$\sigma^2(t) = \frac{D}{\gamma_0} (1 - e^{-2\gamma_0 t}) \quad (7.4.13a)$$

$$\mu(\mathbf{v}_0, t) = \mathbf{v}_0 e^{-\gamma_0 t} \quad (7.4.13b)$$

Then:

$$\hat{P}(k,t) = \exp\left[-ik\mu(\mathbf{v}_0, t) - \frac{k^2}{2}\sigma^2(t)\right] \quad (7.4.14)$$

Taking the inverse Fourier transform of eq. (7.4.14):

$$\begin{aligned} P(\mathbf{v}, t) &= \int_{-\infty}^{\infty} dk e^{-ikv} \exp \left[ -ik\mu(\mathbf{v}_0, t) - \frac{k^2}{2}\sigma^2(t) \right] \\ &= \int_{-\infty}^{\infty} dk \exp \left[ \frac{-\sigma^2(t)}{2}k^2 - ik(\mathbf{v} + \mu(\mathbf{v}_0, t)) \right] \end{aligned} \quad (7.4.15)$$

Using the integral relationship:

$$\int_{-\infty}^{\infty} dx \exp \left[ \frac{-ax^2}{2} + bx \right] = \left( \frac{2\pi}{a} \right)^{1/2} \exp \left[ \frac{b^2}{2a} \right] \quad (7.4.16)$$

Letting:

$$a = \sigma^2(t) \quad (7.4.17)$$

$$b = -i(\mathbf{v} + \mu(\mathbf{v}_0, t)) \quad (7.4.18)$$

Then:

$$P(\mathbf{v}, t) = \left( \frac{2\pi}{\sigma^2(t)} \right)^{1/2} \exp \left[ \frac{-(\mathbf{v} + \mu(\mathbf{v}_0, t))^2}{2\sigma^2(t)} \right] \quad (7.4.19)$$

Which is simply a Gaussian with mean  $\mu(\mathbf{v}_0, t)$  and standard deviation  $\sigma(t)$  as defined in eqs. (7.4.13).

#### 7.4.0.2 Case 2 — Initial Uniform Distribution

For  $\mathbf{v}_0 \in (\mathbf{v}_a, \mathbf{v}_b)$ :

$$P_0(\mathbf{v}_0, t_0) = \frac{1}{\mathbf{v}_a - \mathbf{v}_b} \quad (7.4.20)$$

The Fourier transform is thus:

$$\mathcal{F} [P(\mathbf{v}_0, t_0)] = \hat{P}_0 = \int_{\mathbf{v}_a}^{\mathbf{v}_b} d\mathbf{v} e^{ikv} \frac{1}{\mathbf{v}_a - \mathbf{v}_b} = \frac{e^{ikv_b} - e^{ikv_a}}{ik(\mathbf{v}_a - \mathbf{v}_b)} \quad (7.4.21)$$

## 7.5 Velocity-Energy Scatter Plots

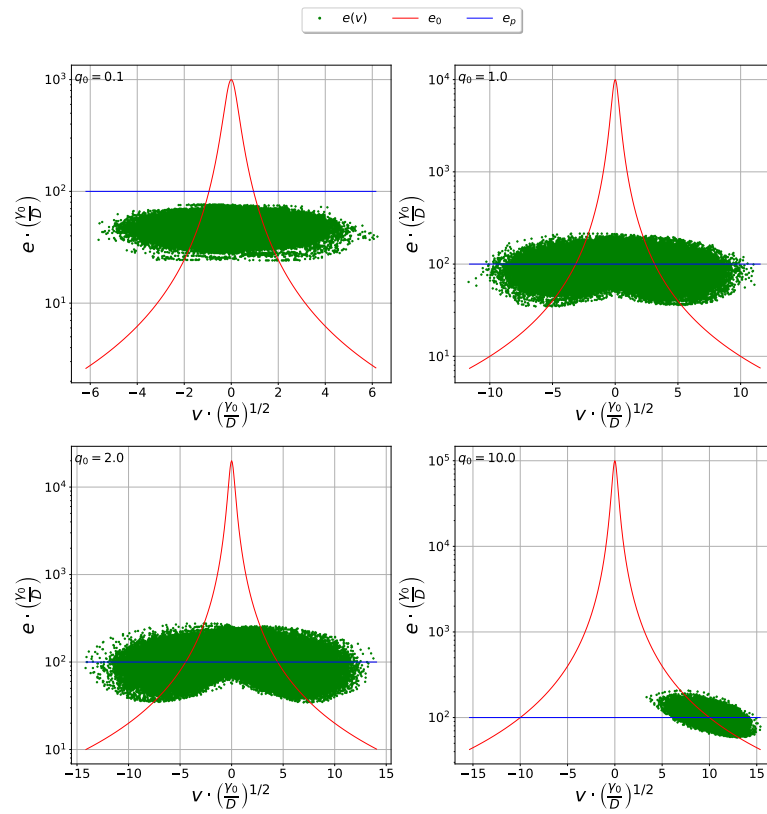


**Figure 7.1:** Scatter plot of particle velocity and energy at intervals of  $\Delta t = 0.1$  for a single particle trajectory of length  $t_{\text{end}} = 30000.0$ . Other parameters  $d_0 = 0.1$ ,  $\gamma_0 = 1.0$ ,  $D = 0.1$ ,  $c = 0.001$ .

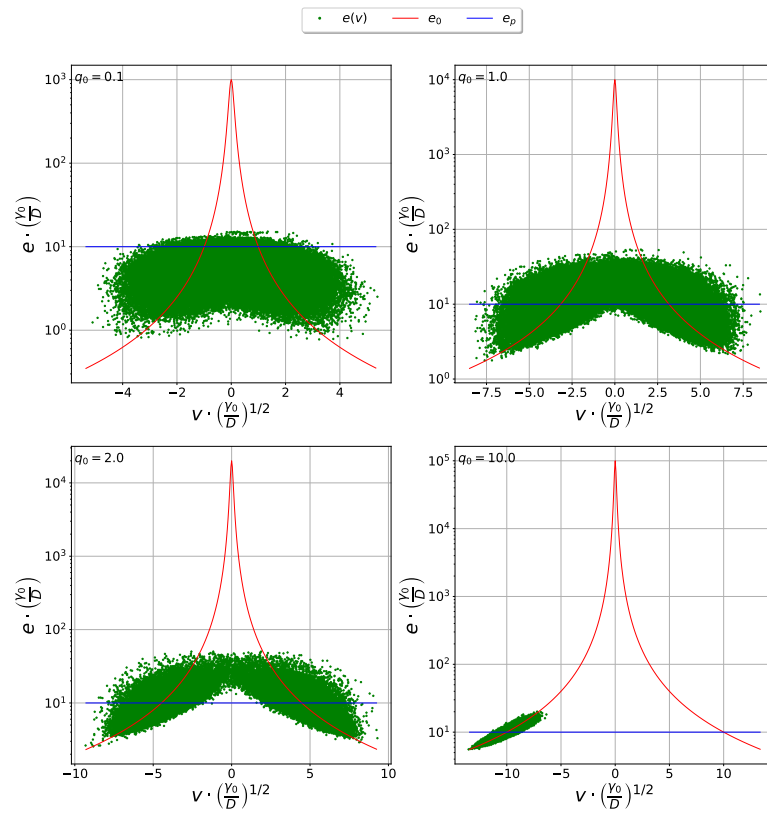


**Figure 7.2:** Scatter plot of particle velocity and energy at intervals of  $\Delta t = 0.1$  for a single particle trajectory of length  $t_{\text{end}} = 30000.0$ . Other parameters  $d_0 = 1.0$ ,  $\gamma_0 = 1.0$ ,  $D = 0.1$ ,  $c = 0.001$ .

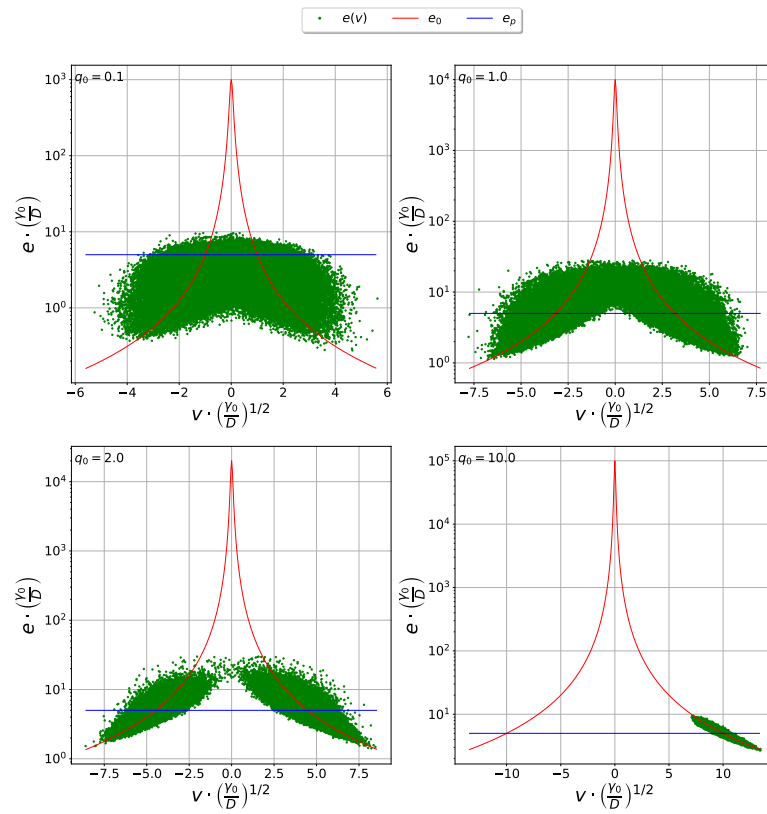


**Figure 7.3:** Scatter plot of particle velocity and energy at intervals of  $\Delta t = 0.1$  for a single particle trajectory of length  $t_{\text{end}} = 30000.0$ . Other parameters  $d_0 = 2.0$ ,  $\gamma_0 = 1.0$ ,  $D = 0.1$ ,  $c = 0.001$ .

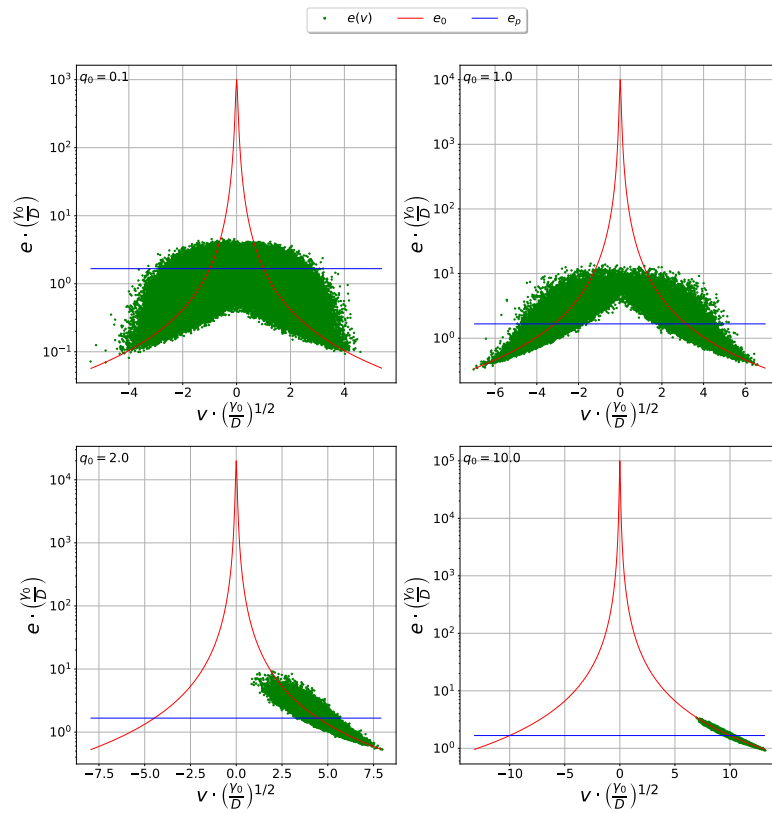


**Figure 7.4:** Scatter plot of particle velocity and energy at intervals of  $\Delta t = 0.1$  for a single particle trajectory of length  $t_{\text{end}} = 30000.0$ . Other parameters  $d_0 = 6.0$ ,  $\gamma_0 = 1.0$ ,  $D = 0.1$ ,  $c = 0.001$ .

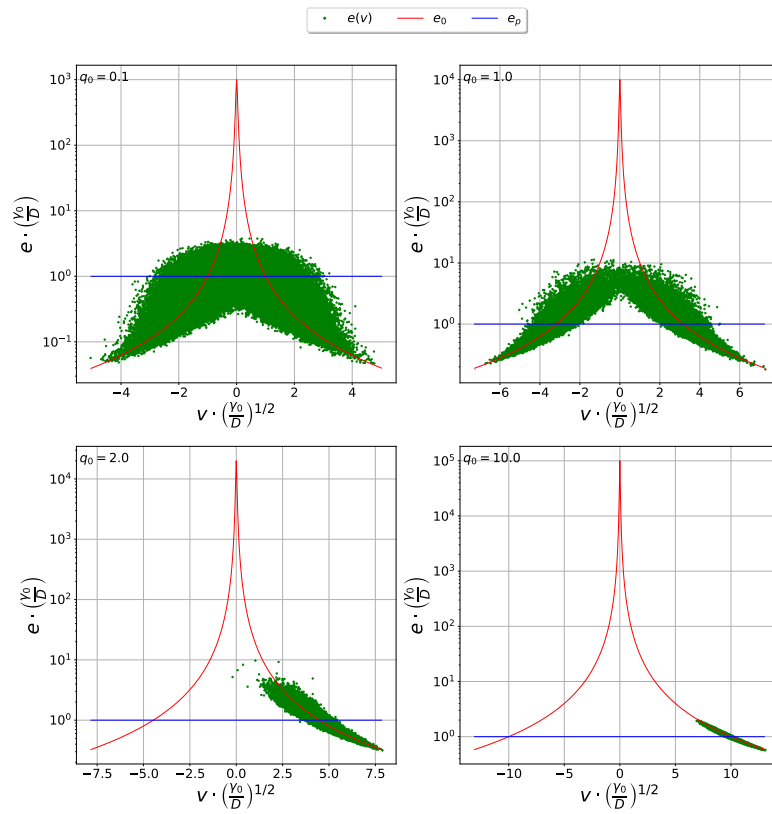


**Figure 7.5:** Scatter plot of particle velocity and energy at intervals of  $\Delta t = 0.1$  for a single particle trajectory of length  $t_{\text{end}} = 30000.0$ . Other parameters  $d_0 = 10.0$ ,  $\gamma_0 = 1.0$ ,  $D = 0.1$ ,  $c = 0.001$ .

## 7.6 First Passage Time Probability

Beginning with the Green's function eq. (7.4.19) for an OU particle as previously derived rewritten for a 1-D system:

$$P(v, \tau|v_0) = \left( \frac{\gamma_0}{2\pi D (1 - e^{-2\gamma_0\tau})} \right)^{1/2} \exp \left[ \frac{-\gamma_0(v - v_0 e^{-\gamma_0\tau})^2}{2D (1 - e^{-2\gamma_0\tau})} \right] \quad (7.6.1)$$

The Green's function  $G(v, \tau|v_0)$  when applying an absorbing boundary condition  $P(v < 0) = 0$  is:

$$G(v, \tau|v_0) = P(v, \tau|v_0) - P(v, \tau|-v_0) \quad (7.6.2)$$

$$G(v, \tau|v_0) = \left( \frac{\gamma_0}{2\pi D (1 - e^{-2\gamma_0\tau})} \right)^{1/2} \left( \exp \left[ \frac{-\gamma_0(v - v_0 e^{-\gamma_0\tau})^2}{2D (1 - e^{-2\gamma_0\tau})} \right] - \exp \left[ \frac{-\gamma_0(v + v_0 e^{-\gamma_0\tau})^2}{2D (1 - e^{-2\gamma_0\tau})} \right] \right) \quad (7.6.3)$$

The survival distribution  $S(\tau)$  is then:

$$S(\tau|v_0) = \int_0^{\infty} dv G(v, \tau|v_0) \quad (7.6.4)$$

$$S(\tau|v_0) = \left( \frac{\gamma_0}{2\pi D (1 - e^{-2\gamma_0\tau})} \right)^{1/2} \int_0^{\infty} dv \left( \exp \left[ \frac{-\gamma_0(v - v_0 e^{-\gamma_0\tau})^2}{2D (1 - e^{-2\gamma_0\tau})} \right] \right) \quad (7.6.5)$$

$$- \exp \left[ \frac{-\gamma_0(v + v_0 e^{-\gamma_0\tau})^2}{2D (1 - e^{-2\gamma_0\tau})} \right] \Bigg) \quad (7.6.6)$$

$$S(\tau|v_0) = \frac{1}{2} \left( \operatorname{erf} \left[ \left( \frac{\gamma_0}{2D (1 - e^{-2\gamma_0\tau})} \right)^{1/2} v_0 e^{-\gamma_0\tau} \right] - \operatorname{erf} \left[ - \left( \frac{\gamma_0}{2D (1 - e^{-2\gamma_0\tau})} \right)^{1/2} v_0 e^{-\gamma_0\tau} \right] \right) \quad (7.6.7)$$

The first passage time distribution can be given thus as:

$$h_0(\tau|v_0) = - \frac{d}{d\tau} S(\tau|v_0) \quad (7.6.8)$$

$$h_0(\tau|v_0) = - \frac{1}{2} \frac{d}{d\tau} \left( \operatorname{erf} \left[ \left( \frac{\gamma_0}{2D (1 - e^{-2\gamma_0\tau})} \right)^{1/2} v_0 e^{-\gamma_0\tau} \right] - \operatorname{erf} \left[ - \left( \frac{\gamma_0}{2D (1 - e^{-2\gamma_0\tau})} \right)^{1/2} v_0 e^{-\gamma_0\tau} \right] \right) \quad (7.6.9)$$

$$h_0(\tau|v_0) = \left( \frac{2v_0^2 \gamma_0^3}{\pi D} \right)^{1/2} \left( \frac{e^{-\gamma_0\tau}}{(1 - e^{-2\gamma_0\tau})^{1/2}} + \frac{e^{-3\gamma_0\tau}}{(1 - e^{-2\gamma_0\tau})^{3/2}} \right) \exp \left( - \frac{\gamma_0 v_0^2}{2D} \frac{e^{-2\gamma_0\tau}}{(1 - e^{-2\gamma_0\tau})} \right) \quad (7.6.10)$$

## 7.7 Stationary Solution of Adiabatic Energy Depot FPE

Recall the LEs for the ED model:

$$\frac{d\mathbf{r}}{dt} = \mathbf{v} \quad (7.7.1a)$$

$$\frac{d\mathbf{v}}{dt} = -\gamma_0\mathbf{v} + e(\mathbf{v}, t)d_0\mathbf{v} + \sqrt{2D}\boldsymbol{\xi}(t) \quad (7.7.1b)$$

$$\frac{de}{dt} = q(\mathbf{r}, \mathbf{v}, t) - (c + d_0\mathbf{v}^2)e(\mathbf{v}, t) \quad (7.7.1c)$$

When particle energy is adiabatic,  $\dot{e} \approx 0$ . Thus eq. (7.7.1c) has the solution:

$$e_0 = \frac{q_0}{c + d_0\mathbf{v}^2} \quad (7.7.2)$$

The FPE for the LEs (7.7.1) given  $e_0$  from eq. (7.7.2) is therefore:

$$\frac{\partial P}{\partial t} = -\frac{\partial}{\partial \mathbf{v}} \left[ \left( -\gamma_0\mathbf{v} + \frac{q_0\mathbf{v}}{\frac{c}{d_0} + \mathbf{v}^2} \right) P + D \frac{\partial P}{\partial \mathbf{v}} \right] \quad (7.7.3)$$

At steady state (SS),  $\frac{\partial P}{\partial t} = 0$  and thus:

$$\int_P \frac{dP'}{P'} = \int_{\mathbf{v}} d\mathbf{v}' \left( \frac{-\gamma_0\mathbf{v}'}{D} + \frac{q_0\mathbf{v}'}{D \left( \frac{c}{d_0} + \mathbf{v}'^2 \right)} \right) \quad (7.7.4)$$

Integrating this yields:

$$\ln \left[ \frac{P}{\mathcal{N}} \right] = \frac{-\gamma_0\mathbf{v}^2}{2D} + \frac{q_0}{2D} \ln \left[ 1 + \frac{d_0\mathbf{v}^2}{c} \right] \quad (7.7.5)$$

Which can be rearranged to give the SS PDF for the velocity of an adiabatic particle, given that the approximation eq. (7.7.2) holds for the system parameters.

$$P_{\text{SS}}(\mathbf{v}) = \mathcal{N} \left( 1 + \frac{d_0}{c} \mathbf{v}^2 \right)^{\frac{q_0}{2D}} \exp \left[ -\frac{\gamma_0}{2D} \mathbf{v}^2 \right] \quad (7.7.6)$$